


This item is held in Loughborough University's Institutional Repository (<https://dspace.lboro.ac.uk/>) and was harvested from the British Library's EThOS service (<http://www.ethos.bl.uk/>). It is made available under the following Creative Commons Licence conditions.




creative
commons
C O M M O N S D E E D


Attribution-NonCommercial-NoDerivs 2.5

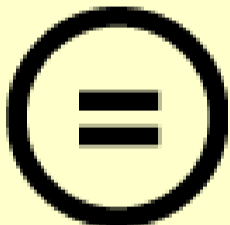
You are free:

- to copy, distribute, display, and perform the work

Under the following conditions:

 **BY:** **Attribution.** You must attribute the work in the manner specified by the author or licensor.


 **Noncommercial.** You may not use this work for commercial purposes.

 **No Derivative Works.** You may not alter, transform, or build upon this work.

- For any reuse or distribution, you must make clear to others the license terms of this work.
- Any of these conditions can be waived if you get permission from the copyright holder.

Your fair use and other rights are in no way affected by the above.

This is a human-readable summary of the [Legal Code \(the full license\)](#).

[Disclaimer](#) 

For the full text of this licence, please go to:
<http://creativecommons.org/licenses/by-nc-nd/2.5/>

**CONTROL OF OUT-OF-BALANCE SERVO MECHANISM SUBJECTED TO
EXTERNAL DISTURBANCES**

by

D.K. DHOLIWAR

A thesis
submitted in partial fulfillment of the
requirements for the award of

Doctor of Philosophy

Loughborough University

August 2007

©Dilip K Dholiwar 2007

In memory of my parents

Summary

There is a category of applications where cantilevered servomechanisms mounted on mobile platforms have to maintain very precise position in inertial space. These systems often referred to as stabilised or line of sight systems have to maintain precise orientation in inertial space in presence of linear and angular external disturbances. Stabilised systems, in general, are designed as balanced systems such that the pivot or centre of rotation coincides with the centre of gravity of the equipment. The research presented in this thesis investigates a general case of stabilising an out-of-balance mechanism; a balanced mechanism is a special case of these systems. The motivation for the research is to remove the requirement for balanced mechanisms enabling engineers to design more effective systems, both in terms of performance and costs, for future needs.

The ultimate aim of the research is to determine whether out-of-balance systems can be stabilised to provide performance comparable with conventionally mounted balanced systems. Stabilisation accuracy is sensitive to nonlinear characteristics of friction. Friction is fairly predictable at moderate speeds but difficult to model close to zero speed where reversals in direction occur. Although many researchers have developed friction models for control system work there is little agreement in the literature on the most appropriate friction model to use both when simulating systems and for use in controller designs. The performance of the most commonly used models is compared with experimental data and recommendations on the models are provided. While the parameters for these models can be obtained in the laboratory using specially designed equipment, or extracted iteratively from a closed loop system, a more direct frequency domain technique is presented which enables the parameters to be obtained from the motion of the mechanism, without the need for a closed loop system.

A novel iterative technique used to determine Coulomb and viscous friction levels has been used to identify the magnitude of system out-of-balance and the nonlinear characteristics of the amplifier. The out-of-balance signal is used to adjust the feedforward controller which enables the stabilisation performance to be maintained

when changes in out-of-balance occur. It is shown that the signal can also be used to automatically adjust controller parameters to maintain desired performance.

Robust control techniques are used to design the control system. It is shown that for this application a control system designed using a lump-parameter model, which results in lower order controller, provides performance similar to that obtained with controllers designed using high order models which have been developed using Finite Element techniques. In this application the dynamic friction models developed by Dahl produced the fastest simulation run times and showed the closest agreement with measured data in the frequency domain.

The conclusions are that out-of-balance systems can be stabilised as effectively as balanced systems if adequate measures are taken to minimise the effects of out-of-balance and friction torques both of which have a marked influence on the stabilisation performance.

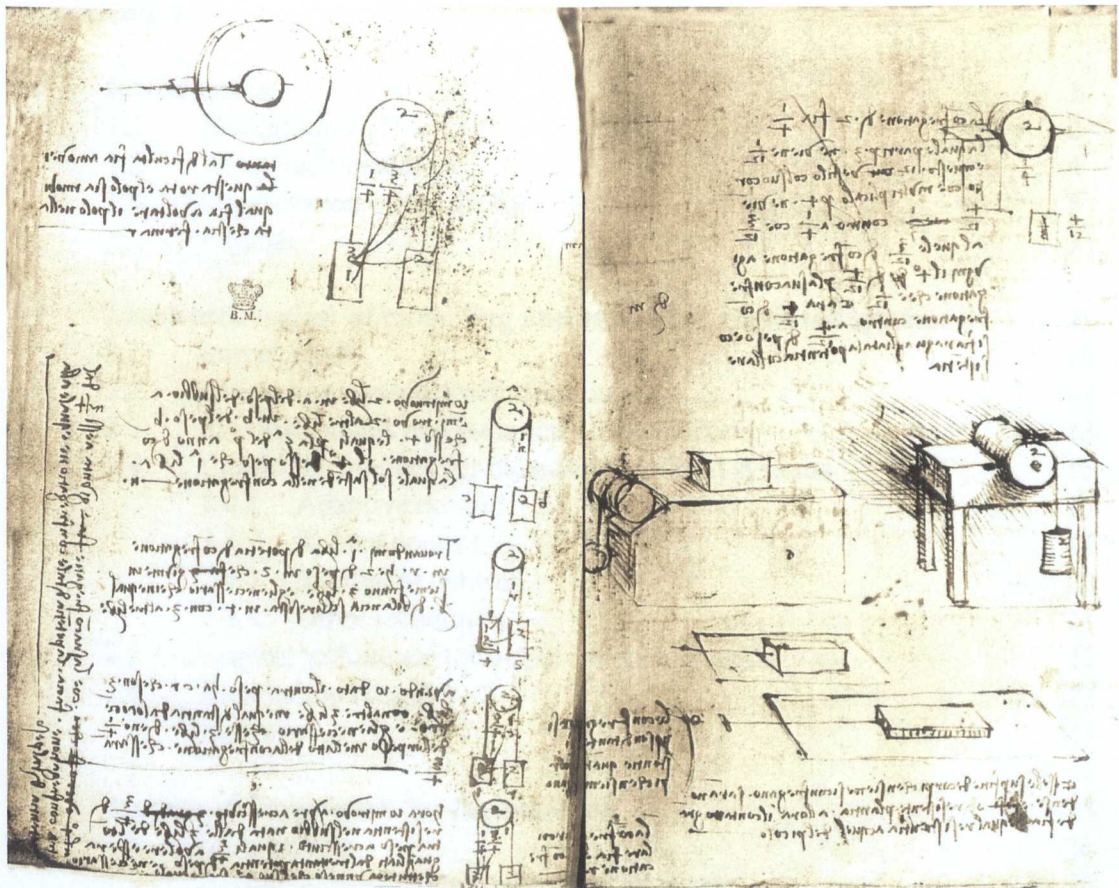
Further work has been identified which involves improving the design of the cantilever mechanism rig and refinement of the experimental techniques. It is recommended that the performance of other control techniques is also assessed. The models developed in this research enable the motions of the tip of the cantilever structure to be predicted. The control of the tip motions, which can cause unacceptable errors, needs to be addressed where the accuracy at the tip is a concern.

Acknowledgments

This work has been carried out under the supervision of Dr. Paul G. Leaney to whom I am indebted for his invaluable guidance, encouragement and patience.

I would like to mention Mr. Tom Forbes for his help on many aspects related to practical work, Mr. Keith Williams for support during long hours of experimental work and Mr. David Lodge for the PAFEC model. The advice and help by Professor Mike Grimble at Strathclyde on the development and use of the robust toolbox has been invaluable. My thanks to Chris Wazynski, Neil Heyes, John Chung, Sean Murray, Ken Peggs and Rob Thornley whose friendship has provided light relief during the final editing.

My gratitude to Vanmala and Ramesh without whom it would not have been possible to complete the work.



© British library2004

‘...circular friction is equal to linear friction’

Leonardo da Vinci (1452-1519)

Arundel Codex ms263 ff40v-41

Contents

<i>Certificate of Originality</i>	<i>i</i>
<i>Summary</i>	<i>ii</i>
<i>Acknowledgments</i>	<i>iv</i>
<i>Contents</i>	<i>vi</i>
<i>Abbreviations</i>	<i>ix</i>
<i>Nomenclature</i>	<i>x</i>
1.0 Introduction	1
1.1 Background	2
1.2 Aims and objectives	4
1.3 Organisation of the thesis	5
Figures	7
2.0 Literature review of modelling and control of stabilised systems	9
2.1 Introduction	10
2.2 Controlling systems with friction	11
2.3 Friction models and parameter measurement	13
2.4 Control techniques for balanced stabilised systems	15
2.4.1 Adaptive control	15
2.4.2 Robust control	17
2.4.3 Intelligent control	20
2.4.4 Other techniques	21
2.5 Control techniques for out-of-balance systems	21
2.6 Concluding remarks	22
Figures	23
3.0 Scope and framework for the research	25
3.1 Introduction	26
3.2 Architecture of the proposed control system	26
3.3 Proposed Research	27
3.3.1 System simulation and control system design	27
3.3.2 Experimental studies and verification of results	30
3.4 Concluding remarks	31
Figures	32
4.0 Description of the cantilever mechanism and experimental setup	34
4.1 Introduction	35
4.2 Description of test rig	35
4.2.1 Mechanical arrangement	35
4.2.2 The nonlinear amplifier characteristics	37
4.2.3 The control system computer	38
4.2.4 Transducer and sensors	38
4.3 The platform motion simulator	38
4.4 Method of assessment and experimental work	39

4.4.1	Measurement of system response	39
4.4.2	External disturbance responses	40
4.5	Concluding remarks	41
	Figures	43
5.0	Simulation of cantilever mechanism	51
5.1	Introduction	52
5.2	Derivation of the system equations	52
5.2.1	Model of the cantilever mechanism	52
5.2.2	Reduced order models	57
5.2.3	The lump-parameter model	60
5.2.4	The gearbox model	61
5.2.5	The servo motor model	62
5.2.6	The servo amplifier model	62
5.2.7	Friction models	63
5.2.8	Transducer models	69
5.2.9	The frequency response analyzer	69
5.3	The SIMULINK models	72
	Figures	74
6.0	Design of the control system	92
6.1	Introduction	93
6.1.1	Control system performance specification	93
6.2	Models for control system design	94
6.2.1	Reduced order models for control system design	95
6.3	Design of controller using FE models	97
6.3.1	Linear model results using FE designed controller	97
6.3.2	Nonlinear model results using FE designed controller	98
6.4	Design of controller using lumped parameter models	99
6.5	Robustness properties	100
6.6	Concluding remarks	103
	Figures	104
7.0	Experimental evaluation	134
7.1	Introduction	135
7.2	Comparing performance of friction models with measured results	135
7.2.1	Combined friction models and their locations	137
7.2.2	Comparing electro-mechanical system (plant) response	138
7.3	Identification of nonlinear parameters	138
7.3.1	Identification of nonlinear gain of the amplifier	140
7.4	Comparing the performance of balanced and out-of-balance system	142
7.4.1	Response of the system to input demand signals	142
7.4.2	Response of cantilever mechanism to external disturbance	144
7.5	Testing robustness properties of the control system	146
7.6	Adapting to changes in out-of-balance	147
7.7	Concluding remarks	149
	Figures	150

8.0	Discussion	188
8.1	Introduction	189
8.2	Modelling of system nonlinearities	189
8.3	Identifying system parameters	190
8.4	Modelling of flexible structure	191
8.5	Design of the control system	192
8.6	Experimental results	193
8.7	Concluding remarks	194
9.0	Conclusions and recommendations for future work	195
9.1	Conclusions	196
9.2	Recommendations for future work	198
10.0	References	200
	Appendices	208
Appendix 1	Other techniques for control of systems with friction	209
Appendix 2	Robust control techniques	212
Appendix 3	Feedforward control	220
Appendix 4	Control system hardware and software development	222
Appendix 5	Details of control system design	227

Abbreviations

ANN	Artificial neural networks
AWTB	Advanced weapon test bed
CACSD	Computer-aided control system design
CFL	Coulomb friction level
CPU	Central processing unit
CVSC	Conventional variable structure control
DC	Direct current
DMRS	Dynamic muzzle reference system
DOF	Degrees of freedom
DPM	Design Plant model
DRA	Defence research agency
DRR	Disturbance rejection ratio
EMF	Electro motive force
FE	Finite element
FFT	Fast fourier transforms
FLC	Fuzzy logic control
FRA	Frequency response analyser
GSLQ	Generalised singular linear quadratic
H_2 and H_∞	Robust control techniques
Hz	Hertz
IKBS	Intelligent knowledge based systems
IWAVM	Integrated weapon armour vehicle model
LIDAR	Laser identification, detection and ranging
LQG/LTR	Linear quadratic gaussian/loop transfer recovery
MBT	Main battle tank
MIMO	Multi-input multi-output
MRAC	Model reference adaptive control
MVSC	Modified variable structure control
PC	Personal computer
PI	Proportional and integral
PID	Proportional integral and derivative control
PMS	Platform motion simulator
PSD	Power spectral density
SISO	Single-input single-output
RMS	Root mean square
STC	Spatial time constant
STR	Self-tuning regulator
TFL	Target feedback loop
TFM	Target function matrix
TFs	Transfer functions
VME	Versa modular euro card
VSC	Variable structure control

Nomenclature

$[]^T$	transpose of matrix	-
$\ F_l(P_G, K)\ _2$	2-norm as in H_2	-
$\ F_l(P_G, K)\ _\infty$	∞ -norm as in H_∞	-
\int_a^b	integral with limits	-
a_0	damping coefficient proportional to mass	-
a_1	damping proportional coefficient to stiffness	-
A	cross sectional area	m^2
A_0, A_c, A_d	non-uniform element area (near, mid, far)	m^2
$[A]_s$	assembly matrix for element s	-
A	plant matrix state space	-
B	input matrix state space	-
C	damping matrix for FE system	N/m/s and Nm/rad/s
$C_{KF}(s)$	complementary sensitivity function	-
C	output matrix state space	-
D_{gb}	damping gearbox	Nm/rad/s
D_h	hub to beam damping	Nm/rad/s
D_v	stick region in Karnopp friction model	m/s (or rad/s)
D	feedforward matrix state space	-
E	Young's modulus	N/m ²
$E(s)$	error state vector	-
f	fiction force (or torque)	N (or Nm)
f_c	coulomb friction force (or torque)	N (or Nm)
f_e	external force (or torque)	N(or Nm)
f_s	stiction force (or torque)	N(or Nm)
f_v	viscous fiction coefficient force (or torque)	N/m/s(or Nm/rad/s)
F_l	lower linear fractional transformation	-
F_m	function describing nonlinear motor friction	-
F_p	function describing nonlinear pivot friction	-
G	control gain matrix	-
$G(j\omega)$	transfer function	-
$ G(j\omega) $	transfer function amplitude	dB
$\angle G(j\omega)$	transfer function phase	rad
$G(s)$	design plant dynamics transfer function	-
$G_a(s)$	actuator transfer function	-
$G_{Amp+mot}$	amplifier and motor transfer function	-
$G_f(s)$	feedforward transfer function	-
$G_{KF}(s)$	loop transfer function matrix	-
$G_1(s)$	control transfer function	-
$G_2(s)$	load transfer function	-
H	filter gain matrix	-
i	solid friction model coefficient	-

i_a	armature current	A
I	second moment of area	m^4
I_0, I_c, I_d	non-uniform element 2 nd moment	m^4
I(T)	imaginary part of transfer function	-
J_b	beam inertia lump-parameter	$kg\ m^2$
J_h	hub inertia-lump parameter	$kg\ m^2$
k	stiffness matrix of each FE element	N/m and Nm/rad
k_{ij}	row and column elements of stiffness matrix	N/m and Nm/rad
K	assembled stiffness matrix for system	N/m and Nm/rad
K_{ac}	accelerometer gain	V/m/s ²
K_e	motor voltage constant	V/rad/s
K_{gb}	stiffness gearbox	Nm/rad
K_{gv}	gyro gain	V/rad/s
K_h	stiffness at hub	Nm/rad
K_{ifb}	current feedback constant	V/A
K_t	motor torque constant	Nm/A
K(s)	compensator	-
K_v	amplifier voltage gain	A/V
L	length	m
L_a	inductance of armature	H
m	mass matrix of each FE element	kg and $kg\ m^2$
m_{ij}	row and column element of mass matrix	kg and kgm^2
M	assembled mass matrix for system	kg and kgm^2
N	gearbox ratio	-
N_c	modal frequency number	-
N_{cy}	number of cycles	-
P	force matrix of each FE element	N and Nm
P	assembled force matrix for system	N and Nm
P_g	generalised plant model	-
P_{xx}	autospectral density (power spectral density)	V ² /Hz
P_{xy}	cross-spectral density	V ² /Hz
r_g	non-uniform element coefficient (stiffness)	-
R_a	resistance	Ω
R(s)	input vector	-
R(T)	real part of transfer function	-
s	Laplace transform	-
S_d	stabilisation factor, $S_d=1$ for $i=1$	-
S_g	non-uniform element coefficient (mass)	-
$S_{KF}(s)$	sensitivity function of TFM	-
$S_{1,2,3}$	forces and torques acting on beam element	N and Nm
t	time	s
T	time(t) at T	s
T_c	constant rolling friction constant	Nm
$T_f(t)$	friction torque	Nm

T_l	load torque	Nm
T_m	motor torque	Nm
T_{oob}	out-of-balance torque	Nm
T_{xy}	transfer function from x to y	-
$T_{1,2}$	torque at 1,2 etc. in gearbox	Nm
$u_{fra}(t)$	input signal at time(t)	V
$u_i(t)$	displacement due to i at beam ends	m or rad
U_{fra}	amplitude of input signal	V
$U(x,t)$	transverse displacement at x, at time t	m
\mathbf{u}	input vector	-
\mathbf{v}	measured variables	-
V	velocity	m/s
V_{o_a}	armature voltage	V
V_{o_g}	generated voltage EMF	V
\mathbf{w}	external signals, eg demand and disturbance	-
\dot{x}_s	Stribeck velocity	m/s or rad/s
\mathbf{x}	state vector	-
$\dot{\mathbf{x}}$	$\frac{dx}{dt}$	-
$y(t)$	output signal at time(t)	V
Y_{fra}	amplitude of system output signal	V
$Y(s)$	output vector	V
\mathbf{y}	output vector	-
z	average bristle deflection	m
\mathbf{z}	error vector	-
α	coefficient in exponential model	-
$\alpha(\dot{x})$	Stribeck effect function	-
α_g	non-uniform element coeff. for 2 nd moment	-
β_g	non-uniform element coeff. for area	-
γ	effective spring rate	N/m or Nm/rad
ζ_{ac}	accelerometer damping ratio	-
ζ_{gy}	gyro. damping ratio	-
ζ_n	damping ratio at mode n	-
θ_b	beam displacement	rad
θ_{gb}	gearbox displacement at input	rad
θ_h	hub displacement	rad
θ_m	motor position	rad
θ_p	pitch of platform	rad
θ_s	gearbox displacement at output	rad
$\dot{\theta}$	speed	rad/s
$\dot{\theta}_m$	motor speed	rad/s
$\ddot{\theta}$	acceleration	rad/s ²

$\ddot{\theta}_m$	motor acceleration	rad/s ²
$\dot{\lambda}$	relative gimbal velocity	rad/s
$\ddot{\lambda}_{RMS}$	relative gimbal acceleration RMS value	rad/s ²
ρ	density	kg/m ³
σ	rest stiffness Dahl model	N/m or Nm/rad
$\sigma_0, \sigma_1, \sigma_2,$	coefficients in friction model	-
$\bar{\sigma}$	maximum singular value	-
τ	time constant	s
τ_a	amplifier time constant	s
τ_{opt}	optimum time constant	s
ϕ	phase angle	rad
ϕ_n	elements of modal matrix Φ	-
Φ	modal matrix	-
$\Phi(s)$	transition matrix	-
$\psi_i(x)$	shape functions i , (x distance along element)	-
ω	frequency of signal	rad/s
ω_{ac}	accelerometer natural frequency	rad/s
ω_{c1}	first break frequency	rad/s
ω_{c2}	second break frequency	rad/s
ω_{gy}	gyro natural frequency	rad/s
ω_n	frequency at mode n	rad/s

CHAPTER 1

INTRODUCTION

1.0 Introduction

1.1 Background

There is a category of applications where cantilevered servomechanisms mounted on mobile platforms have to maintain very precise position in inertial space. These systems often referred to as stabilised or line of sight systems have to maintain precise orientation in inertial space in presence of linear and angular external disturbances, Haessig[1]. Stabilised systems, in general, are designed as balanced systems such that the pivot or centre of rotation coincides with the centre of gravity of the equipment. The research presented in this thesis investigates a general case of stabilising an out-of-balance mechanism; a balanced mechanism is a special case of these systems. The motivation for the research is to remove the requirement for balanced mechanisms enabling engineers to design more effective systems, both in terms of performance and costs, for future needs.

Stabilised systems are encountered in many diverse applications which include airborne radar systems, sighting and surveillance systems, platforms on board ships and weapon systems on attack helicopters, ships and land fighting vehicles. Typical examples of these systems are described by Moorty *et al.*[2], Kennedy[3], Profeta *et al.*[4], Bouazza-Marouf *et al.*[5] and Henry[6]. A selection is illustrated in Figure 1-1. Performance requirements for these systems have steadily increased to reflect the improvements in payload capability, higher maneuverability of host vehicle and overall precision necessary to accomplish the mission objectives. Future applications such as space-based laser systems for communications and high energy laser weapon systems will have to meet more stringent performance requirements, perhaps two or three orders of magnitude better than current systems, Masten *et al.*[7].

Future requirement for higher performance will result in systems where the balanced arrangement cannot be readily accommodated. For example future weapon systems will incorporate larger guns to defeat highly protected targets at longer ranges. Besides being larger the guns will be mounted further forward in the vehicle to accommodate the gun recoil within the turret space. Sighting and surveillance equipment on mobile platforms

will use larger antenna and optical systems and robot arms on mobile platforms will have to provide higher payload capacity and a larger working envelope.

Difficulties in accurate positioning of mechanical systems are primarily caused by the presence of system nonlinearities such as friction and backlash, geometric nonlinearities, joint compliances and the high-order coupled behaviour of mechanical structures. Each of these establishes a limit on the performance; when presented together meeting the performance specifications can be a formidable challenge, Girvin *et al.*[8]. In many motion control applications friction is a dominant factor which limits performance. Failure to account for the effects of friction can lead to tracking errors, limit cycles, undesirable stick-slip motion and unacceptable stabilisation performance, Armstrong-Helouvry *et al.*[9], [10], Radcliffe *et al.*[11]. Control strategies that attempt to compensate for the effects of friction without resorting to high gain feedback loops, require a suitable friction model to predict and compensate for torque or forces due to nonlinear characteristics of friction. Needless to say the accuracy of the friction model, when compared with the actual friction, has a marked influence on the overall system performance.

Future demand for increased reliability, greater operational availability and reduced maintenance costs will require control systems which provide robust performance against changing system parameters. There are many sources which can cause parameters to change some of these include, Maqueira *et al.*[12]:

- Environmental influences such as temperature, pressure and humidity.
- Variations due to manufacturing tolerances and system assembly.
- Aging and wear.
- Distortion and nonlinear behaviour of system components.
- Varying loads and duty cycles.

In cantilevered systems actuators and feedback transducers are usually collocated close to the hub. In systems where the tip accuracy is important this arrangement is not ideal as it ignores the flexing and distortion of the cantilevered structure resulting in poor tip

pointing accuracy. Bird[13], has measured these errors and shown that in mobile weapon systems considerable loss in accuracy at the tip can occur due to the flexing of the gun system resulting in large 'miss distances'.

1.2 Aims and objectives

The ultimate aim of the work presented in this thesis is to determine whether out-of-balance systems can be stabilised to provide performance comparable with conventionally mounted balanced systems. The performance of the control system designed using simulations will be assessed using a specially designed test rig. The rig will enable system parameters to be changed so that the robustness of the control system can be determined. The research program focuses on the following aspects:

- a) **Modelling system nonlinearities:** At present there is little agreement on the most appropriate method for modelling system nonlinearities particularly friction. The rigorous theoretical models, which require measurement of many parameters, are too complex for control systems research while the simpler models may not capture all the salient features of interest. A survey of these models is required to select the most suitable model for use in the simulation of out-of-balance systems.
- b) **Identifying system parameters:** Nonlinearities are difficult to model accurately requiring the measurement of many parameters, which may change with time and operational conditions. While these parameters can be readily measured in the laboratory using specially designed test rigs it may not be practicable to use these techniques in systems operating in the field. Identification techniques are required which will enable the determination of parameters which can be used to tune system performance.
- c) **Modelling of flexible structure:** Whether the system is modelled as a set of lumped mass, spring and damping components, finite elements or assumed modes, the essential difficulty of modelling a distributed parameter system with a finite number of coordinates remains. Control systems designed using low

order or truncated models can result in performance degradation caused by spillover effects, Joshi and Kelkar[14], Balas[15]. Large order models with many hundreds of degrees of freedom are too complex for control systems work. The effects of neglected higher modes will be investigated by comparing the performance of controllers designed using finite element models with those designed using lump-parameter techniques.

- d) **Design of the control system:** A control system will be designed for the out-of-balance system and its performance verified using nonlinear models. The robustness properties of the control system will be investigated. The control system will be implemented in hardware and its performance tested in the laboratory. The robustness properties of the system to changes in several system parameters will be verified.

- e) **Experimental verification of results:** A test rig, which closely resembles a real system, is required which can be used to verify the theoretical results predicted by the simulations. An extensively instrumented test rig needs to incorporate facilities which enable system parameters such as out-of-balance, inertia, friction, and backlash to be varied so that the sensitivity of the system performance to parameter changes can be investigated. The stabilisation performance will be measured using a platform motion simulator. However, platform motion simulators are designed to test stabilisation performance of balanced systems and therefore do not simulate the linear motions. An experimental method is required which will overcome the limitations of the simulator and enable the performance of out-of-balance systems to be tested. The simulator will use measured disturbance data obtained from field trials as input. The stabilisation performance will also be determined in the frequency domain to complement the techniques used in the design of the controller.

1.3 Organisation of the thesis

The thesis is organised in 9 chapters. The research work commences with a literature review, described in chapter 2, which examines control techniques applicable to the

stabilisation of out-of-balance systems. The wide ranging review examines techniques such as adaptive control, robust control, and intelligent control. Techniques which are specifically designed to compensate for system nonlinearities and modelling of the nonlinearities are given particular prominence in the survey. The results of the review are used to provide a framework for the research and scope for the issues to be addressed which are outlined in chapter 3. A structure of the control system to be used for the research is proposed and the features to be incorporated in the design of the rig for experimental work are established.

Details of the specially designed rig, referred to as the ‘cantilever mechanism’, for the experimental work are provided in chapter 4. The equations used to simulate the system are derived in chapter 5 and details of the models developed using SIMULINK® are provided. Chapter 6 presents the design of the control system and simulation results for a typical generic application. The theoretical predictions are compared with the experimental results in chapter 7. The discussion is followed by conclusions and recommendations presented in chapter 8 and 9. The last two sections cover references and appendices.

FIGURES CHAPTER 1

INTRODUCTION

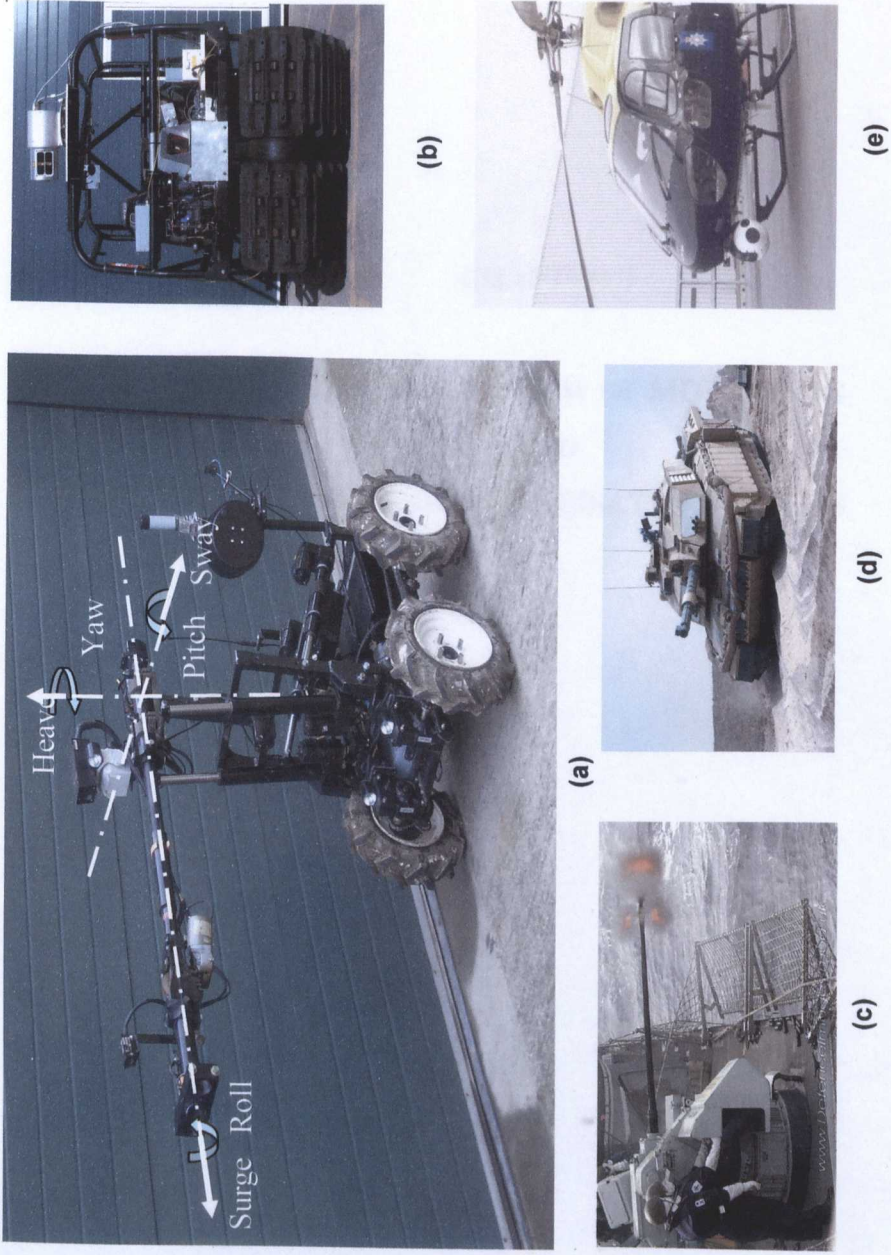


Figure 1-1: Examples of stabilised systems. (a) Remotely controlled robot arm on mobile platform. (b) LIDAR system on unmanned ground vehicle. (c) Naval gun system. (d) Armoured fighting vehicle gun system. (e) Surveillance sight system.

CHAPTER 2

LITERATURE REVIEW OF MODELLING AND CONTROL OF STABILISATED SYSTEMS

2.0 Literature review of modelling and control of stabilised systems

2.1 Introduction

Most of the research described in the literature considers the inertial stabilisation of balanced systems. Using feedforward compensation described by Bigley and Schupan[16], which they refer to as strong stabilisation, it is fairly straight forward to design a controller for linear systems which is able to reject the effects of external disturbances to acceptable levels. However, stabilised systems are sensitive to the nonlinear characteristics of friction especially close to zero speed where reversals in directions occur. In this region changes in forces occur due to effects of stiction and Coulomb friction, and negative gradients are experienced due to the Stribek effect.

In an excellent experimental study using a stabilised airborne pointing and tracking system Walrath[17] shows that the classical friction model, which has its origins in the experimental work of Leonardo da Vinci[18],[19], does not adequately represent friction. The results show that friction has dynamic characteristics which are represented by a first order differential equation, where the time constant is inversely proportional to acceleration. Walrath uses this model to predict friction forces which are then incorporated in a feedforward controller to reduce errors in stabilisation.

Close examination has shown that the model is related to a dynamic model of friction first proposed by Dahl[20],[21], the main conflict being that in Dahl's model the time constant is inversely proportional to speed. Based on Dahl's work several other dynamic models have been proposed and the most commonly used in control system research are described in papers by Haessig and Friedland[22], and Canudas de Wit *et al.*[23]. The classical representation is an example of a static model as it maps friction force as a nonlinear function of speed. Static friction models developed by Tustin[24] and Karnopp[25] have been used in servo control systems research by Gilbert and Winston[26], by Johnson and Lorenz[27] and several other authors. At present there is little agreement in the literature on the most appropriate friction model to use both when simulating systems and for use in controller designs which use friction models to estimate friction forces.

Many different control techniques have been used in research studies to improve the performance of balanced stabilised systems. These techniques can be broadly classified under the following titles:

- i. Adaptive control
- ii. Robust control techniques
- iii. Intelligent control
- iv. Other techniques

The review examines these techniques applied to balanced systems followed by a review of work on the control of out-of-balance systems. As background the review first provides a very brief summary of the problems associated with the control of systems with friction followed by a review of friction models and the determination of the parameters for the models. Other related papers which do not fit in the above categories are examined in section 2.4.4.

2.2 Controlling systems with friction.

Electro mechanical servo systems which do not change direction and do not operate close to zero speed can be controlled quite satisfactorily using PID or similar control techniques as friction in these regions is typically a linear function of speed. However in systems which operate close to zero speed or change direction, such as robots, position controlled apparatus and stabilised systems, PID control has to provide high stiffness (proportional term) and damping (derivative term) to avoid limit cycling and tracking errors. The use of PD and PID controller in systems which perform positioning and tracking tasks has been investigated by several authors. Dupont *et al.*[28] summarise the work of these authors and the different models used in the analysis. Radcliffe *et al.*[29], Kubo *et al.*[30], and others have shown that a system with Coulomb friction and PD control will not exhibit hunting and Kubo has also established that while tracking PD control will not show stick-slip motions.

Integral control is almost always necessary for tracking or positioning systems to reduce the steady state errors. However, the integral action can introduce limit cycling in

systems. One method of reducing limit cycling is to include a deadband as input to the integrator. Shen *et al.*[31] have shown that the deadband decreases linearly with ramp rate and propose controlling the deadband in response to the input rate. Integral windup, which occurs during velocity reversals, is usually overcome by resetting the integral action at velocity reversals. Hansson *et al.*[32] in a novel method use fuzzy logic to control windup in control systems.

To overcome these difficulties a friction model, sometimes referred to as friction observer, is used to estimate the nonlinear torque which is then scaled and summed into the main feedback loop. With perfect match and no delays due to actuator dynamics the estimated torque cancels the actual friction torque and the system appears to be linear. The model based method can be used as either feedforward or feedback compensation as illustrated in Figure 2-1. In feedback implementation the torque or force is estimated using the information such as velocity and position from the output of the system. Where these cannot be directly measured estimates are used. In feedforward implementation the command or demand signals are used as inputs to the friction model. The feedforward scheme, also referred to as open-loop compensation, has the advantage that the input signals to the friction model are known and therefore no additional transducers are required and it is easier to implement as it does not modify the feedback controller. The feedback arrangement provides better estimates of torques as it uses the actual measurements, but additional filtering may be required to maintain system stability, Johnson and Lorenz[27], and Himmel *et al.*[33].

There are a number of other non-model based techniques which have been used to control systems with friction. Typical examples are: impulse control described by Hojjat *et al.*[34] and Deweerth *et al.*[35]; dither control by Lee and Meerkov[36] and Godfrey[37]; joint torque control by Luh *et al.*[38], and Hashimoto *et al.*[39] and the use of magnetic bearings (suspension) to reduce the nonlinear effects of friction by Bleun and Stuart[40]. The work on magnetic suspension is of particular interest as the experimental study shows that considerable improvement in stabilisation performance is achieved by using magnetic suspension systems when compared to conventional bearing mounted systems. Their work on the azimuth axis of an electro-optic system showed the stabilised system performance is improved from -35dB to -60dB. The main

disadvantage of the system is the complexity and the additional power requirements associated with the electro-magnetic system. Brief descriptions of the non-model based techniques mentioned above are provided in appendix 1.

2.3 Friction models and parameter measurement

The classical friction model is the most commonly used representation of friction. The model simply maps friction force against velocity with a discontinuity at zero velocity to account for direction related Coulomb friction. This simple model does not capture any dynamics associated with friction and at zero velocity it can have any value between the Coulomb friction limits. When this model is used in simulations, or for friction compensation, the main difficulty arises in locating the zero crossing. This difficulty is overcome by Karnopp[25] who introduces a small zone at zero velocity which enables the system to 'stick'. Momentum equations are used to determine the forces in this zone which enables the system to 'break free' when the applied force exceeds the stiction force. Although the model is computationally very efficient the complexity of the model increases as additional masses are added to the system. Karnopp demonstrates the increase in complexity for a two mass system. The model also requires accurate values of the masses or inertias, which is not the case with other friction representations. In earlier work Tustin[24] proposed a model which accurately predicted friction forces close to zero velocity. Experimental work has shown the model to be 90% accurate in predicting the friction forces, Armstrong-Helouvry *et al.*[41],[10]. A general form of the model is referred to as the exponential model proposed by Bo and Pavelescu[42].

The classical, Karnopp, Tustin and exponential models are classified as static models as they do not include pre-sliding displacement which occurs at the contact interface. One of the first dynamic friction models was developed by Dahl[20],[21], based on experimental work using ball bearings. The pre-sliding displacement caused by elastic deformation of surface asperities is often referred to as the Dahl effect. The main drawback of the Dahl model is that it does not include stiction or account for the Stribeck effect. However, it is simple to use and computationally very efficient. Heassig and Friedland[22] have developed the bristle and the reset integrator models which provide the desired characteristics. The bristle model is computationally very

inefficient and generally the reset integrator model, which is simplified development of the bristle model, is used in control systems research. Based on the bristle model Canudas de Witt *et al.*[43] proposed a model which displayed the stick-slip behaviour during velocity reversals, the hysteresis effect and the spring-like stiction characteristics. The model is more complex than the Dahl and the reset integrator models. The friction models described above are the most commonly used models in control system research, however other models have been developed by researchers such as Bo and Pavelescu[42], Bilman and Sorine[44]. Details of the models used in this research are provided in the chapter 5 on system simulation.

Whichever sets of equations are used to model friction, it is necessary to measure or identify friction coefficients accurately for effective compensation and modelling of systems. While these parameters can be determined in the laboratory using bespoke tools and rigs, Harnoy[45], Dahl[21], it is advantageous to be able to measure them by more direct methods. Specialist instrumentation such as load cells and torque transducers can be integrated into systems. In a paper by Luh *et al.*[46], on robot application, a torque transducer is installed in the system to measure friction torques. This arrangement has the disadvantage that the hardware has to be modified which results in changes in system dynamics and additional costs are incurred.

Several researchers have developed methods for identifying the parameters directly from the control signals. Walrath[17], Leonard and Krishnaprasad[47], are typical examples. Johnson and Lorenz[27] describe an experimental technique applied to a robot gripper which is used to iteratively extract the friction characteristics from the control signal. The advantage of the technique is that no modifications to the system hardware, such current probes or torque transducers, are required and the technique can be used in situ. In some applications, such safety critical systems, where adaptive control cannot be used or in systems where parameters have to be identified in the field the use of iterative technique is particularly attractive. Johnson and Lorenz intimate that other parameters may also be identified using this technique. The identification of out-of-balance torque and amplifier nonlinear gain is of particular interest in the proposed research.

2.4 Control techniques for balanced stabilized systems

2.4.1 Adaptive control

The adaptive control proposed by Walrath uses measurements from existing system sensors to adjust, on-line, the time constant in the friction model. However, the control system has two limitations; firstly it does not adapt to changes in the rolling or Coulomb friction levels and secondly extensive experimental work is required to derive the relationship between the time constant and acceleration. Walrath's model also does not agree with Dahl's model as described earlier. The limitation regarding the estimate of changes in Coulomb friction is recognized by Kennedy *et al.*[48] who propose a scheme for updating the rolling friction parameter in Walrath's model. They do not provide any results but comment that simulation results show improvements in performance when compared to conventional rate loops and that significant improvements would be necessary to warrant the additional complexity of their scheme. Maqueira and Matsen[12] describe an adaptive control scheme applied to a sighting system. In their work they use relative rate of the gimbal and the controller output signal to determine two variables called Coulomb friction level (CFL) and spatial time constant (STC), which is a measure of the disturbance rise time. The friction model is a first order model whose time constant is updated using estimates of STC and CFL is the gain of the model. Advantage is taken of the relationship between relative rate zero-crossing and reversals in friction disturbance polarity. Filters are used to process the control signal to remove high frequency noise and DC offsets in the control signal. Zero-crossing detectors applied to relative rate signal are used to trigger the estimators.

Several papers describe friction compensators which are based on the input demand signal and load motion. A very simple adaptive friction compensator for a spacecraft gimbal system is described by Himmel *et al.*[33] who compare the performance on an open-loop friction compensator with a closed-loop friction compensator which adapts to changes in friction parameters of a spacecraft gimbal system. In their scheme the friction estimator twice differentiates the position signal and scales the result with the moment of inertia of the load. This represents an estimate of the torque applied to the load. When this torque is subtracted from the actual commanded torque an estimate of the friction torque is obtained. The parameters of the friction model can then be updated

to new values. The results of the work show, as expected that the open-loop compensator outperforms the closed-loop compensator when the assumed friction torque is closed to the actual value and achieves its best performance when the assumed value is the same as the actual value. Results of a hybrid system, which combines the fast response of the open-loop system with insensitivity of the closed-loop system, outperforms both approaches over the full range of operation.

A model reference adaptive compensation for an optical tracking telescope based on Liapunov's direct method is described by Gilbert and Winston[26]. The friction levels in the telescope change with orientation and with direction of travel. Coulomb friction levels of the classical model are updated and used in a feedback compensator. Results show significant improvements in performance for both constant speed operations and sinusoidal inputs. They do not discuss the speed of adaptation but the input demand speed is 0.005degree/second.

Leonard and Krishnaprasad[47] carry out a study in which they compare the performance of several adaptive friction compensation methods with a PID control system for two bi-directional low velocity tracking systems. Although the application is not a stabilized system it provides an interesting comparison on the performance of these techniques. In their work they compare the performance of adaptive control systems based on: (a) Gilbert and Winston[26], (b) Walrath[17] and (c) Craig[49] methods with (d) standard PID and (e) PID augmented with a dither signal. In the controller which uses the Craig's method they use three types of static friction models; Coulomb with viscous friction model, asymmetric characteristics in the Coulomb with viscous model and a model with Stribek friction characteristics.

The results of their work provide the following conclusions:

- i. The three adaptive controllers out perform the PID and PID with dither signal controllers. However, the dither signal frequency was restricted to 25 Hz due to the sampling rate of the controller which may have limited the improvements.

- ii. Walrath's method was reliable and provided the best performance. However, it should be noted that the Coulomb friction levels were not changed. The experiments showed that the time constant in Walrath's model was inversely proportional to speed, agreeing with Dahl's model, and not related to acceleration.
- iii. Gilbert's adaptive system was slow to adapt before it produced the best results.
- iv. Craig's controller overestimated the values of Coulomb friction and the values of viscous friction were poor and the estimated values also drifted. Using the more complicated models did not provide significant improvements in performance.

2.4.2 Robust control

Robust control refers to the use of fixed controllers to the control of plants with unknown disturbance signals, uncertain dynamics and parameters which are not precisely known. Robust control techniques enable the design of fixed controllers which provide acceptable performance in the presence of plant and input certainty, Paraskevopoulous[50].

Table 2-1, from the MATLAB Robust control toolbox user's guide, summarises the advantages and disadvantages of the three most common robust control techniques used to control stabilised equipment. Details of these three techniques are provided in appendix 2, which also includes references which give fuller details.

Pee *et al.* [51] apply the LQG/LTR technique to design a controller for a main battle tank based on a two-inertia model of the system. They compare the performance of the controller with a conventional PI controller and conclude that LQG/LTR provides improved performance for both gun stabilisation and a step demands. The improvement in stabilisation is about 50% and the overshoot present in the PI controller, due to step demand, is eliminated in the LQG/LTR controller. The effect of parameter changes such as gyroscope bandwidth (30% change), system inertia (100%) and resonant frequency (80%) due to gearbox compliance are also investigated. The LQG/LTR controller demonstrates good robustness but the paper does not report on the robustness

performance of the PI controller. They do not report on the effects of changes in friction and it is not clear whether a friction observer is used. Details of the friction model used in the study are not provided.

Method	Advantages	Disadvantages
LQR/LTR	<ul style="list-style-type: none"> • Guaranteed stability margin • Systematic design procedure 	<ul style="list-style-type: none"> • High gain controller • Possibly many iterations • Design focus on one point
H_2	<ul style="list-style-type: none"> • Addresses stability and sensitivity • Almost exact loop shaping • Closed loop always stable 	<ul style="list-style-type: none"> • Possibly many iterations
H_∞	<ul style="list-style-type: none"> • Addresses stability and sensitivity • Exact loop shaping • Direct one step procedure 	<ul style="list-style-type: none"> • Requires special attention to plant parametric robustness

Table 2-1: Summary of the various robust control techniques Mathworks® [52]

Mattice *et al.* [53] use a laboratory test rig, illustrated in Figure 2-2, to compare the performance of three robust control techniques, LQG/LTR, generalized singular linear quadratic (GLSQ) and H_∞ . The rig simulates the azimuth axis of a gun system, and incorporates several interesting features. It has a cantilever flexible beam which represents the gun system, provision for changing the backlash, friction and drive train compliance. In their study, they conclude that all three controllers provide the desired performance with the H_∞ controller showing the best robustness properties. The LQG/LTR controller becomes unstable due to control saturation and backlash. Details of the models used in the design process are not provided.

Rao *et al.*[54], use a model of the above rig to study the performance of the controller based on the LQG/LTR technique. In the study, they encountered convergence/numerical integration problems in a simulation of the controller with a nonlinear plant. The controller is redesigned using a reduced order model. The full order model is reduced using balanced truncation method. The comparisons show that the performance of the redesigned controller is satisfactory and spillover problems are not encountered. The main advantage of the reduced order model is simplification in implementation. The same authors in two separate studies [55], [56] compare the results of four model reduction techniques. They conclude that models reduced by optimal projection, balanced truncation, Litz's modal, and Routh's methods produce similar results with excellent low frequency match between original and reduced order models. Changes in performance of both 'full order' and reduced order models when system parameters are perturbed by 5% are provided. Both models show degradation in step responses. None of the studies give any indication of the stabilisation performance.

In the above studies the models are derived from first principles based on physical laws but in some instances it is easier to fit transfer functions to measured data. A typical example is presented by Moorthy and Marthe[57] in their design of H_{∞} control for a stabilized sighting system. They compare the measured data with a third order model and seventh order model. The third order model is used for the design of the controller and the modelling errors at high frequencies are regarded as multiplicative uncertainties. The measured results show the controller meets the design requirements such as steady state tracking, gain and phase margins but they do not present results of stabilization or test the robustness properties of the controller. The same authors [58] have also applied the LQG/LTR control technique to the stabilisation of a sighting system. They report that the control system achieved the designed goals and achieved stability robustness requirements.

2.4.3 Intelligent control

There are three basic approaches to intelligent control: Knowledge-based expert systems, fuzzy logic, and neural networks. Fuzzy logic control (FLC) is the most commonly used intelligent control technique for the stabilisation problem.

Li *et al.*[59] present a simulation study which assess the effectiveness of FLC when applied to a gun control problem. They use the FLC as an outer loop to enhance the performance of a robust control system. The FLC is used in conjunction with GSLQ and H_{∞} . In both these cases the new system shows considerable improvements in the response times, i.e. the rise time. In the steady state period the authors state that the robust control takes charge to ensure stability as the FLC control signal diminishes to zero. The use of robust control, which is 18th order, simplifies the representation of the FLC. The paper does not present results of the stabilisation performance but comment that both the robust controllers had met the designed requirements with the FLC controller. An example of system controlled entirely by FLC is provided by Moorthy *et al.*[60],[2] who apply FLC to a naval gun system. In this application the gun is slaved to a stabilised electro-optic sight system. This type of system is often referred to as a gun director system and is commonly used for naval applications. In modern land system applications it is usual to have both the gun and the sight system stabilized. In the first paper a FLC is applied to the sight system. The second applies FLC to the slaved gun system which receives its command signals from the stabilised sight system. Using a nonlinear simulation the performance of the FLC controller is compared with a controller designed using classical techniques based on a linear model of the system. The FLC controller outperforms the classical controller by a factor of about two. In both cases the actuator reaches saturation where the FLC controller is able to use nonlinear control laws. It should be noted that in well designed systems actuator saturation is generally avoided. Neither the FLC nor the conventional controller uses a friction observer which may have improved the performance of the conventional controller.

2.4.4 Other techniques

Several other techniques which do not fit in the above categories have also been considered. Nonlinear servomechanism theory and variable structure control (VSC) are two nonlinear control techniques which have been used on the gun-turret application. Haung *et al.* [61], have applied nonlinear servomechanism theory to control a test rig which represents the azimuth axis. In their study they consider the backlash, Coulomb friction and saturation as the three dominant nonlinearities. The simulation studies compare the performance of a control law based on a linear model with control laws based on nonlinear control design. The linear control law shows satisfactory performance on the linear model but poor response in presence of the nonlinearities. The nonlinear control shows performance which is comparable to the linear controller for the linear model case. The nonlinear controller is also able to achieve high precision tracking in the presence of torque disturbances from a firing impulse. Dana *et al.* [62] have applied variable structure control to the elevation axis of an MBT system. They show both simulation and experimental results for a conventional VSC (CVSC) which uses a linear switching line. The results of the simulation showed good agreement with the experimental work and the controller show good robustness to parameter changes. The experimental results however show chatter, which drained the battery supply. The authors also show a modified VSC (MVSC) which uses curved trajectories. The results of the simulation study did not show the expected improvements with the modified method. The experimental work and the simulation studies considered a static vehicle case.

2.5 Control techniques for out-of-balance systems

Out-of-balance systems are very common and are encountered in robot arms, cranes and large gun systems. In the vertical plane the main disadvantage in these systems is the force or torque due to gravitational acceleration, which can be quite large when compared to the forces required for motion control. In very large guns such as mobile howitzers, an equilibrator, a pneumatic spring, is used to reduce the static out-of-balance torque, which enables smaller servo drive components to be used resulting in lower power requirements, smaller size envelope, and cost. While the static force due to gravity can be reduced by springs or similar devices in stabilised systems the effect of

out-of-balance torque disturbance due to heave acceleration can cause unacceptable stabilisation errors. Grumble *et al.*[63] have developed a toolbox for the control of out-of-balanced systems based on the H_2 robust control technique. As an example they design a control system for a large gun, using a lumped-parameter model. The out-of-balance system is assumed to be statically balanced and a classical friction model is used in the nonlinear models. The results show substantial improvements in performance when feedforward control is used for heave compensation. There are two aspects of the work which need further investigation. The first is the effect of the higher modal frequencies which are neglected by the lump-parameter model, and the second is the effect of a more representative friction model. In a statically balanced system Purdy[64], using a controller based on classical techniques, compares the performance of an out-of-balance system with a balanced system and concludes, from a theoretical study, that the performance of out-of-balance systems is 11.4% worse and an increase of 15.9% in power is required. Both these studies are based on simulation work. They do not address the changes in system parameters, and the results need to be confirmed by experimental work.

2.6 Concluding remarks

In this chapter, a variety of techniques which address the stabilisation of equipment mounted on mobile platforms are reviewed. Although many papers consider the stabilisation of balanced systems the case of out-of-balance systems has not been fully investigated. The papers which consider out-of-balance generally assume that both the out-of-balance and the friction characteristics are known and do not change. Experimental data on control of out-of-balance systems is not provided by any of the studies.

The effect on stabilisation performance due to changes in parameters has only been partially addressed for systems which use the robust control techniques. In publications where experimental results are presented they are for laboratory test rigs of the azimuth axis, such as Figure 2-2, but in general the severest disturbance in stabilised system occurs in the vertical plane or pitch axis.

FIGURES CHAPTER 2

**LITERATURE REVIEW OF MODELLING
AND
CONTROL OF STABILISATED SYSTEMS**

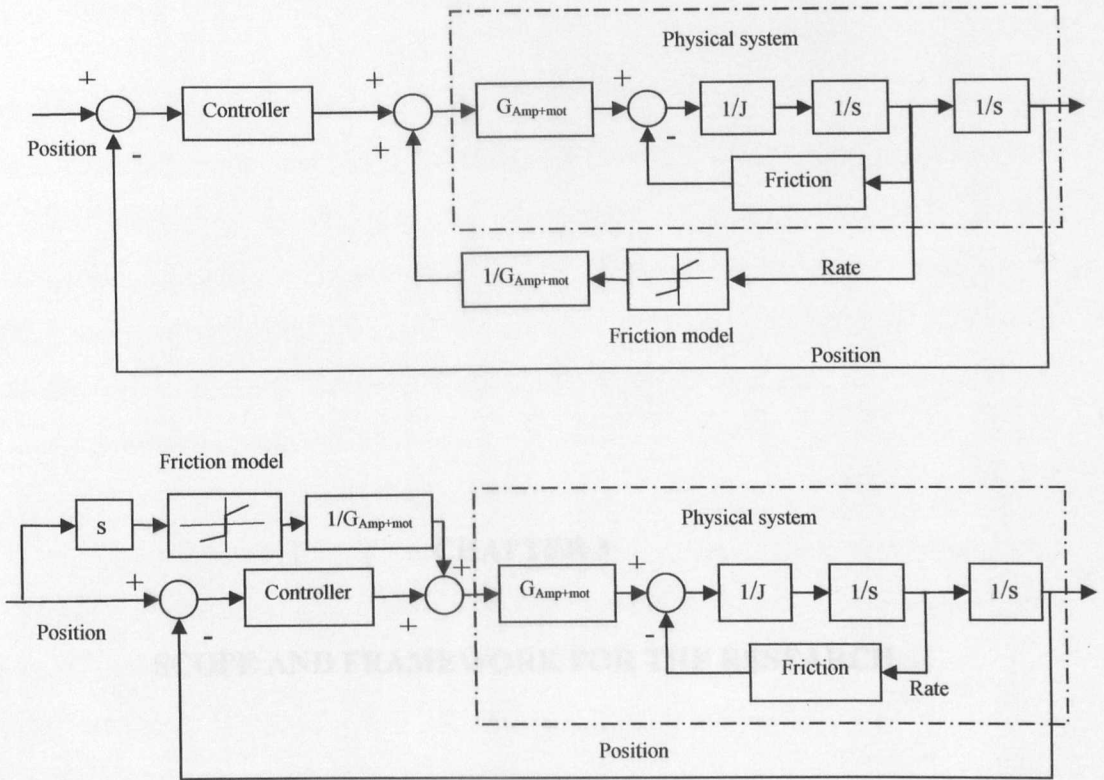


Figure 2-1: Friction model used as feedback compensation (top diagram) and feedforward compensation (bottom) (Amp+mot refers to amplifier and motor).

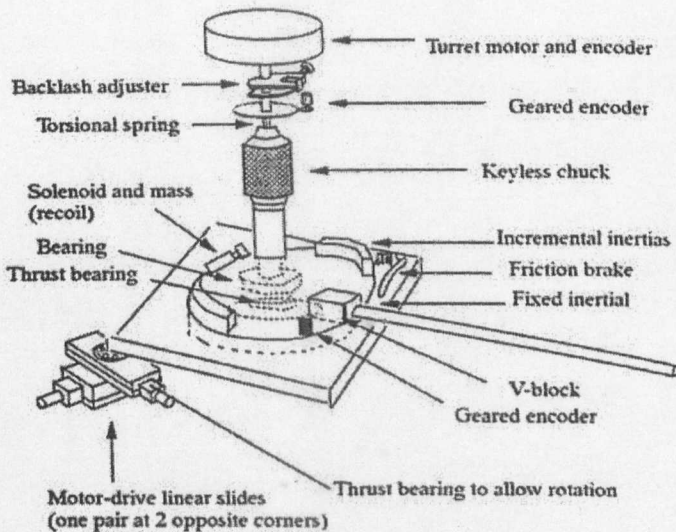


Figure 2-2: Advanced Weapon Test Bed used for stabilisation experiments Mattice et al. [53].

CHAPTER 3

SCOPE AND FRAMEWORK FOR THE RESEARCH

3.0 Scope and framework for the research

3.1 Introduction

The ultimate aim of the research described in this thesis is to develop a control system for out-of-balance stabilised equipment which provides performance similar to that obtained for the balanced case. In order to demonstrate the effectiveness of the control system the theoretical predictions, based on simulation studies, need to be supported by experimental results obtained from a rig which closely resembles, in size and configuration, a real system.

In developing an outline for the research programme to obtain the above objectives, it is helpful to summarise the issues encountered in stabilisation of equipment, both balanced and out-of-balanced, which are highlighted in the literature review.

- System nonlinearities have a marked influence on performance but there is little agreement on the most appropriate method for modelling of friction, the dominant nonlinearity in stabilised systems.
- Although the changes in performance due to variation in friction, inertia, and sensor bandwidth have been addressed the effects of changes in out-of-balance have not been investigated or the effect of changes in system gain as of result of nonlinear amplifier characteristics.
- Parameter identification techniques are required which can be used in the field to manually tune system performance where automatic tuning of systems is not permissible.
- The effect of neglected modes of vibration needs to be considered to avoid spill over effects.

3.2 Architecture of the proposed control system

The architecture proposed for the control system for a single axis of a stabilised mechanism is illustrated in Figure 3-1. The system consists of two major feedback loops and a nonlinear compensator. The primary function of the inner loop is to provide system stabilisation by decoupling the payload, in this case the cantilever

mechanism, from the disturbances caused by the motion of the platform. The decoupling is carried out by the feedback controller using inertial sensors such as rate gyros. The stabilisation of the system is further enhanced by incorporating two feedforward elements which use the angular (pitch) and the linear (heave) motions of the platform as their input. In balanced systems only the feedforward for pitch disturbances is required. In linear systems, if the disturbance can be measured precisely and the actuator dynamics are known, feedforward controllers can nullify the effects of the disturbance to acceptable levels. The effects of feedforward controllers are discussed by Bigley and Schupan[16] for stabilised systems and for more generally applications by D'Souza[65], McNab[66], Kavranoglu[67] and a brief analysis is provided in appendix 3

The function of the second feedback loop is to position the system in response to the demand input, i.e. control the orientation of the mechanism. The position can be derived directly by integrating the rate gyro signals or by using separate position sensors. In systems that need to follow moving objects an additional tracking compensator has to be incorporated to eliminate velocity and acceleration lags. As the primary interest of the work described in this thesis is concerned with system stabilisation the design of the outer loop and the tracking controller will not be addressed. In Figure 3-1 the main components of the control to be addressed by this research are shown in bold.

3.3 Proposed Research

3.3.1 System simulation and control system design

Modelling system nonlinearities and determining parameters

As already noted in chapter 2 gross nonlinearities, in particular friction, have a marked influence on servo system performance. At moderate speeds the effects of friction are fairly predictable but it is difficult to model at low speeds or in systems which undergo velocity reversals. As a result inadequate friction models are used or their effects ignored during the system design process only to discover that in reality, friction can

lead to steady state errors, tracking errors, limit cycles or stick-slip motions. Many researchers such as Tustin[24], Dahl[20], [21], Karnopp[25], Canudas *et al.*[23], Walrath *et al.*[17] and Haessig *et al.*[22] have developed simplified models which are suitable for control systems work. A study will be carried out which will compare the performance of a selection of these friction models to establish which model is the most appropriate for this application. It is not clear whether the accuracy of the friction models is related to the complexity of the models or how the complexity affects the simulation run times. The results of the models will be compared with measured friction characteristics.

While the parameters for these models can be obtained in the laboratory using specially designed equipment it is proposed that the research will investigate whether the parameters can be obtained directly by observing the motions of the platform and the stabilised cantilever mechanism. In studies by Walrath[17], and Leonard and Krishnaprasad[47] the parameters for their models are obtained by using a closed loop system and a first order model for friction is assumed.

Identification of parameters

Johnson and Lorenz[27] and others have shown that Coulomb and viscous friction can be identified using control systems signals. They also intimate that other parameters may also be determined from these signals. In addition to the above friction characteristics the identification of out-of-balance, and other nonlinear characteristics of the drive system will be investigated. The method for identification of these additional parameters will be established using the simulations and then verified using a test rig.

Modelling the flexible structure

Structural dynamicists generate and analyse models with many hundreds of dynamic degrees of freedom (DOF). However, it is very difficult to design controllers based on full order models and the tools used by control analysts fail when more than a dozen or so modes are considered. Whether the system is modelled as a set of lumped mass and springs, finite elements or assumed modes, the essential difficulty of modelling a distributed parameter system with finite number of coordinates remains.

The use of reduced-order models for controller design can lead to control and observation spill over effects which can cause loss of performance or system instability. Control spill over is an excitation of residual modes (modes not included in reduced-order models) by the control action and observation spill over is the contamination of sensor readings by the residual modes.

In this work a Finite Element (FE) model of the system will be developed using a large number of elements (which have constant cross-section) to provide good approximation of the geometry of the structure. A second set of models will be developed using elements with non-uniform cross-sections, which enables the geometry of structure to be approximated using fewer number of elements. The results of the models will be compared with measured modal analysis of the system. Model truncation techniques will then applied to further reduce the size of the model for control system design and analysis.

In addition to the FE model a lump-parameter model will also be developed which neglects the higher modes of the cantilever mechanism i.e. flexible structure. The model will be used in the design of a low order control system. The performance of the control systems designed using FE and lump-parameter models will be compared on the FE model of the system.

Control system design

While the development of precision hardware, such as the use of magnetic suspension, Bluen and Stuart[40], can provide improvements in performance, the approach can lead to high recurring costs and also has restricted areas of application. The work described in this thesis will attempt to provide improvements in system accuracy and performance through control techniques rather than specialised hardware designs.

The control system will be based on the work of Grimble *et al.*[63] and use the toolbox developed [68] for control of an out-of-balanced system. The choice for this controller is based on the promising results obtained by robust control techniques together with a readily available toolbox enabling for rapid development of

controllers. The controller design in Grimble's work is based on a low order lump-parameter model which does not include the effects of structural flexibility. It is proposed that the technique is used on higher order model to compare the performance of the two systems.

3.3.2 Experimental studies and verification of results

The predicted simulation results will be verified using a specially designed test rig based on a real system. To confirm the robustness properties of the control system the test rig, referred to as the cantilever mechanism, will incorporate facilities which enabled system parameters to be varied as follows:

- Out-of-balance of the mechanism.
- Friction in the servo system components.
- Inertia of the system.
- Backlash in the servo drive system.

Ultimately, the stabilisation performance of the system has to be assessed in its operating environment. However, for research work the use of mobile platforms have several disadvantages such as repeatability of tests cannot be guaranteed as they rely on the operator of the vehicle to perform consistently, the terrain may alter due to the churning of the ground and the vehicle characteristics may change. In addition it is difficult to arrange for controlled inputs such as sinusoidal and triangular signals, without a great deal of expense. Delays due to the availability of a host vehicle, the operator and adverse weather conditions etc. can further add to the difficulties. Ideally research studies need to be carried out in the laboratory using a platform motion simulator which enables a variety of repeatable signals to be used which cannot be achieved in field trials. Platform motion simulators are designed to test stabilisation performance of balanced systems and therefore do not simulate the effects of heave motions. A test method is required which will enable the performance of out-of-balance systems to be investigated using a conventional platform motion simulator.

3.4 Concluding remarks

In this chapter a framework for the research programme is established. The research will cover theoretical aspects which will be supported by experimental data obtained from a specially designed test rig. The architecture of the proposed control system is presented and the requirements of the models for the theoretical investigations are discussed. The requirements of test rig are outlined and the experimental procedures to be used to assess the performance of the control system are addresses.

FIGURES CHAPTER 3

SCOPE AND FRAMEWORK FOR THE RESEARCH

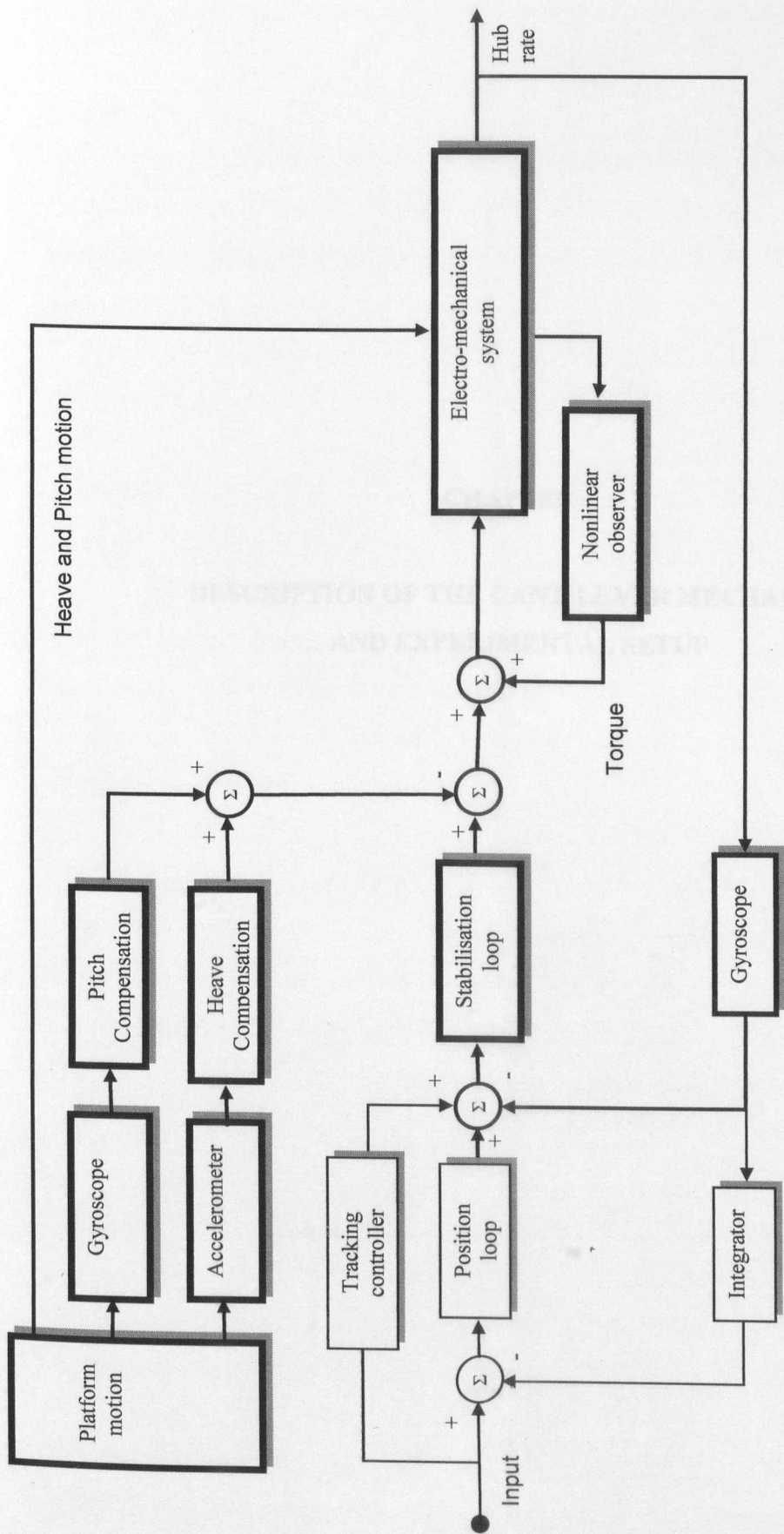


Figure 3-1: Typical control system for stabilised mechanisms with pitch, heave and nonlinear friction observer. The observer is shown as a feedback. In balanced systems the heave compensation is not used. The heavy boarders indicate scope of research.

CHAPTER 4

DESCRIPTION OF THE CANTILEVER MECHANISM AND EXPERIMENTAL SETUP

4.0 Description of the cantilever mechanism and experimental setup

4.1 Introduction

This section provides the details of the cantilever mechanism to be stabilised and the experimental setup used in the laboratory. Salient features of the control system hardware and instrumentation are provided while details of the control software and computer system are consigned to appendix 4. The operation of the platform motion simulator (PMS) used to measure system stabilization is described and the experimental procedures are outlined in this chapter and covered more fully in chapter 7.

4.2 Description of test rig

4.2.1 Mechanical arrangement

The cantilever mechanism illustrated in Figure 4-1 is a real system which has been modified for this research to enable experimental work to be carried out. The primary features are as follows:

- It is a close representation of a typical system.
- The system has been modified to enable system parameters to be readily changed.
- Extensive instrumentation and data logging facilities are incorporated which enable system performance to be measured, recorded and analysed.
- Software development environment used enables rapid modification of control system algorithms.

The layout of the experimental setup is presented as a schematic in Figure 4-2. The figure shows the cantilever mechanism on its platform mounted on the PMS. The sensors incorporated are listed and a pictorial representation of the instrumentation together with a block diagram of the computer system is provided in the figure.

The mechanical system, Figure 4-1, to be stabilised consists of a cantilever mechanism which is pivoted at the hub. The mechanism consists of a beam which is attached to the hub. A support structure is incorporated in the design which increases the stiffness of

the system by a factor of two and a half. The addition of the support structure increases the system out-of-balance. An electric motor-gearbox assembly is coupled to the cantilever mechanism through a large driving gear located at the hub. The rig design enables parameters such as inertia, out-of-balance, backlash and friction to be changed. The components used to change these parameters are identified in Figure 4-1 and the method used is outlined below. As the parameter values for the system are commercially sensitive and classified, Table 4-1 summarises the changes in parameter values as percentage of the values of the system in normal out-of-balance configuration.

System inertia

The method for changing inertia consists of a dumb-bell arrangement which is attached to the main shaft. The inertia is varied by adding masses to the dumb-bell. There is provision for adding four masses (installed as two pairs) which together with the dumb-bell give three inertia variations. Addition of all the inertia masses also changes the overall system mass to 136% of normal.

Out-of-balance

The system balance is changed by adding masses at the hub end of the mechanism. The out-of-balance is increased (towards the tip) by removing masses or reduced by adding masses. When all the masses are installed the system is balanced and with all masses removed it is in the normal out-of-balance state. Further masses can also be added to the front of hub (nearest to the tip) to increase the out-of-balance. In the balanced state the system has the largest moment of inertia which is 133% of the normal out-of-balance value and the mass increases to 196%.

System backlash

Increasing the gap between the large driving gear located on the main shaft and the motor-gearbox assembly varies the backlash in the drive system. The gap is changed by adding spacers between gearbox mounting flanges and the platform, as illustrated in Figure 4-2. The system is calibrated so that the change in backlash is known for each spacer.

Friction at the pivot

The friction in the system is varied using a disc brake mounted on the main shaft. The disc brake is operated by a pneumatic cylinder which is connected to the laboratory supply via a pressure regulator. Although, the control of the friction is not very precise an indication of changes in control system performance can be assessed at several friction levels. The graph of friction torque against the pressure is shown in Figure 4-3. The graph shows peak friction values but does not provide details of the various components of friction. A more precise characterization of the friction can not be obtained due to the limitations of system design.

4.2.2 The nonlinear amplifier characteristics

The amplifier used in the system has a nonlinear characteristic which was measured using a current measuring transducer. The measurements were made with the motor stalled, so that there is no back EMF generated. The characteristics of the amplifier are illustrated in Figure 4-4.

Out-of-balance		Inertia		Backlash		Friction	
Mass no.	%	Mass	%	Spacer	%	Pressure	torque
none (normal)	100%	none (normal)	100%	None (normal)	100%	0 bar	normal
3	75%	Dumb-bell	112%	2 spacers	200%	0.25 bar	50Nm
3&4	37%	2 masses	125%	4 spacers	300%	0.68 bar	100Nm
3&4&5 (balanced)	0%	4 masses	137%	8 spacers	500%	1.0 bar	150Nm
1&2	148%						

Table 4-1: Changes in system parameters as percentage of normal values. (System parameters are commercially classified. Normal values are given as 100%). Mass number 1 and 2 are installed at the front of the hub to increase out-of-balance while 3, 4 and 5 installed at the back of the hub reduce out-of-balance.

4.2.3 The control system computer

The rig is controlled using a digital system based on VME bus architecture. The system uses a MOTOROLA M68000/30 Central Processing Unit (CPU). Interface cards installed in the system enable it to be connected to the rig, provide communication links to other computer systems and input signals to control the rig. The system has 32 differential analogue input channels with 16 bit resolution and 8 analogue output channels with 12 bits resolution. A resolver input board, which has two channels, is used to measure the speed of the motor. Further details of the system are included in appendix 4.

4.2.4 Transducers and sensors

The two primary measurements are heave and pitch motions of the system, relative to inertial space. These are measured using accelerometers and gyroscopes. The system has two gyroscopes located adjacent to the pivot, as shown in Figure 4-8. One gyroscope, located on the platform measures the disturbance into the system and the second mounted on the mechanism, measures the motion of the cantilever mechanism to be stabilised. The gyroscope located on the platform has two functions, firstly it provides a measure of the external disturbance (pitch) acting on the system and secondly it is incorporated in the control system design as input to the feedforward controller. Similarly an accelerometer mounted on the platform adjacent to the pivot measures the vertical accelerations (heave) acting on the system and is used as input to the second feedforward controller.

Position and speed transducers mounted on the cantilever mechanism pivot measure the motions of the mechanism relative to the platform. A tachometer integrated into the servo motor measures the speed of the motor.

4.3 The platform motion simulator

The platform motion simulator only provides pitch motions in the vertical plane therefore the response of the system to heave disturbances can not be obtained directly. This limitation is overcome by mounting the test rig so that it is offset from the

rotational axis of the simulator, as shown in Figure 4-2 and 4-8(a). The heave acceleration and pitch accelerations are simply related by the offset measurement. This arrangement has the limitation that pitch and heave motions cannot be controlled independently.

Tests were carried out to ensure that the above arrangement gave a good approximation of the heave acceleration. Figures 4-5 and 4-6 compare pitch and heave motions produced by the PMS using trials data as the input signal. The results, Figure 4-5, show that the PMS produces pitch motions which are a good match with the measured data from the trial. Close examination of the data shows that there is a delay in the PMS output signal which increases with time. This is attributed to delays in the data logging system and the computer (PC based system) used to control the PMS. Comparison of the heave disturbance data from the trial with the output of the PMS in general shows similar trends but the PMS output shows marginally larger amplitudes, Figures 4-6. A closer agreement would have been obtained by reducing the offset in the rig mounting position and the PMS centre of rotation. A Power Spectral Density (PSD) analysis of the input signal (Figure 4-7(a)), and output signals, (Figure 4-7(b)), show reasonable agreement between the measured data and output motions of the PMS.

4.4 Method of assessment and experimental work

The performance of the system is assessed using the frequency-domain and time-domain tests commonly used to specify control system requirements. In addition to these the ability of the system to reject the effects of an external disturbance referred to as system stabilization are measured using a platform motion simulator. The terminology used to describe the tests refers to Figure 4-8 and 4-9 which show the component diagram and block diagram of the system.

4.4.1 Measurement of system response

The frequency-domain responses of the closed-loop system and the plant (comprising the amplifier, motor, gearbox, cantilever mechanism and transducers) are measured

using the frequency response analyser, Solartron [69]. The time-domain responses are obtained using function generators to provide the input signals.

a) Plant responses

The responses of the plant are measured to validate the model of the electro-mechanical system. These responses are obtained by applying input voltages to the amplifier and the outputs measured by the gyroscope located at the hub. Tests are carried out at several input amplitudes to determine the effects of system nonlinearities. In these tests the controller is not connected to the system.

The plant response tests differ from open-loop tests which include the controller with the feedback disconnected.

b) Closed-loop responses

Closed-loop tests follow the same procedures as the plant tests described above but with the feedback signal enabled and input applied to the system via the controller as illustrated in Figure 4-8 and 4-9.

4.4.2 External disturbance responses

Response of the plant to external disturbances

In the vertical plane the plant response can only be measured on the balanced system as any out-of-balance causes the system to drift to the lower limits under the influence of gravitational force. In a perfectly balanced system vertical acceleration has no effect on the mechanism. However, the tests on the balanced system were carried out with the rig mounted on the PMS with zero offset to minimise errors due to any imbalance in the system. The plant response is measured with the motor disconnected from the amplifier so that the forces driving the mechanism are due to friction in the gears, bearings and seals. In the frequency-domain tests sinusoidal signals are used to drive the PMS system; which is the input disturbance and the output is the motion of the mechanism. The input rate and the output rate are measured using the two gyroscopes located on the platform and the hub of the cantilever mechanism respectively.

Stabilisation response of the closed-loop system

The stabilisation performance of the system is assessed in both the frequency and time-domain. The closed-loop frequency-domain tests follow the same procedure as described above for the plant response tests but with the control system activated. The stabilisation performance of the system sometimes is referred to as the Disturbance Rejection Ratio (DRR) is calculated in decibels as follows:

$$\text{DRR} = 20 \cdot \log_{10} (\text{output response of mechanism} / \text{input motion of platform})$$

A low value of DRR indicates good stabilisation performance.

In the frequency-domain tests described above the stabilisation response of the system is obtained at several individual amplitudes and frequencies. While this provides a method for assessing the performance in the laboratory it does not give an overall, or average response for the system in its operating environment. To assess the response of the system to disturbances encountered in a typical operating environment, measured data from field trials is used as input to the PMS. Disturbance Rejection Ratio using time-domain data is obtained as follows [70]:

$$T_{xy}(f) = \frac{P_{xy}(f)}{P_{xx}(f)}$$

Where P_{xx} = auto-spectral density

P_{xy} = cross-spectral density

T_{xy} = transfer function from x to y

4.5 Concluding remarks

Chapter 4 provides the details of the cantilever mechanism to be stabilised and the experimental setup used in the laboratory. An outline of the test procedures is provided and following limitations of the experimental setup are noted.

a) Platform Motion Simulator limitations

The PMS only provides pitch motions and therefore independent control of heave motions is not available. However, tests have shown that by mounting the rig so that it is offset from the main rotational axis of the PMS provides a good approximation of heave disturbance.

b) Changes in out-of-balance and inertia of the system

The out-of-balance is changed by adding masses to the system. While this varies the out-of-balance it also changes the inertia of the system. Similarly when masses are added to the dumb-bell arrangement to vary the inertia the overall mass of the mechanism also changes.

c) Changes to friction levels

The friction levels in the system are changed using a disc brake operated by a pneumatic system. It is not possible to fully characterise the friction but the system provides an indication of the change in peak friction values.

FIGURES CHAPTER 4

DESCRIPTION OF THE CANTILEVER MECHANISM AND EXPERIMENTAL SETUP

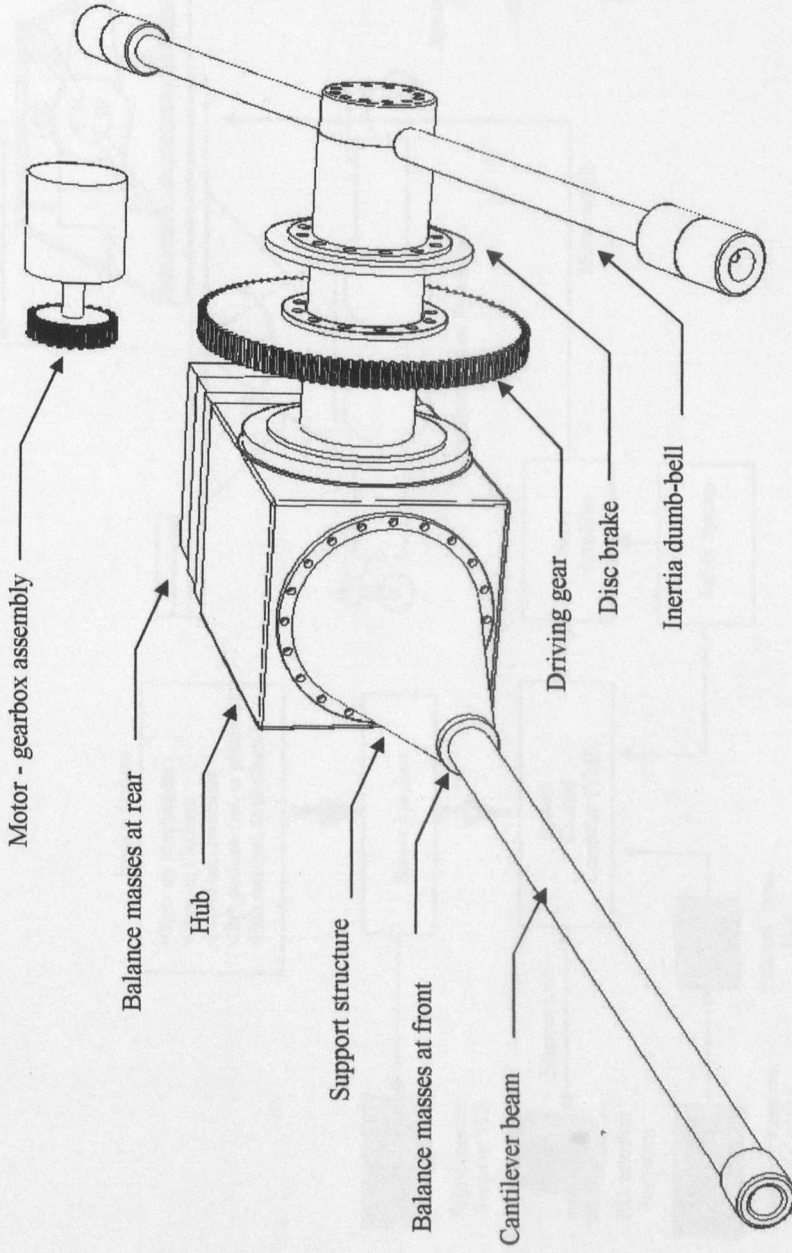


Figure 4-1: Schematic of the cantilever mechanism. The gap between motor - gearbox assembly and driving gear, shown separated for clarity. The balance masses at front also not shown for clarity.

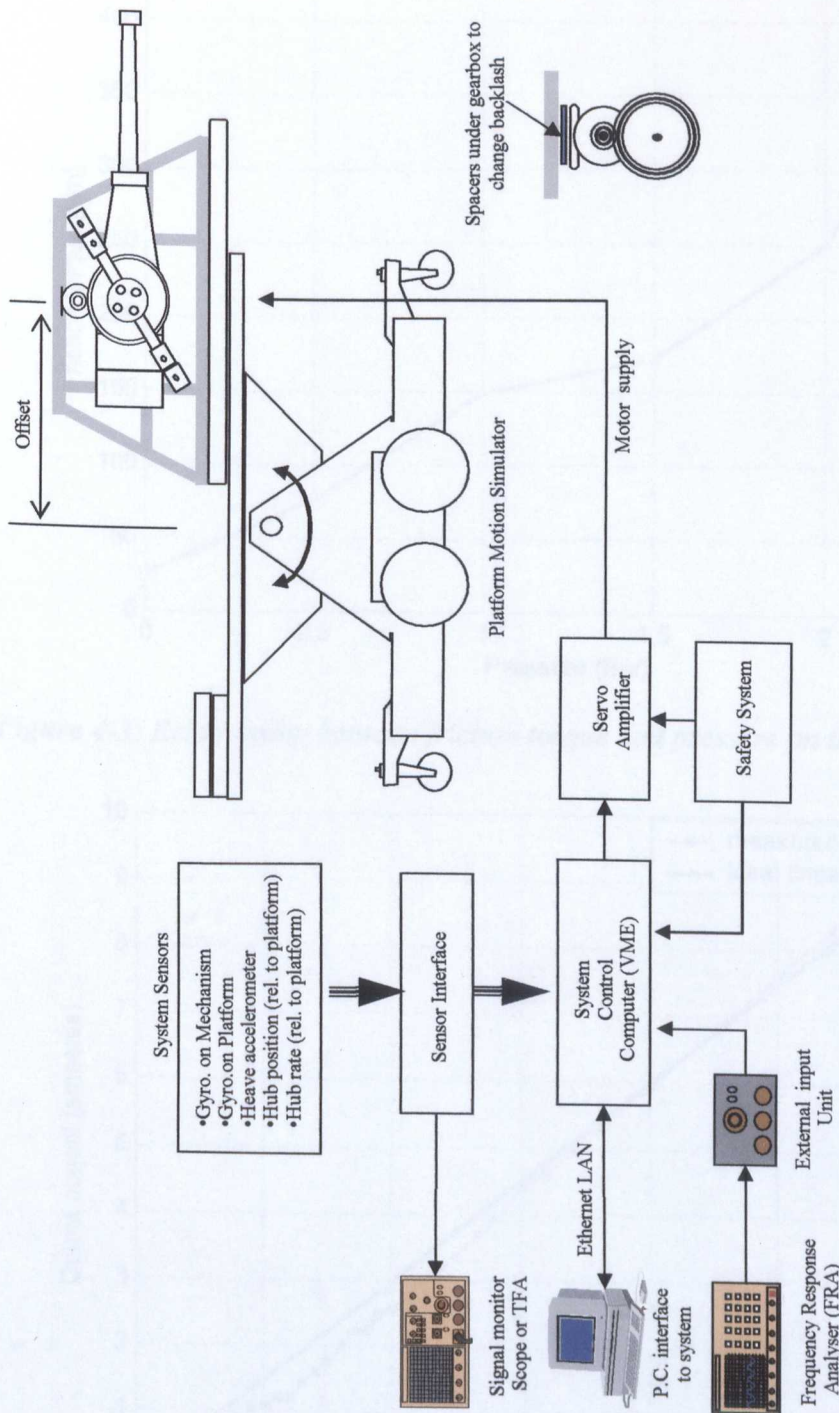


Figure 4-2: Block diagram of the rig and the platform motion simulator. Rig is mounted so that it is offset from rotational axis of PMS to simulate heave disturbance.

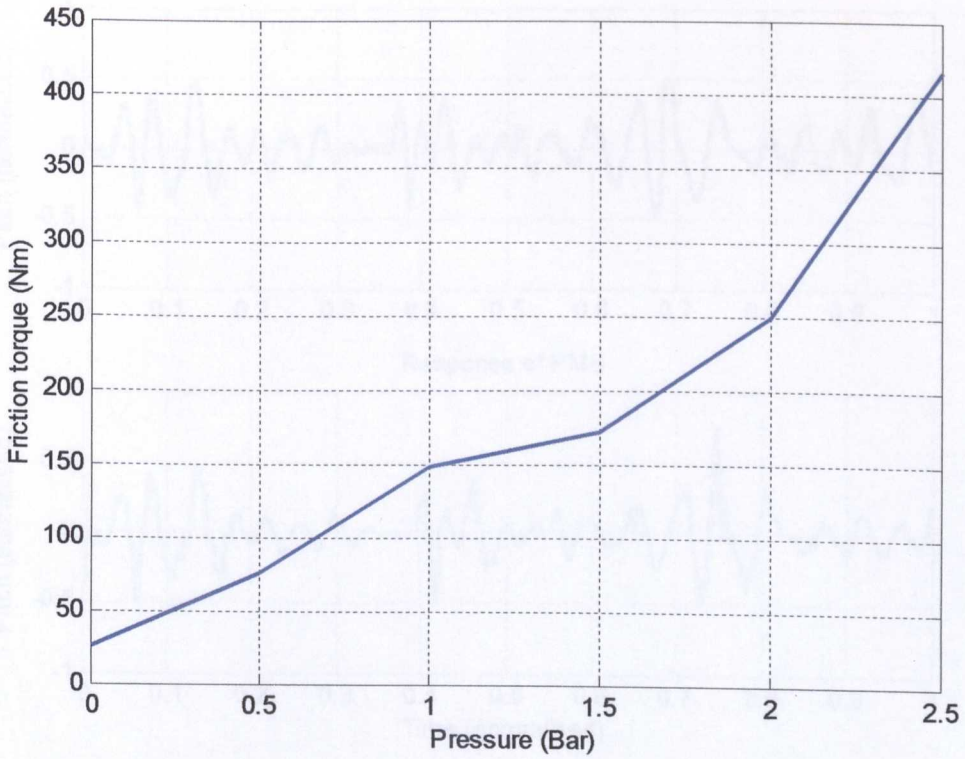


Figure 4-3: Relationship between friction torque and pressure on the disc brake

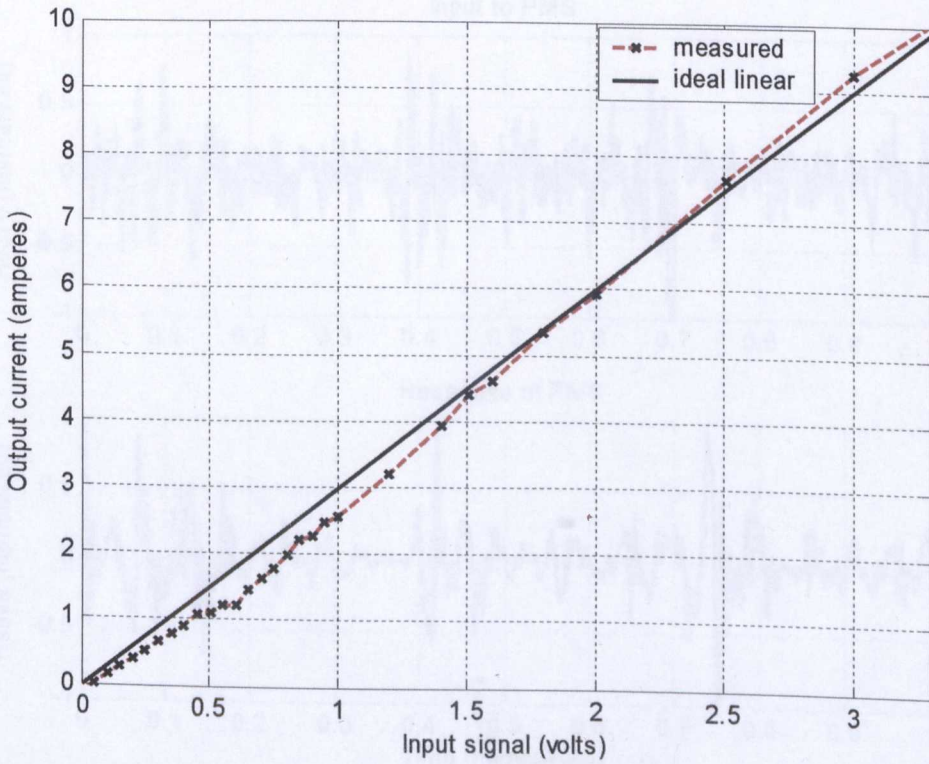


Figure 4-4: The nonlinear characteristics of the amplifier

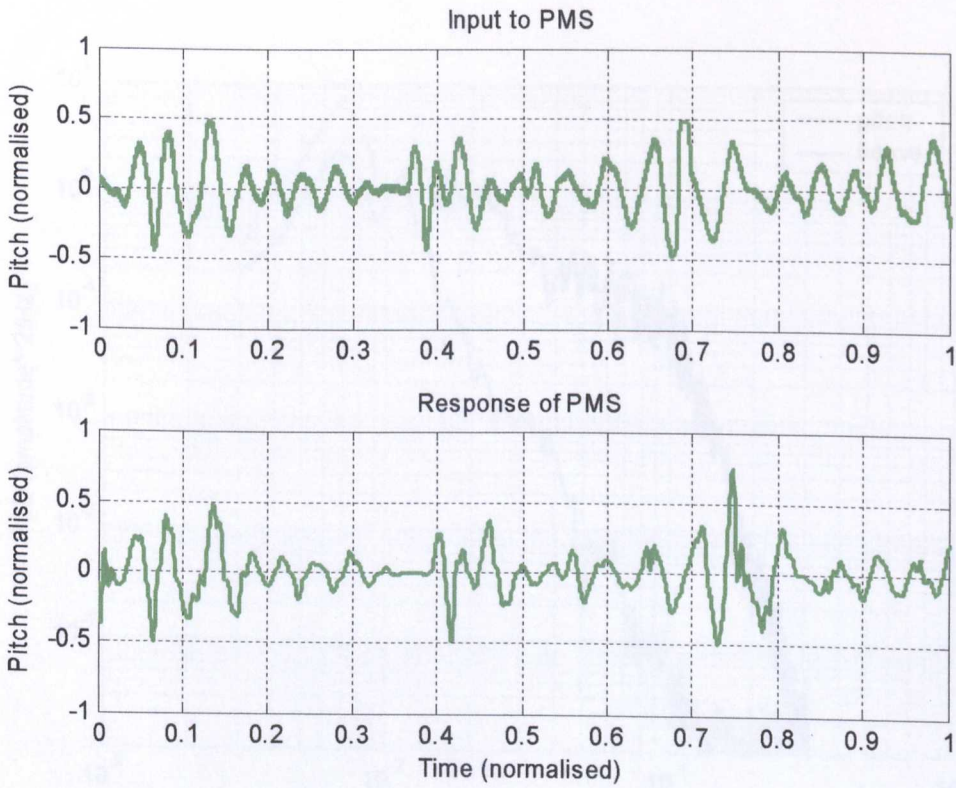


Figure 4-5: Comparison of measured pitch disturbance (top) with output of the platform motion simulator

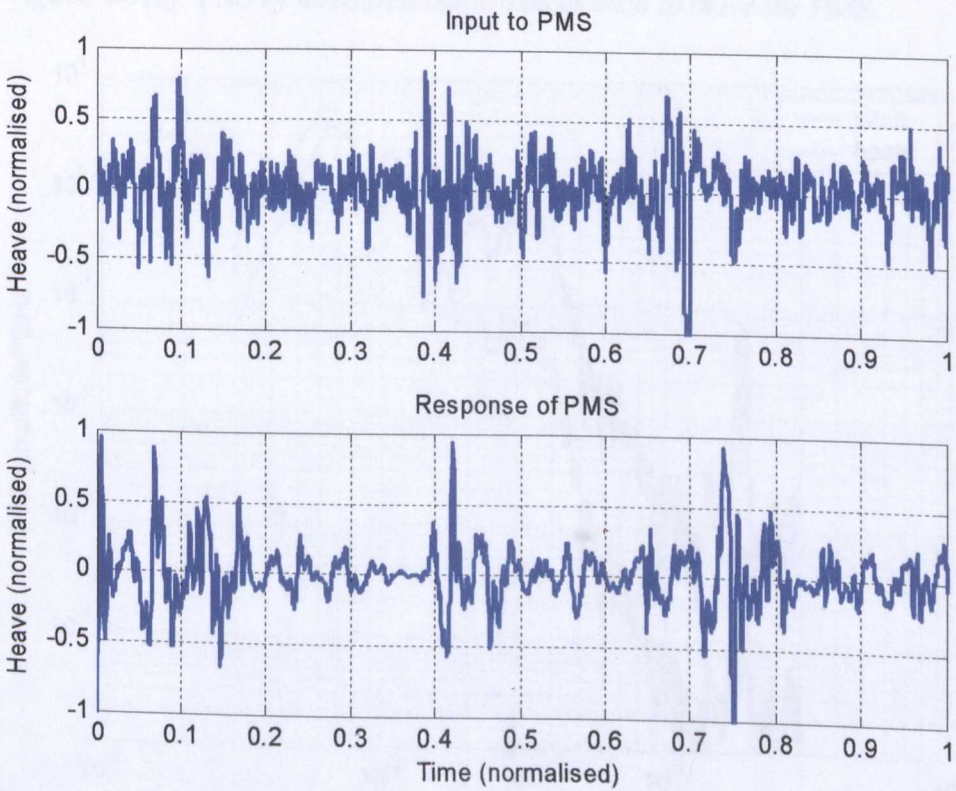


Figure 4-6: Comparison of measured heave disturbance (top) with output of the platform motion simulator

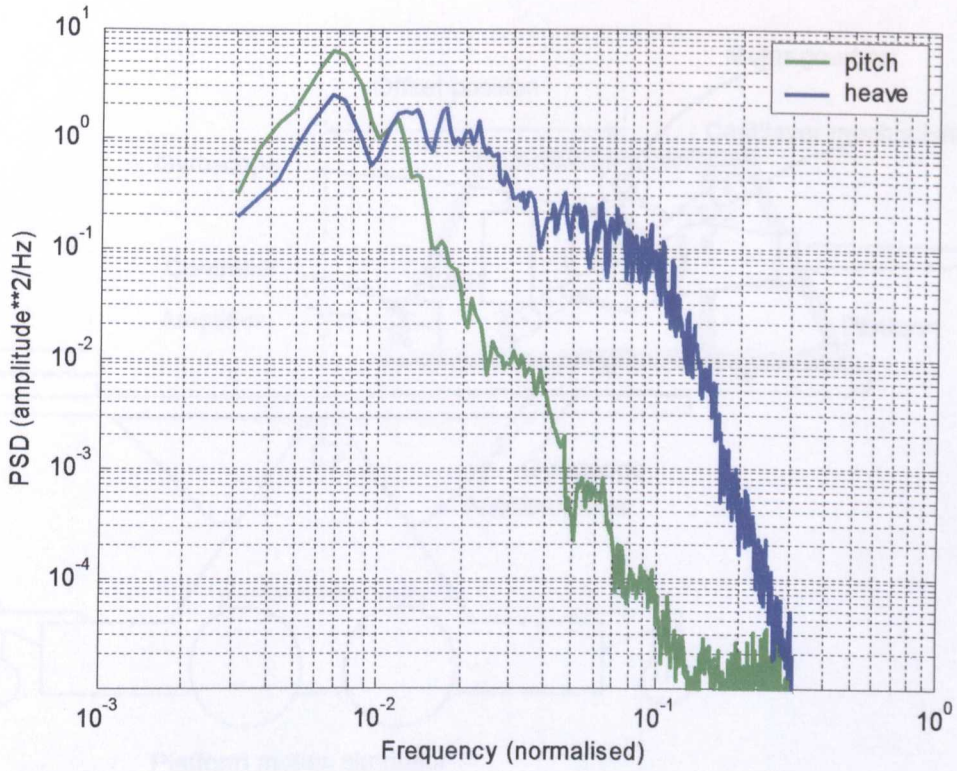


Figure 4-7(a): PSD of measured disturbances used to drive the PMS

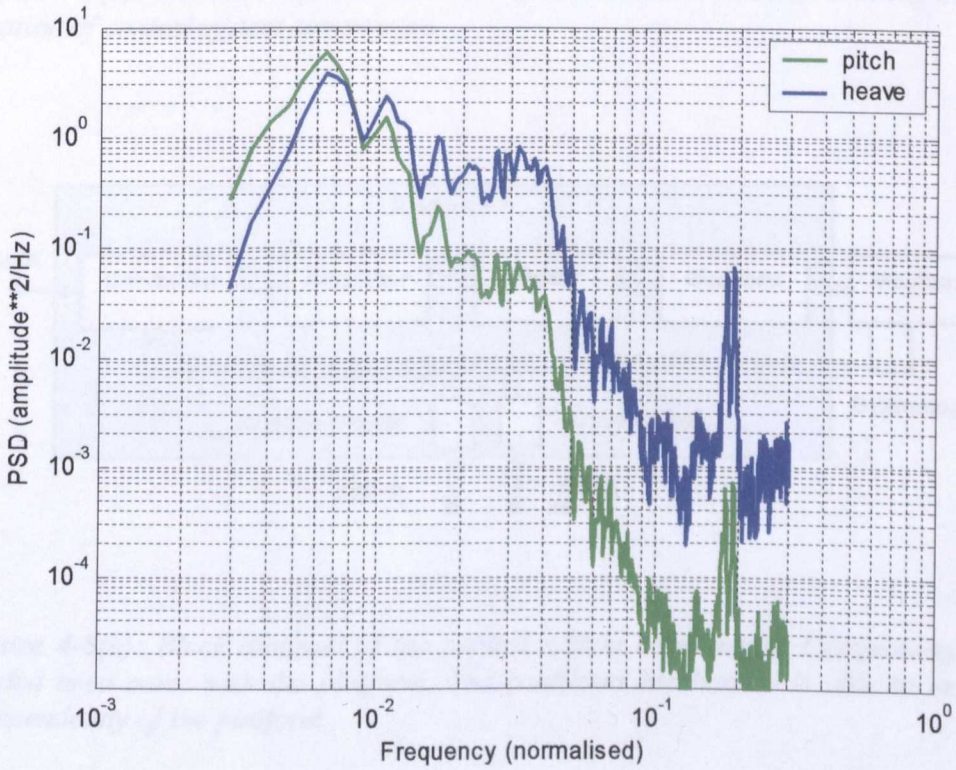


Figure 4-7(b): PSD of output of the platform motion simulator

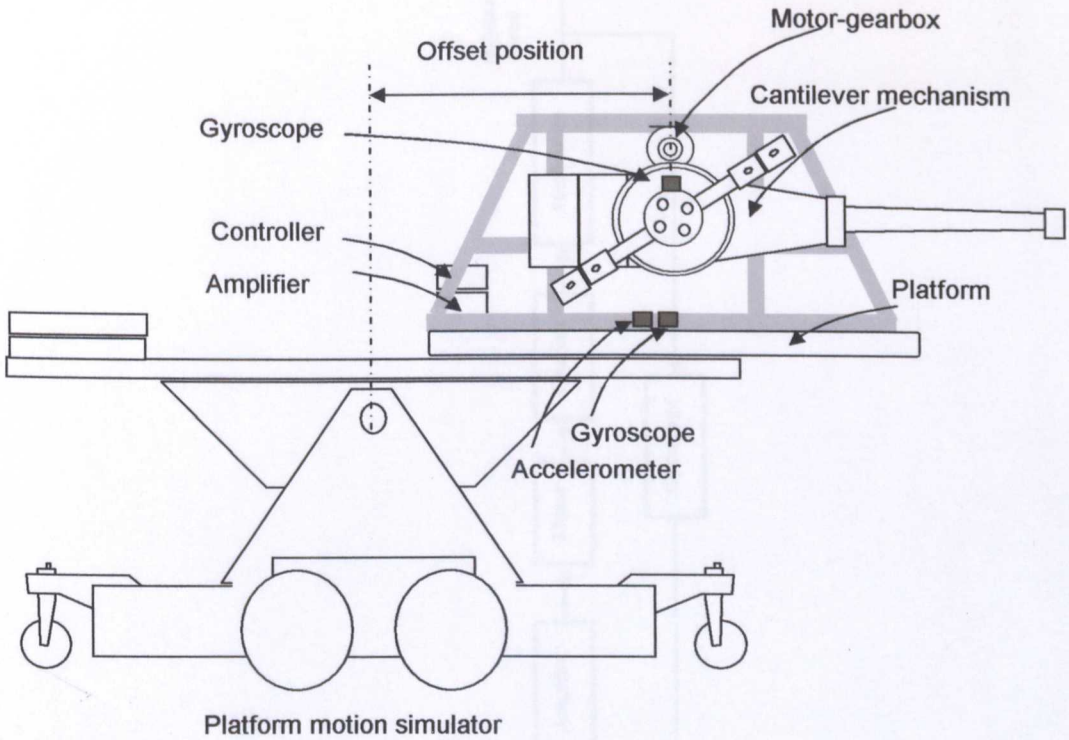


Figure 4-8(a): Schematic of cantilever mechanism mounted on PMS showing the location of control system components

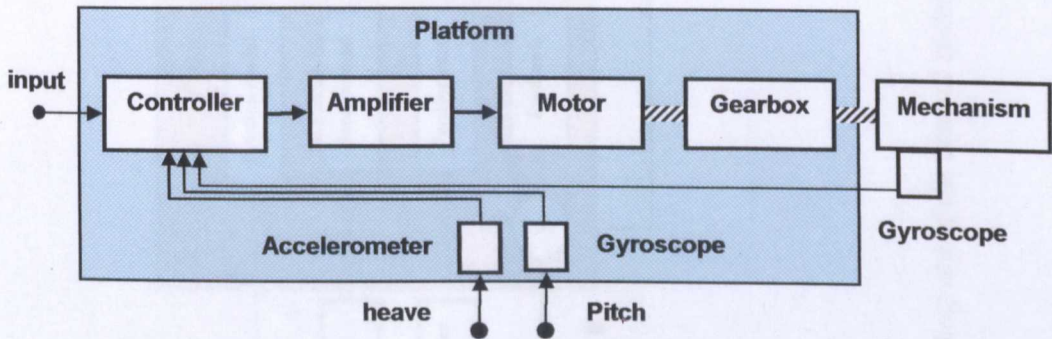


Figure 4-8(b): Block diagram of the control system components. Components in shaded area move with the platform. The cantilever mechanism is able to move independently of the platform

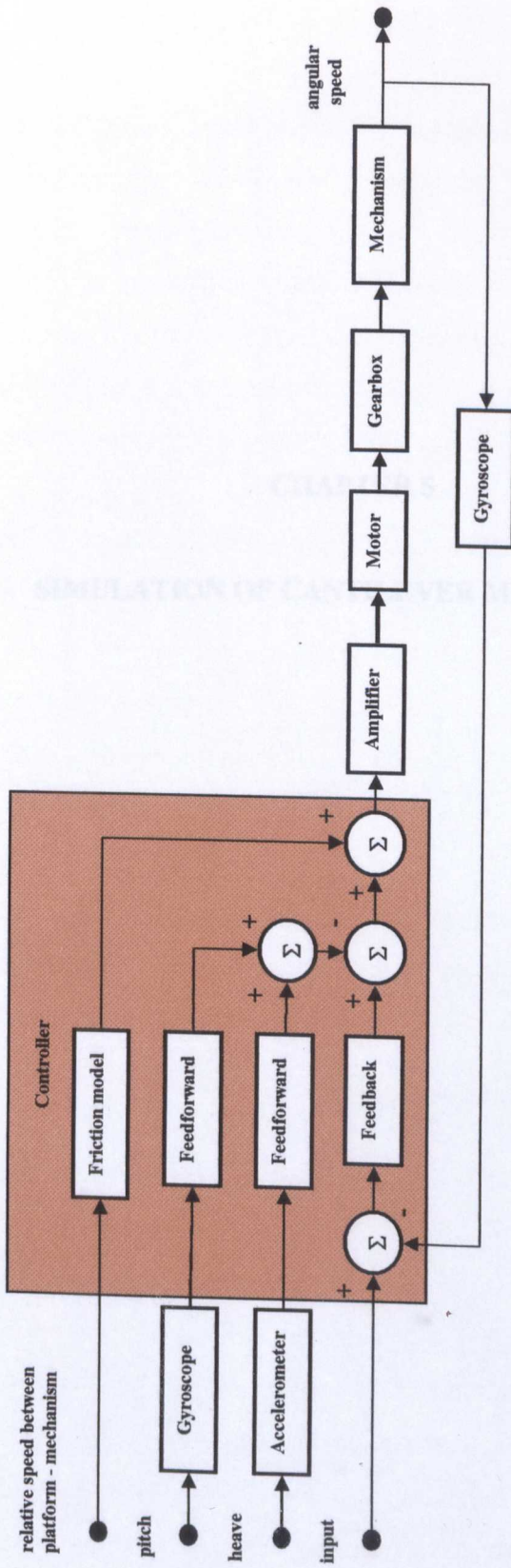


Figure 4-9: Block diagram of the control system and components.

CHAPTER 5

SIMULATION OF CANTILEVER MECHANISM

5.0 Simulation of cantilever mechanism

5.1 Introduction

This section describes simulation of the system which is developed using MATLAB and SIMULINK packages. The simulation is produced in modules which represent system components such as the motor, gearbox, amplifier, etc. This approach has the advantage that the modules can be easily updated or changed to incorporate different types of system components, improved component models, or control system algorithms. The modules are developed using transfer functions, primitive blocks provided in the package, and customized routines using M files.

The simulation incorporates the following features of interest to this research.

- Generic model of the out-of-balance servo system.
- Effects of heave and pitch external disturbances acting on the system due to motions of the platform.
- System nonlinearities such as friction, backlash and gains etc.
- Structural flexibility of the cantilever mechanism.

A model of the frequency response analyser (FRA) is also developed to enable frequency domain analysis to be carried out on the nonlinear simulation for direct comparison with measured experimental results.

5.2 Derivation of the system equations

5.2.1 Model of the cantilever mechanism

The details of a generic non-uniform flexible cantilever mechanism to be stabilised are shown in Figure 5-1. In systems which are stiff or where the tip movement is not needed the mechanism can be modelled using lump-parameter techniques. The two inertia lump-parameter model, one inertia representing the hub and a second the beam, has been used to represent the dynamics of such systems by Clephan[71], Oats *et al.*[72]. The main advantage these models provide are fast simulation run times and small system matrices which avoids the difficulties encountered in design of control

systems due to large or ill conditioned matrices. However, control systems designed using low order or truncated models can result in performance degradation caused by spillover effects Joshi and Kelkar[14], Balas[15].

To study these spillover effects both lumped and distributed parameter models are developed. The distributed parameter model is developed using the finite element (FE) technique which enables an accurate model to be obtained directly from the physical dimensions of the structure. The accuracy of the model, which can cover modes of vibrations ranging from a few Hz to several kHz, is determined by the number of elements used to approximate the structure. In general these models are too complex for control system studies and have to be simplified by using reduction and truncation techniques to cover frequencies for the first few modes of vibration. In the section 5.3.1.2 several methods for reducing the size of the system matrices are described and the use of elements with non-uniform characteristics, which may improve model accuracy, are considered.

Whether the system is modelled as a set of lumped mass, spring and damping components, finite elements or assumed modes, the essential difficulty of modelling a distributed parameter system with a finite number of coordinates remains. In this study the models are validated using modal analysis.

5.2.1.1 The distributed parameter FE model

In the FE technique a complex structure is subdivided into many simple shaped elements, which can be easily modelled. The elements are then assembled together to obtain an approximation of the whole structure. The non-uniform beam structure is divided into several cylindrical shaped elements which have constant cross-sections. The tapered sections are approximated as cylindrical elements using the average cross-sectional values.

Each element is modelled using Bernouli-Euler theory, Meriovitch[73] , Craig[74]. Figure 5-2 shows a beam element with uniform cross-section capable of resisting axial forces, bending moments about the two principal axes in the plane of its cross-section

and twisting moments about its centroidal axis. In the vertical plane only the transverse motion needs to be considered as shown in Figure 5-3. The transverse displacement within the element is approximated by considering the displacements at the two ends.

$$U(x,t) = \sum_{i=1}^4 \psi_i(t) u_i(t) \quad (5-1)$$

The shape functions $\psi_i(x)$ shown in Figure 5-3 are obtained by statically loading the beam at the two ends.

$$\psi_1(0) = 1, \quad \dot{\psi}_1(0) = \psi_1(L) = \dot{\psi}_1(L) = 0 \quad (5-1a)$$

$$\dot{\psi}_2(0) = 1, \quad \psi_2(0) = \psi_2(L) = \dot{\psi}_2(L) = 0 \quad (5-1b)$$

$$\psi_3(L) = 1, \quad \psi_3(0) = \dot{\psi}_3(L) = \dot{\psi}_3(0) = 0 \quad (5-1c)$$

$$\dot{\psi}_4(0) = 1, \quad \psi_4(0) = \dot{\psi}_4(L) = \psi_4(L) = 0 \quad (5-1d)$$

The Bernoulli-Euler stiffness, mass and generalised force matrices are obtained by substituting the shape functions into the following:

$$k_{ij} = \int_0^L EI \dot{\psi}_i \dot{\psi}_j dx \quad (5-2)$$

$$m_{ij} = \int_0^L \rho A \psi_i \psi_j dx \quad (5-3)$$

$$p_i = \int_0^L P(x,t) \psi_i dx \quad (5-4)$$

which result in the following stiffness and mass matrices.

$$k = \left(\frac{EI}{L^3} \right) \begin{bmatrix} 12 & 6L & -12 & 6L \\ & 4L^2 & -6L & 2L^2 \\ & & 12 & -6L \\ \text{symm.} & & & 4L^2 \end{bmatrix} \quad (5-5)$$

$$m = \left(\frac{\rho AL}{420} \right) \begin{bmatrix} 156 & 22L & 54 & -13L \\ & 4L^2 & 13L & -3L^2 \\ & & 156 & -22L \\ \text{symm.} & & & 4L^2 \end{bmatrix} \quad (5-6)$$

These matrices are assembled together using

$$K = \sum_{s=1}^n [A]_s^T [k]_s [A]_s \quad (5-7)$$

$$M = \sum_{s=1}^n [A]_s^T [m]_s [A]_s \quad (5-8)$$

$$P = \sum_{s=1}^n [A]_s^T [p]_s \quad (5-9)$$

and for each element $[A]_s$ takes the form

$$[A]_1 = \begin{bmatrix} 1 & 0 & 0 & 0 & 0 & 0 \\ 0 & 1 & 0 & 0 & 0 & 0 \\ 0 & 0 & 1 & 0 & 0 & 0 \\ 0 & 0 & 0 & 1 & 0 & 0 \end{bmatrix}, [A]_2 = \begin{bmatrix} 0 & 0 & 1 & 0 & 0 & 0 \\ 0 & 0 & 0 & 1 & 0 & 0 \\ 0 & 0 & 0 & 0 & 1 & 0 \\ 0 & 0 & 0 & 0 & 0 & 1 \end{bmatrix} \text{ etc.} \quad (5-10)$$

Damping

Element damping matrices can be obtained using techniques similar to those described above. Damping in solids and structures is not as well defined and it is difficult to attribute precise values for each element. Damping in structures is dominated by external influences such as joints, pivots, surface covering, friction etc. It is usual to

define the damping properties for the whole structure. One commonly used method called Rayleigh damping, Clough[75], Weaver[76], is defined by: -

$$C = a_0 M + a_1 K \quad (5-11)$$

Where a_0 and a_1 can be obtained by considering damping at two modes using

$$\zeta_n = \frac{1}{2} \left(\frac{a_0}{\omega_n} + a_1 \omega_n \right) \quad (5-12)$$

where $a_0 M$ produces damping inversely proportional to ω_n and $a_1 K$ provides damping proportional to ω_n as shown in Figure 5-4.

Rayleigh's method enables damping to be specified at two nodes, however when precise control of damping is required at several modes the following equation is used.

$$C = \sum_{n=1}^{N_c} \left(\frac{2\zeta_n \omega_n}{M_n} \right) (M\phi_n)(M\phi_n)^T \quad (5-13)$$

The above produces no damping for modes greater than N_c or when $\zeta_n = 0$. The equation can be modified so that modes beyond N_c have a higher damping than N_c as follows: -

$$C = a_1 K + \sum_{n=1}^{N_c-1} \left(\frac{2\zeta_n \omega_n}{M_n} \right) (M\phi_n)(M\phi_n)^T \quad (5-14)$$

where $a_1 = \frac{2\zeta_{N_c}}{\omega_{N_c}}$ and ϕ_n are elements of modal matrix Φ .

System matrices and state space formulations

When the elements have been assembled and damping incorporated the following equation of motion results

$$[M]\{\ddot{x}\} + [C]\{\dot{x}\} + [K]\{x\} = \{P\} \quad (5-15)$$

These equations can be readily converted into state space form

$$\dot{\mathbf{x}} = \mathbf{A}\mathbf{x} + \mathbf{B}\mathbf{u}$$

$$\mathbf{y} = \mathbf{C}\mathbf{x} + \mathbf{D}\mathbf{u}$$

$$\begin{Bmatrix} \ddot{\mathbf{x}} \\ \dot{\mathbf{x}} \end{Bmatrix} = \begin{bmatrix} M^{-1}C & -M^{-1}K \\ I & 0 \end{bmatrix} \begin{Bmatrix} \dot{\mathbf{x}} \\ \mathbf{x} \end{Bmatrix} + \begin{bmatrix} M^{-1} \\ 0 \end{bmatrix} \{\mathbf{u}\} \quad (5-16)$$

$$\mathbf{A} = \begin{bmatrix} M^{-1}C & -M^{-1}K \\ I & 0 \end{bmatrix} \quad (5-16a)$$

$$\mathbf{B} = \begin{bmatrix} M^{-1} \\ 0 \end{bmatrix} \quad (5-16b)$$

\mathbf{C} = output matrix and \mathbf{D} = feedforward matrix

5.2.2 Reduced order models

The FE method produces high order structural models which have many degrees of freedom. These high order models are unsuitable for control system work as the tools used to design the controllers fail due to ill conditioned matrices or result in large order controllers which are difficult to implement in hardware. Simulations which incorporate large order models and contain discontinuous nonlinear characteristics also require long run times. Several methods for model reduction have been developed which are described in the review by Craig *et al.*[77]. Typical examples are modal truncation [77], Guyan reduction, Guyan [78], and balanced model reduction, Moore[79]. Many of these techniques have been incorporated in MATRIX_x tool box described in reference by ISI[80] on model reduction.

5.2.2.1 Non-uniform element model

The cantilever mechanism to be controlled is very approximately a tapered beam which can be modelled using constant cross-section (uniform) beam elements. The accuracy of the model is improved by increasing the number of elements used. Unfortunately this also results in large order system matrices. The use of non-uniform beam element is considered as a means of reducing the size of system matrices while still retaining the accuracy, as illustrated in Figure 5-5.

The non-uniform beam element, illustrated in Figure 5-6, described in reference by Gallagher[81] has the following mass and stiffness properties which directly replace the linear element matrices described earlier. (Note the 2nd and 3rd row and columns have been exchanged so that the coordinates correspond to the linear element discussed earlier).

The elements of the mass matrix are given by:

$$m_{11} = \rho A_0 L \left[\frac{156}{420} + s_g \left(\frac{1}{\beta_g + 1} - \frac{1}{\beta_g + 3} + \frac{1}{\beta_g + 4} + \frac{1}{\beta_g + 5} - \frac{1}{\beta_g + 6} + \frac{1}{\beta_g + 7} \right) \right]$$

$$m_{21} = -\rho A_0 L \left[\frac{22}{420} + s_g \left(\frac{1}{\beta_g + 2} - \frac{2}{\beta_g + 3} - \frac{2}{\beta_g + 4} + \frac{8}{\beta_g + 5} - \frac{7}{\beta_g + 6} + \frac{2}{\beta_g + 7} \right) \right]$$

$$m_{31} = \rho A_0 L \left[\frac{54}{420} + s_g \left(\frac{3}{\beta_g + 3} - \frac{2}{\beta_g + 4} + \frac{9}{\beta_g + 5} + \frac{12}{\beta_g + 6} - \frac{4}{\beta_g + 7} \right) \right]$$

$$m_{41} = \rho A_0 L \left[\frac{13}{420} + s_g \left(\frac{1}{\beta_g + 3} - \frac{1}{\beta_g + 4} - \frac{3}{\beta_g + 5} + \frac{5}{\beta_g + 6} - \frac{2}{\beta_g + 7} \right) \right]$$

$$m_{22} = \rho A_0 L^3 \left[\frac{4}{420} + s_g \left(\frac{1}{\beta_g + 3} - \frac{4}{\beta_g + 4} + \frac{6}{\beta_g + 5} - \frac{4}{\beta_g + 6} + \frac{1}{\beta_g + 7} \right) \right]$$

$$m_{32} = -\rho A_0 L^2 \left[\frac{13}{420} + s_g \left(\frac{3}{\beta_g + 4} - \frac{8}{\beta_g + 5} + \frac{7}{\beta_g + 6} - \frac{2}{\beta_g + 7} \right) \right]$$

$$m_{42} = -\rho A_0 L^3 \left[\frac{3}{420} + s_g \left(\frac{1}{\beta_g + 4} - \frac{3}{\beta_g + 5} + \frac{3}{\beta_g + 6} - \frac{1}{\beta_g + 7} \right) \right]$$

$$m_{33} = \rho A_0 L \left[\frac{156}{420} + s_g \left(\frac{9}{\beta_g + 5} - \frac{12}{\beta_g + 6} + \frac{4}{\beta_g + 7} \right) \right]$$

$$m_{43} = \rho A_0 L^2 \left[\frac{22}{420} + s_g \left(\frac{3}{\beta_g + 5} - \frac{5}{\beta_g + 6} + \frac{2}{\beta_g + 7} \right) \right] \quad (5-17)$$

$$m_{44} = \rho A_0 L^3 \left[\frac{4}{420} + s_g \left(\frac{1}{\beta_g + 5} - \frac{2}{\beta_g + 6} + \frac{1}{\beta_g + 7} \right) \right]$$

and the elements of stiffness matrix are as follows:-

$$k_{11}, k_{33}, -k_{33} = \frac{12EI_0}{L^3} \left[1 + 3r_g \left(\frac{1}{\alpha_g + 1} - \frac{4}{\alpha_g + 2} + \frac{4}{\alpha_g + 3} \right) \right]$$

$$k_{21}, -k_{32} = \frac{-6EI_0}{L^2} \left[1 + 2r_g \left(\frac{2}{\alpha_g + 1} - \frac{7}{\alpha_g + 2} + \frac{6}{\alpha_g + 3} \right) \right]$$

$$k_{22} = \frac{4EI_0}{L} \left[1 + r_g \left(\frac{4}{\alpha_g + 1} - \frac{12}{\alpha_g + 2} + \frac{9}{\alpha_g + 3} \right) \right] \quad (5-18)$$

$$k_{41}, -k_{43} = \frac{-6EI_0}{L^2} \left[1 + 2r_g \left(\frac{1}{\alpha_g + 1} - \frac{5}{\alpha_g + 2} + \frac{6}{\alpha_g + 3} \right) \right]$$

$$k_{42} = \frac{2EI_0}{L} \left[1 + 2r_g \left(\frac{2}{\alpha_g + 1} - \frac{9}{\alpha_g + 2} + \frac{9}{\alpha_g + 3} \right) \right]$$

$$k_{44} = \frac{4EI_0}{L} \left[1 + r_g \left(\frac{1}{\alpha_g + 1} - \frac{6}{\alpha_g + 2} + \frac{9}{\alpha_g + 3} \right) \right]$$

From reference Gallagher [81] the coefficients $r_g, s_g, \alpha_g, \beta_g$ are defined by the following:-

$$r_g = \left(\frac{I_d}{I_o} - 1 \right), \alpha_g = \log \left(\frac{I_c - I_o}{I_d - I_o} \right) \div \log(0.5) \quad (5-19)$$

$$s_g = \left(\frac{A_d}{A_o} - 1 \right), \beta_g = \log \left(\frac{A_c - A_o}{A_d - A_o} \right) \div \log(0.5) \quad (5-20)$$

The subscripts refer to the following:-

- c properties at the center of the element
- d properties at furthest (deep) end of the element
- o properties at the near end of the element

5.2.3 Lump-parameter model

The lump-parameter model of the mechanics of the cantilever mechanism is shown in Figure 5-7. In systems which are stiff or where the tip position is not needed the structure can be modelled as a two inertia system; one inertia representing the hub and a second the beam which are linked together using lumped stiffness and damping. The equations of motion for an out-of-balance system, referring to Figure 5-8a, are as follows: -

Beam

$$J_b \ddot{\theta}_b = (\theta_h - \theta_b) K_h + (\dot{\theta}_h - \dot{\theta}_b) D_h \quad (5-21)$$

Hub

$$J_h \ddot{\theta}_h = (\theta_{gb} - \theta_h) K_{gb} + (\dot{\theta}_{gb} - \dot{\theta}_h) D_{gb} - (\theta_h - \theta_b) K_h - (\dot{\theta}_h - \dot{\theta}_b) D_h - F_p (\dot{\theta}_h - \dot{\theta}_p) \quad (5-22)$$

5.2.4 The gearbox model

Although, it is possible to produce a detailed model of the gearbox, for control systems work it is usually unnecessary. In this simulation a two gear model is used which incorporates the dominant features associated with a gearbox such as inertia, stiffness, friction, and backlash. The model is illustrated in Figure 5-8b and the following equations describe its operation.

Equations at the motor end of the gearbox

$$T_m = J_m \ddot{\theta}_m + F_m (\dot{\theta}_m) + T_1 \quad (5-23)$$

Equations at gearbox output

$$T_2 = (\theta_{gb} - \theta_h) K_{gb} + (\dot{\theta}_{gb} - \dot{\theta}_h) D_{gb} + T_{oob} \quad (5-24)$$

T_{oob} includes static torque due to gravitational acceleration and due to acceleration of the platform.

The external motion of the platform modifies the gearbox output as follows

$$T_2 = (\theta_{gb} + \theta_p - \theta_h) K_{gb} + (\dot{\theta}_{gb} + \dot{\theta}_p - \dot{\theta}_h) D_{gb} + T_{oob} \quad (5-25)$$

The motor side and the gearbox outputs are related by

$$\theta_m = N \theta_{gb} \quad (5-26)$$

$$T_2 = N T_1 \quad (5-27)$$

The total backlash and the stiffness in the servo drive system are incorporated at the output of the gearbox. The backlash characteristic used in the model is illustrated in Figure 5-9. The gearbox inertia is modelled at the input of the gearbox and combined with the motor inertia.

5.2.5 The servo motor model

In its simplest form the servo motor can be modelled as a simple gain which converts current to a torque. However, this model does not take into account the effects of armature or stator resistance, inductance and back electro motive force (EMF) which add damping to the system and also determine the maximum speed of the motor under no-load conditions. Figure 5-10 shows a schematic of the motor.

The voltage in the armature is given by

$$V_{O_a} = R_a i_a + L_a \frac{di_a}{dt} + V_{O_g} \quad (5-28)$$

With constant flux the voltage generated by the armature moving through the flux is given by

$$V_{O_g} = K_e \dot{\theta}_m \quad (5-29)$$

The torque generated by the motor is given by

$$T_m = K_t i_a \quad (5-30)$$

5.2.6 The servo amplifier model

The servo amplifier is a complex system which converts the input signal to three phase output. The amplifier is a switching amplifier whose output power is controlled by varying the pulse-width ratio, Anon [82], Kuo[83]. The switching frequency of these amplifiers can be as high as 100kHz. Because of the high switching rates accurate models of the amplifiers require small integration time steps which results in long simulation run times. To overcome this difficulty the amplifier is modelled as an equivalent linear amplifier. Linear servo amplifiers use a combination of current and voltage feedback for stable operation as shown in Figure 5-11. The gain of an ideal amplifier is constant and independent of frequency, however most practical amplifiers have a limited band width typically between 50 and 100 Hz.

$$V_{O_a} = \frac{K_v}{(\tau_a s + 1)} (V_{O_i} - i_a K_{ifb}) \quad (5-31)$$

The model of the amplifier can be further simplified as a simple gain which converts input voltage to current output. This model assumes that the amplifier has high bandwidth and the current feedback from the motor is dominant. When this representation of amplifier is used the servo motor simplifies to a simple gain term which converts current to torque as described earlier.

5.2.7 Friction models

Friction is difficult to model accurately as it is effected by many factors such as relative velocity between the surfaces, lubrication, temperature, normal force, rate at which tangential force is applied, dwell time etc. The survey in chapter 2 noted that several different types of friction models have been developed which range from detailed seven parameter model developed by Armstrong-Helouvry *et al.* [9],[10], to a simple classical model. Several authors have noted that the classical model is not adequate for control systems work and that the seven parameter model is too complex requiring parameter measurements which are difficult to obtain. To overcome these difficulties alternative models which capture of friction characteristics while being simple to use have been proposed.

Friction models are broadly classified as either static or dynamic models. Static friction models simply map friction force as a function of velocity and normal load. In addition to forces due to velocity, dynamic friction models account for pre-sliding displacements and hysteresis in friction force due to varying velocity which occur in the low velocity and pre-sliding regions.

A toolbox of friction models is developed in this thesis to investigate how accurately these models represent the friction in the test system and to determine their effect on system stabilization. The salient features of each are summarised below while details can be found in the references.

5.2.7.1 Static models

Classical model [19]

The elementary representation of the classical friction model as a function of relative velocity between the contacting surfaces is shown in Figure 5-12(a). When the relative velocity is zero the friction force is indeterminate and can take any value between the Coulomb friction limits. This simple model which does not include viscous friction, stiction or the Stribeck effect is represented by: -

$$f = f_c \operatorname{sgn}(V) \quad (5-32)$$

Figure 5-12(b) shows a model which includes both Coulomb and viscous friction, a force proportional to velocity.

$$f = f_c \operatorname{sgn}(V) + f_v V \quad (5-33)$$

A model with stiction is illustrated in Figure 5-12(c). Stiction is static force which occurs when two surfaces are at rest. The Stiction force is larger than the Coulomb friction which disappears when the surfaces start to move. The following equations describe the stiction forces which can be added to the above equations.

$$f = f_e \quad \text{if } V = 0 \text{ and } |f_e| < f_s$$

or

$$(5-34)$$

$$f = f_s \operatorname{sgn}(f_e) \quad \text{if } V = 0 \text{ and } |f_e| \geq f_s$$

These effects can be combined in different ways and the resulting models are all referred to as the classical model.

Tustin model [24]

Tustin developed a model which describes the friction force at velocities close to zero.

Experimental studies have shown that the model can predict friction forces with an accuracy of 90%.

$$f = f_c \operatorname{sgn}(V) + (f_s - f_c)e^{-(V/V_s)} + f_v V \quad (5-35)$$

A more general form of the model is referred to as the exponential model.

Exponential model [43]

$$f = f_c \operatorname{sgn}(V) + (f_s - f_c)e^{-(V/V_s)^\alpha} + f_v V \quad (5-36)$$

When $\alpha = 2$ the model is known as Gaussian exponential. Other models similar to the above are the polynomial model and the Lorentzian models. These models are described in reference Armstrong-Helouvry [9],[10].

Karnopp model [25]

In the representation of friction shown in Figure 5-12 at zero velocity friction is multi-valued and can assume any value between the Coulomb or stiction limits. One approach used to overcome this difficulty is to use a large gain at zero velocity. This model has two limitations, firstly the model cannot predict stick-slip motions and secondly the steep gradient can result in very short integration time steps and numerical instability. Karnopp developed a model which overcomes the anomaly at zero velocity. In Karnopp's model, illustrated in figure 5-13, a small region $\pm D_v$ at zero velocity is introduced to ensure the system 'sticks' such that the friction force equals the driving or applied force. When the driving force exceeds the stiction force the body accelerates and moves beyond D_v . Other friction characteristics which depend on velocity then apply to the system.

Although, the model is very efficient in terms of computing time the primary drawback is that its complexity changes with the complexity of the system being modelled. Karnopp demonstrates the increase in complexity of the friction model by considering two bodies which move relative to each other over a fixed surface. For such systems the

friction model can not be incorporated as a modular element and a new model has to be developed for each application.

5.2.7.2 Dynamic models

Dahl model [20],[21].

Dahl developed a solid friction model following experimental work on ball bearings. From further experimental work using servo systems which used ball bearings he was able to show that bearing friction and solid friction have similar characteristics. Although, Dahl describes two models in reference [20] the second model, illustrated in Figure 5-14, which is easier to use is favoured by most studies. Dahl uses the fact that friction stress is a function of displacement and can be differentiated with respect to time.

$$\frac{df}{dt} = \frac{df}{dx} * \frac{dx}{dt} \quad (5-37)$$

Dahl considers characteristics for the function $\frac{df}{dx}$ and from experimental work has determined that a square law is the most suitable function.

$$\frac{df}{dx} = \gamma(f - f_0)^2 \quad (5-38)$$

where f_0 is the peak sliding friction and γ is the effective spring rate. In a second paper [21] Dahl provides a more general solution to this model.

$$\frac{df}{dx} = \sigma \left| 1 - \frac{f}{f_c} \operatorname{sgn}\left(\frac{dx}{dt}\right) \right|^i S_d \quad (5-39)$$

Where i is the solid friction model coefficient

Dahl's model captures the forces of Coulomb friction but it does not capture stiction or the velocity related Stribeck effect shown in Figure 5-12(d). Models similar to Dahl's have been used in adaptive control applications and one such model is described below which was developed by Walrath.

Walrath model [17]

The Walrath model developed for an airborne tracking application is represented by the following equation:

$$T_f(t) + \tau \frac{dT_f(t)}{dt} = T_c(\text{sign}\dot{\lambda}) \quad (5-40)$$

$\text{sign}\dot{\lambda} = (+1 \text{ or } -1)$ the relative gimbal velocity

From experimental work it is found that τ is related to acceleration by a linear relationship as follows:-

$$\frac{1}{\tau_{opt}} = 1 + 0.37\ddot{\lambda}_{RMS} \quad (5-41)$$

Walrath uses this model as a feedforward element in the controller to improve the stabilisation performance of the system.

Haessig and Friedland model [22]

Haessig and Friedland, who use the work of Dahl and Karnopp, present two models referred to as the bristle model and the reset integrator model. The bristle model attempts to model the distortion of surface asperities which causes the 'sticking' phenomenon at zero velocity. The surface asperities, which are similar to mountain peaks and troughs, are modelled as bristles which bend and distort. The model is numerically very inefficient and they propose the reset integrator model which does not capture details of the sticking phenomenon but exhibits behavior similar to the Karnopp's model. Although, the reset integrator model is not as efficient as the Karnopp's model it has the advantage that the friction model can be readily incorporated into simulations regardless of the complexity of system. A block diagram of the reset

integrator model is shown in Figure 5-15. Using the nomenclature provided in reference by Olsson et al.[84]

In the reset integrator model the friction force is given by:

$$f = (1 + a(z)) \sigma_0(V)z + \sigma_1 \frac{dz}{dt} \quad (5-42)$$

and

$$\frac{dz}{dt} = 0, \text{ if } (V > 0 \text{ and } z \geq z_0), \quad (5-43)$$

or $(V < 0 \text{ and } z \leq -z_0)$,

otherwise it is V .

$\sigma_1 \frac{dz}{dt}$ is a damping term which is active only when sticking occurs

and stiction is given by the term

$$a(z) = a \text{ if } |z| < z_0$$

or 0 for other values

Sticking occurs when $|z| < z_0$ and the force is a function of z . The force when slipping occurs is given by the function $\sigma_0(V)$.

LuGre model [23]

The LuGre model described by Canudas de Wit *et al* [23] is a dynamic friction model which is related to the bristle model described by Haessig *et al*. [22]. The model captures all the static and dynamic properties of friction likely to be of interest in precision control systems applications. The model describes steady state characteristics, hysteresis due to friction lag, spring like behaviour in the pre-sliding region and the breakaway force which is dependent on rate of the applied force. Using the same nomenclature as above.

$$f = \sigma_0 z + \sigma_1 \dot{z} + \sigma_2 \dot{x} \quad (5-44)$$

$$\dot{z} = \dot{x} - \alpha(\dot{x}) |\dot{x}| z \quad (5-45)$$

z is the unmeasurable average deflection of the bristles and $\sigma_0, \sigma_1, \sigma_2$, are coefficients of forces due to stiffness of the bristles, damping in the bristles and viscous friction due to velocity. The Stribeck effect is modelled using the following function for $\alpha(\dot{x})$

$$\alpha(\dot{x}) = \frac{\sigma_0}{f_c + (f_s - f_c) e^{-(\dot{x}/\dot{x}_s)^2}} \quad (5-46)$$

As before f_c is Coulomb friction, f_s is stiction and \dot{x}_s is the Stribeck velocity.

5.2.8 Transducer models

The gyroscopes

The electromechanical gyroscopes used to measure the hub and platform motions are modelled as damped second order systems.

$$\frac{\text{output voltage}}{\text{input rate}} = K_{gy} \frac{\omega_{gy}^2}{s^2 + 2\zeta_{gy}\omega_{gy}s + \omega_{gy}^2} \quad (5-47)$$

The accelerometers

The solid-state accelerometers used in the system also have a second order damped response and are modelled using the following transfer function

$$\frac{\text{output voltage}}{\text{input acceleration}} = K_{ac} \frac{\omega_{ac}^2}{s^2 + 2\zeta_{ac}\omega_{ac}s + \omega_{ac}^2} \quad (5-48)$$

5.2.9 The frequency response analyser model

The performance of control systems is often measured and analysed in the frequency domain using classical techniques such as Bode, Nyquist, Nichols charts. The experimental measurements are carried out using frequency response analysers (FRA) such as a Solartron 1250 or Hewlett-Packard 3562A dynamic signal analyser.

Most CACSD packages provide facilities for frequency response analysis. However, the algorithm produced by Laub[85], used in these packages requires that the system is linear. A nonlinear system can be linearised about an operating point using the facilities provided in the packages. These linearising algorithms are based on Taylor theorem. For systems which have continuous nonlinearities the results can be quite accurate. However, when discontinuous nonlinearities are present the algorithms fail or produce poor results when compared to those measured in the laboratory. In some instances, where a single discontinuous nonlinearity is present, describing function approximations can be used to obtain approximate responses, Dholiwar[86].

A model of a frequency response analyser has been developed which enables direct comparison of measured results with outputs generated by the simulations. The basic operation of the analyser is described below while the theoretical details can be found in the references by Wellstead[87] and Luksic[88]. Referring to Figure 5-16 the following equations describe the operation of the FRA.

$$u_{fra}(t) = U_{fra} \sin \omega t \quad (5-49)$$

$$y_{fra}(t) = Y_{fra} \sin(\omega t + \phi) \quad (5-50)$$

where $Y_{fra} = U_{fra} |G(j\omega)|$ and $\phi = \angle G(j\omega)$

Then the sine channel output $R(T)$ is given by

$$R(T) = \frac{U_{fra}}{T} |G(j\omega)| \int_0^T \sin \omega t \cdot \sin(\omega t + \phi) dt \quad (5-51)$$

$$= \frac{U_{fra}}{T} |G(j\omega)| \left[\cos \phi \left(\frac{T}{2} - \frac{\sin 2\omega T}{4\omega} \right) - \sin \phi \left(\frac{\cos 2\omega T}{4\omega} - \frac{1}{4\omega} \right) \right] \quad (5-52)$$

so when $T = \frac{N_{cy}\pi}{\omega}$ $N_{cy} = 1, 2, 4, \dots$ the sine channel output is

$$R\left(\frac{N_{cy}\pi}{\omega}\right) = \frac{U_{fra}}{2} |G(j\omega)| \cos \phi \quad (5-53)$$

similarly the cosine channel output $I(T)$ is given by

$$I(T) = \frac{U_{fra}}{T} |G(j\omega)| \int_0^T \cos \omega t \sin(\omega t + \phi) dt \quad (5-54)$$

which can be evaluated for $T = \frac{N_{cy}\pi}{\omega}$ as

$$I\left(\frac{N_{cy}\pi}{\omega}\right) = \frac{U_{fra}}{2} |G(j\omega)| \sin \phi \quad (5-55)$$

The gain and phase are then obtained using

$$\text{Gain} = \sqrt{(R^2 + I^2)} \quad (5-56)$$

$$\text{and using } Y_{fra} = U_{fra} |G(j\omega)| \quad (5-57)$$

$$\text{Gain} = \frac{Y_{fra}}{2} \sqrt{(\cos^2 \phi + \sin^2 \phi)} \quad (5-58)$$

$$|G(j\omega)| = \frac{Y_{fra}}{U_{fra}} \quad (5-59)$$

$$\text{dB} = 20 * \log_{10} \left(\frac{2 * \text{Gain}}{U_{fra}} \right) \quad (5-60)$$

$$\text{Phase} = \text{Arc tan} \left(\frac{I}{R} \right) \quad (5-61)$$

The above equations form the core of the frequency response analyser called TFA_SINGLE. As frequency responses take a long time to generate, a second program, named TFA_MAP, is developed which enables the responses over a range of frequencies and amplitudes to be produced by running the simulations in batch mode.

5.3 The SIMULINK model

Figure 5-17 shows the model of the complete system. The model consists of three super blocks which represent the controller, amplifier and motor, and mechanics which comprises the mechanics of the motor, the gearbox and the cantilever mechanism. The three main inputs to the mechanics block are the amplifier and motor super block output, pitch disturbance (rad/s) and heave acceleration (m/s/s). The tip and hub motions, and the motor speed are the primary outputs. The model shows the transducer models and the nonlinear compensation block. The three inputs into the system, shown on the left side, are the demand input (sinusoidal, step and triangular wave inputs), the heave and pitch disturbances. Several outputs are incorporated in the simulations which enable parameters to be monitored for system validation and performance measurement, typical examples being the controller outputs. Brief details of each super block are described in the following subsections.

The flexible beam

Models of the flexible structure are illustrated in Figure 5-18. The state space model has two inputs and several outputs which provide the rate and position at the boundary of each element. The position and rate outputs at hub and the tip are saved for further processing. The second diagram in the Figure 18b shows the differential equation implementation.

The amplifier and motor

The model of the amplifier and the electrical components of the motor are illustrated in Figure 5-19. The amplifier has three input signals, the first is the demand signal and two feedback signals, speed and current, from the motor. The output of the amplifier feeds into the motor armature which produces current. The figure also shows a simple linear amplifier model and a nonlinear gain amplifier (using measured data) which converts the input voltage to a current output. The input to the amplifier is provided by the controller illustrated in Figure 5-20. The design of the three transfer functions in the controller are described in chapter 6.

The motor and gearbox model

The model incorporates several friction models which are shown in the detailed motor and gearbox block, Figure 5-21. The models can be selected by connecting their output to the motor torque summing junction, identified as motor_friction variable. The Karnopp model cannot be connected directly into the system and an alternate model of the motor with Karnopp friction has been included.

The friction models

The friction models are shown in Figures 5-21 to 5-26. Each model follows the equations described in section 5.2.7.

- Tustin model (Figure 5-22)
- Karnopp model (Figure 5-23)
- Dahl model (Figure 5-24)
- Haessig and Friedland reset integrator model (Figure 5-25)
- LuGre model (Figure 5-26)

The transducer models.

The gyroscopes and the accelerometers used are modelled using transfer function block provided in SIMULINK.

FIGURES CHAPTER 5

SIMULATION OF CANTILEVER MECHANISM

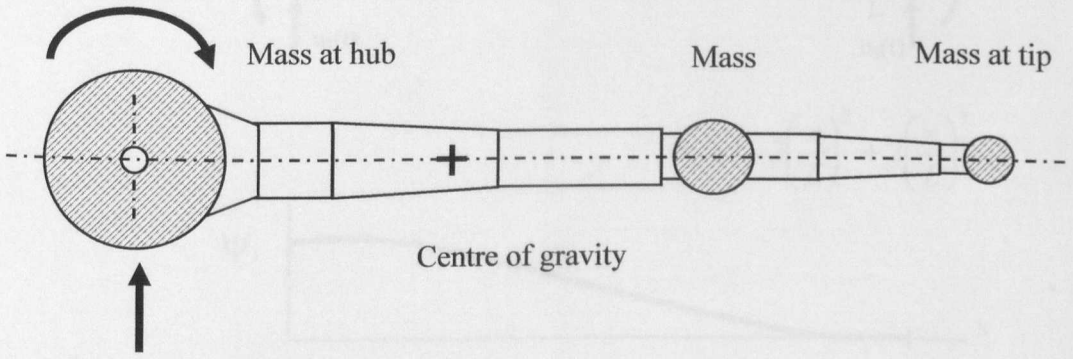


Figure 5-1: Schematic of the cantilever mechanism showing the hub and flexible beam

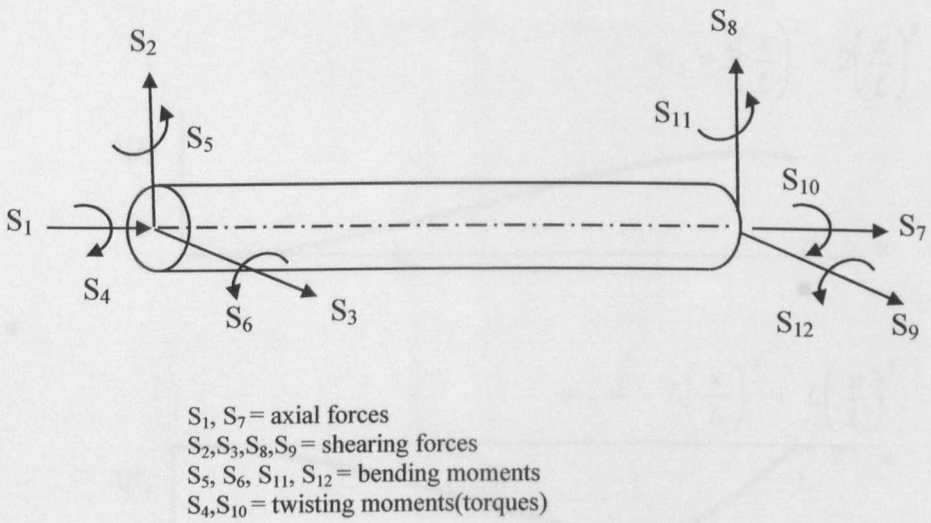
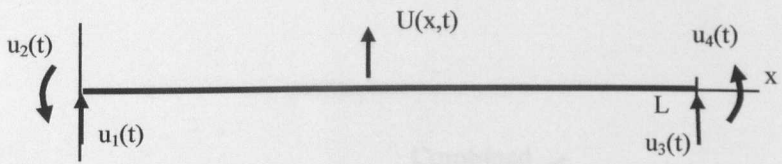
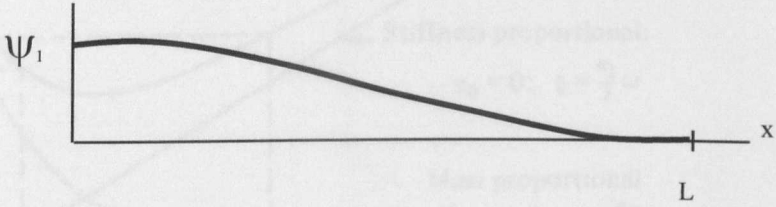


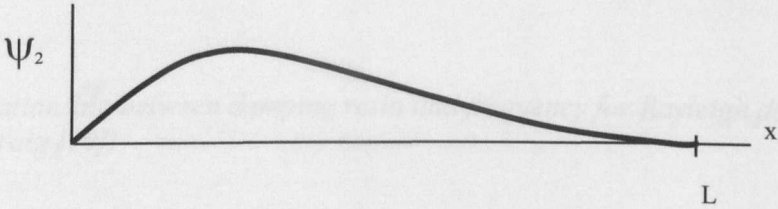
Figure 5-2: A beam element showing forces and moments



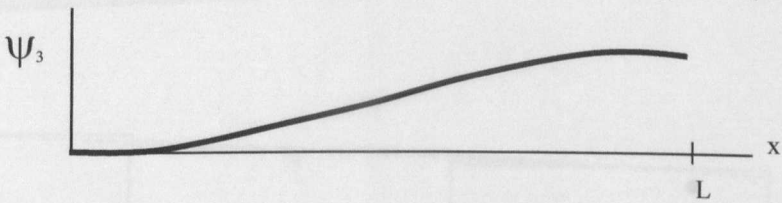
$$\psi_1 = 1 - 3\left(\frac{x}{L}\right)^2 + 2\left(\frac{x}{L}\right)^3$$



$$\psi_2 = x - 2L\left(\frac{x}{L}\right)^2 + L\left(\frac{x}{L}\right)^3$$



$$\psi_3 = 3\left(\frac{x}{L}\right)^2 - 2\left(\frac{x}{L}\right)^3$$



$$\psi_4 = -L\left(\frac{x}{L}\right)^2 + L\left(\frac{x}{L}\right)^3$$

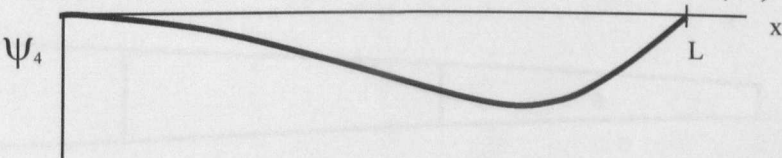


Figure 5-3: Uniform beam in transverse motion and the shape functions

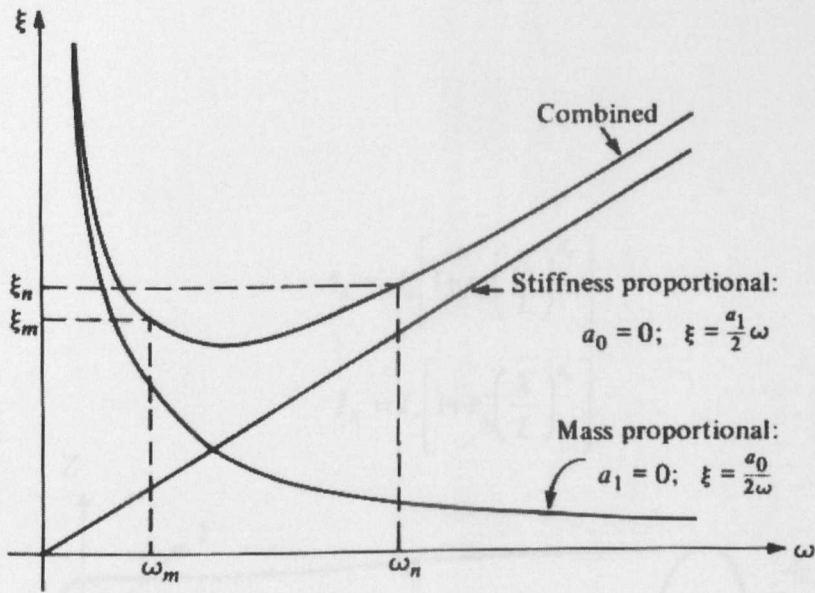


Figure 5-4: Relationship between damping ratio and frequency for Rayleigh damping (Clough [89], Craig [90])

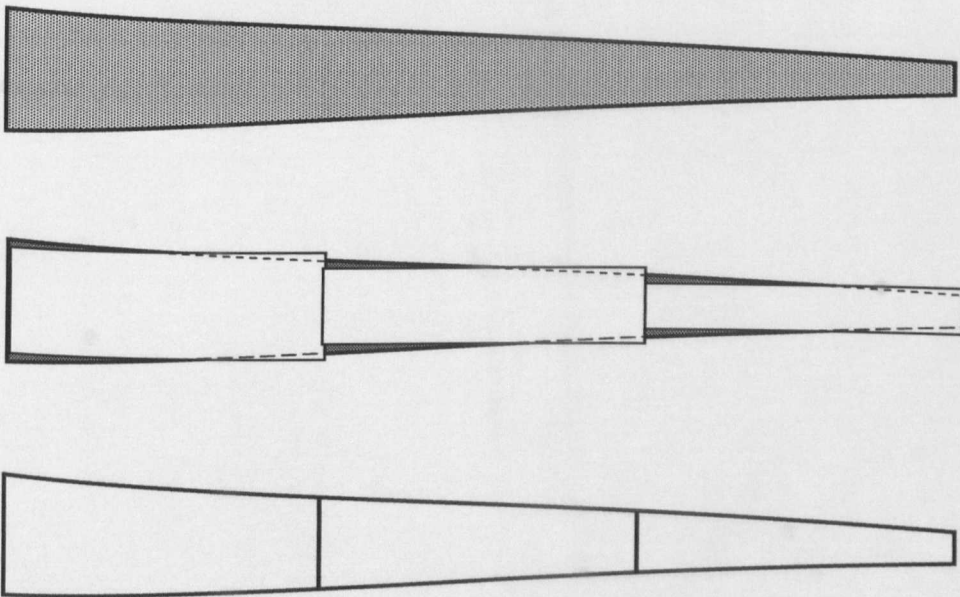


Figure 5-5: Tapered structure to be modelled (top), using uniform elements (centre), using non-uniform elements (bottom)

$$A_X = A_o \left[1 + s_g \left(\frac{X}{L} \right)^{\beta_g} \right]$$

$$I_X = I_o \left[1 + r_g \left(\frac{X}{L} \right)^{\alpha_g} \right]$$

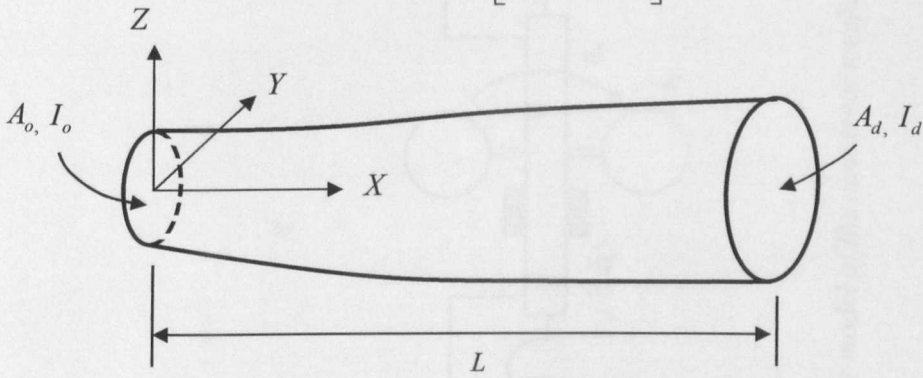


Figure 5-6: Non-uniform beam element (Gallagher [95])

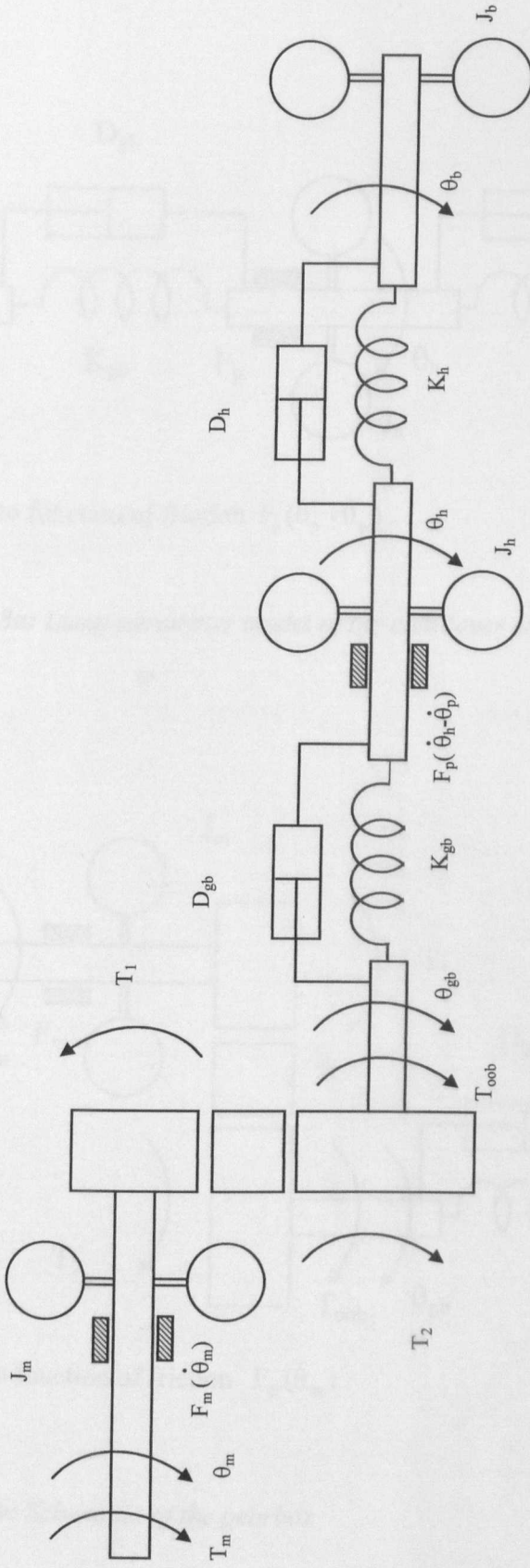
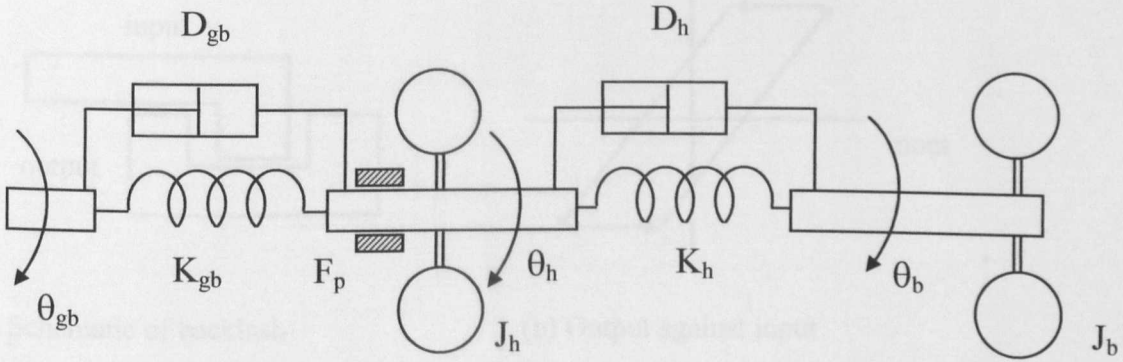
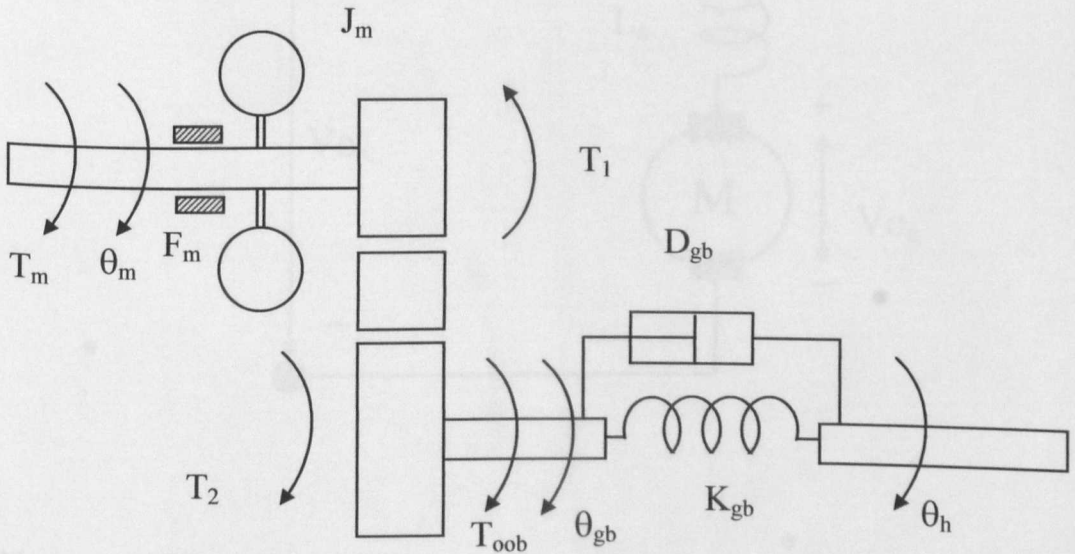


Figure 5-7: Lump parameter model of the cantilever mechanism



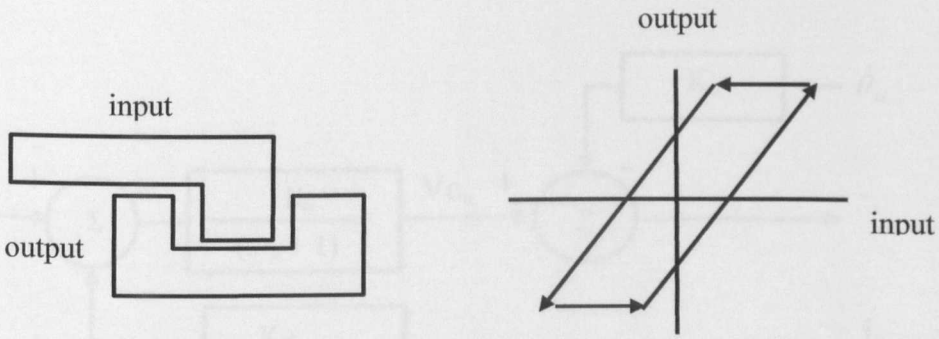
F_p refers to function of friction $F_p(\dot{\theta}_p - \dot{\theta}_h)$

Figure 5-8a: Lump parameter model of the cantilever structure



F_m refers to function of friction $F_m(\dot{\theta}_m)$

Figure 5-8b: Schematic of the gearbox



(a) Schematic of backlash

(b) Output against input

Figure 5-9: Details of the backlash model

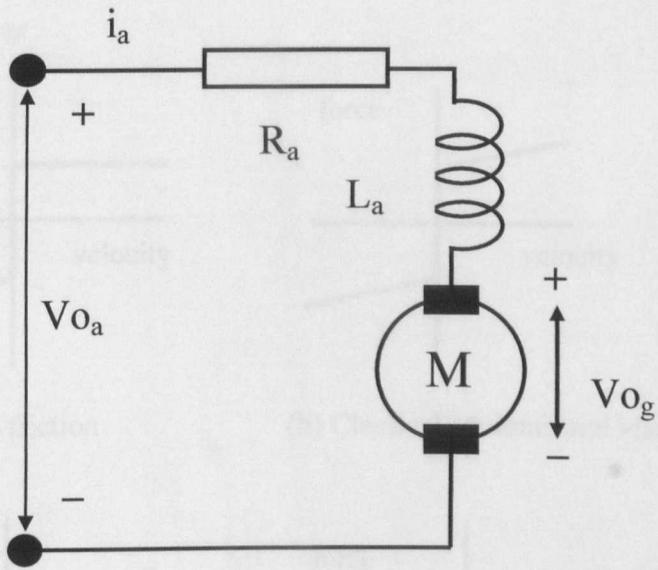


Figure 5-10: Schematic of a DC motor

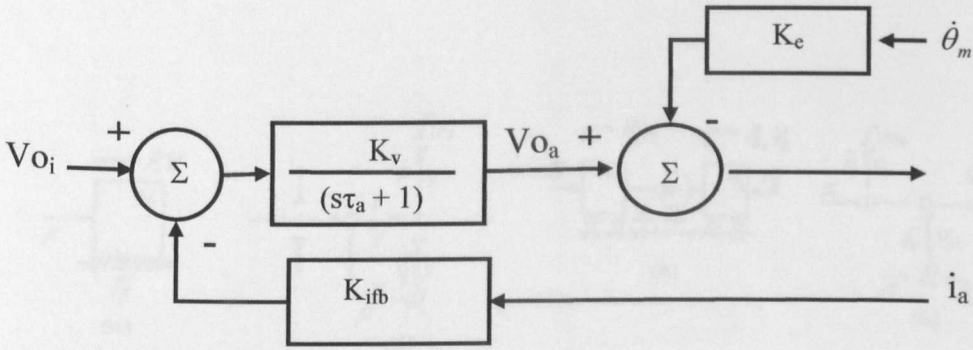
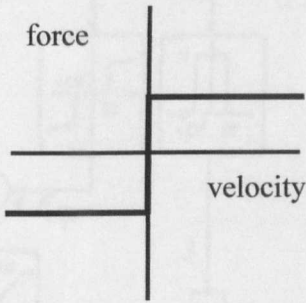
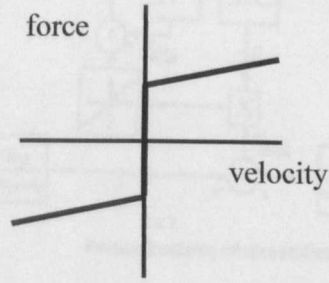


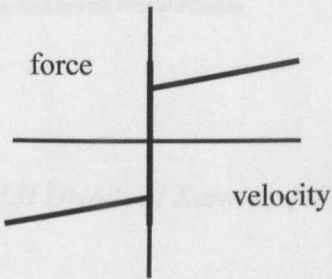
Figure 5-11: An ideal linear amplifier with current feedback



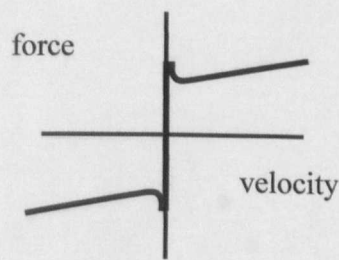
(a) Classical coulomb friction



(b) Classical coulomb and viscous



(c) Classical coulomb, viscous and stiction



(d) Friction with Stribeck effect

Figure 5-12: Static friction model characteristics

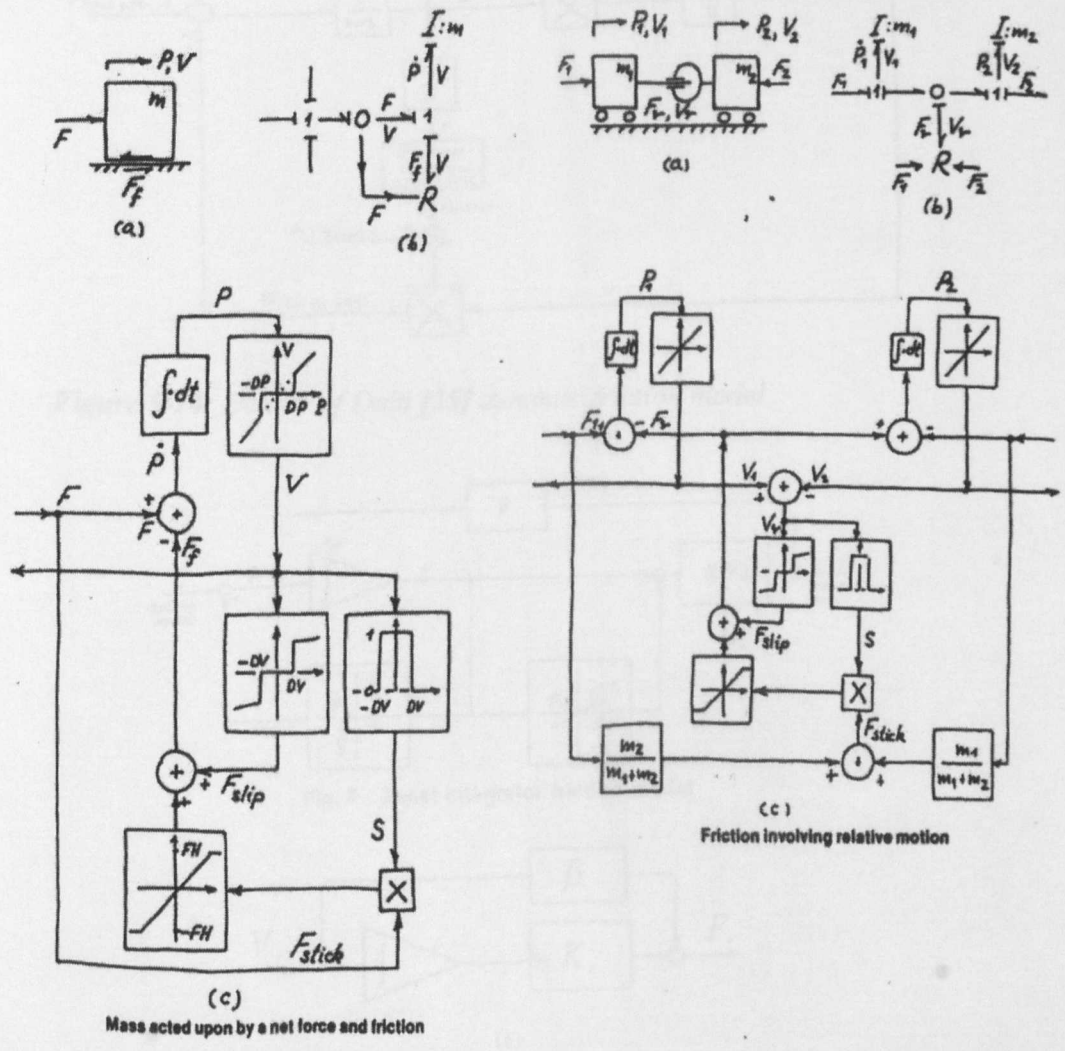


Figure 5-13: Details of Karnopp [48] model

FREQUENCY RESPONSE ANALYSER

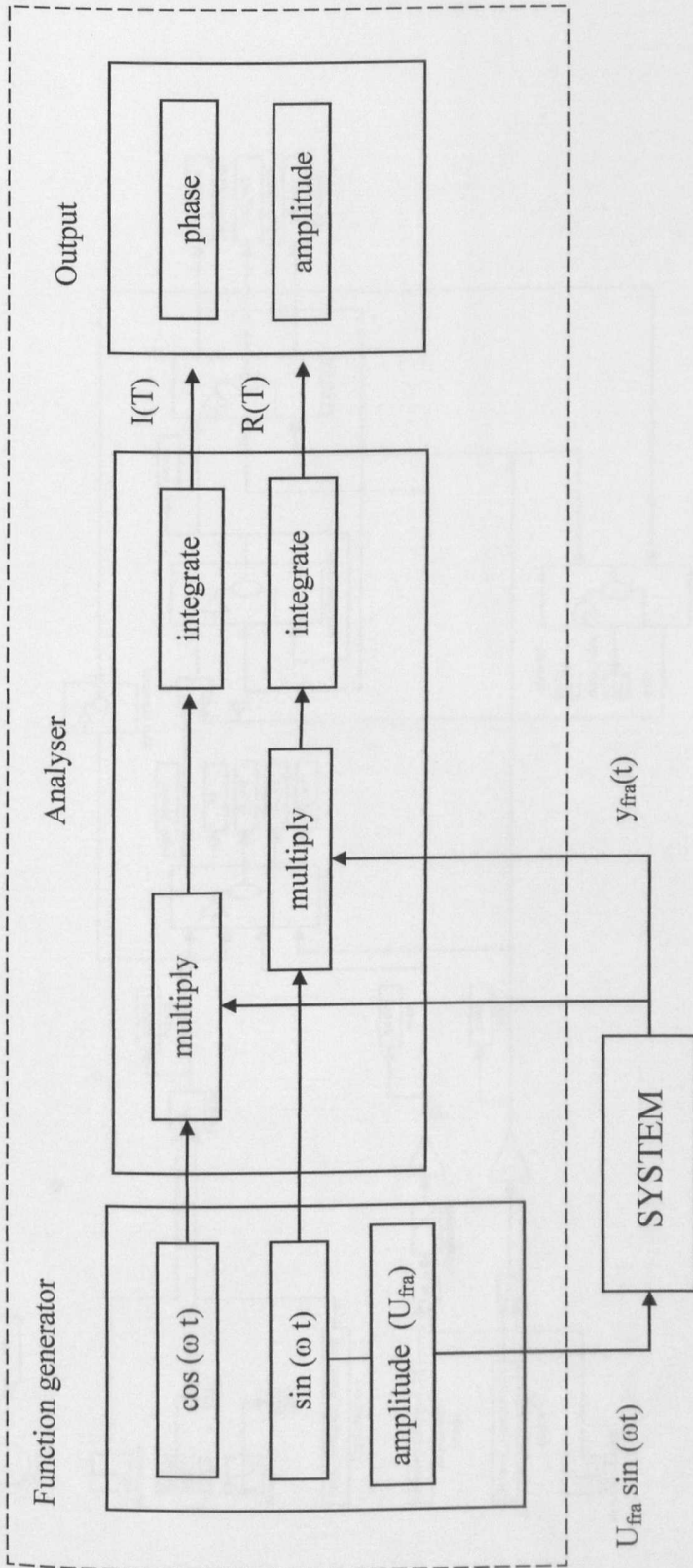


Figure 5-16: Frequency response analyser and system

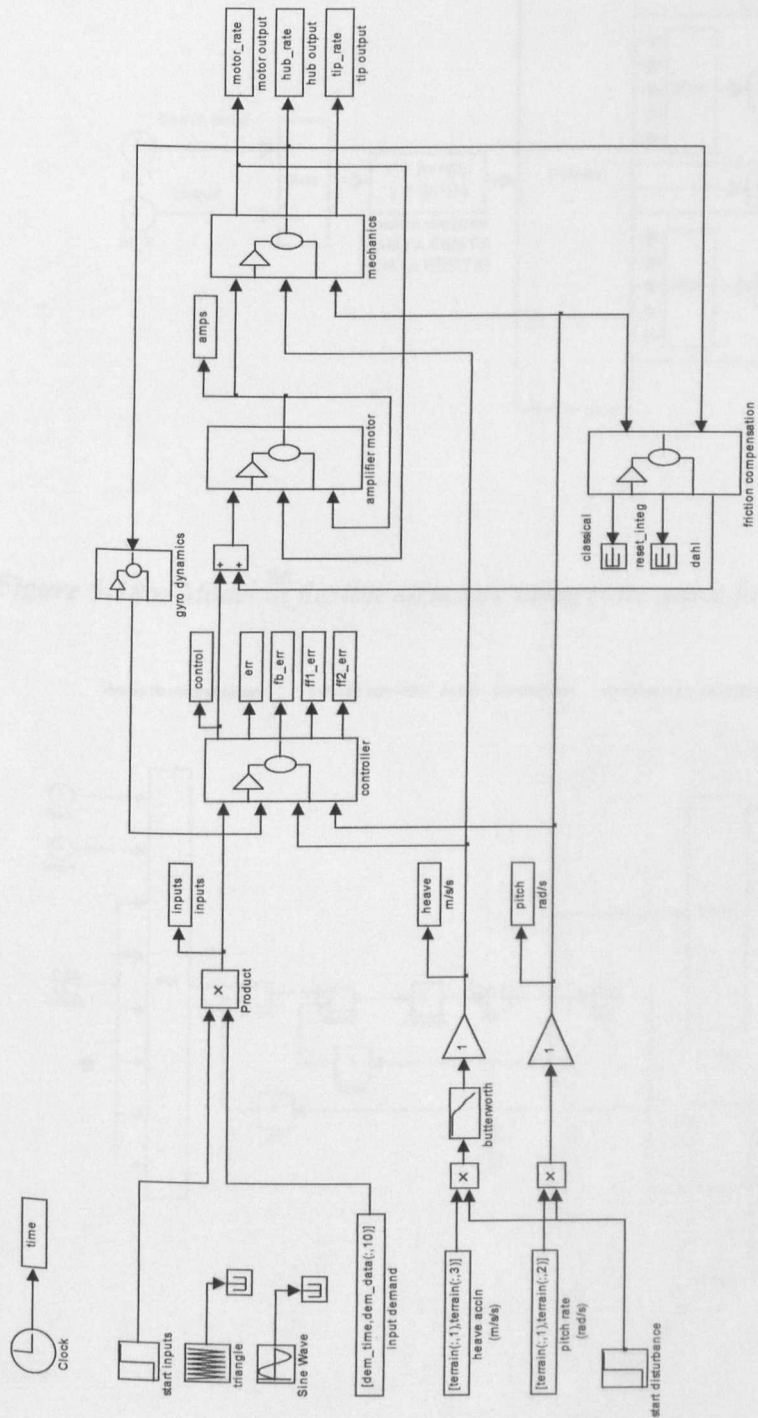


Figure 5-17: Simulation block diagram of the full system

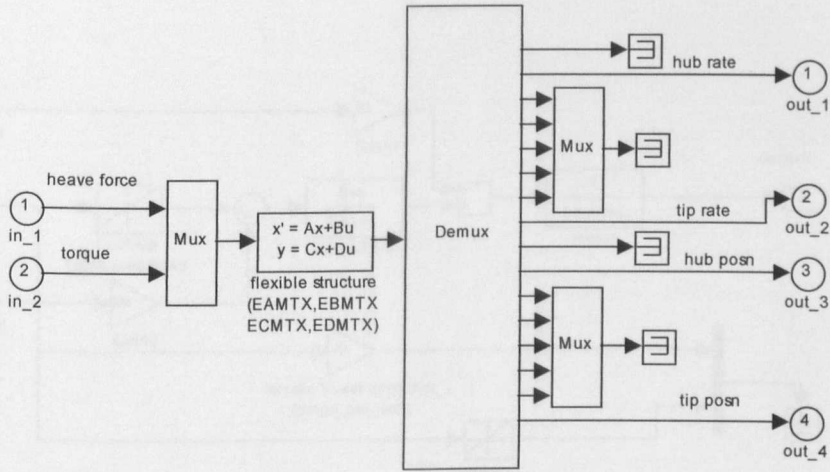


Figure 5-18a: Model of flexible structure using state space formulation

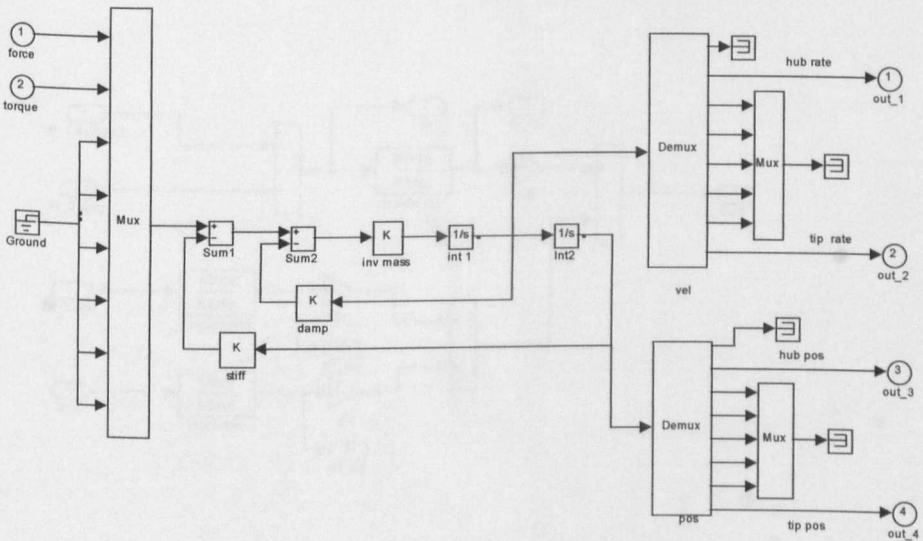


Figure 5-18b: Model of the flexible structure using mass, stiffness and damping matrices

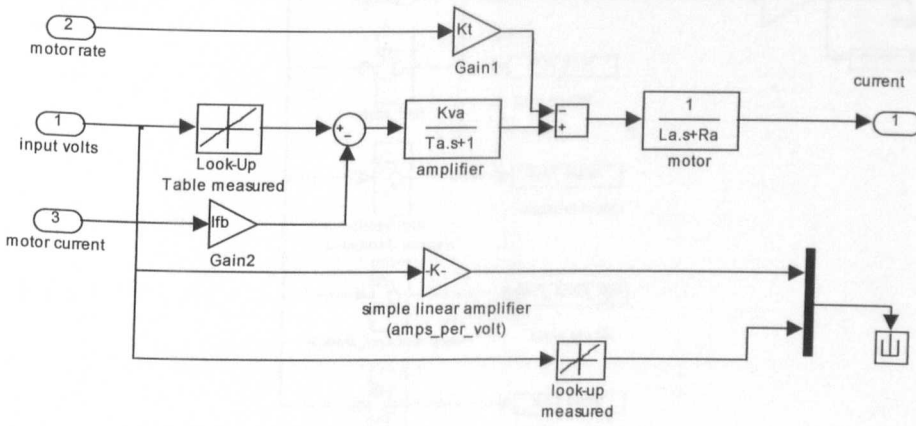


Figure 5-19: Servo amplifier and the motor model (electrical)

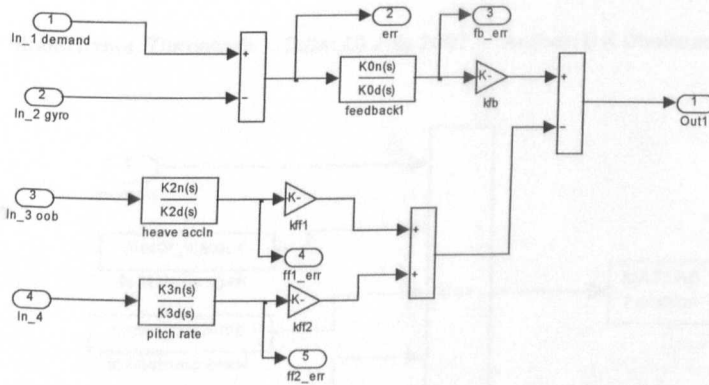


Figure 5-20: Controller block diagram

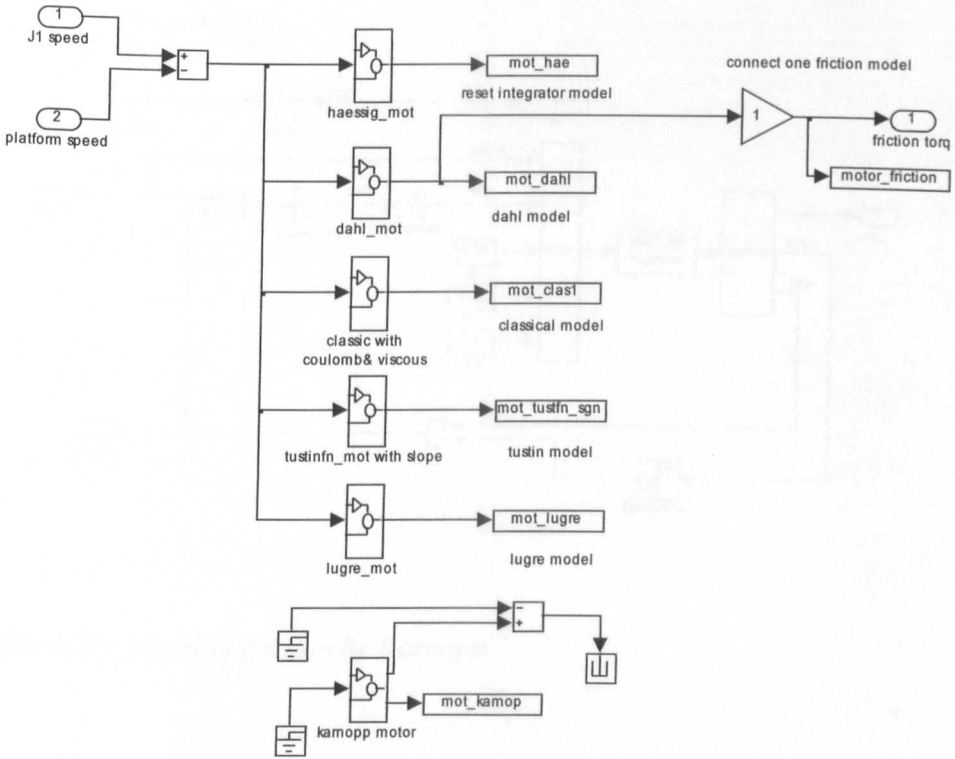


Figure 5-21: The motor and gearbox model showing the friction models

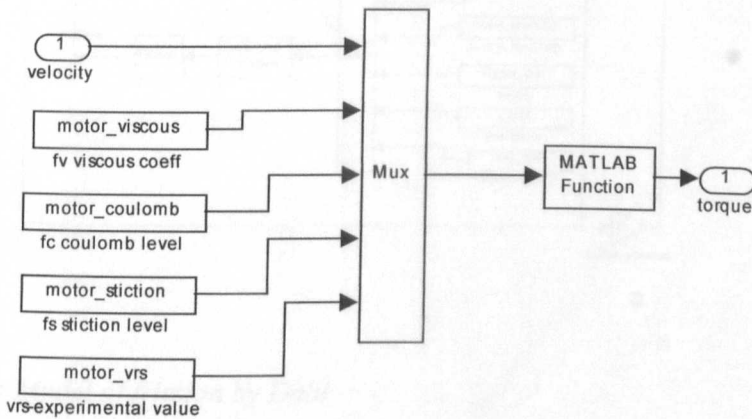


Figure 5-22: Model of friction by Tustin

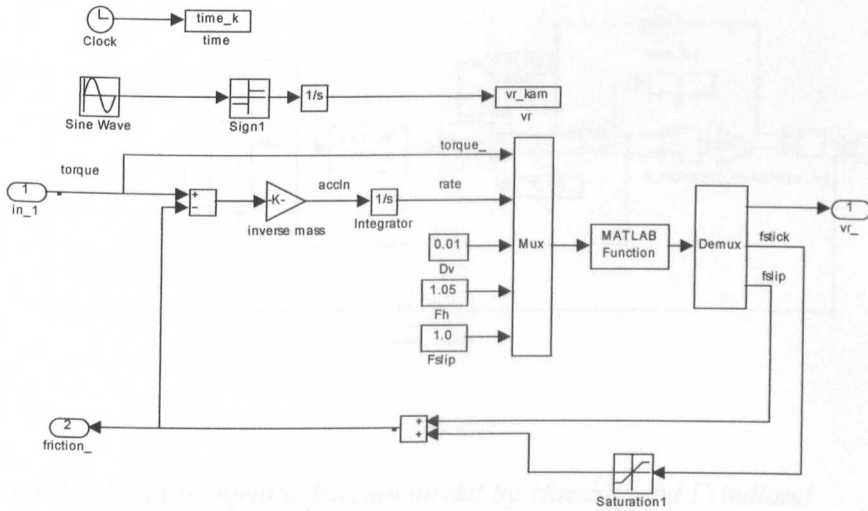


Figure 5-23: Model of friction by Karnopp

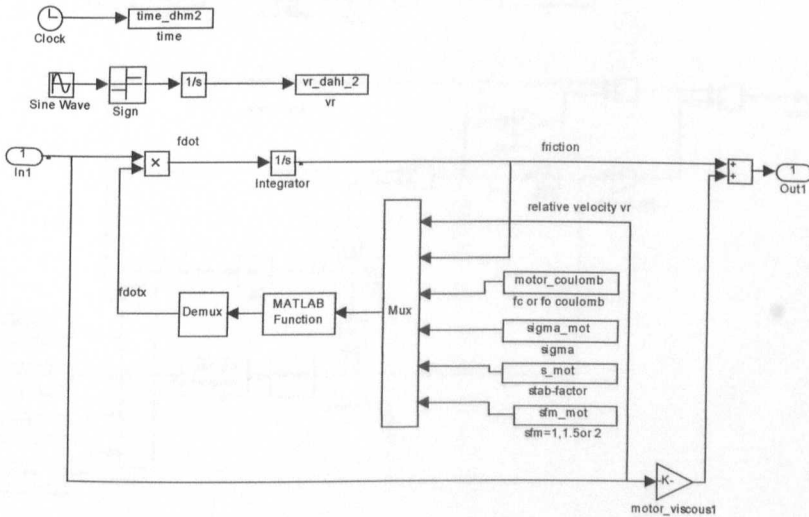


Figure 5-24: Model of friction by Dahl

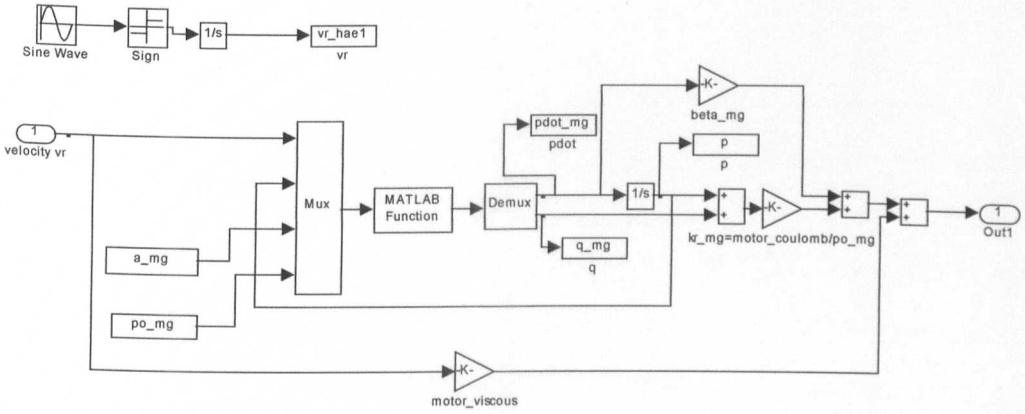


Figure 5-25: Reset integrator friction model by Haessig and Friedland

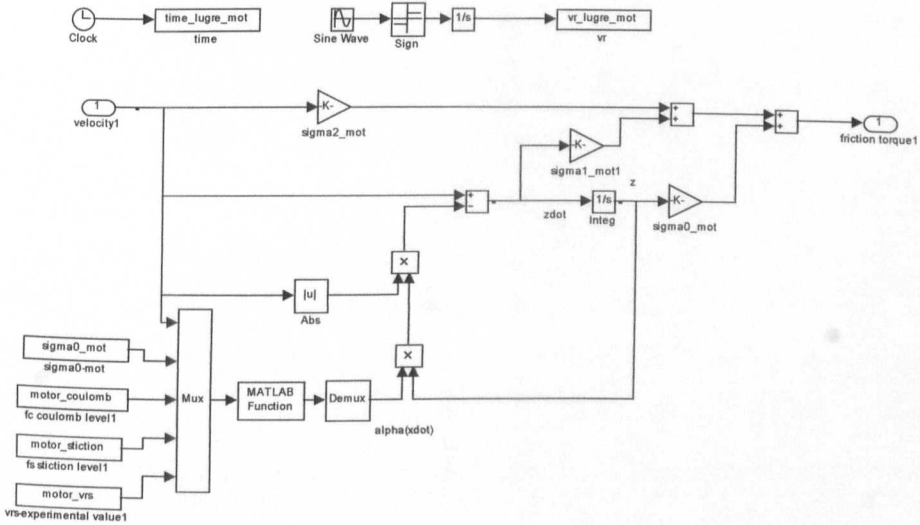


Figure 5-26: LuGre friction model by Canudas de Wit et al.

CHAPTER 6

DESIGN OF THE CONTROL SYSTEM

6.0 Design of the control system

6.1 Introduction

This section presents the design of a control system for the generic simulation of the cantilever mechanism described in chapter 5. The design is based on the robust control technique described by Grimble [63] and uses the toolbox developed by Strathclyde University [68]. While previous work, described in chapter 2, use simple models based on lump-parameter techniques and static friction characteristics, the study presented in this chapter uses a more representative model of the system.

The aims of this section are to:

- a) Design of controllers for realistic system models which incorporate structural flexibility of a cantilever beam and dynamic friction models.
- b) Investigate the degradation in performance due to spill over effects by comparing the performance of controllers designed using lump-parameter and FE models.
- c) Investigate the robustness properties of the system to parameter changes such as out-of-balance, friction, inertia and backlash.

A model based nonlinear observer is used to minimise the effects of friction. An experimental technique, which varies from that described by Johnson and Lorenz *et al.*[27] in that it is applied directly to the H_2 controlled system, is used to obtain the parameters for the observer. In chapter 7, which covers experimental work, the technique is extended to extract other system parameters such as out-of-balance torques and nonlinear amplifier gain.

6.1.1 Control system performance specification

In common with many applications the control system in this research has to provide acceptable response to input demand signals and has to maintain the desired accuracy in the presence of external disturbances. The exact requirements are specified using performance criteria such as peak-overshoot, rise-time and steady-state errors in the

time-domain and bandwidth, gain and phase margins in frequency-domain, Dutton[89]. In addition to these commonly used criteria, the performance of stabilised systems is measured by their ability to reject the external disturbances using Disturbance Rejection Ratio (DRR). The ratio is derived by dividing the amplitude of the output, the cantilever mechanism hub motion, by the amplitude of the disturbance which is the input to the system. In the resulting frequency response graphs low gain indicates good stabilisation. The measurement of DRR is described more fully in chapter 4.

The stabilisation performance of the control system without the feedforward controllers, i.e. the performance of the feedback control system, is first established and then the improvements provided by the two feedforward control systems are quantified. As the H_2 design technique is based on linear theory the performance is first analysed using the linear models and then assessed using nonlinear models.

6.2 Models for control system design

The FE simulation packages used by structural dynamicists generate models with many hundreds of dynamic degrees of freedom (DOF). However, while these models are highly accurate, it is very difficult to design controllers based on large order models and the tools used by control analysts fail when more than a dozen or so modes are considered. Hughes[90] has shown that for practical designs the dynamics of flexible structures can be adequately modelled using a small number of elements.

The performance of a control system designed using FE models is compared with a control system designed using low order lump-parameter models. The control system complexity, i.e. order of the controllers, is governed by the order of the model used in the design process. The main advantage of using the lump-parameter model is that low order control systems are produced which can be implemented in hardware relatively easily without resorting to transfer function reduction techniques. The cost of implementation is also reduced as lower specification processors can be used which can be critical in price sensitive products. The main disadvantage is that the effects of neglected modes can cause severe degradation in performance due to spill over effects discussed in chapter 2. However, it is likely that in this application with the practical

constraints of band-limited sensors and actuators, unmodelled high frequency dynamics become less significant and their effects on control design is minimal.

6.2.1 Reduced order models for control system design

FE models for control system design

Several models of the structure are developed using different numbers of elements. The results are compared with measured data and with models developed using PAFEC [91], a commercial FE package. The PAFEC ^[a] model uses 129 elements to model the flexible cantilever structure. The variations in modal frequencies for different number of finite elements used to model the system, described in section 5, are summarised in Table 6-1. The table compares the predicted modal frequencies with the experimental measurements for the free-free case for the structure. The structure, which has a cross section that is approximately tapered, is first modelled using elements which have uniform cross-sections. The diameter of the element is the average diameter of the tapered section. The accuracy of the model increases with the number of elements used. In an attempt to improve the accuracy or reduce the number of elements, the structure is modelled again using non-uniform elements with tapered cross-sections as illustrated in Figure 5-5.

The 14-element model shows good agreement with the measured and the 129-element model for the first 5 modes showing a variation of less than 4 %. The three-element model shows good agreement, error of less than 1%, while the model using non-uniform elements shows an error of less than 0.2% for the first mode. The higher modes are not as close in either of the 3-element models when compared to the 14-element model. Interestingly, the first mode in the 14-element model is not as accurate as the 3-element models. The model which uses the non-uniform FE element in general shows closer agreement with measured results than the model which uses uniform cross-section elements.

[a] PAFEC model and modal frequency data provided by Mr D Lodge

Mode no.	Measured data	FE package results	Uniform cross-section element results				Non-uniform cross-section element results		
		129 element	14 element	3 element	2 element	1 element	3 element	2 element	1 element
1	0.02762	0.02762	0.02660	0.02786	0.02692	0.03789	0.02767	0.02728	0.03615
2	0.07571	0.07565	0.07309	0.08852	0.09432		0.08539	0.08998	
3	0.14697	0.14695	0.14513	0.18058		0.12943	0.18678		0.14492
4	0.24347	0.24476	0.24804		0.21506			0.21827	
5	0.36075	0.36401	0.37300	0.34298	0.38128		0.35964	0.43451	
6	0.49436	0.49938	0.53523	0.53652			0.53998		
7	0.64727	0.66354	0.72310						
8	0.82007	0.84169	0.95422	0.96069			0.94393		
9	1.00000	1.06295	1.24417						

Table 6-1: Comparison of predicted modal frequencies for various cases and with measured data (normalised to measured 9th mode frequency).^[b]

For H₂ control system design the order of the model is further reduced by using modal reduction techniques described in section 3. The transfer function for the plant with input at the actuator and output at the hub is 21st order. The reduction is carried out by using minimum realization (pole/zero cancellation) followed by discarding the higher modes, using the modred function in MATLAB[92]. The reduced transfer function used for the control system design is 11th order. The frequency responses of the 3-element model and the reduced order models used for the control system design are shown in Figure 6-1 for the three inputs. Figure 6-1(a) shows the response of the plant to input demand signal applied to the amplifier, while Figures 6-1(b) and (c) show the response to heave and pitch disturbances. The outputs of the system are hub rate.

[b] All figures in this chapter normalised to the same values. Frequency response graphs normalised to the measured 9th mode frequency.

Lump-parameter models for control system design

The transfer functions of the plant derived using the lump-parameter model are compared with the TFs obtained with the FE model in Figure 6-2(a), (b) and (c). The lump-parameter TFs show good agreement with the FE model TFs for all three inputs. However, in the lump-parameter model the higher modal frequencies are not present. The lump-parameter model TF is 11th order.

6.3. Design of controller using FE models

Details of the H_2 controller design, summarised in Figure 6-3, are provided in appendix 5. The frequency responses of the feedback controller, which incorporates integral action and the two feedforward controllers are illustrated in Figures 6-4(a), (b) and (c).

6.3.1 Linear model results using FE designed controller

Frequency-domain

The frequency responses of the system are illustrated in Figures 6-5. The gain and phase margins and the bandwidth using the open-loop and closed-loop responses, Figure 6-5(a) and (b), are as follows:

Gain margin:	12 dB
Phase margin:	60 degrees
Bandwidth(-3dB):	3.8e-3 (normalised frequency)

Time-domain

The outputs of the closed-loop linear system to the three inputs are illustrated in Figures 6-6. The response of the system to a unit step input, Figure 6-6(a), shows the following performance indices:

Overshoot:	13%
Peak time:	0.025 (normalised)
Time to steady-state:	0.23 (normalised)

The effectiveness of feedforward control in eliminating the errors caused by external disturbances is investigated by examining the stabilisation of the system for each

disturbance individually followed by the study of the combined effect of the two disturbances acting simultaneously. In an ideal system each feedforward controller should eliminate the effects of each disturbance completely. Figure 6-6(b) shows the effect of the heave disturbance acting on the system with only the feedback control. The improvements provided by the heave feedforward control, illustrated in Figure 6-6(c), shows that feedforward control provides a substantial reduction in errors (almost eliminated) caused by the external disturbance. Similarly, Figure 6-6(d) shows the effect of pitch disturbance acting on the system. The feedback controller reduces the peak disturbances by a factor of 13. The improvements in system stabilisation, illustrated in Figure 6-6(e), show that the effects of the pitch disturbance on the hub motion are substantially reduced by the pitch feedforward controller. The effects of both these disturbances, acting simultaneously, are illustrated in Figures 6-6(f) and (g). In these graphs both the heave disturbance and pitch disturbance are included to provide a visual indication of the improvements in performance. The results in Figure 6-6(g) show that the feedforward controllers provide substantial improvements in system stabilisation.

6.3.2 Nonlinear model results using FE designed controller

The nonlinear simulation results are presented in the same sequence as the linear results to enable direct comparison of the two cases. In the nonlinear simulations a friction observer is used to improve the system performance, as described in section 6-1.

Time-domain results

The responses of the nonlinear closed-loop model to the three inputs are shown in Figures 6-7. The results compare very favourably with those obtained for the linear model, illustrated in Figure 6-6, for all the three inputs. The response of the system to unit step input, Figure 6-7(a) shows the following:

Overshoot:	15%
Peak time:	0.0255 (normalised)
Time to steady state:	0.24 (normalised)

Comparing these Figures with the linear case, the nonlinear system is under damped showing a larger overshoot, higher amplitude oscillations and takes longer to reach settling time. The steady-state errors are the same as the linear model. These differences are primarily due to the effects of the linearisation process, which is an approximation, and therefore cannot model discontinuous effects of Coulomb friction, backlash etc.

The effects of heave disturbance on the hub motions are illustrated in Figures 6-7(b) and (c). The effect of the disturbances acting on the system without feedforward compare favourably with the corresponding linear results shown in Figures 6-6(b). The nonlinear model shows some higher frequency oscillation and noise which is not present in the linear results. Inclusion of the feedforward controller provides marked improvements in system performance, showing similar results to those in the linear case. However, the results show some deterioration in the stabilisation performance and high frequency oscillations. The results for the nonlinear model to pitch disturbance again compare favourably with the linear case shown in Figure 6.6(d) and the results with the feedforward controller shows greater errors than the linear case but these are marginal. Figure 6-7(f) and (g) show the system response to the combined heave and pitch disturbances. The rejection of the external disturbances is only marginally worse than those in the linear model but they show good overall agreement.

In all the nonlinear model results some minor high frequency oscillations are noted. These are attributed to the effects of discontinuous nonlinearities which cannot be accounted for by the linearisation process and also due to the nonlinear observer which cannot completely compensate for the effects of friction. The control system can be tuned further by additional iterations of the design process summarised in Figure 6-3 and covered in appendix 5, which also provides examples of controllers with other characteristics.

6.4 Design of controller using lump-parameter models

The design of the lump-parameter model controller follows the same process to that described for the FE model controller, presented in section 6.3. It is interesting to

compare the transfer functions of the controllers produced by the two methods. The feedback controllers Figure 6-4(a), the FE model controller, and Figure 6-8(a), the lump-parameter model controller, are very similar. The heave controllers Figure 6-4(b) and 6-8(b) also show very close agreement. Similarly the pitch controllers Figure 6-4(c) and 6-8(c). It is interesting to note that at higher frequencies the truncation of the FE transfer functions produce the same results as the lump-parameter results which are not truncated.

The results of using these controllers are very similar to those obtained for controllers designed using the FE controllers.

6.5 Robustness properties

Sections 6-3 and 6-4 are primarily concerned with design of controllers using H_2 Robust control technique. This section examines the robustness properties of the controller when subjected to variations in system parameter which may occur due to changes in operating environment, wear, aging, maintenance etc. In a complex system under consideration there are a large number of parameters which can change, ranging from variations in sensor characteristics to structural deformations of the mechanical components. Parameters may also change gradually or abruptly. An exhaustive study of all the likely combinations would be a mammoth undertaking well beyond the scope of this chapter. While recognising that in an operational environment several parameters may change simultaneously, in this study simultaneous changes in two or more parameters are not considered. In the nonlinear model results presented in this section the parameters are changed at the start of each simulation run.

Changes in hub inertia

The robustness properties of the control system are investigated by examining the changes in system response to inputs demand signals and the two external disturbances. The responses of the system to a step input are illustrated in Figure 6-9(a). In the Figure the results are shown for 100% increase in inertia, which corresponds to double the standard inertia value, and 50% reduction, which corresponds to half the standard inertia value. The transient response, first overshoot, shows an increase to 20.5% and reduced

to 13% for the increased and reduced inertia values respectively. The time at which the first peak occurs also changes with longer time for the increased inertia case showing the expected slower system response.

The stabilisation responses of the system, with and without feedforward control, are illustrated in Figure 6-9(b) and Figure 6-9(c). The results are shown without the external disturbances to enable closer comparison of variations in system response. In both cases the results shows only minor changes in system stabilisation performance.

Changes in friction

The robustness properties of the system to changes in friction are examined by changing the nonlinear friction, by 100% (double the standard value) and 50% (half the standard value). The results for the two cases are compared in Figures 6-9(d) to Figure 6-9(f). As with the inertia case described above the system shows variations in performance when the friction changes are introduced. The reduction in friction increases the amplitude of the first peak and an increase in friction reduces the amplitude. The time of the first peak is the same for the two cases when compared to the standard system.

The stabilisation results, Figure 6-9(e) and Figure 6-9(f), show degradation in performance for both with and without feedforward control. When the parameters of the friction observer are changed the step responses and the stabilisation performance is restored to be similar to the standard system.

Changes in backlash

The changes in system performance due to variations in backlash are illustrated in Figure 6-9(g) to Figure 6-9(i). The results to the changes in backlash, 100% and 50%, show minimal degradation in system performance. The 100% case shows marginally higher amplitudes, while the 50% case shows lower amplitudes when compared to the standard model for step inputs. Similarly the results for stabilisation shown in Figure 6-9(h) and Figure 6-9 (i).

Changes in system out-of-balance

The variations in system performance are most marked when changes in system out-of-balance are introduced. The results are illustrated in Figures 6-9(j) to Figures 6-9(l). The step input results in Figure 6-9(j) show similar performance for all three cases. However, the stabilisation results show wide variations when compared with the standard case. In Figure 6-9(k), results without feedforward control, the variation appears to be proportional to the changes in the out-of-balance. The increased in out-of-balance produces larger stabilisation errors, while reduction in out-of-balance lowers the stabilisation errors.

In the fully compensated system which includes the two feedforward controllers, Figure 6-9(l), changes in system out-of-balance increases the stabilisation errors for both cases. The errors increase by a factor five for increased out-of-balance and four for reduced out-of-balance when compared to the standard case.

These changes are primarily due to the heave feedforward controller. Redesigning the controllers with the modified out-of-balance, illustrated in Figures 6-10(a) to Figure 6-10(c), it is observed the feedback and the pitch disturbance feedforward controllers remains unchanged for all three out-of-balance cases. The heave feedforward controller for the three out-of-balance cases illustrated in Figure 6-10(b) shows the changes the controller characteristics. Results of the fully compensated system with the redesigned controllers and the standard case are shown in Figure 6-10(d). Comparison of the three shows that the changes in the out-of-balance can be accommodated if the heave feedforward controller is modified.

For the system to provide acceptable performance when variation in system out-of-balance occurs a mechanism for changing the gain of the heave feedforward controller is required. In chapter 7 a method is presented which enables the heave feedforward controller characteristics to be changed, to reflect the changes in system out-of-balance thus maintaining the required performance.

6.6 Concluding remarks

This chapter describes the design of control systems and the assessment of their performance using both linear and nonlinear models. The performances of the system are assessed using step inputs and external disturbances, typically experienced by the system. The conclusions from this chapter are as follows:

- The results of the controller design process show that for this application low-order controller designed using lump-parameter models gives similar performance to those designed using FE models. The simulation results do not show any degradation of performance due to spill over effects. Integral action in the feedback controller does not cause the system to oscillate or limit cycle.
- The feedback controller, in conjunction with the nonlinear observer, shows that the system remains stable and no degradation in stabilisation performances is noted when large changes in inertia and backlash are introduced. Change in friction causes degradation in stabilisation performance which is restored when the parameters of the friction observer are updated.
- However, the stabilisation performance is particularly poor when system out-of-balance is changed. The primary cause for the degradation is due to the limitations of the heave feedforward controller. A scheme is required which can be used to update the feedforward controller to maintain desired performance.

FIGURES CHAPTER 6

DESIGN OF THE CONTROL SYSTEM

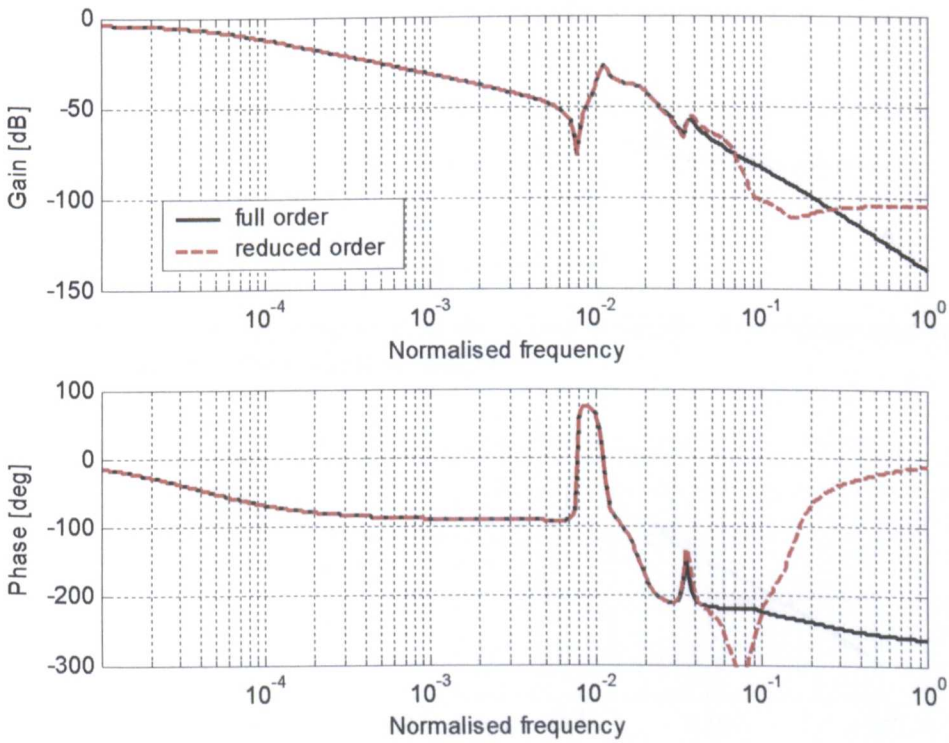


Figure 6-1(a): Frequency response of the plant to input signal and reduced order model used for control system design. ^[b]

[b] All figures in this chapter normalised to the same values. Frequency response graphs normalised to the measured 9th mode frequency.

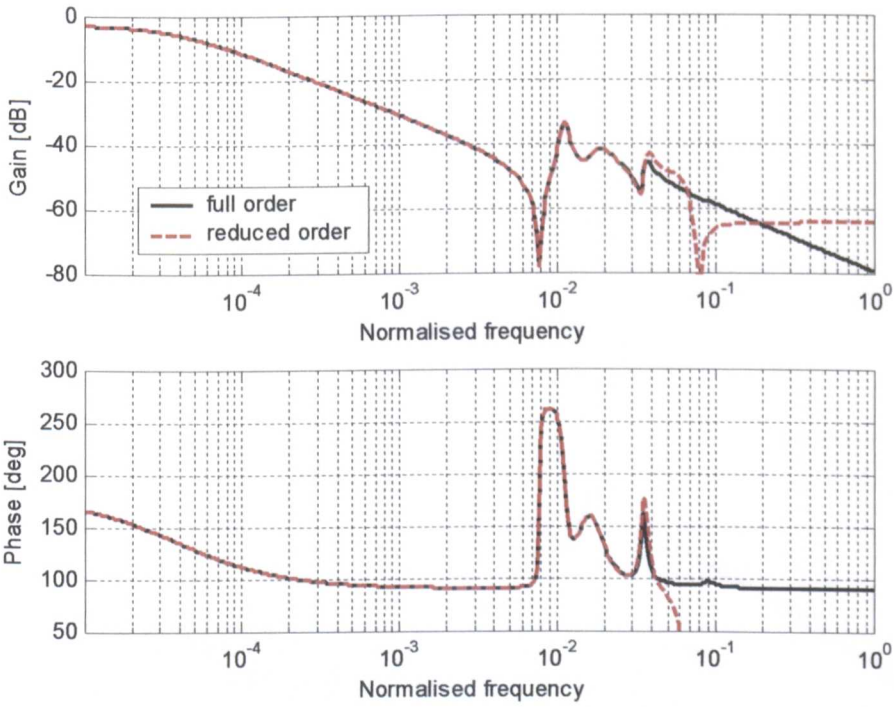


Figure 6-1(b): Frequency response of the plant to heave disturbance and reduced order model used for control system design.

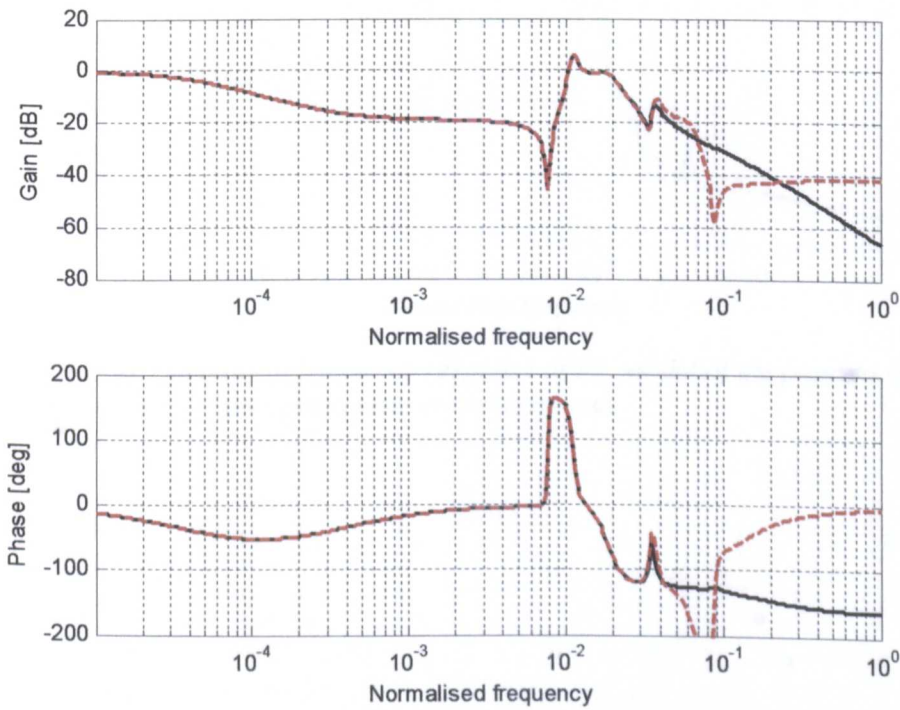


Figure 6-1(c): Frequency response of the plant to pitch disturbance and reduced order model used for control system design.

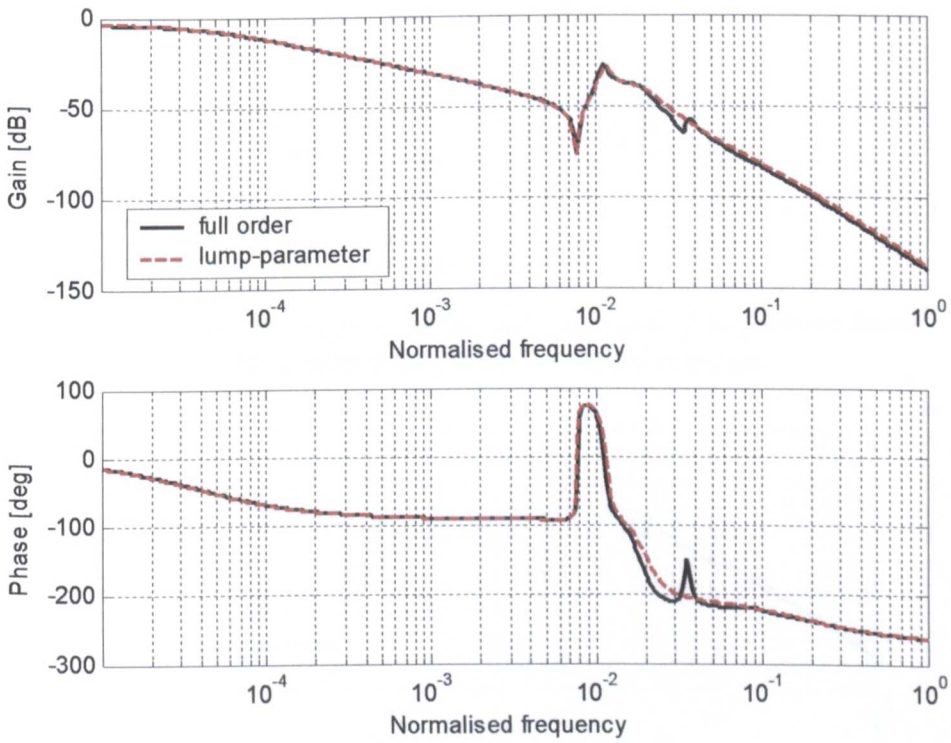


Figure 6-2(a): Comparing frequency response of FE model of the plant to input signal with corresponding lump-parameter model response.

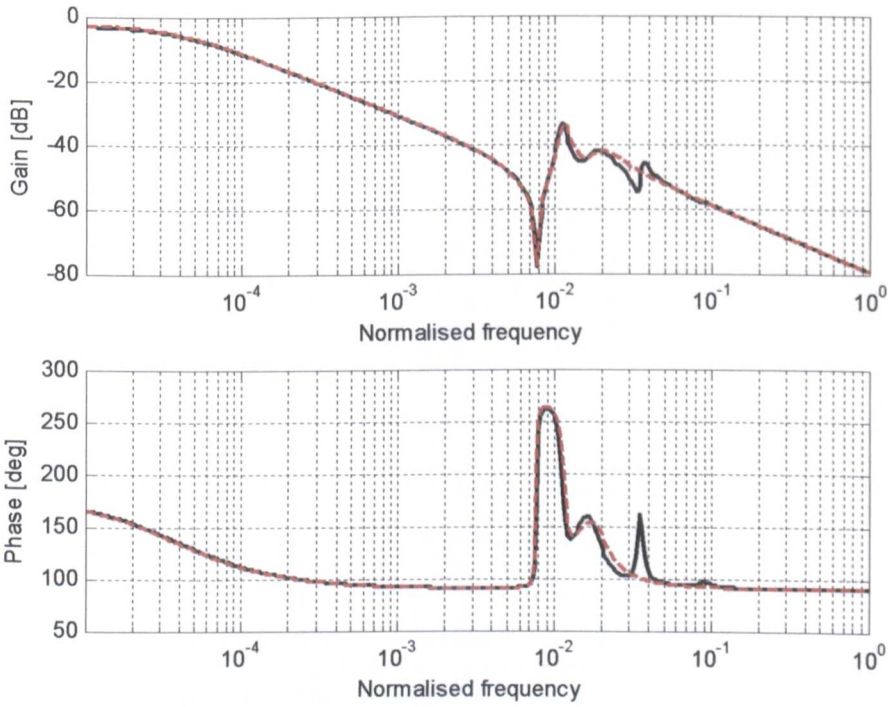


Figure 6-2(b): Comparing frequency response FE model of the plant to heave disturbance with corresponding lump-parameter model response.

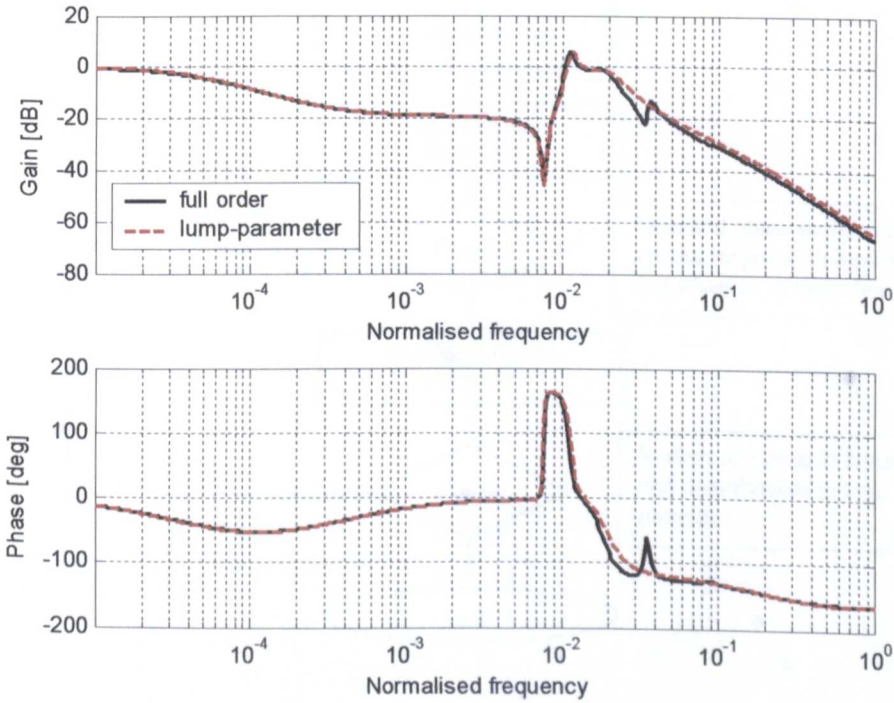


Figure 6-2(c): Comparing frequency response FE model of the plant to pitch disturbance with corresponding lump-parameter model response.

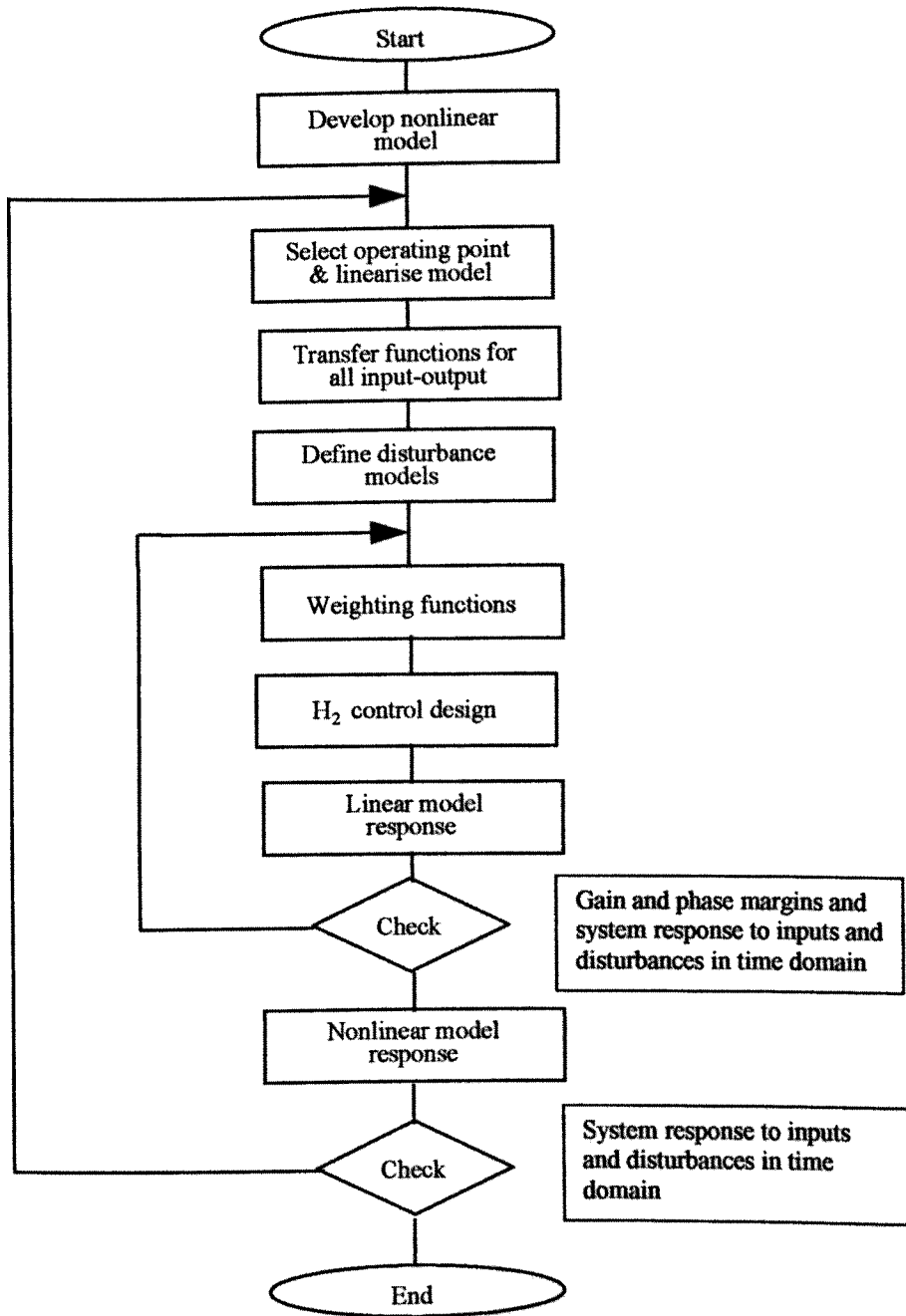


Figure 6-3: Outline of the H_2 controller design process.

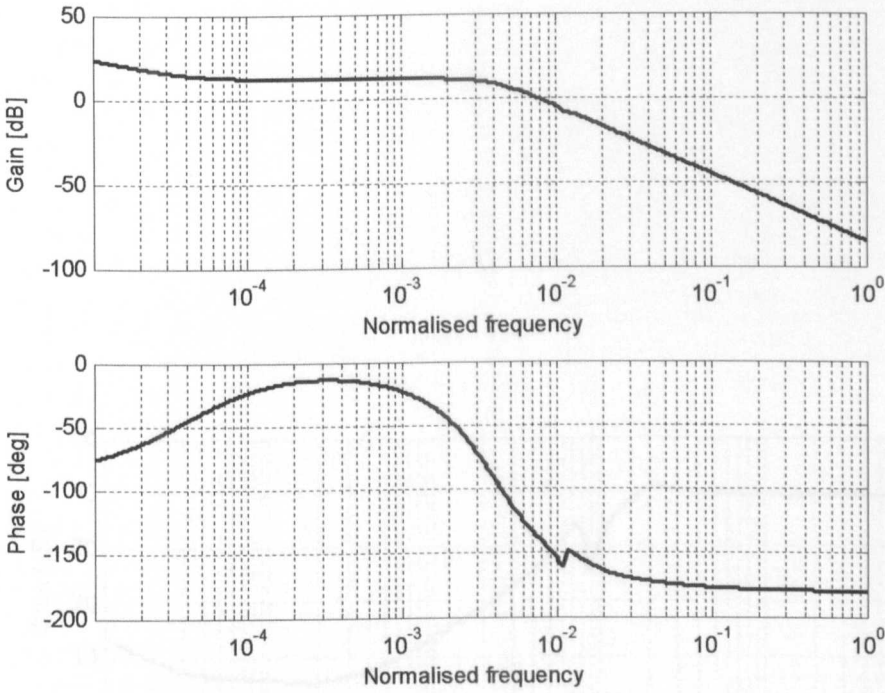


Figure 6-4(a): Frequency response of feedback controller which incorporates an integrator.

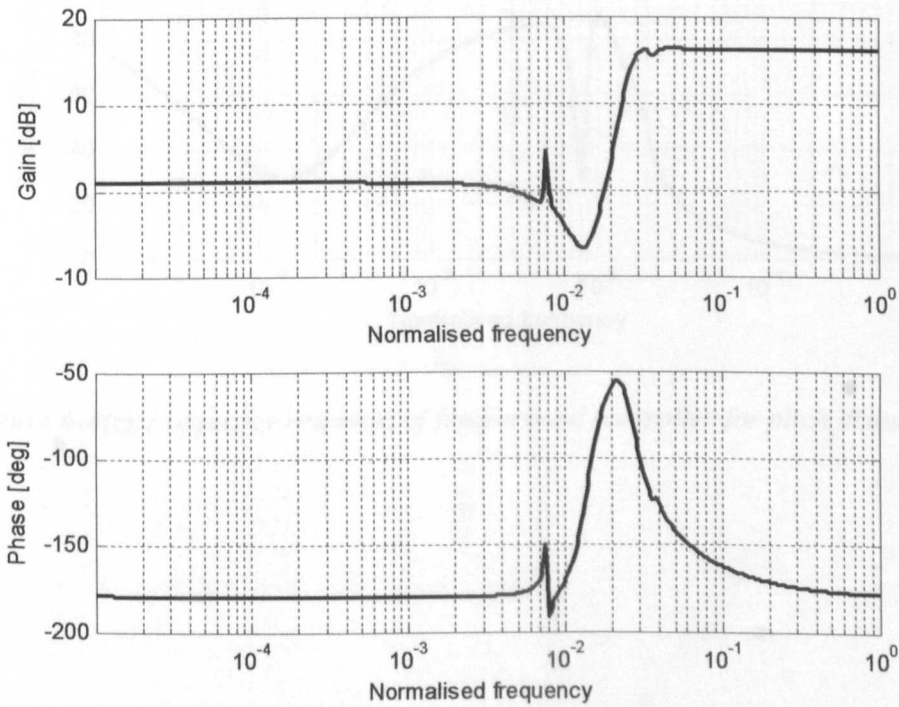


Figure 6-4(b): Frequency response of feedforward controller for heave disturbance.

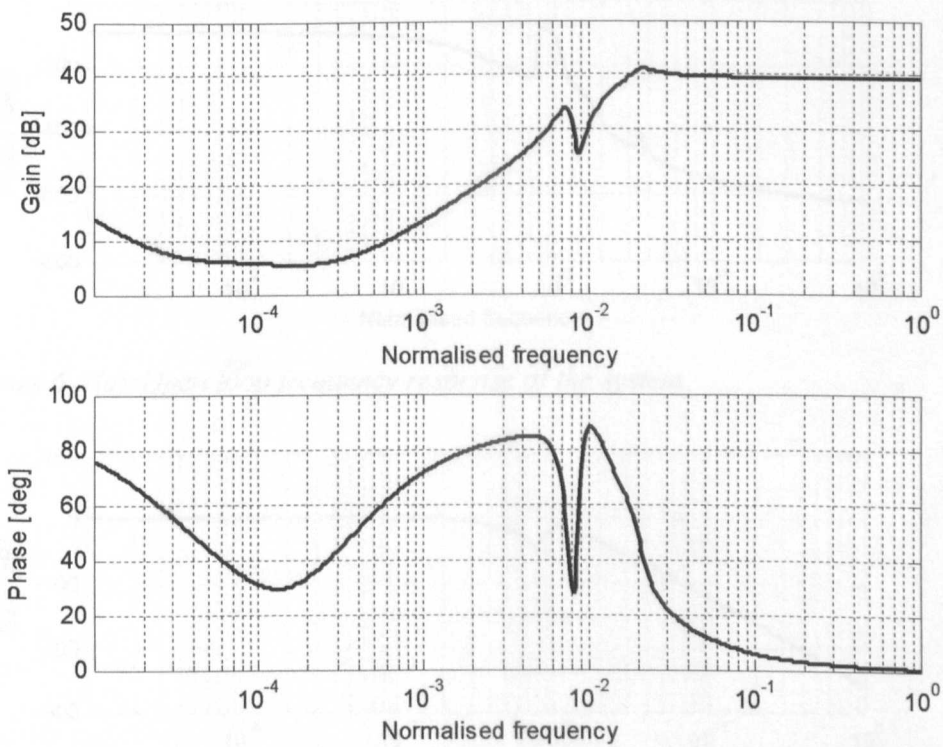


Figure 6-4(c): Frequency response of feedforward controller for pitch disturbance.

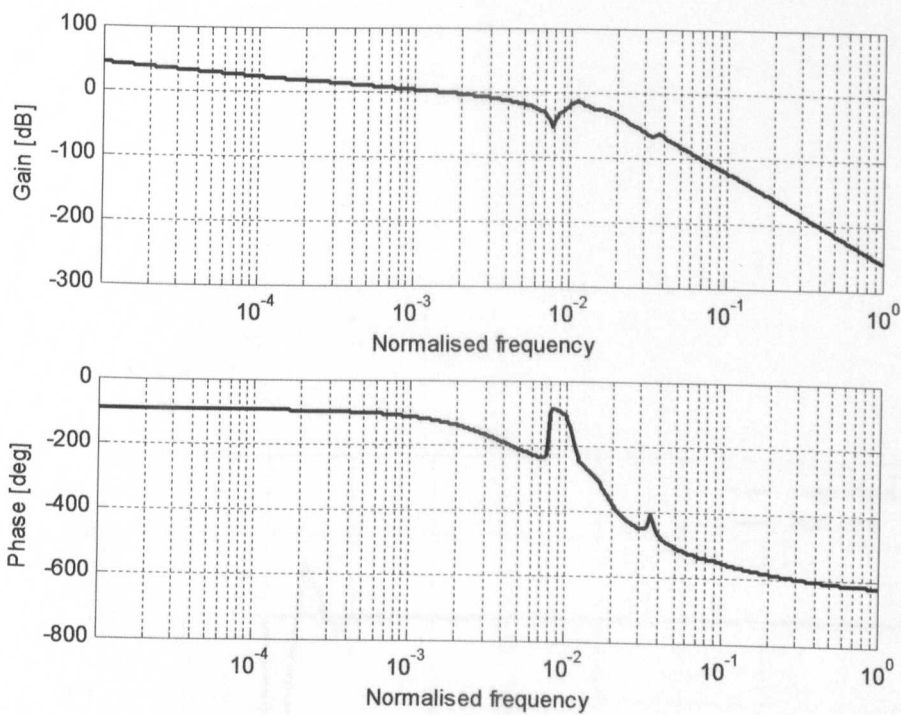


Figure 6-5(a): Open loop frequency response of the system.

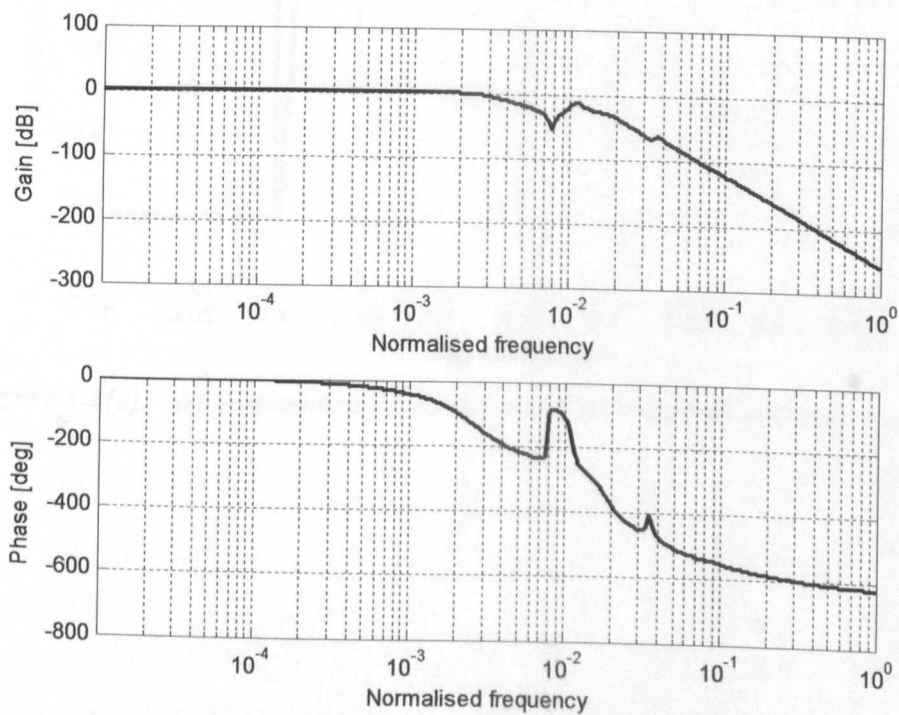


Figure 6-5(b): Closed loop frequency response of the system.

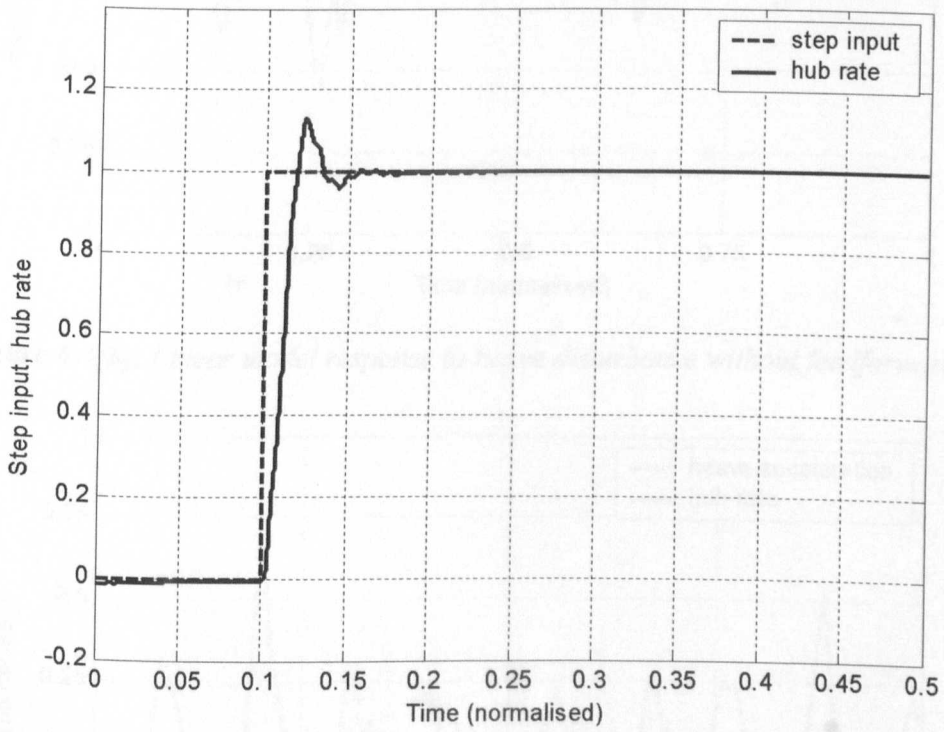


Figure 6-6(a): Step response of the linear model showing hub response.

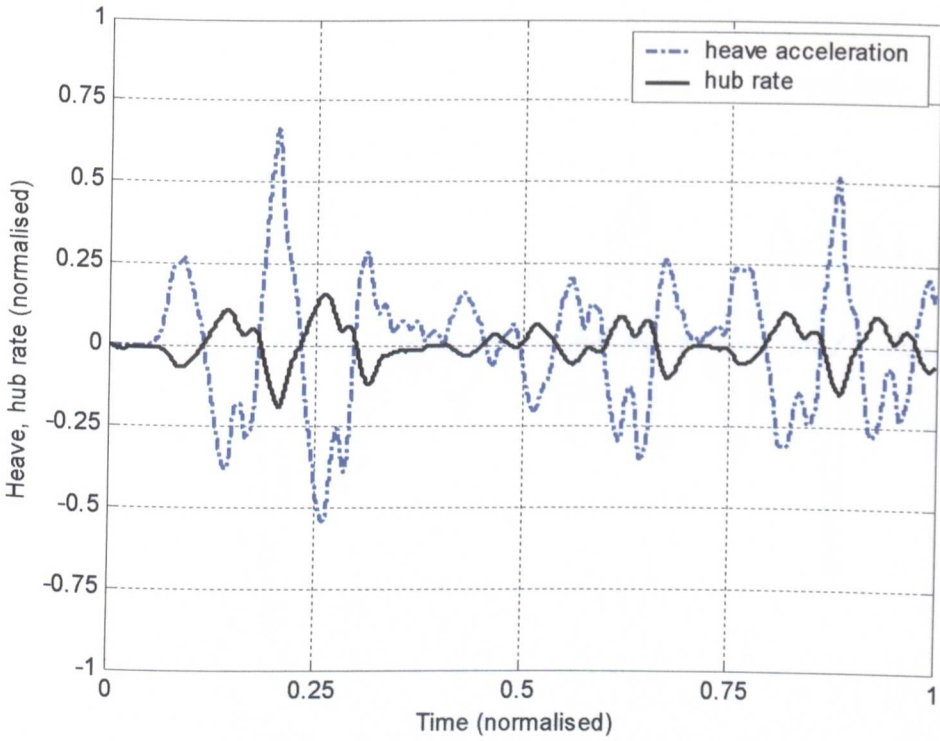


Figure 6-6(b): Linear model response to heave disturbance without feedforward.

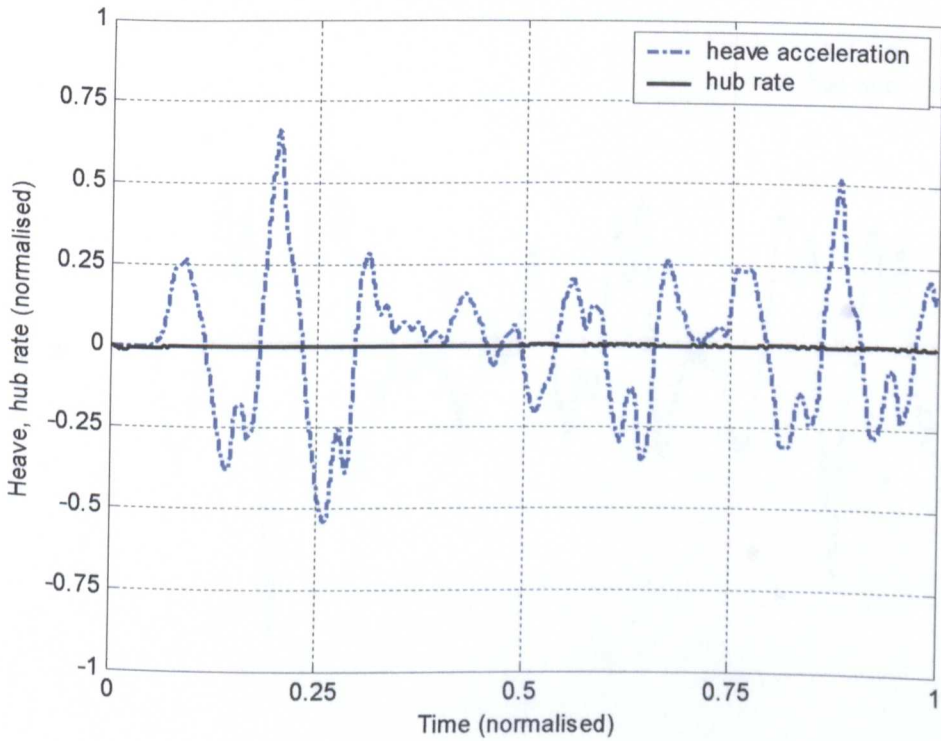


Figure 6-6(c): Linear model response to heave disturbance with feedforward control

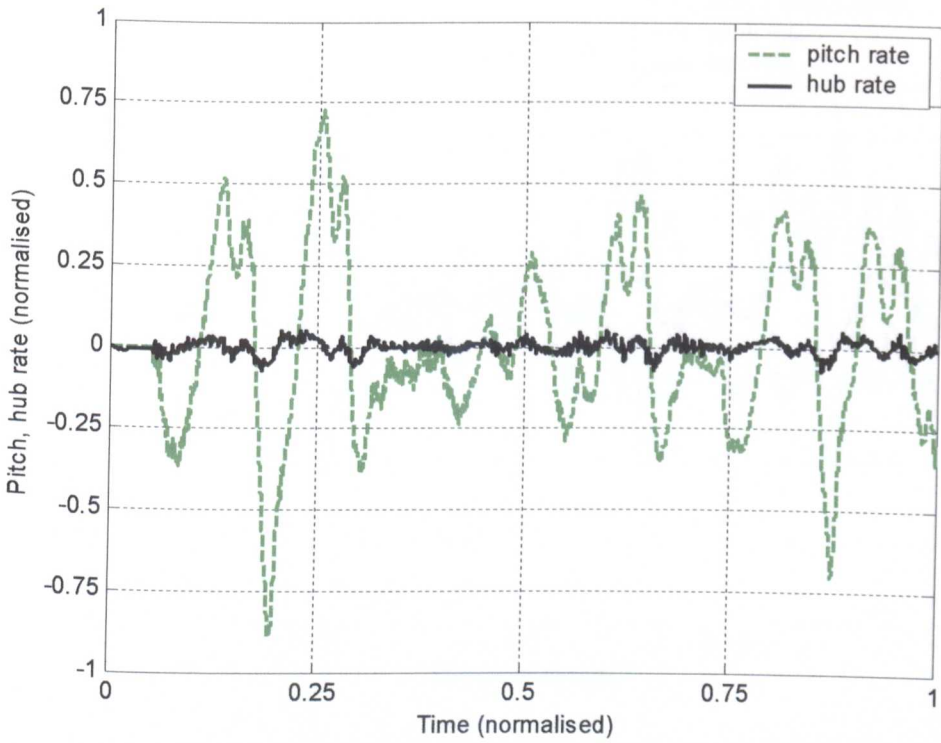


Figure 6-6(d): Linear model response to pitch disturbance without feedforward.

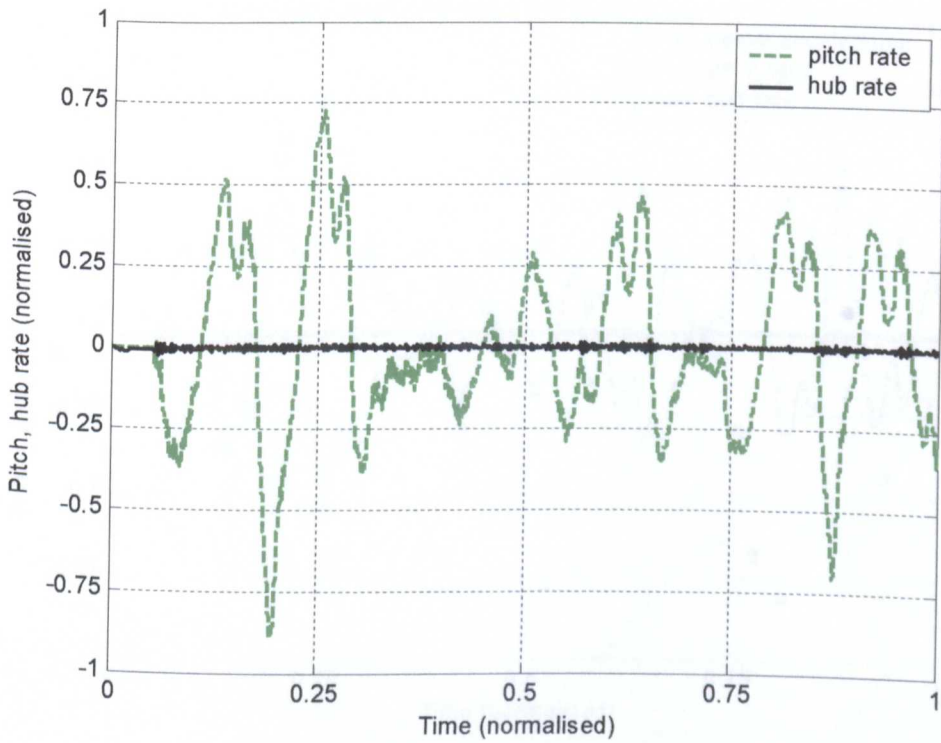


Figure 6-6(e): Linear model response to pitch disturbance with feedforward.

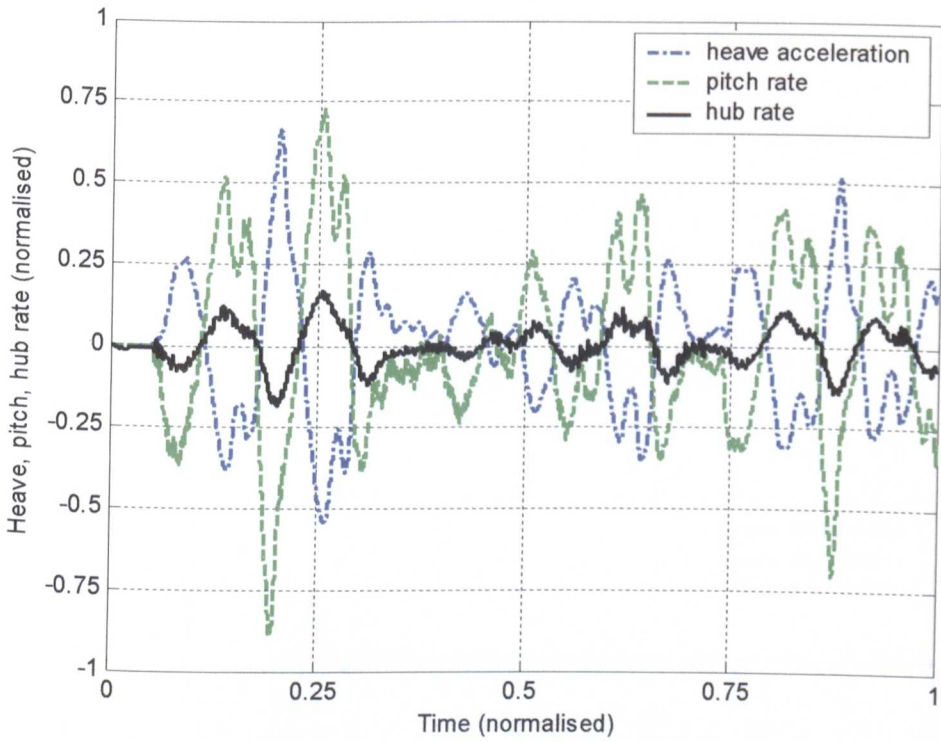


Figure 6-6(f): Linear model response to simultaneous heave and pitch disturbances without feedforward control.

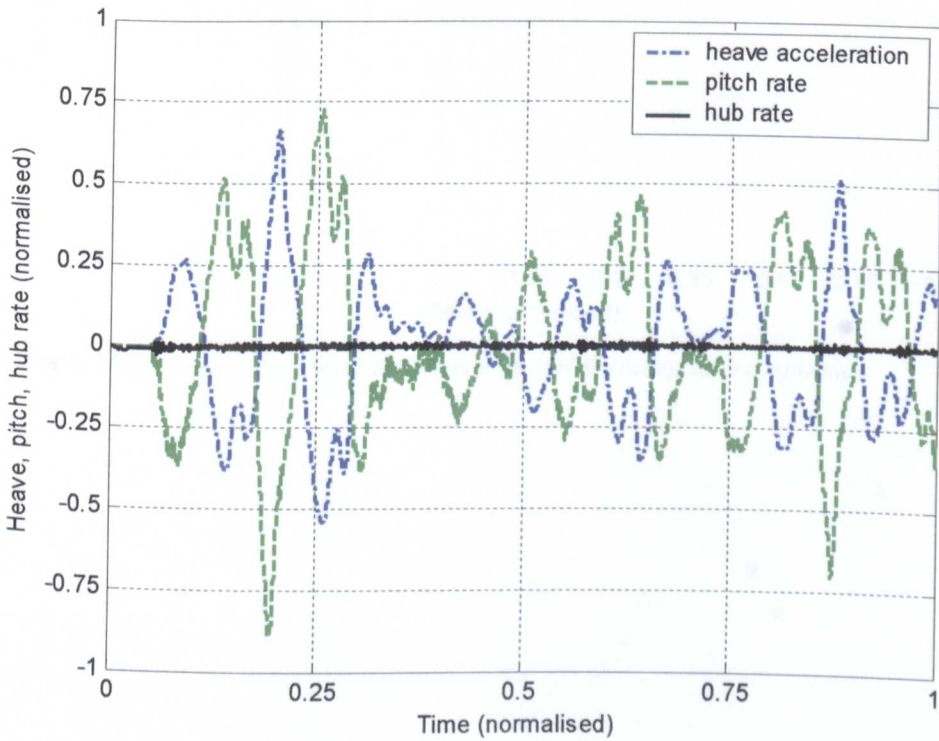


Figure 6-6(g): Linear model response to simultaneous heave and pitch disturbances with feedforward control.

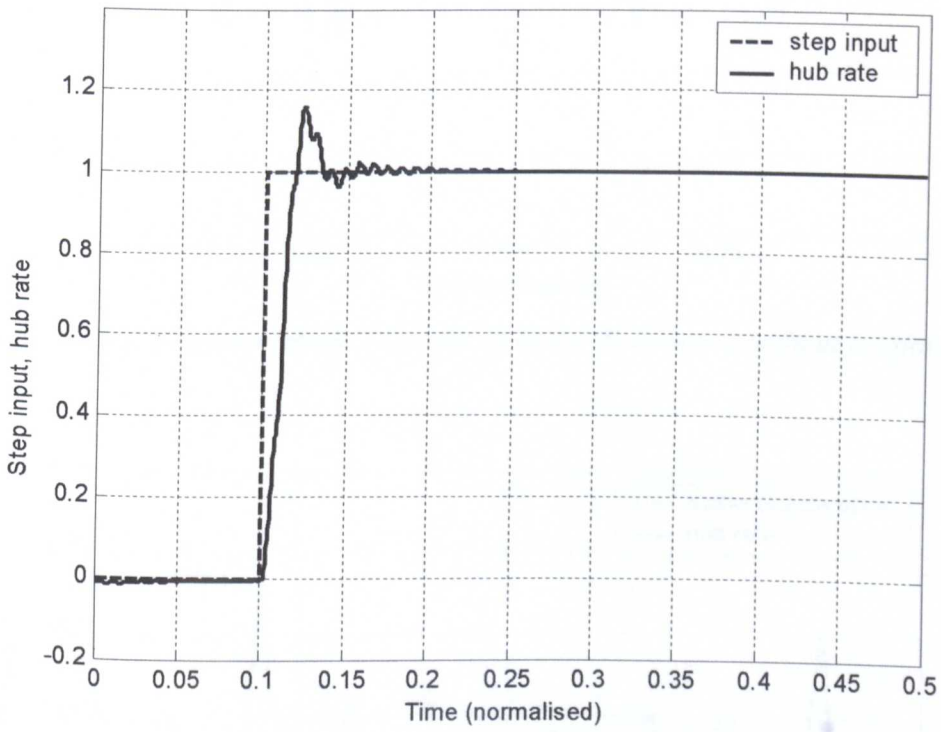


Figure 6-7(a): Step response of nonlinear model showing hub response.

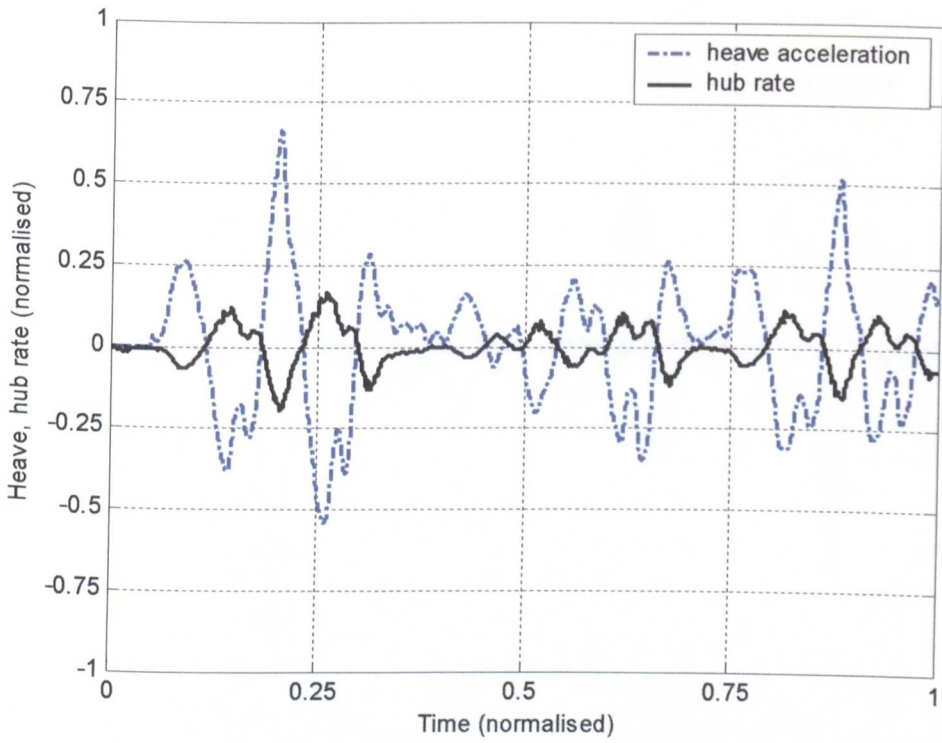


Figure 6-7(b): Nonlinear model response to heave disturbance without feedforward.

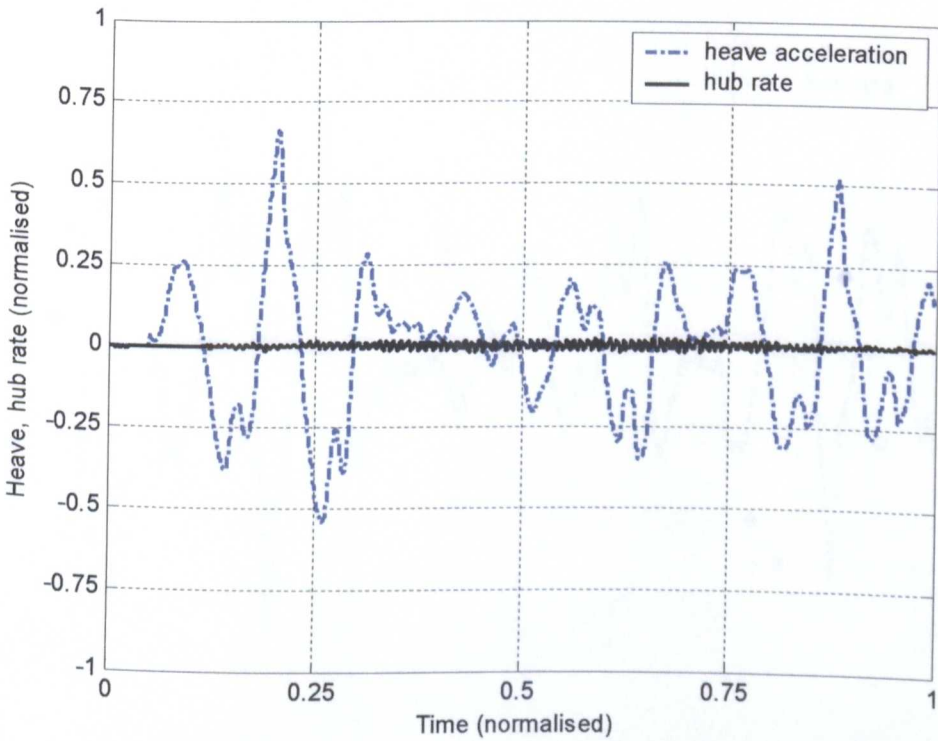


Figure 6-7(c): Nonlinear model response to heave disturbance with feedforward.

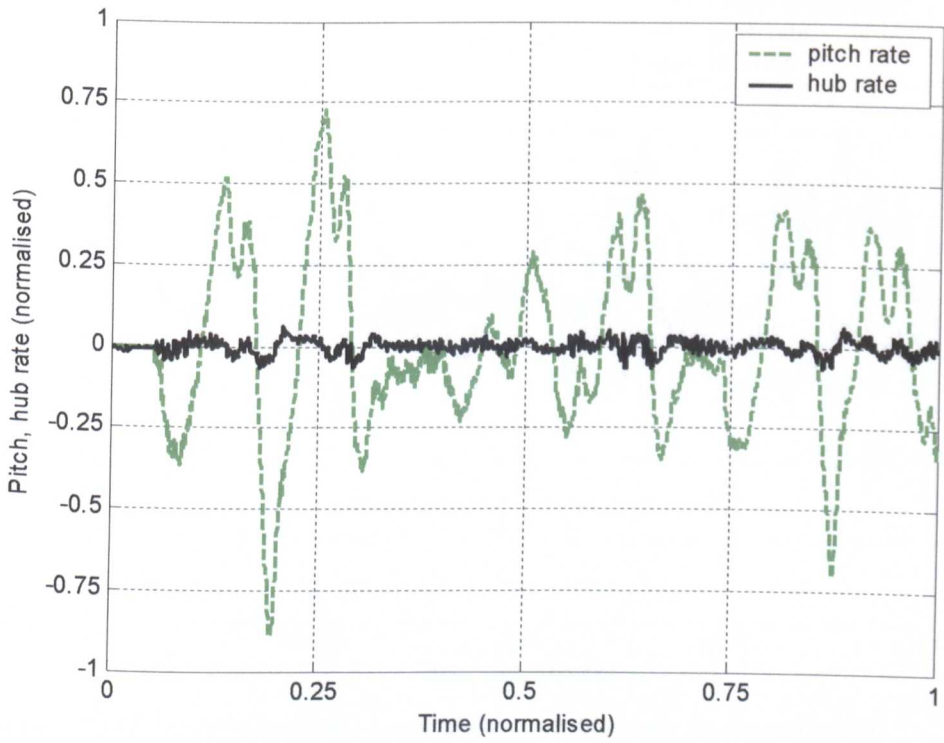


Figure 6-7(d): Nonlinear model response to pitch disturbance without feedforward.

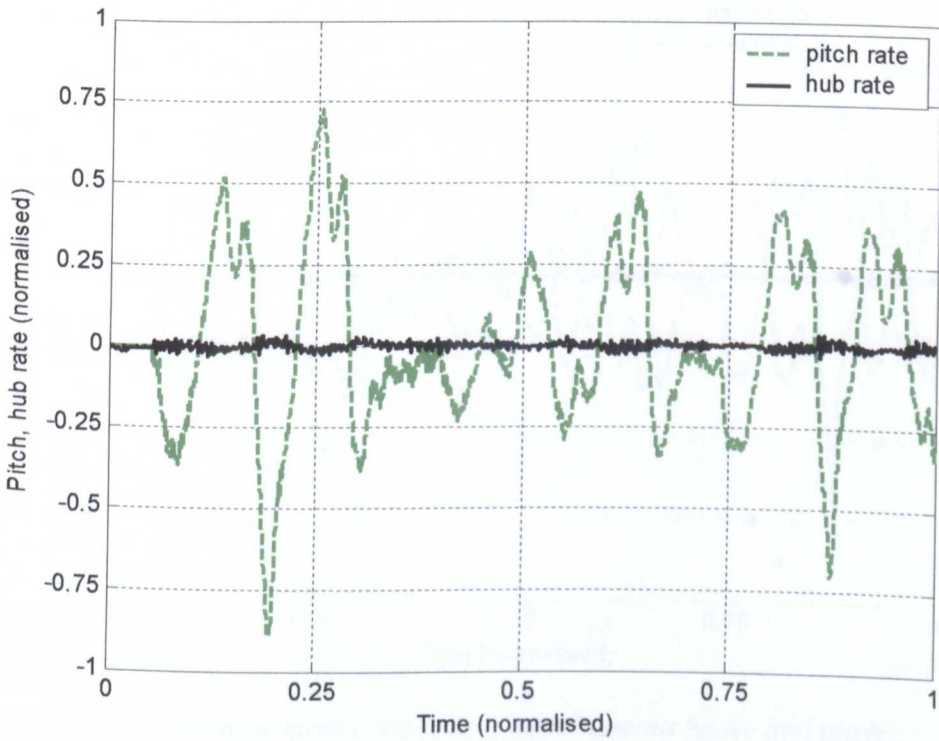


Figure 6-7(e): Nonlinear model response to angular disturbance with feedforward.

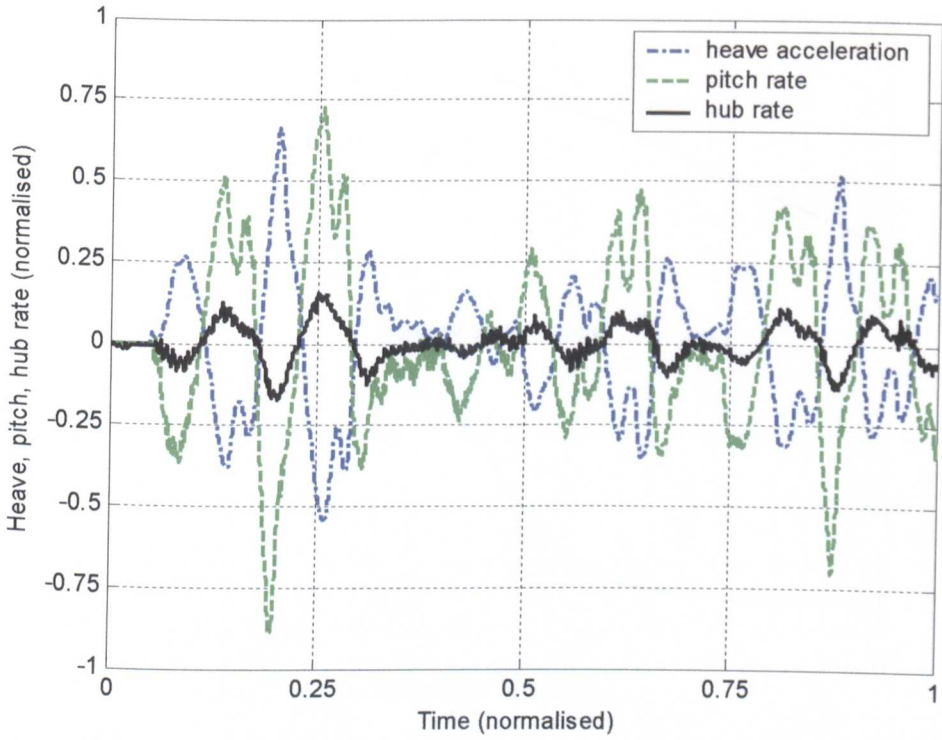


Figure 6-7(f): Nonlinear model response to simultaneous heave and pitch disturbances without feedforward control.

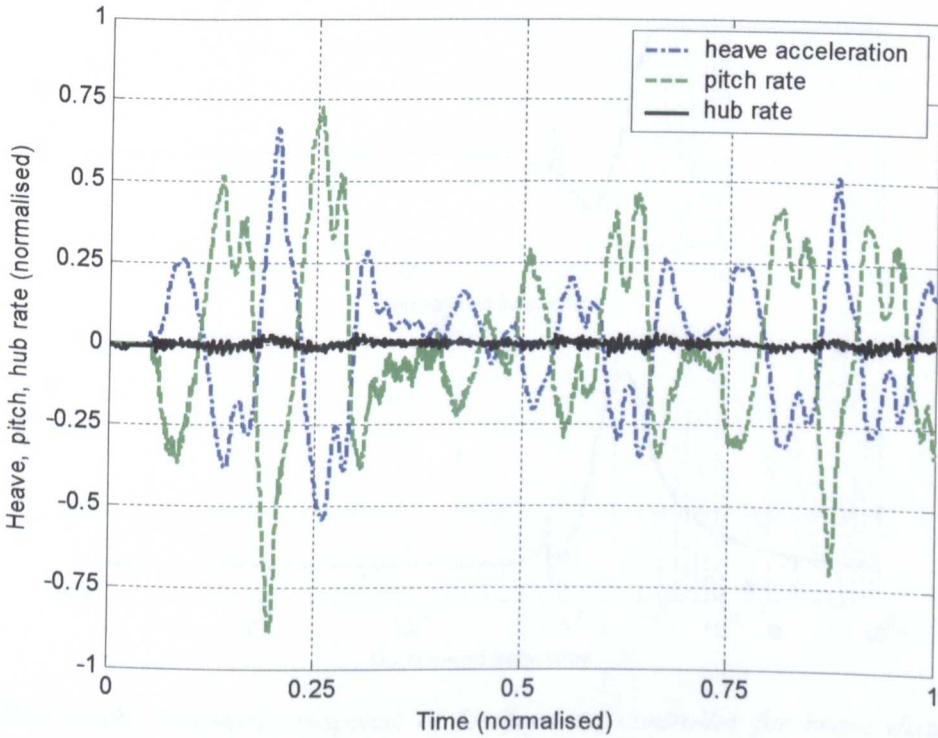


Figure 6-7(g): Nonlinear model response to simultaneous heave and pitch disturbances with feedforward control.

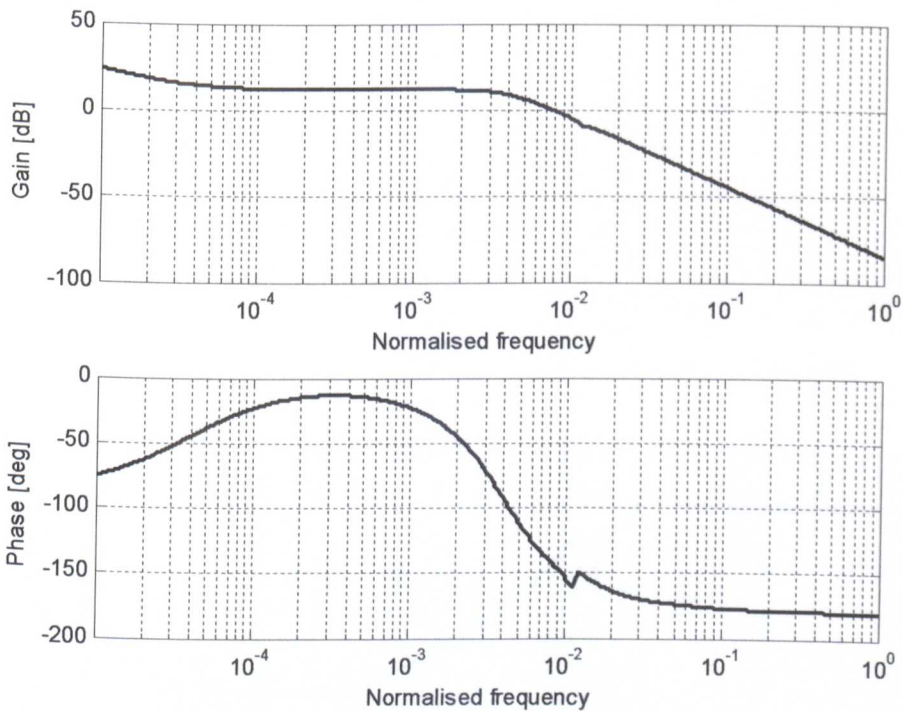


Figure 6-8(a): Frequency response of feedback controller designed using lump-parameter model which incorporates an integrator.

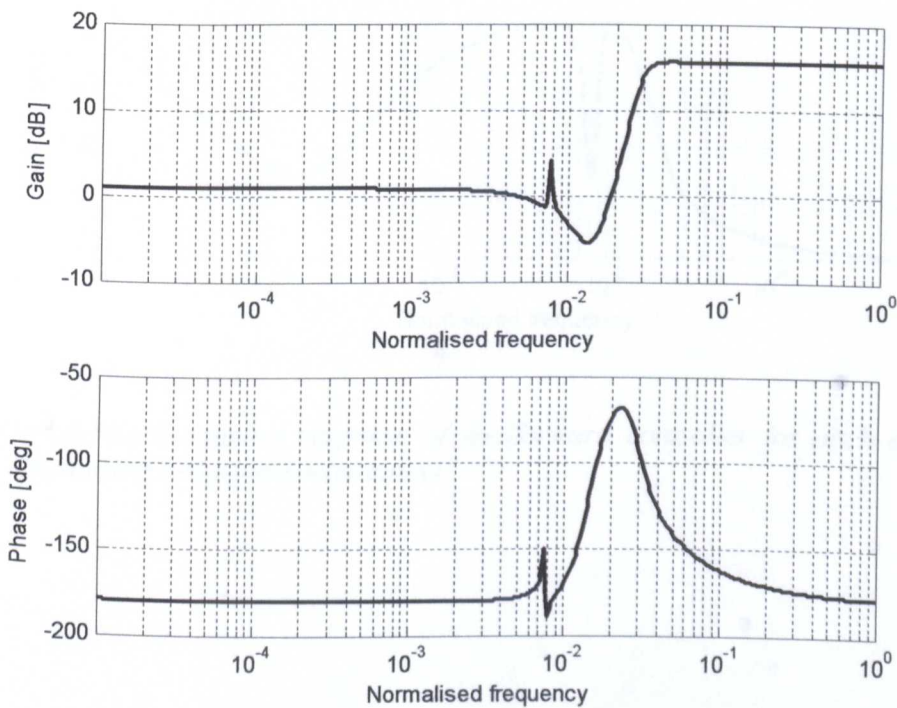


Figure 6-8(b): Frequency response of feedforward controller for heave disturbance designed using lump-parameter model.

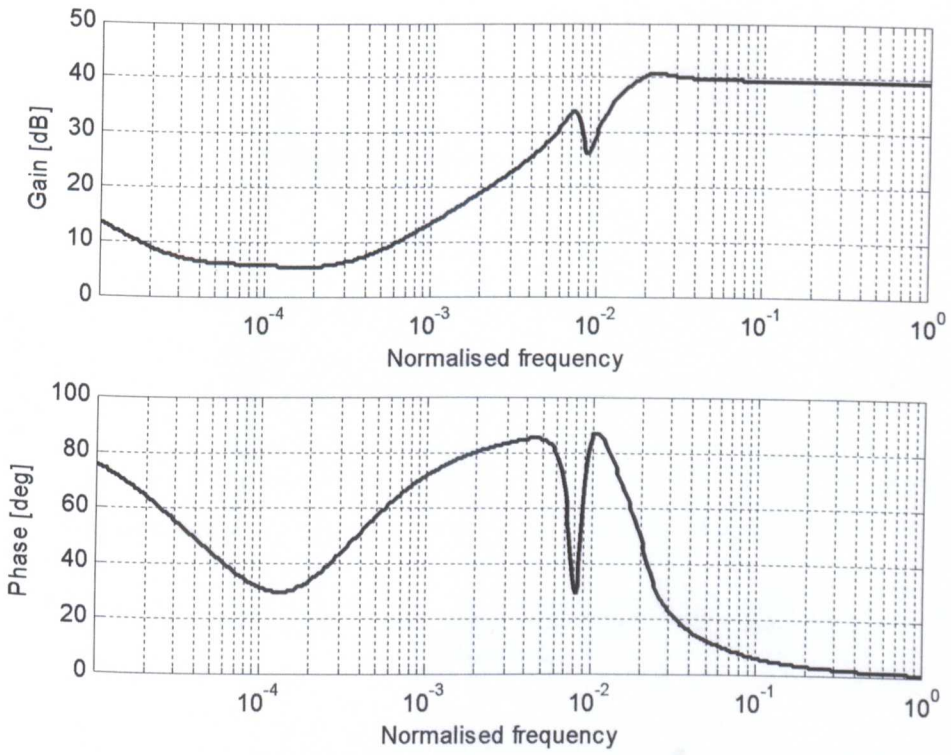


Figure 6-8(c): Frequency response of feedforward controller for pitch disturbance designed using lump-parameter model.

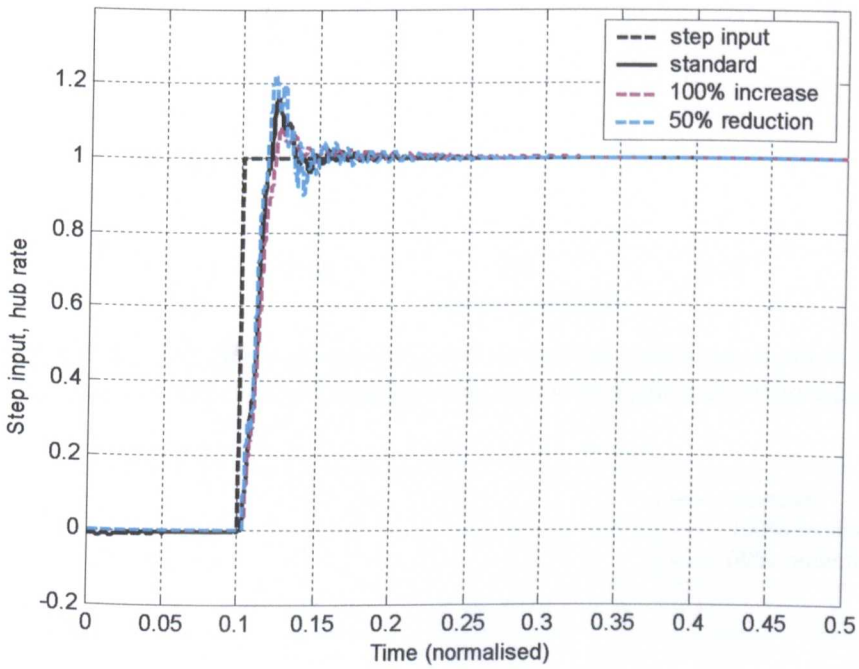


Figure 6-9(a): The effect of changing hub inertia on step response. (100% increase doubles the standard inertia and 50% reduction halves the inertia value)

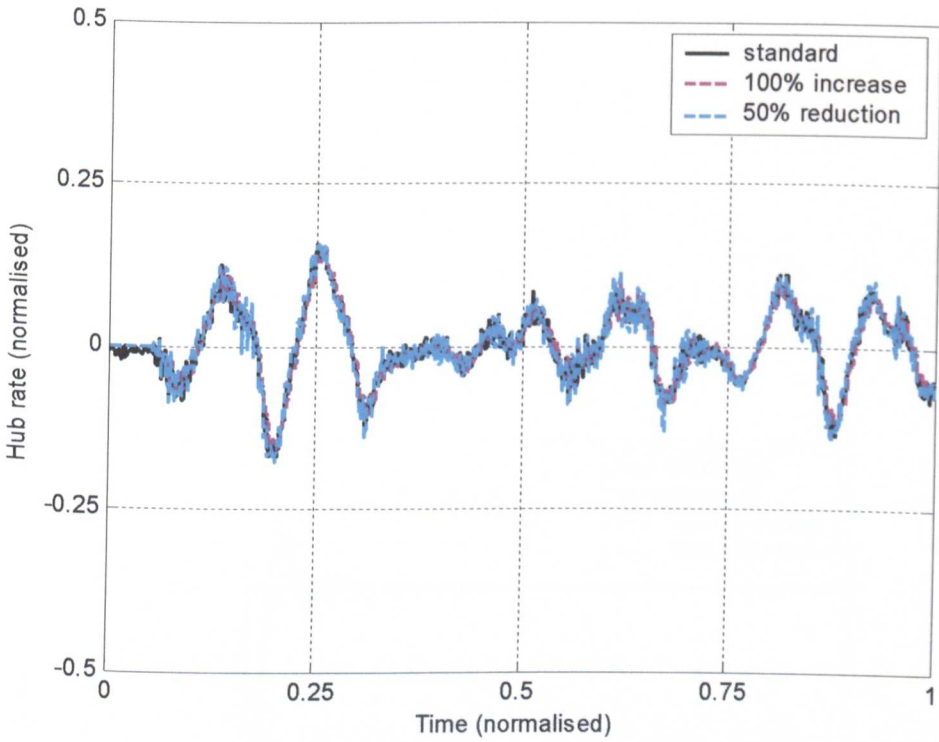


Figure 6-9(b): The effect of changing hub inertia on stabilisation performance without feedforward control (simultaneous heave and pitch disturbances).

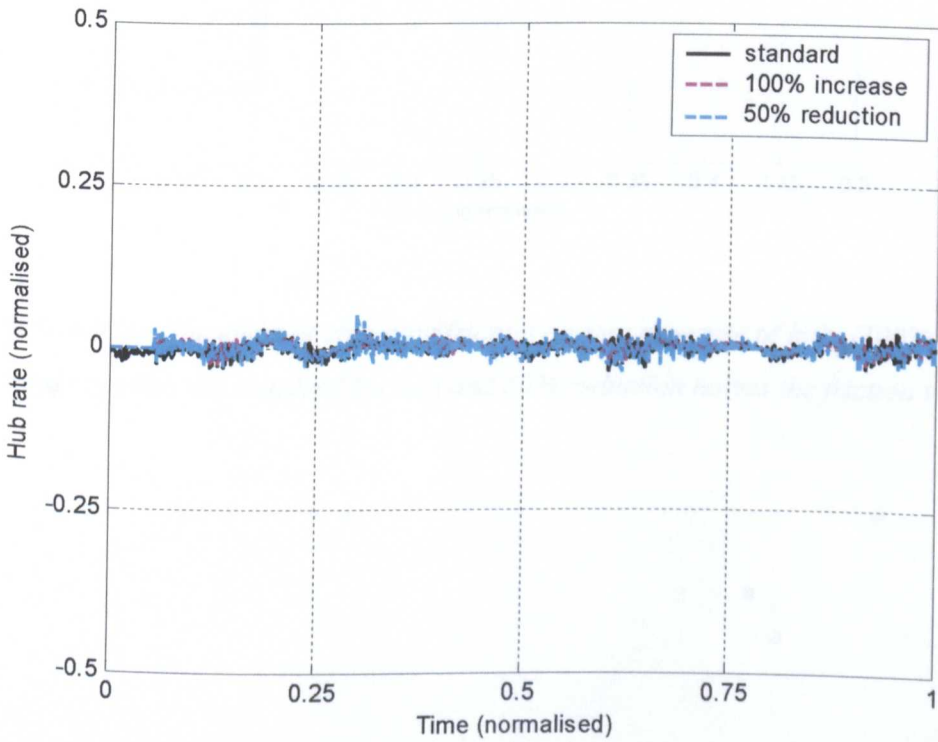


Figure 6-9(c): The effect of changing hub inertia on stabilisation performance with feedforward control (simultaneous heave and pitch disturbances).

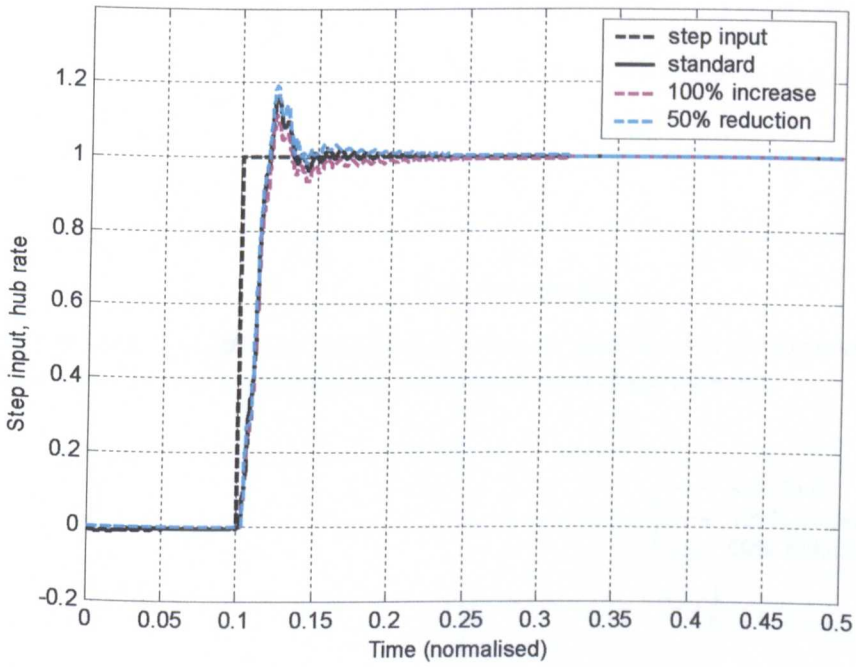


Figure 6-9(d): The effect of changing friction on step response of hub. (100% increase doubles the standard friction and 50% reduction halves the friction value)

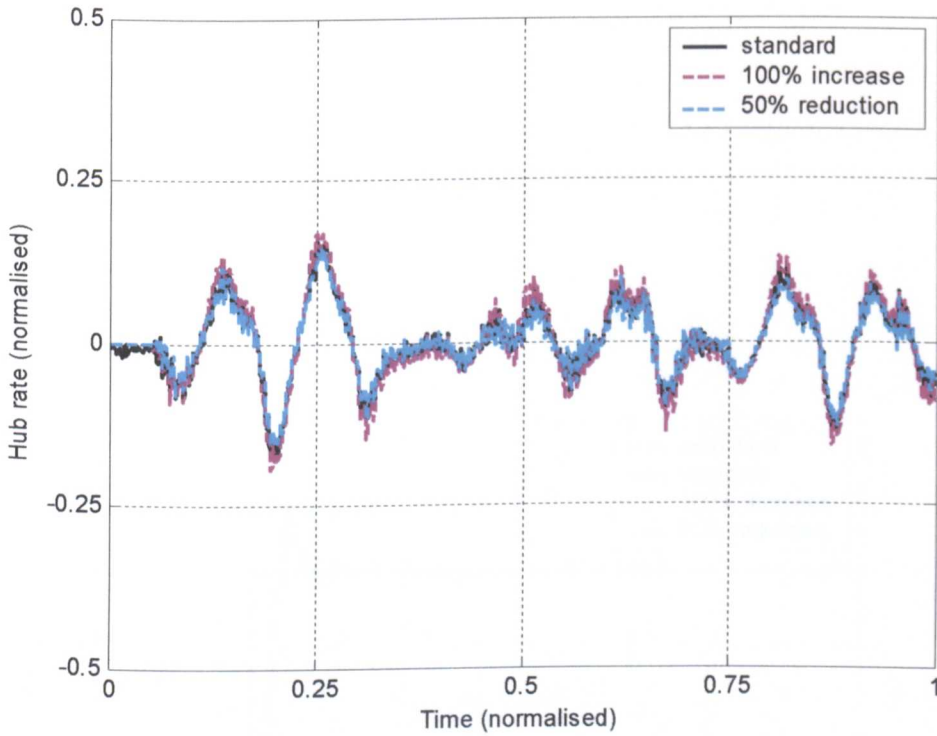


Figure 6-9(e): The effect of changing friction on stabilisation performance without feedforward control (simultaneous heave and pitch disturbances).

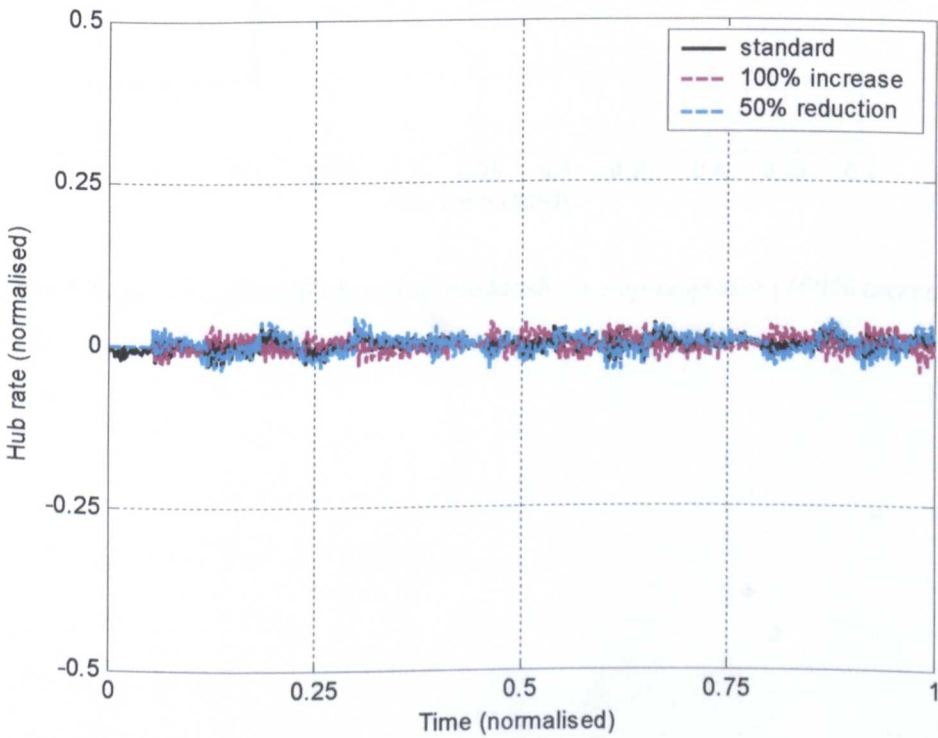


Figure 6-9(f): The effect of changing friction on stabilisation performance with feedforward control (simultaneous heave and pitch disturbances).

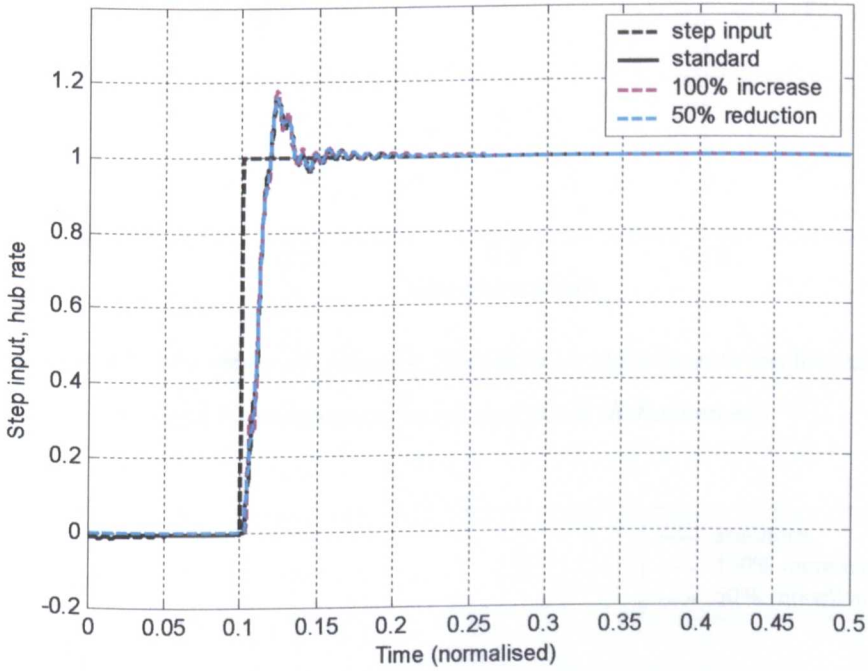


Figure 6-9(g): The effect of changing backlash on step response (100% increase doubles the standard backlash and 50% reduction halves the backlash value).

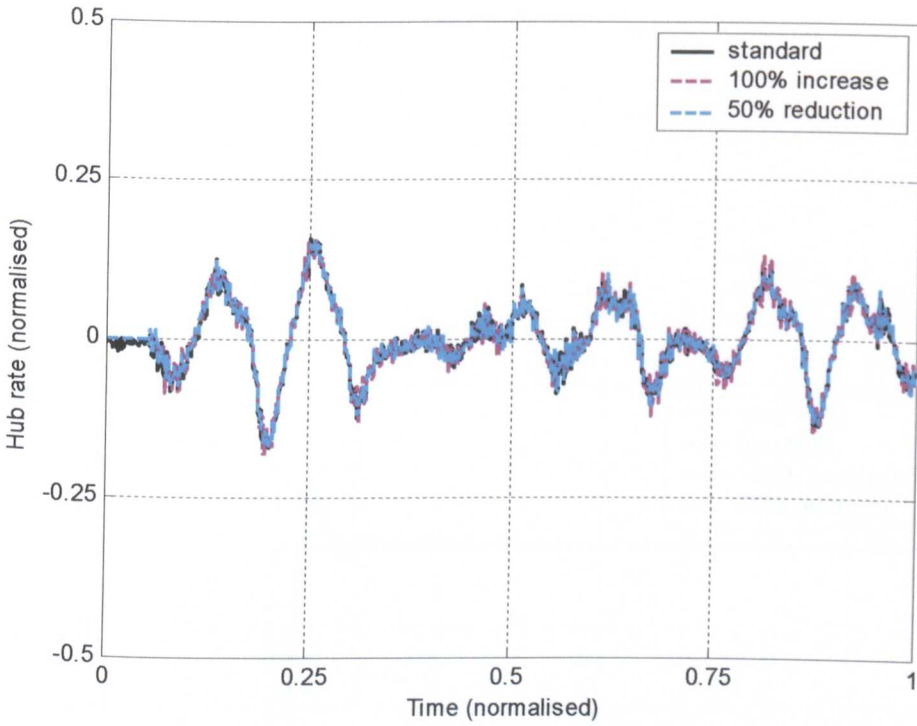


Figure 6-9(h): The effect of changing backlash on stabilisation performance without feedforward control (simultaneous heave and pitch disturbances).

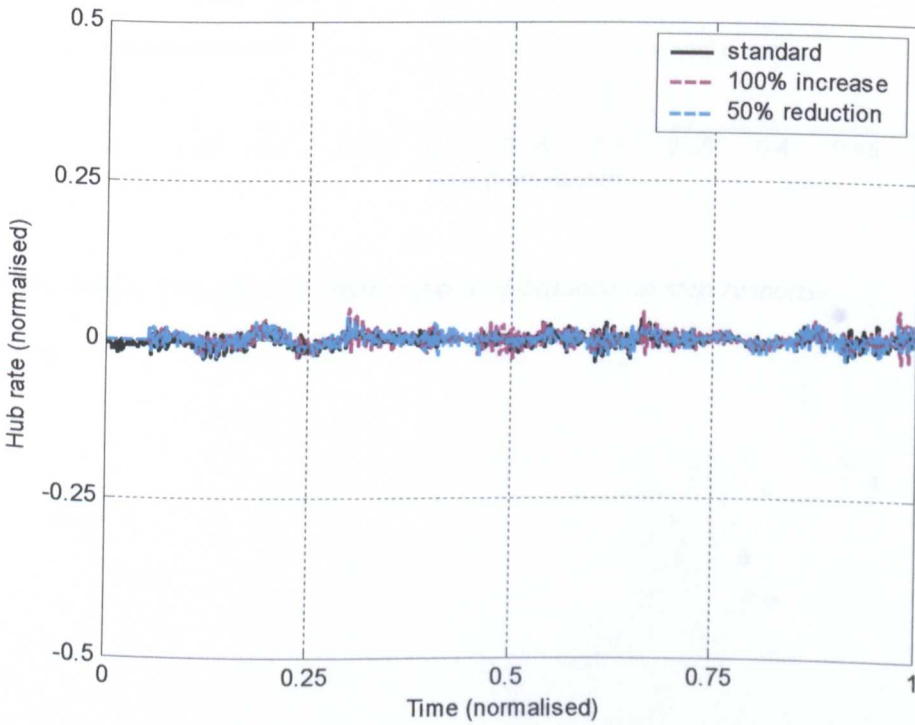


Figure 6-9(i) The effect of changing backlash on stabilisation performance with feedforward control (simultaneous heave and pitch disturbances).

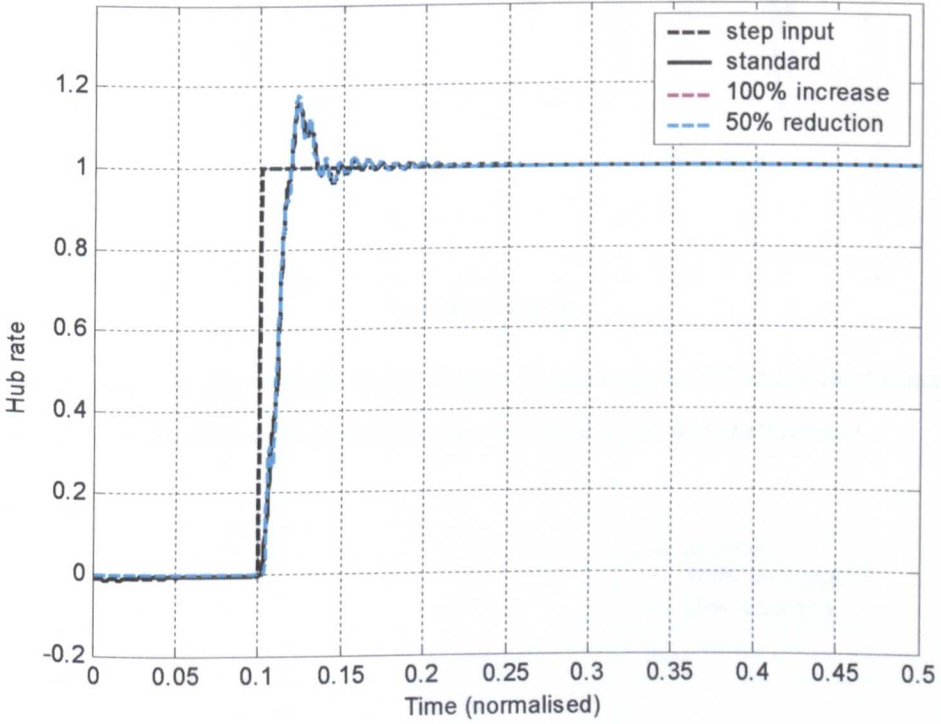


Figure 6-9(j): The effect of changing out-of-balance on step response

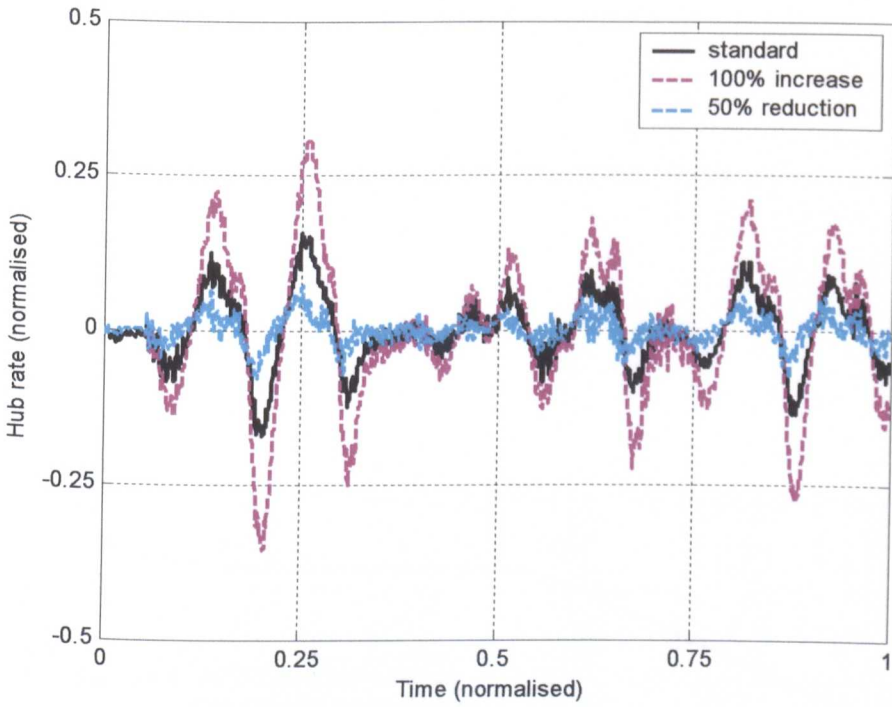


Figure 6-9(k): The effect of changing system balance on stabilisation performance without feedforward control (simultaneous heave and pitch disturbances)

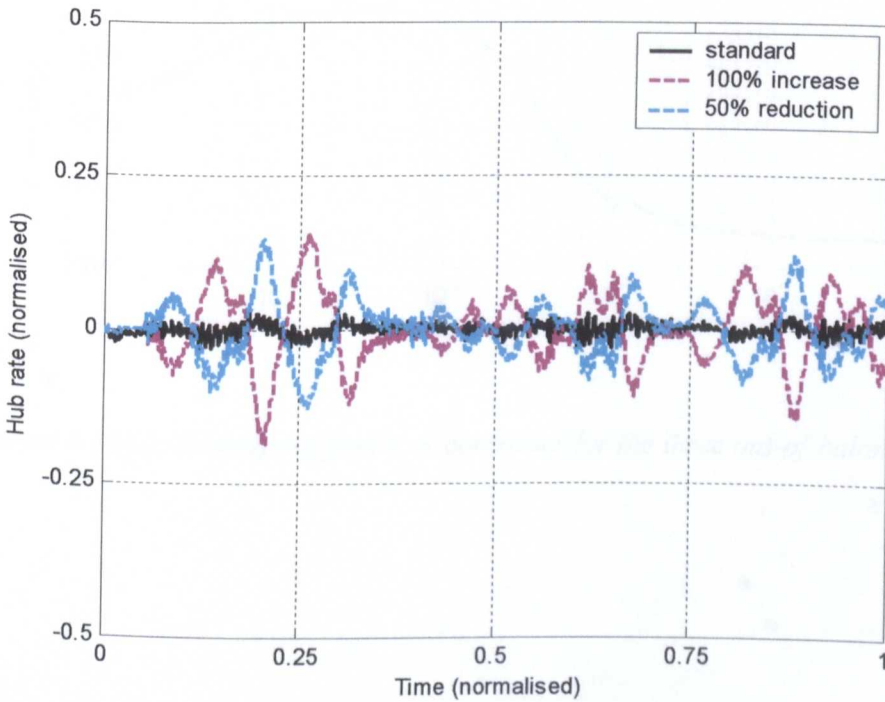


Figure 6-9(l): The effect of changing system balance on stabilisation performance with feedforward control (simultaneous heave and pitch disturbances)

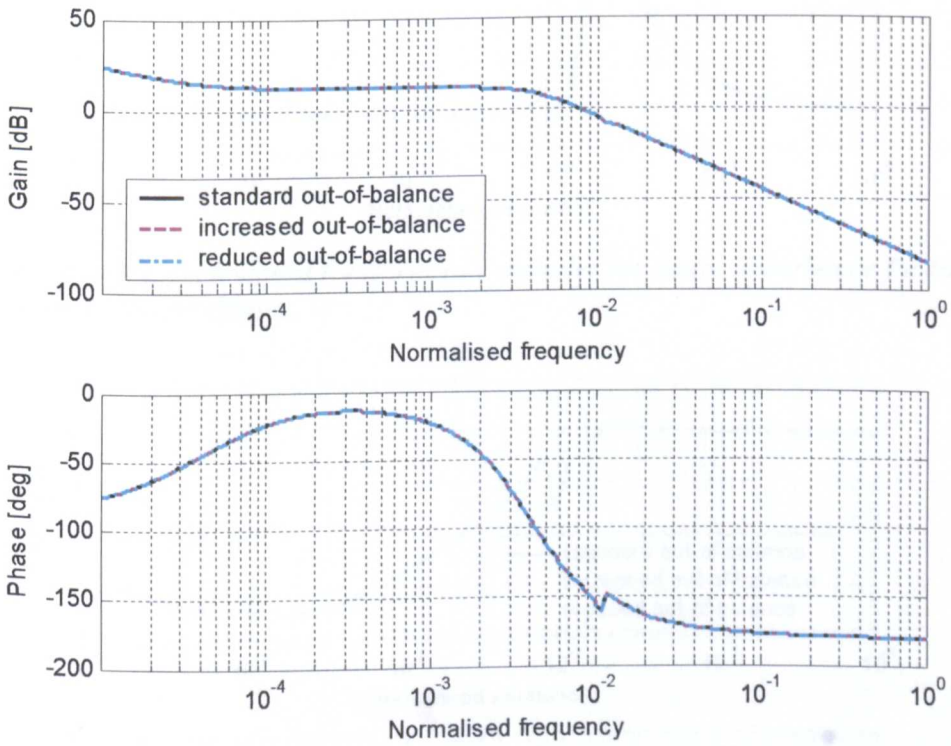


Figure 6-10(a): Redesigned feedback controller for the three out-of-balance cases.

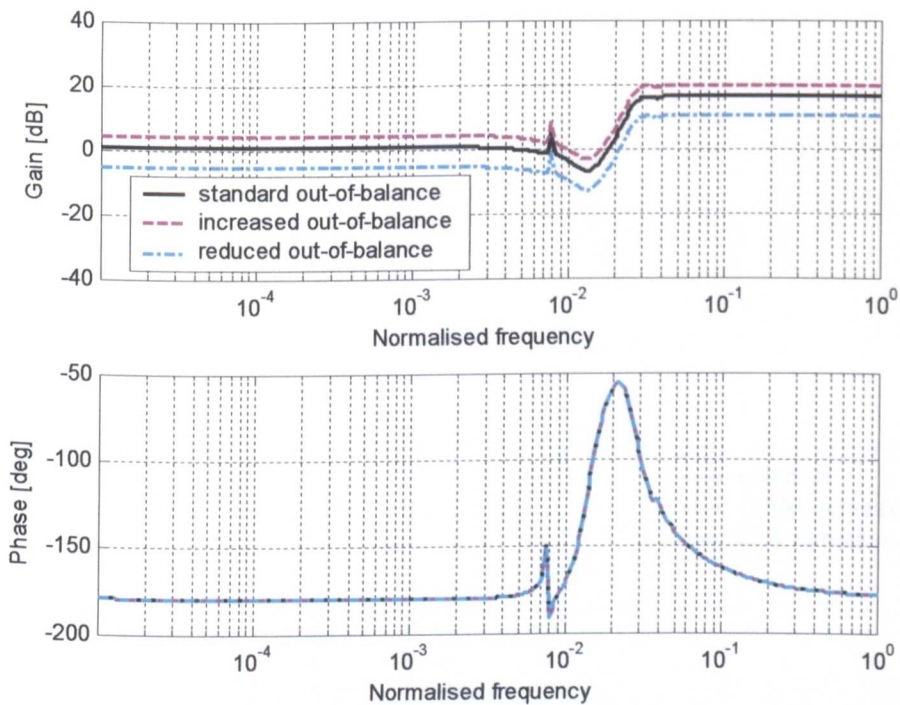


Figure 6-10(b): Redesigned feedforward controller for heave disturbance for the three out-of-balance cases.

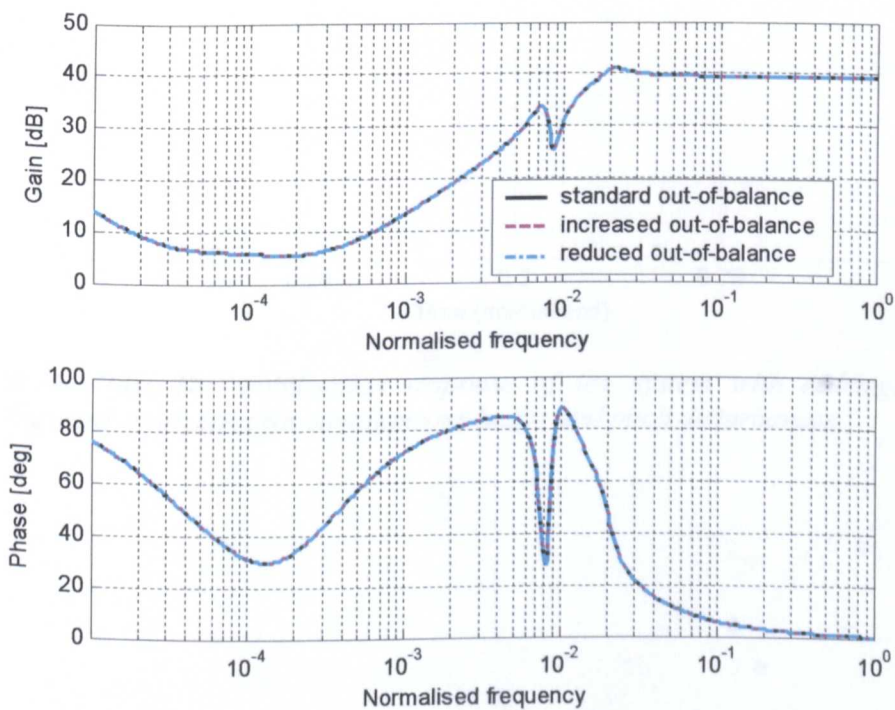


Figure 6-10(c): Redesigned feedforward controller for the angular disturbance for the three out-of-balance cases.

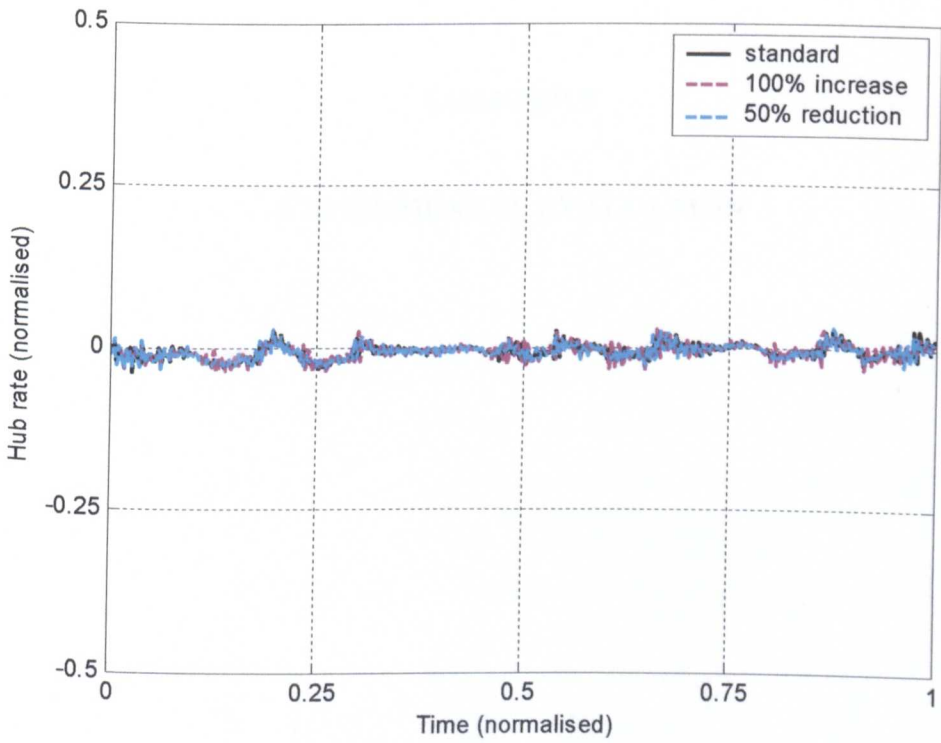


Figure6-10(d): The stabilisation response of the system with redesigned heave feedforward controllers for simultaneous heave and pitch disturbances.

CHAPTER 7

EXPERIMENTAL EVALUATION

7.0 Experimental evaluation

7.1 Introduction

In this chapter simulation outputs produced using the models developed in chapter 5 are compared with experimental results. A sound knowledge of system characteristics is of primary importance for controller selection and design if high performance electromechanical servo systems are to meet the desired objectives. Especially, detailed information regarding the linear, nonlinear, static and dynamic characteristics. To meet this requirement the chapter commences, in section 7.2, by examining the plant characteristics and validation of the plant model. The performance of several friction models are compared with measured results using a technique based on the input and output motions of the cantilever mechanism. The objective is to select the most appropriate friction model in terms of accuracy and speed. The work then progresses, section 7.3, to describe a novel identification technique used to determine the various nonlinear parameters of the system. The predicted and experimental results of the control system performance for the balanced and out-of-balance system are compared in section 7.4 followed by results of tests carried out to assess the robustness properties of the control system in section 7.5. In section 7.6 simulation results are presented for a control system which automatically adjusts the parameters of the feedforward controller to account for changes in system out-of-balance. The conclusions are presented in section 7.7.

7.2 Comparing performance of friction models with measured results

In Walrath's[17] work on stabilised airborne electro-optical pointing and tracking equipment the friction characteristics are obtained by adjusting the time constant of a dynamic friction model of a closed loop system. The base of the stabilised system is perturbed using a sinusoidal signal over a range of amplitudes (RMS speed) and frequencies. The time constant of the friction model is adjusted by observing the amplitude of the stabilised element until a minimum value is obtained. It is found that the time constant is inversely related to the RMS value of acceleration. It is further shown that a system incorporating the friction model is fairly robust to changes in the values of the time constant.

A more direct method is used in this research to obtain the friction characteristics based on measuring the frequency response between the platform and the cantilever mechanism. The main advantage of the method over that used by Walrath is that it does not require a closed loop system, and it does not assume structure of the friction model. The principles of the experimental method are shown in Figure 7-1(a). The response is obtained by mounting the rig on the Platform Motion Simulator (PMS). Sinusoidal signals at various speed amplitudes (RMS) over a range of frequencies are used as input to the PMS and the output signal is the response of the cantilever mechanism. Gyroscopes located on the platform and the hub measure the input disturbance and the output response. The phase and gain are generated by a frequency response analyzer (FRA). The limitations of the experimental setup are shown in Figure 7-1(b). In the cantilever mechanism as all the component masses (and their centre of gravity) are located along the longitudinal axis and the system is balanced in the vertical plane the effects of the horizontal and vertical translations are negligible or zero. The measured and simulation results presented in this section are for a balanced system configuration with the amplifier disconnected from the motor.

The measured results at several speed amplitudes over a range of frequencies are shown in the frequency response diagram in Figure 7-2. The corresponding simulation results for five friction models are shown in Figures 7-3 and 7-4, the static and dynamic friction models respectively. In the simulations the gain and phase are obtained using a model of the FRA enabling direct comparison with the measured results. All five models show good agreement with measured results for the two larger input amplitudes. At the larger input amplitudes the effects of pre-sliding displacements are less prominent than at lower amplitudes. However, the simulation results for the three smaller amplitudes show that the static models in Figure 7-3(a), (classical model) and Figure 7-3(b) (Tustin's model) compare poorly with measured results. At the smaller amplitudes the effects close to zero speed become more prominent.

Simulation results using dynamic friction models are illustrated in Figure 7-4(a), (b) and (c). The Dahl model illustrated in Figure 7-4(c) shows excellent agreement with measured results at all amplitudes and frequencies. The accuracy of the model is further confirmed by comparing the time domain results at selected frequencies and amplitudes shown in

Figure 7-5. The value of the rest stiffness parameter (σ) in the Dahl model is used to tune the simulation results to match the measured data and the value of exponent parameter and stabilizing factor are both set to 1 as described by Dahl[20],[21]. The results for the Haessig and Friedland's reset-integrator model[22] and the LuGre model[23] presented in Figure 7-4(a) and 7-4(b) show fair agreement with measured data at four amplitudes but both models show poor results for 0.083 amplitude at higher frequencies. Simulations which use the Dahl model run about 1.5 times faster than the reset-integrator model and about 3 times faster than the LuGre model. The results also confirm that, for this application, the time constant is related to the RMS value of speed and not the RMS value of acceleration as observed by Walrath. All the simulation results presented in this chapter use the Dahl model.

7.2.1 Combined friction models and their locations

In many studies, such as Haessig [22], a single friction model is used which is either located at the input (motor side) or the output (load side) of the gearbox. This simplification is not ideal as in high ratio gearboxes the speed at the input will be considerably different to that at the output. As a result the input shaft may be operating in a part of the friction characteristic which is different to that at the output shaft. Clearly in a gearbox each gear may be operating in different part of the friction characteristic. It is cumbersome and not practicable to include a friction model at each gear. An investigation is carried out using two friction models one located at the input and the other at the output to determine the most effective method of modelling the system. The ratio of the friction forces is varied between the two models such that zero percentage at input results in hundred percentage friction at the output and vice versa. A triangular wave input signal is applied to the closed loop system. The input signal, control signal and output signals are recorded. The results are illustrated in Figure 7-6(a) and (b). Figure 7-6 (b) shows the measured control signal plotted against the output signal. The simulation results for various combinations of the friction models are illustrated in Figures 7-7. The results with a single friction model, Figure 7-7(a) at input and Figure 7-7(b) at output, show poor agreement with the measured results presented in Figure 7-6(b). The results with friction divided equally, Figure 7-7(e), between the input and the output shows very good agreement with the measured results. However, for out-of-balance systems further

experimentation has shown that a ratio of 10-90% (motor-load) gives the most accurate results.

7.2.2 Comparing electro-mechanical system (plant model) response

Frequency-domain response of the plant

The above section is primarily concerned with modelling of friction and validation of the mechanical system. For control system design the characteristics of the electro-mechanical plant are required. The frequency responses of the plant are measured by applying an input voltage at the amplifier and output rate is measured by a gyroscope located at the hub. The experimental and simulation results are presented in Figure 7-8(a) and (b) respectively. The tests are carried out at four input amplitudes to gain insight into the nonlinear behaviour of the system. The simulation results obtained using a model FRA show reasonable agreement with the measured data and confirm the amplitude dependent nonlinear behaviour of the system.

Time-domain response of the plant

Figure 7-9 shows the response of the plant to step demands. As the total travel of the structure is limited to +15 and -15 degrees the input to the system is controlled manually, indicated by the variable time step. Simulation results are generated using the same input data as that used on the rig. In general the simulation results show good agreement with the measured data.

7.3 Identification of nonlinear parameters

The identification of the nonlinear parameters is based on the technique described by Johnson and Lorenz[27]. Unlike their work, which uses a three term controller, the technique presented in this chapter is applied directly to the H_2 controlled closed-loop system with the primary aim of identifying the friction parameters, out-of-balance torque and amplifier nonlinearities.

As the controller is designed for the out-of-balance case the identification process is first described for this system. A triangular wave input signal is applied to the closed-loop system and the angular rate of the hub and controller output voltages are measured. Figure 7-10(a) compares the measured and the simulation results for the system without nonlinear compensation. Both the controller output signal, the top part of the figure, and the hub rate, which is the gyroscope signal are shown in volts. For clarity the triangular input signal is not shown. In the graph the simulation results are shown in blue and cyan and the measured data in red and magenta.

The nonlinear characteristics of the plant are more clearly defined by plotting the controller output voltage against the hub rate as shown in Figure 7-10(b). In these graphs the offset voltage is the measure of the out-of-balance torque. The discontinuity at zero hub rate is a measure of the total Coulomb friction and stiction. The gradient of the two lobes either side of zero speed is due to combined value of the viscous friction and any other effects proportional to the speed. The width of the loop ΔV voltage is proportional to the inertia of the system.

The nonlinear observer used in this example employs a Dahl friction model which is implemented as a feedback observer but a feedforward observer also produces similar results. Figure 7-10(c) compares the response of the original system with the response of the system which incorporates friction and out-of-balance compensation. The response of the system on time axis is illustrated in Figure 7-10(d) which can be compared directly with Figure 7-10(a), the original system without compensation. The most noticeable features are the elimination of discontinuity at zero crossing in the hub rate and the offset in the controller signal.

In all the results the experimental and the simulation data show fair agreement, however the measured results show additional minor oscillations which are not present in the simulation outputs. These oscillations, also seen in Figure 7-6, are due to experimental noise and higher order effects. Similar oscillations are noted by Dahl [21], which experimental work has shown to be caused by worn bearing surfaces.

7.3.1. Identification of nonlinear gain of the amplifier

Amplifiers used in servo drive systems are generally assumed to have linear characteristics. However, the amplifier used in this research has nonlinear characteristics which change with amplitude of the input voltage. The measured nonlinear characteristics of the amplifier, together with the linear gain are illustrated in Figure 7-11. The nonlinear characteristics are obtained by locking the cantilever mechanism to the platform so that the motor is stalled. Voltage is applied to the amplifier and the output current measured using a Hall-effect current probe. The results show that the system is nonlinear at low input voltages, at intermediate voltages the gain approaches the ideal linear characteristics and at high inputs it follows the ideal characteristics as defined by the manufacturers.

By extending the method described above it will be shown the nonlinear characteristics of the amplifier can be extracted from the measured results without the need to carry out specific tests on the amplifier. The results for a balanced system are shown in Figure 7-12(a) which compares the measured data with simulation results for a system with a linear gain amplifier. In Figure 7-12(b), the controller output voltage is plotted against speed which gives clearer indication of the discrepancy between the measured and simulation results.

As a first estimate assume that measured and simulation hub rates, red and blue lines, and accelerations, gradient of the two lines, are approximately equal - a reasonable first assumption from Figure 7-12(a) if the transients near zero speed are ignored. As the speed and the accelerations are approximately equal, then the resulting torques due to speed such as viscous friction, and inertial torque due to acceleration will be approximately equal. The torque produced at the motor for both cases is therefore approximately equal, and therefore the current into the motor is also approximately equal for the two cases.

For any selected speed the differences in the controller output voltage between the measured (magenta) and simulation results (cyan) are therefore due to the nonlinear gain of the amplifier. The controller output voltage is the input signal to the amplifier. Using the linear amplifier characteristic in Figure 7-11, amplifier current can be obtained for any input voltage. Table 7-1 below shows errors at selected points for the balanced system.

Time (s)	Measured (volts)	Simulation (volts) linear amplifier	Amplifier (amps)
1.85	0.32	0.25	0.75
2.0	0.42	0.28	0.84
2.25	0.51	0.32	0.96
2.4	0.54	0.35	1.05
2.5	0.57	0.36	1.08
2.55	0.59	0.375	1.125
2.7	0.44	0.27	0.81
2.8	0.38	0.24	0.72
2.95	0.34	0.23	0.69
3.15	0.28	0.2	0.6
3.4	0.22	0.16	0.48
3.7	0.12	0.09	0.27

Table 7-1: Summary of data for amplifier for the balanced system

The next set of points can be obtained in a similar manner for a different out-of-balance case. As an illustration simulation results are used for an out-of-balance case midpoint between the balanced and default out-of-balance. Simulation results for the linear and nonlinear amplifier are shown in Figure 7-12(c) and (d) and selected points are provided in Table 7-2 below.

Time (s)	Simulation(volts) nonlinear amplifier	Simulation (volts) linear amplifier	Amplifier (amps)
1.85	1.24	1.14	3.42
1.95	1.27	1.18	3.54
2.0	1.275	1.19	3.57
2.1	1.29	1.21	3.63
2.25	1.32	1.24	3.72
2.4	1.34	1.27	3.81
2.5	1.24	1.15	3.45
2.65	1.22	1.13	3.39
2.8	1.20	1.1	3.3
3.0	1.17	1.05	3.15
3.2	1.135	1.02	3.06
3.3	1.12	1.0	3
3.4	1.04	0.93	2.79
3.75	0.53	0.32	0.96
3.8	0.49	0.3	0.9
4.0	0.4	0.25	0.75

Table 7-2: Summary of data for amplifier for midpoint out-of-balance system

In the default out-of-balance case the results for the linear amplifier are very close to the measured results as shown in Figure 7-10(a) and (b) indicating that the amplifier gain is linear. Figure 7-11 shows the correction in the amplifier gain after the first iteration, marked with + symbol. The results show close agreement with the measured amplifier characteristics. The process can be repeated again if necessary until the simulation results match the measured data. Figure 7-12(e) and (f) compare the simulation results using the nonlinear gain amplifier model with measured response for the balanced system. Comparing these with the linear amplifier results, Figures 7-12(a) and (b), shows the marked improvements in the simulation results with close agreement with measured results.

7.4 Comparing the performance of balanced and out-of-balance systems

In this section the performance of the balanced and out-of-balance system are compared in both frequency and time domain. The response of the systems to input demand signals is assessed and then the ability of the control systems to reject external disturbances is established. The results are presented in graphical form which can be readily assimilated rather than summarised as a list of numbers in tabulated form. Performance criteria such as overshoot, rise time steady state errors, bandwidth, damping etc. can be readily obtained by inspection of the graphs.

7.4.1 Response of the system to input demand signals

Frequency-domain response of the closed-loop system

There are some control systems which have peculiar requirements but in general control systems have to provide fast response, short settling time and good steady state performance. The system should provide a linear response to input demand signals, a bandwidth which covers the expected range of external disturbance frequencies and a roll-off rate to reject high frequency resonances and noise. Frequency responses of the closed-loop out-of-balanced system, which incorporates the nonlinear observer, are presented in Figure 7-13(a) and (b), the experimental and simulation results respectively. The system shows a damped response with a bandwidth of 0.1, normalised frequency, which exceeds

the range of disturbance frequencies, illustrated in the PSD Figure 4.7. The system shows a linear response to input demand signals. The simulation results show good agreement with the measured results up to the system bandwidth, but beyond this frequency they do not correspond as well but generally show similar behaviour with roll-off rate. The measured results show two lightly damped resonances which are not as well defined in the simulation results.

The above results show the response of the system which incorporates the nonlinear observer. The results for the out-of-balance system without the nonlinear observer are illustrated in the Figures 7-13(c) and (d), measured and simulation respectively, which show the marked improvements provided by the observer, shown in Figure 7-13(a) and 7-13(b). The improvements in system performance provided by the nonlinear observer are more clearly demonstrated in the time domain results presented in the next section. The responses of the balance system are shown in Figure 7-13(e) and (f). The simulation results for the balanced system, while similar, show greater variation when compared with the measured results. The variation is particularly noticeable for the lowest input amplitudes.

The measured responses for the balanced and out-of-balance systems, Figure 7-13(a) and (e) show similar bandwidth and damped responses. Within experimental variations the close agreement between the two measured responses confirms that the feedback controller is robust to large changes in amplifier gain, 2 amps/volt for the balanced compared to 3 amps/volt for the out-of-balance system, and changes in system inertia. In the balanced case the inertia is increased to 133%, as a result of adding masses at the hub to balance the system.

Time-domain response of the closed-loop system

The closed-loop step responses of the out-of-balance system are shown in Figure 7-14(a) and (b). The response of the system without nonlinear observer, Figure 7-14(a), shows a slow response which takes about 0.05 time (normalized) to reach steady-state. Figure 7-14(b) shows the improvements in the system response when a nonlinear observer is

incorporated in the control system design. The corresponding results for the balanced system are shown in Figure 7-14(c) and (d).

Comparing the closed loop results of the balanced and out-of-balance system, the step responses show very similar performance. The overshoot in both cases is similar—marginally higher for balanced system which also shows lower damping which results in settling time which is marginally longer for the balanced system. The steady state performance is the same for both systems. The results confirm the robustness properties of the feedback controller which is able to cope with changes in amplifier gain and system inertia. The changes in amplifier gain, described in section 7.3.1, are illustrated in Figure 7-11. The responses of the system to triangular wave inputs, are discussed in section 7.3 and illustrated in Figures 7-10 and 7-12.

7.4.2 Response of cantilever mechanism to external disturbance (stabilisation)

This section presents the results of the study carried out to compare the stabilisation performance of the balanced and out-of-balance system. The time-domain responses of the system to external disturbances are obtained using PMS which is controlled using measured data from field trials as described in section 4. To recap the stabilisation performance, sometimes referred to as disturbance rejection, is the ratio of the output divided by the input. The output is the motion of the cantilever mechanism and the input is the disturbance or the motion of the PMS. For good stabilisation a low value for disturbance rejection ratio is required. Time and frequency domain results are presented and compared for the two systems.

Out-of-balance system

Predicted and measured responses for the out-of-balance case are presented in Figures 7-15(a) to (d). In these Figures the hub responses are presented along side motions of the platform to provide a visual illustration of the ability controllers to isolate the system from external disturbances. Both the simulation and measured results show that feedback control, Figures 7-15(a) and (c), is fairly effective at rejecting the external disturbances but substantial improvements are provided by feedforward control as illustrated in Figures 7-

15(b) and (d). The simulation results compare favourably with the measured results when closer examination is undertaken as in Figures 7-15(e) and (f) which show the motions of the hub. In these figures the simulation start time and the finish time does not correspond exactly with the measured results. The simulation results, top graph in Figures 7-15(e) and (f), show similar trends as the measured data but as in other results the measured data contains high frequency experimental noise. The simulation results show some high amplitude peaks which are not present in the measured results.

The disturbance rejection response, obtained from the time domain results, for the feedback controller and the feedforward controllers are shown in Figure 7-15(g) and (h) respectively. In both the measured and simulation results the improvements in system performance due to the feedforward control are clearly demonstrated. The simulation results with the feedforward controller, Figure 7-15(h) show better stabilisation than the measured results. The differences are not as marked in the time domain results shown in Figure 7-15(f).

Balanced system

The performance of the controller, designed for the out-of-balance system, when used on a balanced system is presented in Figures 7-16(a) to (i). Figures 7-16(a) to (c) show the simulation results for the system

- without feedforward
- with both feedforwards
- pitch feedforward only

Pitch feedforward, Figure 7-16(c), improves the stabilisation when compared to the feedback controller, Figure 7-16(a). While the introduction of both heave and pitch feedforward controllers reduce the stabilisation as illustrated in Figure 7-16(b). The simulation results show good agreement with the measured results for the three cases as illustrated in the detailed examination in Figures 7-16(d) to (f). The corresponding overall frequency response results, generated using time-domain data, are illustrated in Figure 7-16(g) to (i). In general the simulation results for the balanced system are in closer agreement with the measured responses than the out-of-balance system.

Comparing the balanced system stabilisation, Figures 7-16(i) with the out-of-balance stabilisation, Figure 7-15(h) shows that the out-balance system provides better stabilisation than the balanced system. This may be due to increased inertia of the balanced system (133% of out-of-balance system), due to lower amplifier gain (33% lower than out-of-balance system) or due to system backlash. The out-of-balance torque preloads the gears reducing the effects of backlash as discussed in section 7.5.

7.5 Testing robustness properties of the control system

Tests are carried out to assess the variation in system stabilisation due to changes in mechanical parameters. Besides the change in system balance and amplifier gain described above three other parameters are changed. Variations in the parameters studied may occur due to operating conditions, environmental changes, wear, aging, duty cycles or due to maintenance schedules etc. The changes in system performance are assessed using the frequency-domain tests which are summarised on a single graph, by comparing the performance at one input amplitude which has normalised amplitude of 0.333. The tests are carried out on the out-of-balance system where the amplifier gain is linear.

Variation in system backlash

In addition to the default backlash value used in the above studies the backlash tests are carried out at three other settings. The measured and simulation results are presented in Figures 7-17(a) and (b). In both results the backlash has little effect on system stabilisation. In an out-of-balance system the static torque due to gravitational acceleration preloads the system so that the gears are forced to one end of the backlash region. In the stabilisation tests carried out the forces and torques acting on the system are unable to overcome these preload forces. As a result the gears maintain contact and the system behaves as if there is zero backlash. Preloading of systems components is often used to negate the effects of backlash in mechanical systems as described by Black *et al.* [93].

Variation in hub inertia

The inertia of the system was increased in three steps. The simulation and the measured results are illustrated in Figures 7-17(c) and (d). The inertia values used in the tests have

little effect on the stabilisation. The magnitude of the inertia changes which represent the typical changes in a system under consideration were not sufficient to effect the system performance.

Variation in friction

Tests are carried out to assess the effects of changing friction on system stabilisation. Friction is changed using a disc brake mounted close to the hub bearing on the main shaft. Variations in friction are obtained by adjusting the pressure in a pneumatic actuator which operates the calipers acting on the disc. The graph of friction torque verses the pressure provided by the manufacturers is shown in Figure 4-4 and the details of the mechanical arrangement are discussed in chapter 4. As precise friction characteristics for the disc brake are not available changes in Coulomb friction values at the hub bearing are used in the simulations to model the disc brake. The experimental and simulation results, Figure 7-17(e) and (f), show that increasing friction reduces system stabilisation. In the measured results the first increase in friction value, 50 Nm, shows similar performance to the default case. This may be due to the characteristics of the disk brake not being as precise as suggested by the manufacturers at low input pressures. At other values the simulation results compare fairly with the measured results.

7.6 Adapting to changes in out-of-balance

The results presented in section 6 and section 7.5 show that the stabilisation performance is sensitive to changes in friction and to changes in system out-of-balance. Several papers discussed in section 2 present techniques which can be used to overcome the loss in performance due to changes in friction parameters. In this section a technique is presented which adjusts control system parameters to maintain stabilisation performance in presence of changes to system out-of-balance. In chapter 6 it was shown that the gain of the feedforward controller is related to system out-of-balance. In the iterative parameter identification technique presented in section 7.3 it shown that the control signal contains information about the system out-of-balance. This control signal is used to estimate the magnitude of the out-of-balance which is incorporated in the adjustment mechanism for the heave feedforward controller. The adjustment of the feedforward controller can be

carried out manually, continually (such as every second), or automatically on detection of change in out-of-balance or loss in stabilisation performance. The results presented in this section consider abrupt changes in out-of-balance such as those which may occur due to different weight of components picked-up by robots, changes in camera systems installed or ammunition natures used in gun system, etcetera.

To demonstrate the adaptive process in operation first consider a system with linear amplifier characteristics. Figure 7-18(a) shows various signals for the default out-of-balance system. The magnitude of out-of-balance is estimated by taking the average value of the control signal over a set period. Acceptable results are obtained when the estimation period is set at 0.03 time (normalized) as it provides a fast response and a fairly reliable estimate of the out-of-balance. In Figure 7-18(b) a step change in out-of-balance is introduced at 0.3 time(normalized) shown in the trace (i). Trace (ii) shows the estimated out-of-balance value, which has a delay, of 0.03 time(normalized), while the estimation process is in progress. The variation in the control signal due to out-of-balance change is shown in trace (iv) and the subsequent degradation in stabilisation performance, hub rate gyro, is shown in trace (v). Trace (iii) shows the controller update signal, which is not used in case.

Figure 7-18(c), shows the same system but with the controller updated at 0.7 time(normalized), as shown in trace (iii). The immediate improvement in hub rate performance is seen in trace (v), the hub rate gyro signal. The performance after the controller is updated is very similar to the system shown in Figure 7-18(a) when no change in out-of-balance occurs. In Figure 7-18(d) the controller update starts at 0.03 time(normalized). As in the previous case the system shows improvement in system performance which is similar to that in Figure 7-18(a), the default out-of-balance. A deterioration in hub rate is noted at 0.3 time(normalized) during the estimation.

The effectiveness of the adaptive system is demonstrated in a system which experiences several changes, increase and decrease, in system out-of-balance. The degradation in system stabilisation due to step changes in out-of-balance is illustrated in Figure 7-18(e). The adaptive control system restores the system stabilisation to original levels as shown in Figure 7-18(f).

The effect of nonlinear amplifier gain on adaptation process

In the above example linear amplifier gain is used. The effects on the system performance due to nonlinear amplifier gain are investigated and the results are illustrated in Figures 7-18(g) and 7-18(h). These Figures can be compared directly with the corresponding, linear amplifier gain results in Figures 7-18(d) and 7-18(f). A slight deterioration in performance is noted in Figure 7-18(h) when the out-of-balance is at its lowest value. This is due to slight variation in the estimate of the out-of-balance, but in general the system operates satisfactorily providing significant improvement over the system without adaptation as observed by comparing with Figures 7-18(b) and 7-18(e).

7.7 Concluding remarks

In chapter 7 theoretical results from simulation studies are compared with experimental data. The measured stabilisation response of the cantilever mechanism is obtained by mounting the system on a platform motion simulator and perturbing it over a range of frequencies and speed amplitudes, for frequency domain results, and for time domain results measured data from field trials is used to drive the simulator. A detailed comparison of the performance of balanced systems and out-of-balance systems is presented and in general the simulation results show reasonable agreement with the measured results. The performance of several friction models is compared with test data in the frequency domain and wide variations in the accuracy and performance (simulation speed) of the models is observed. A novel experimental technique developed for identifying friction parameters is used to determine the magnitude of the out-of-balance and is modified to obtain the nonlinear gain characteristics of the amplifier. The results of robustness study show that the system is sensitive to changes in friction parameters and system out-of-balance. An adaptive technique is presented which automatically adjusts the controller parameters to maintain stabilisation performance when changes in system out-of-balance occur.

FIGURES CHAPTER 7

EXPERIMENTAL EVALUATION

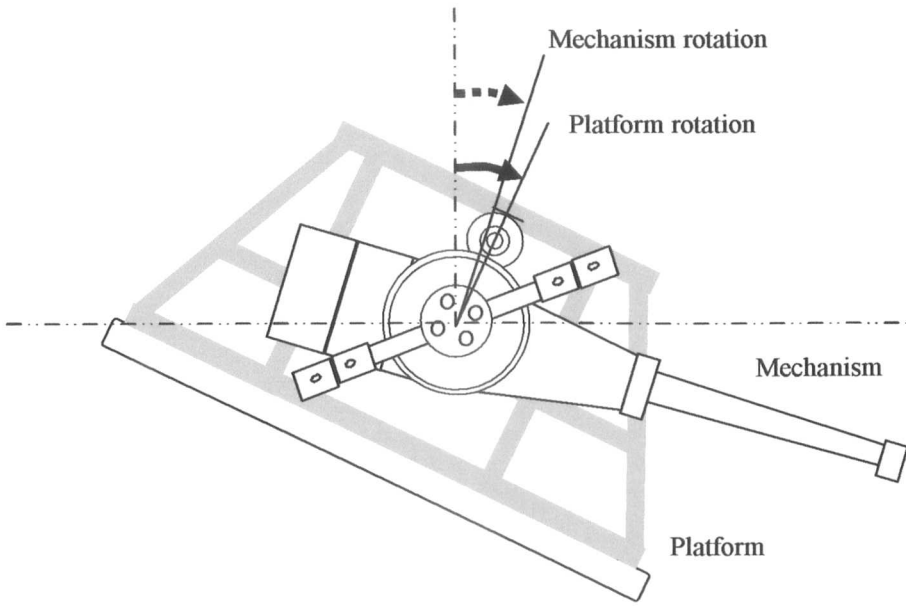


Figure 7-1(a): The rotation of the platform and the cantilever mechanism. The rotational centres of the PMS and the cantilever mechanism coincide with each other. (Not to scale)

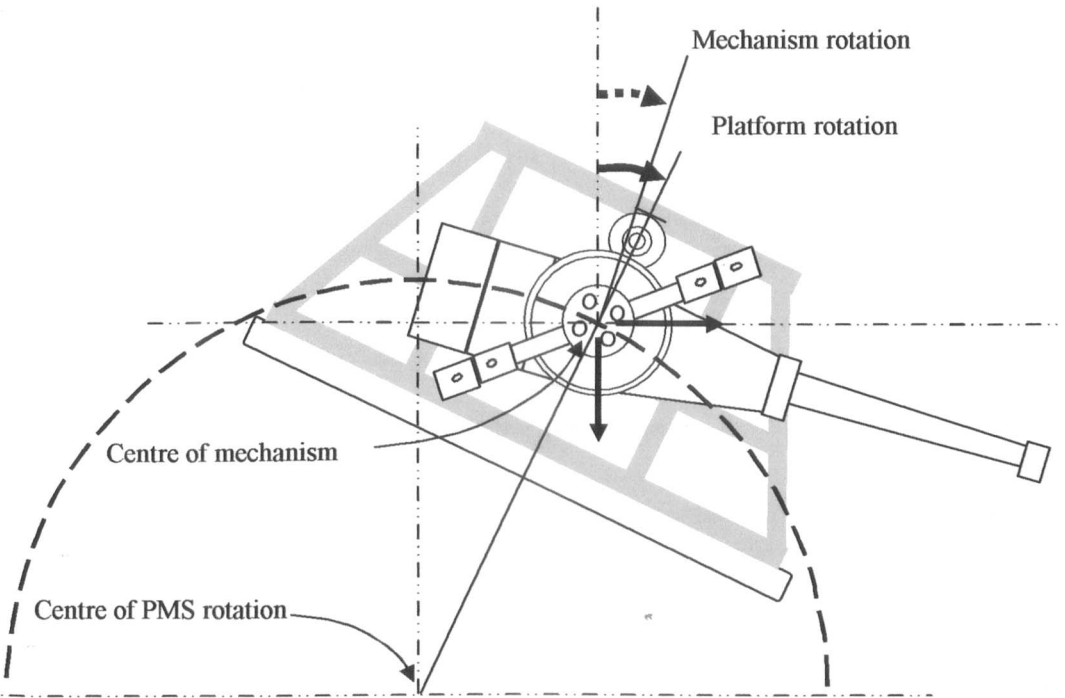


Figure 7-1(b): The rotation and translation due to the rotational centres of the PMS and the cantilever mechanism not coinciding. The effects of the translations are negligible if the system is balanced along the longitudinal and perpendicular axes. (Not to scale)

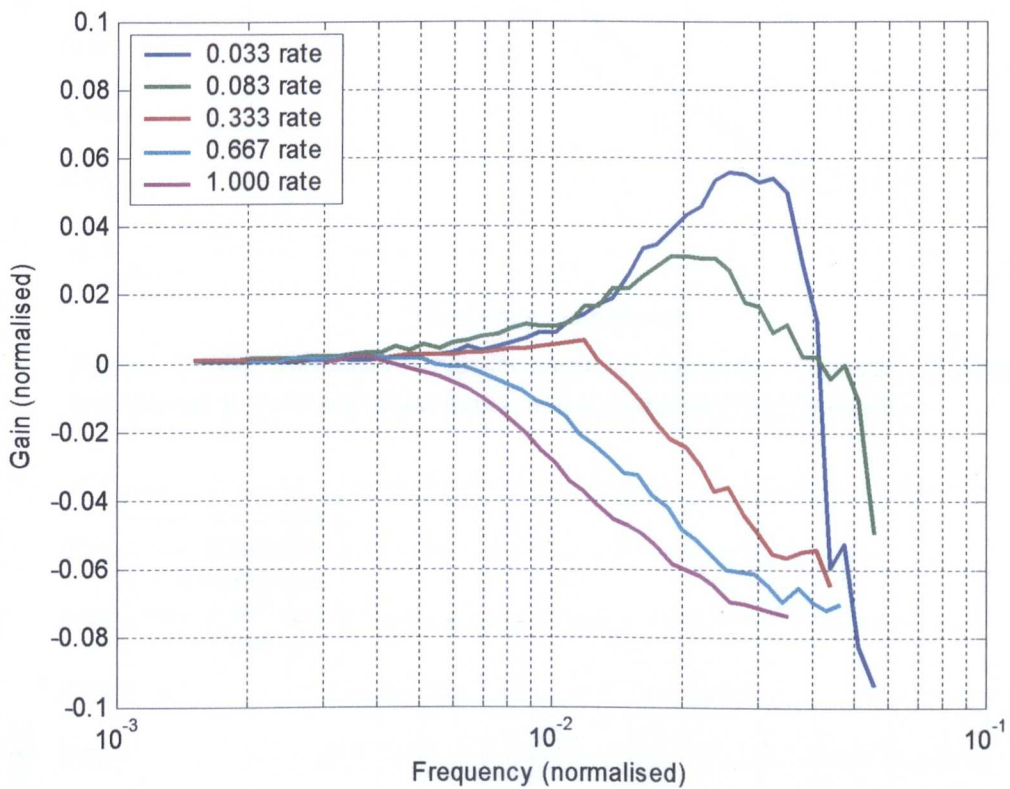


Figure 7-2: Measured frequency response of cantilever mechanism to external disturbance. The frequency, gain and input rates are normalised (input rates normalised to largest RMS amplitude).^[c]

[c] All figures presented in this chapter normalised using same frequency, gain, and time values

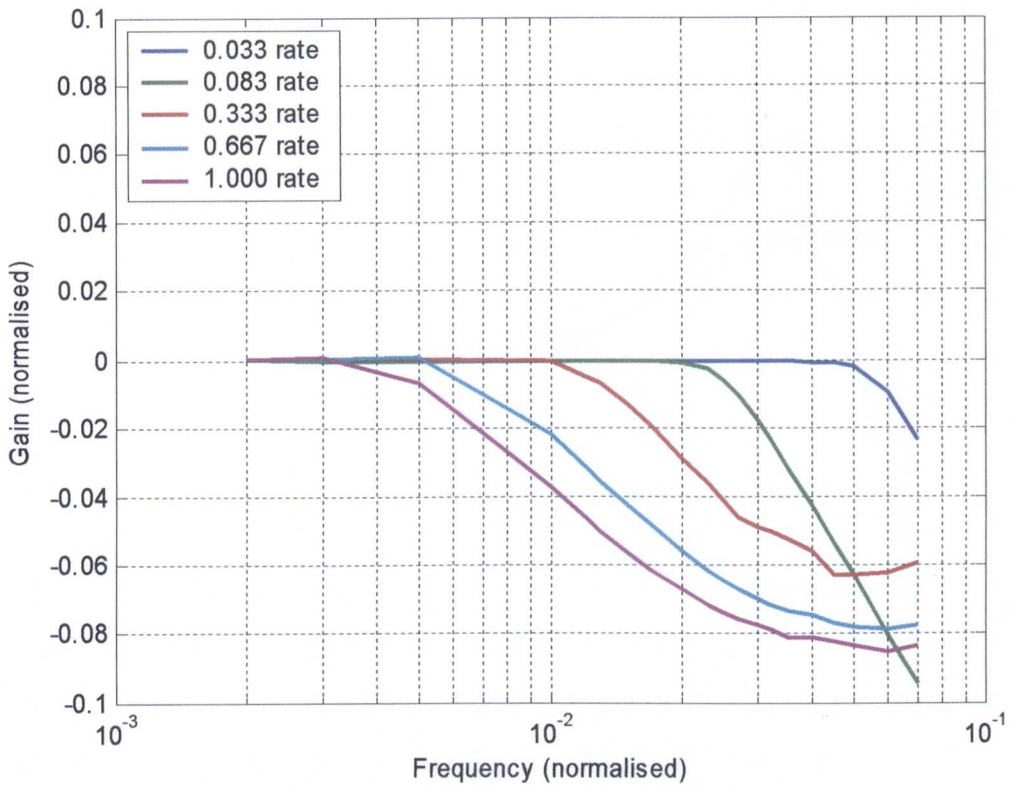


Figure 7-3(a): Simulation results showing frequency response of cantilever mechanism to external disturbance using classical friction model.

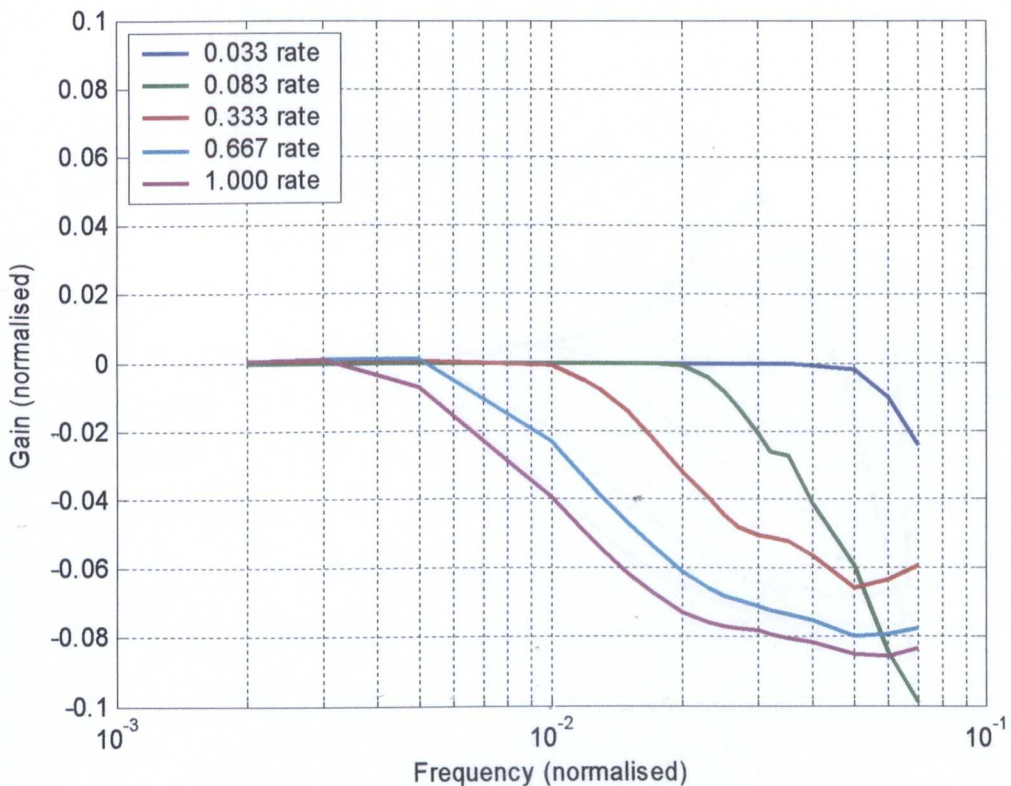


Figure 7-3(b): Simulation results showing frequency response of cantilever mechanism to external disturbance using Tustin's friction model.

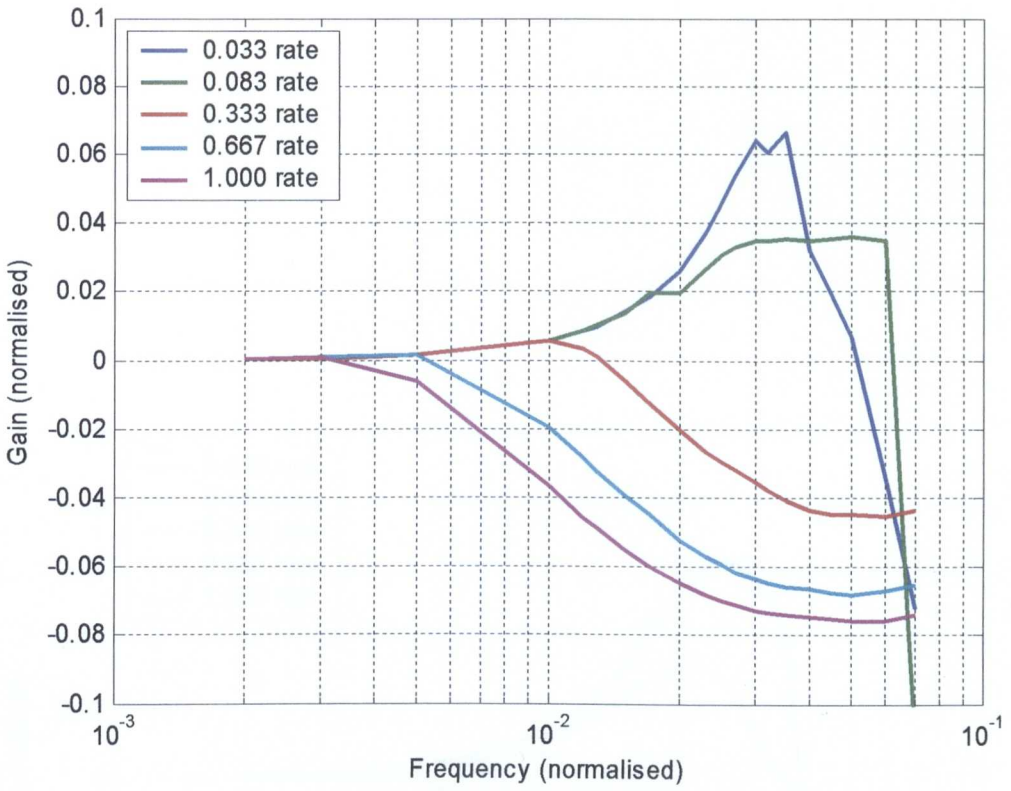


Figure7-4(a): Simulation results showing frequency response of cantilever mechanism to external disturbance, using reset-integrator friction model.

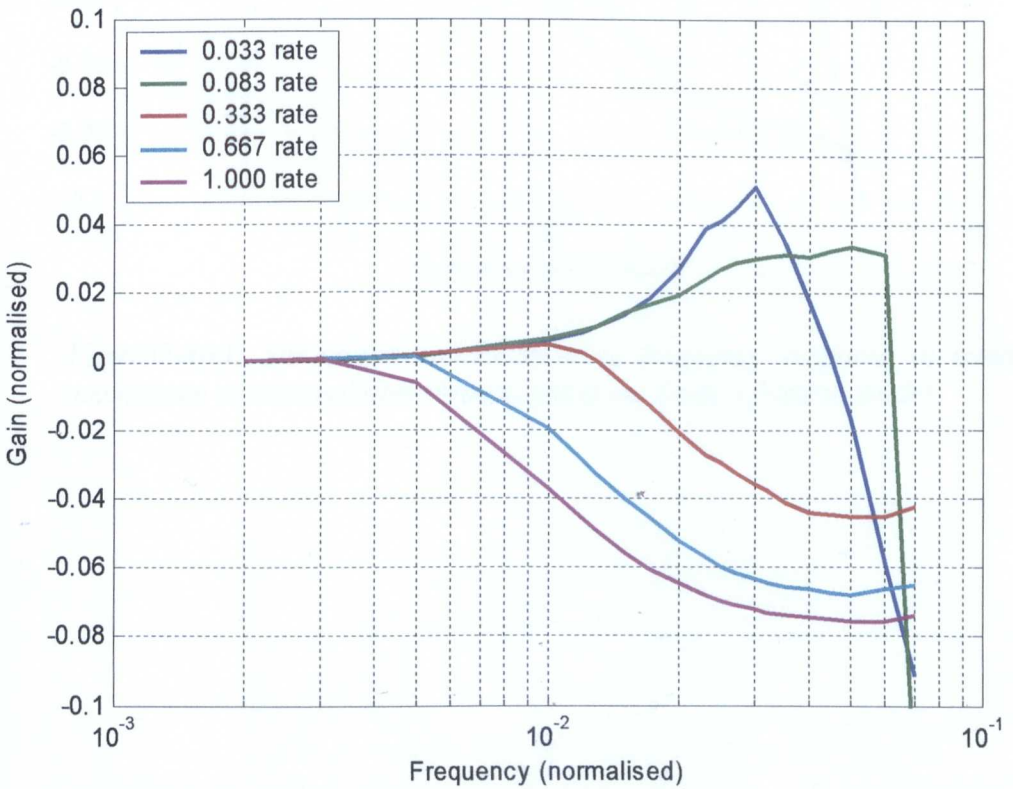


Figure7-4(b): Simulation results showing frequency response of cantilever mechanism to external disturbance, using LuGre friction model.

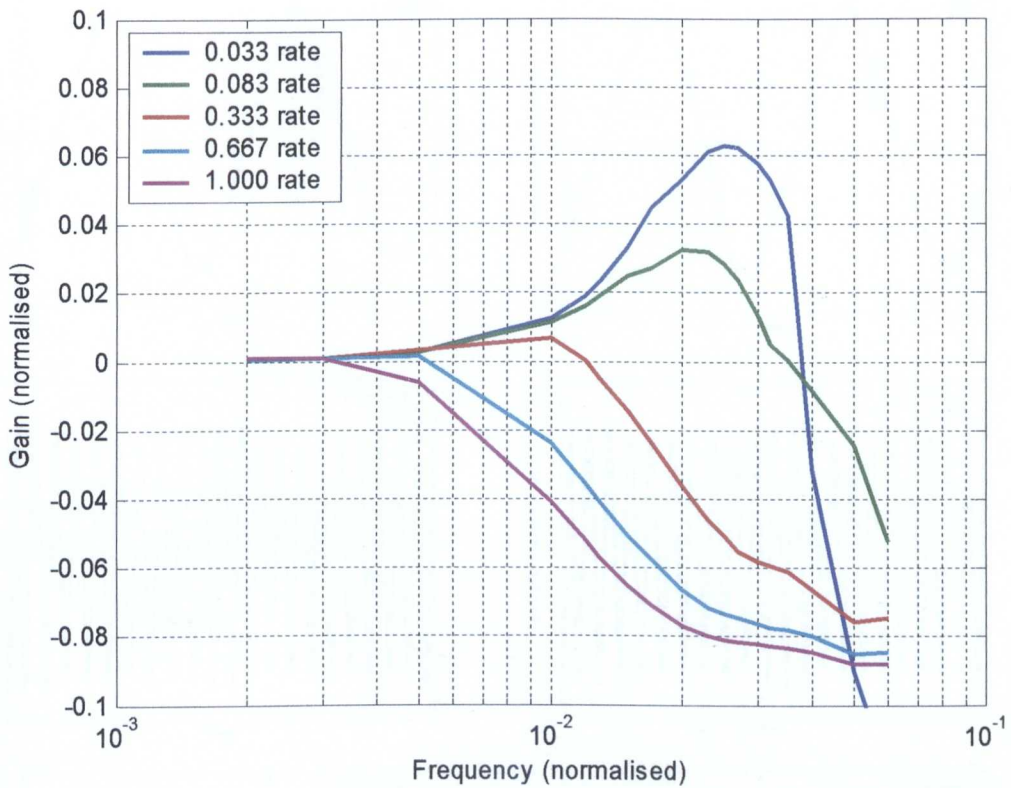


Figure 7-4(c): Simulation results showing frequency response of cantilever mechanism to external disturbance, using the Dahl's friction model.

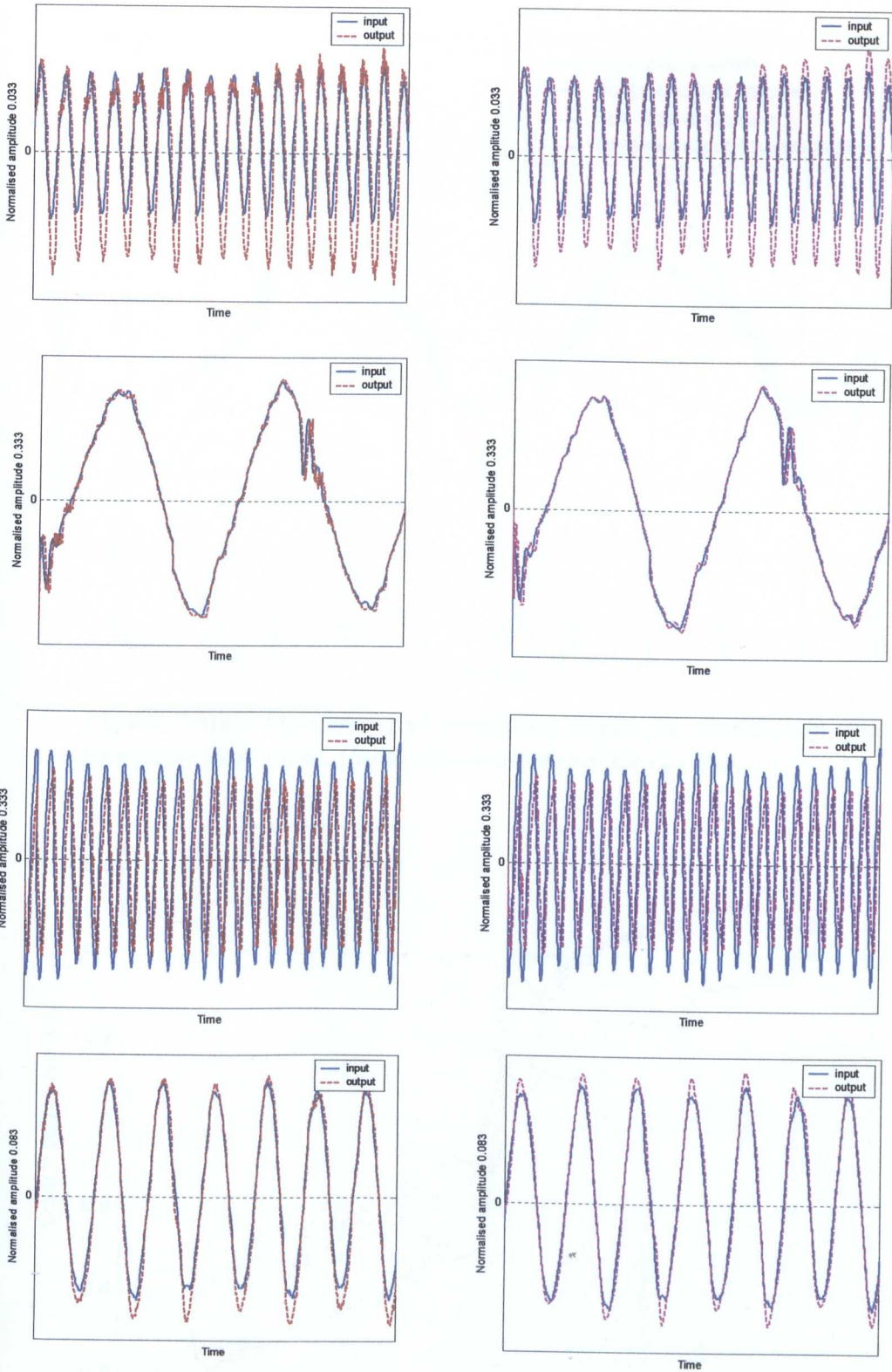


Figure 7-5: Measured results (left) and the corresponding simulation results (right) for various input amplitudes and frequencies. The simulation results are shown for Dahl's friction model.

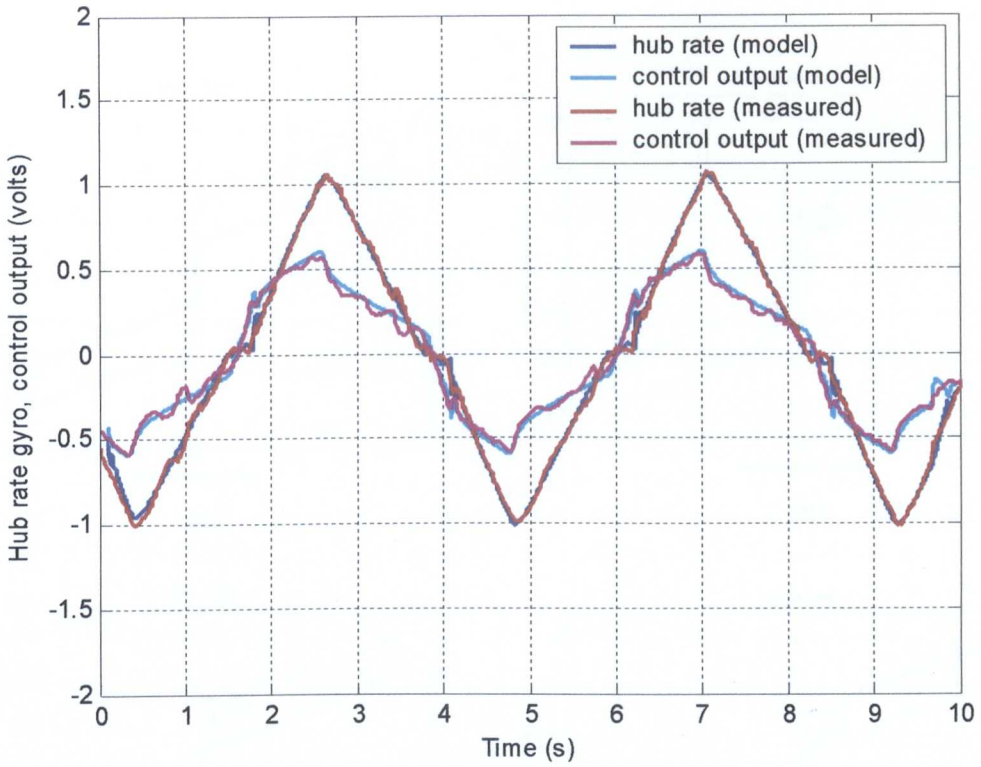


Figure 7-6(a): Measured and simulation results for closed-loop system with triangular wave input. (Input signal not shown for clarity)

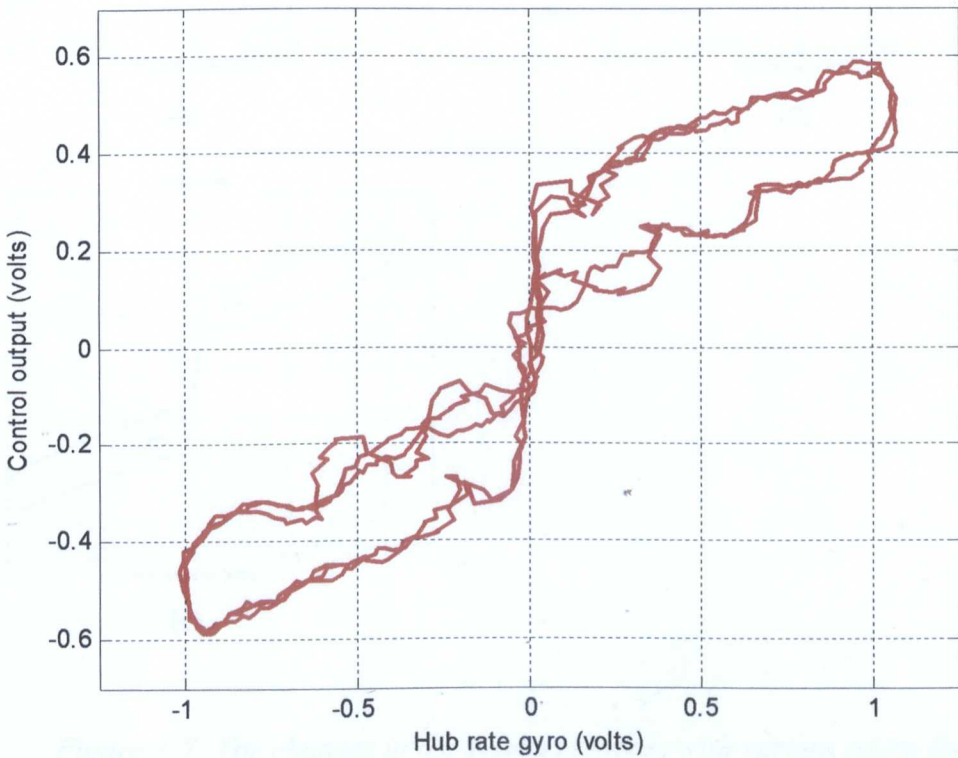
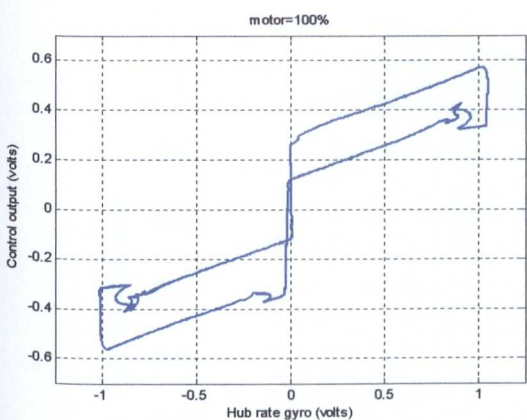
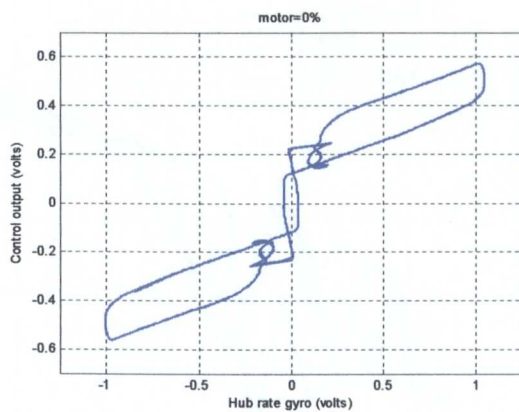


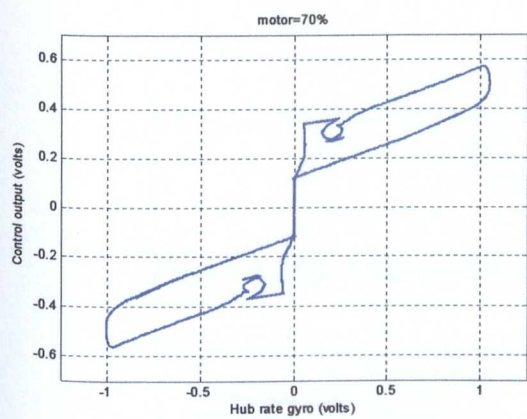
Figure 7-6(b): Control output plotted against hub rate for measured results.



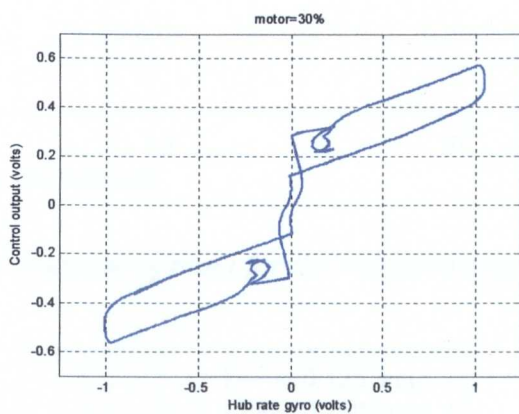
(a)



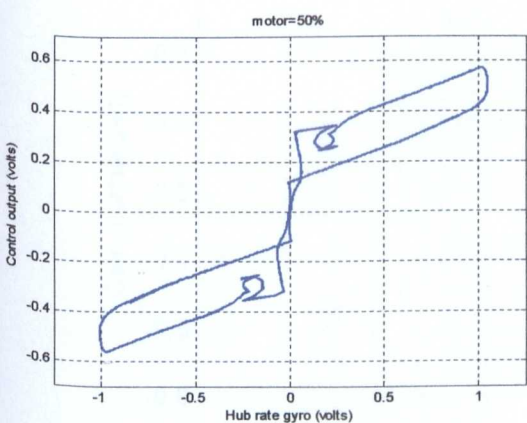
(b)



(c)



(d)



(e)

Figure 7-7: The changes in the system response with various ratios for the two friction models located at input and output of gearbox for balanced system.

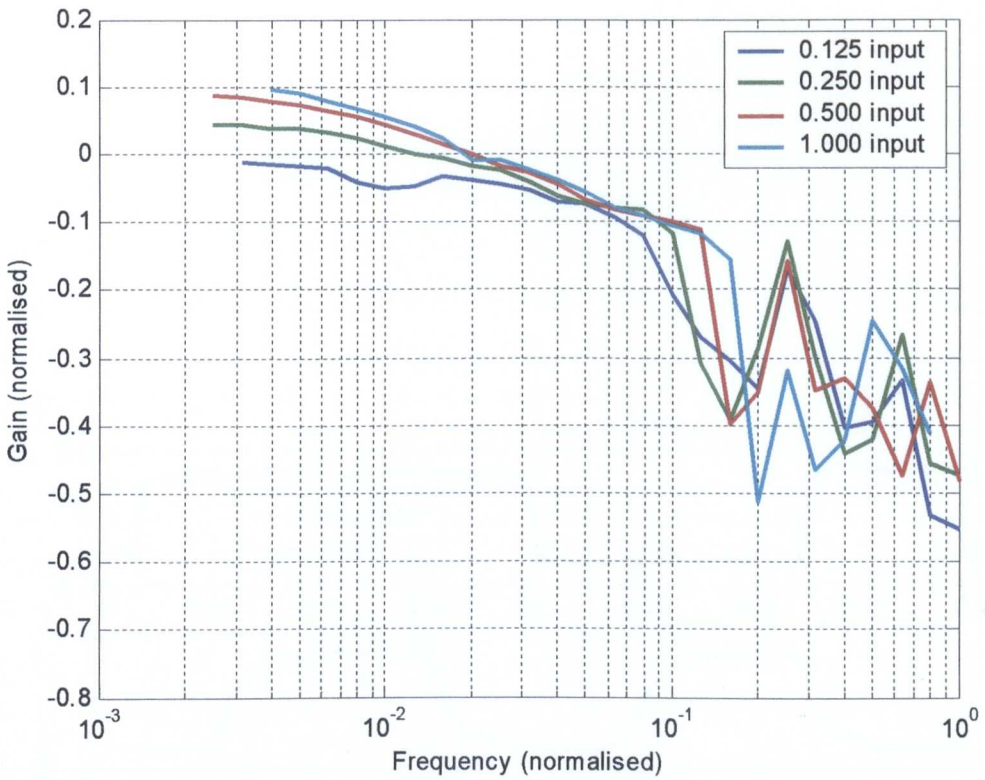


Figure 7-8(a): Measured frequency response of plant for the balanced system.

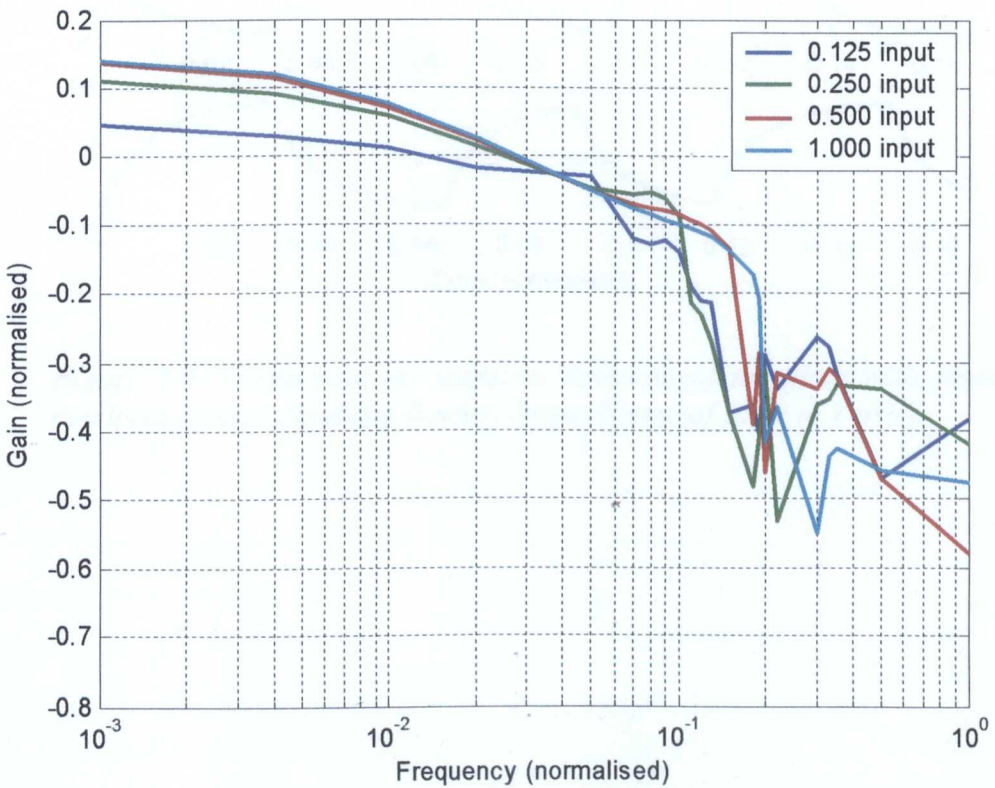


Figure 7-8(b): Simulated frequency response of plant for the balanced system.

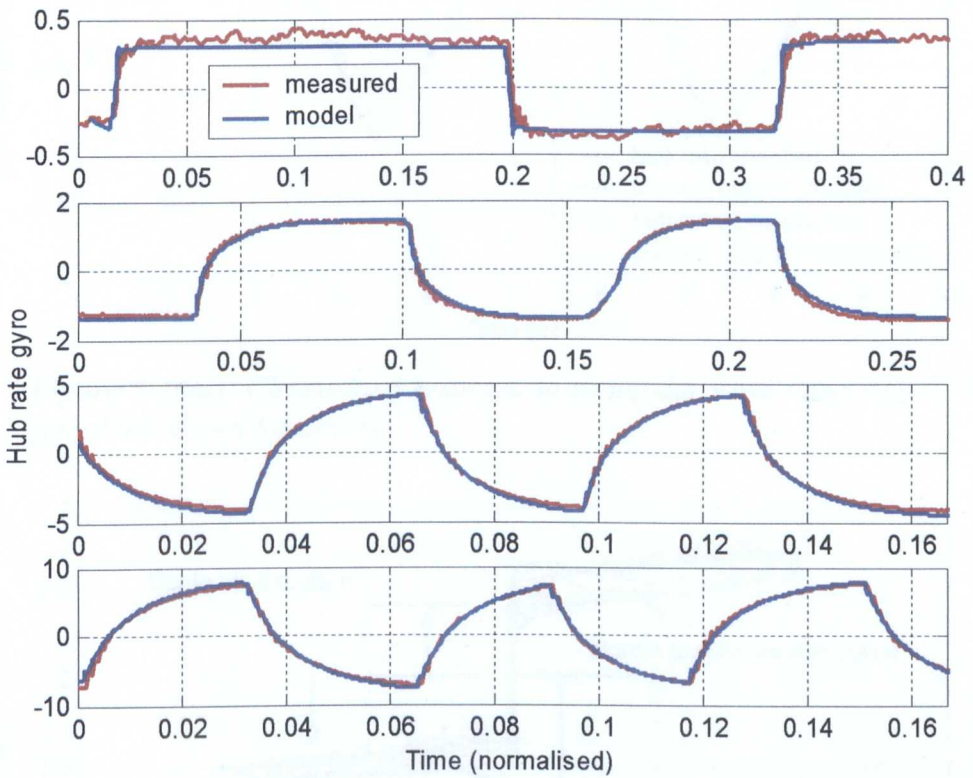


Figure 7-9: Comparing the transient response of the plant with simulation results at several input amplitudes, (Note change of scale in Y axis).

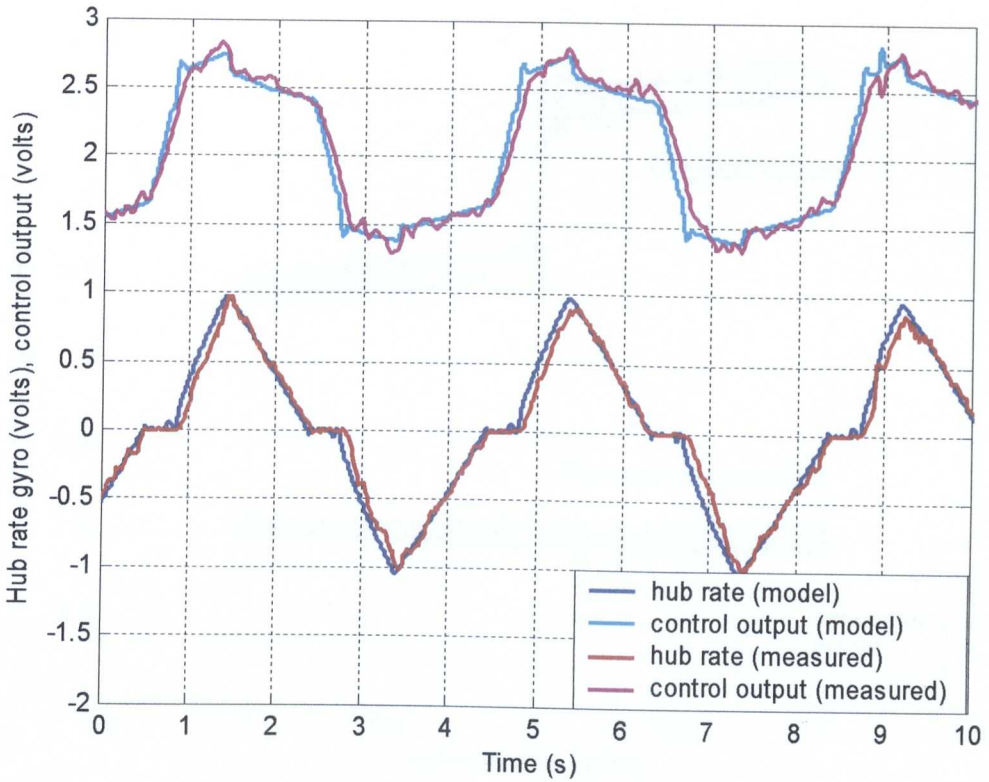


Figure 7-10(a): Closed-loop response to triangular wave input signal. (Input signal not shown for clarity)

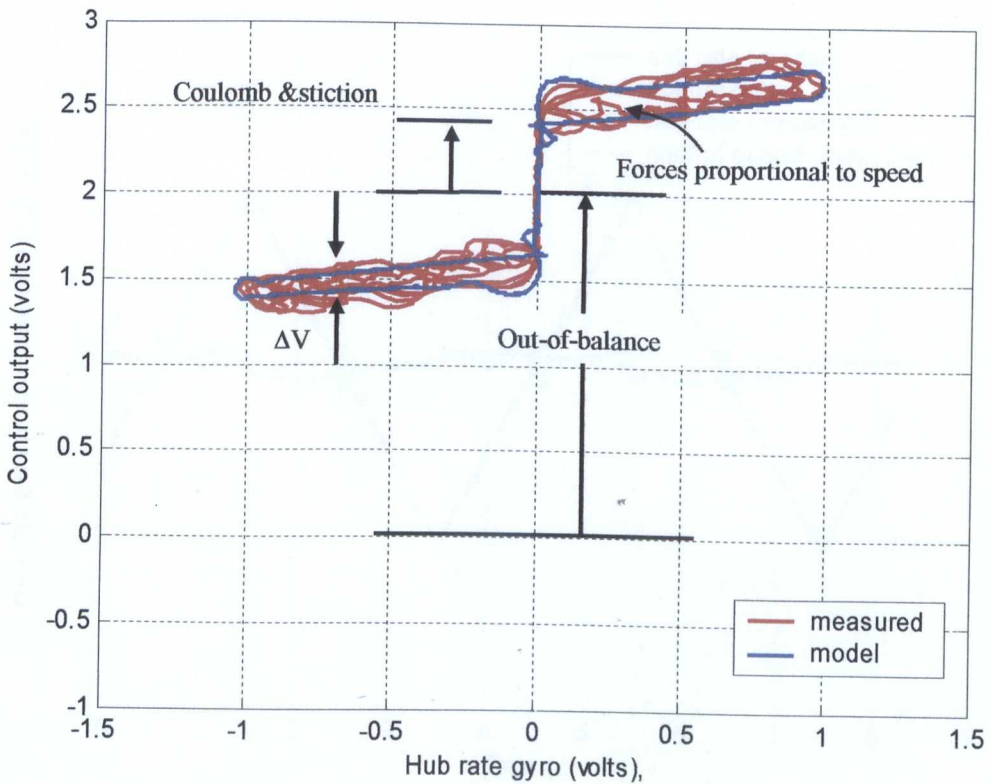


Figure 7-10(b): Control output plotted against hub rate.

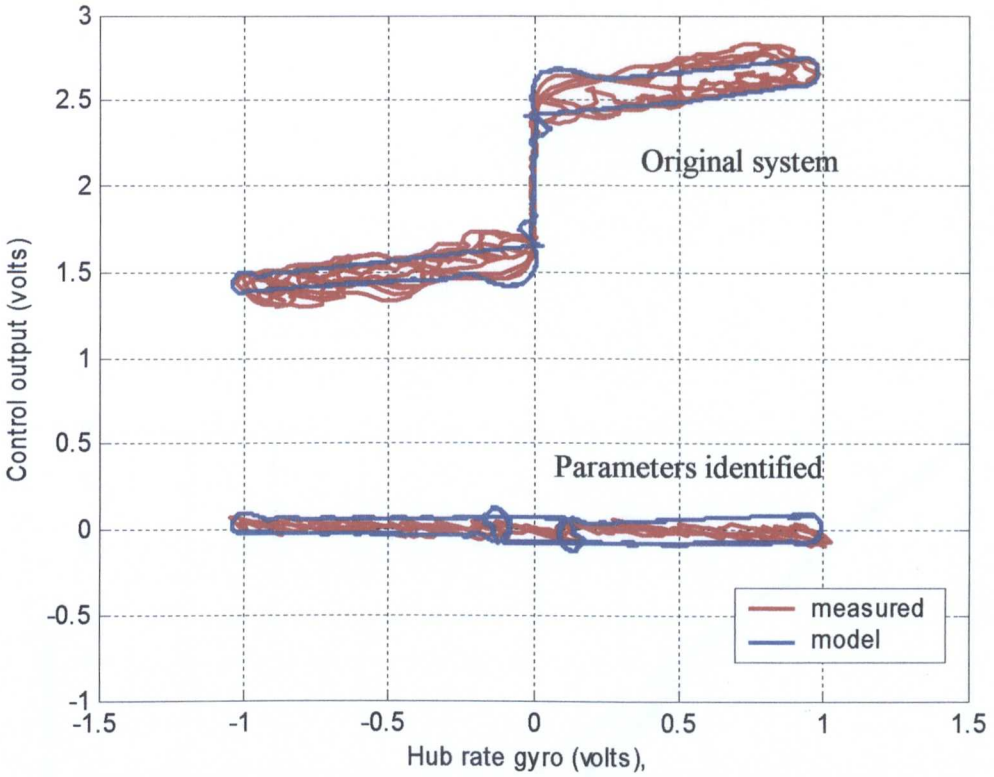


Figure 7-10(c): System response with out-of-balance, Coulomb friction and speed related forces identified.

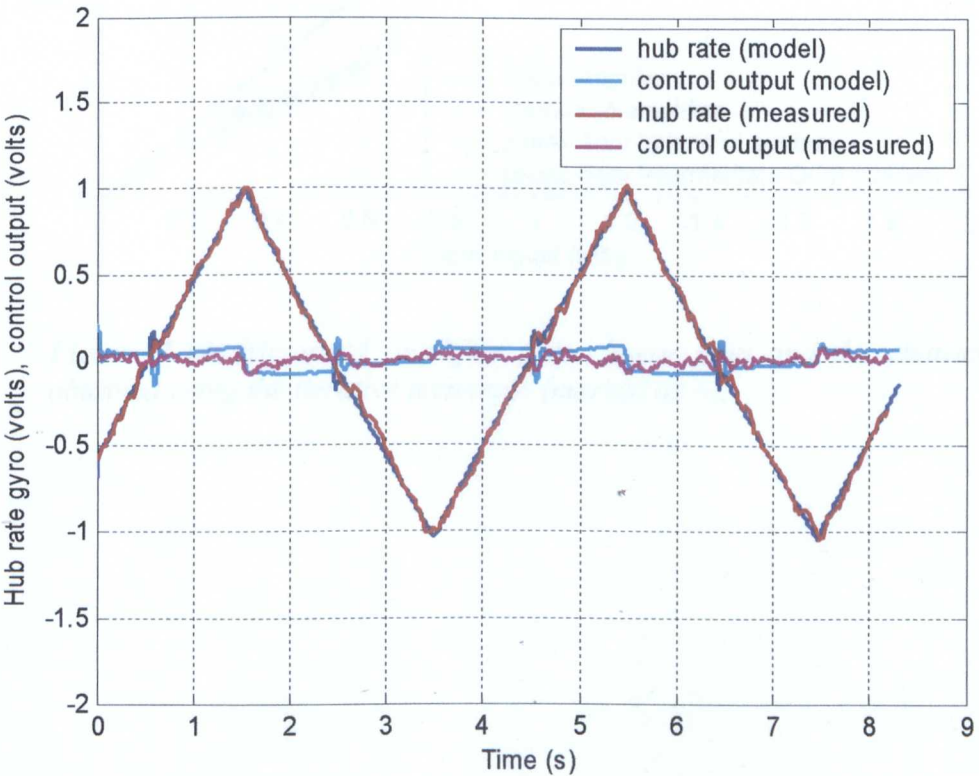


Figure 7-10(d): Closed-loop response to triangular wave input for fully compensated system.

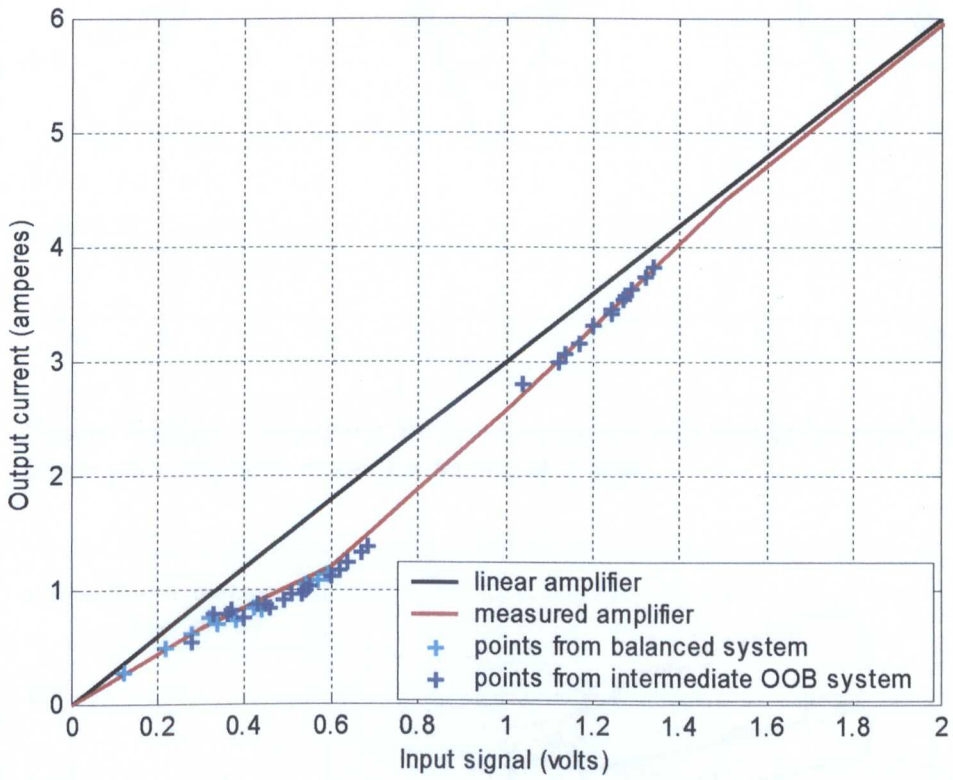


Figure 7-11: Measured amplifier gain, linear gain and the characteristic obtained using the iterative technique (marked as +).

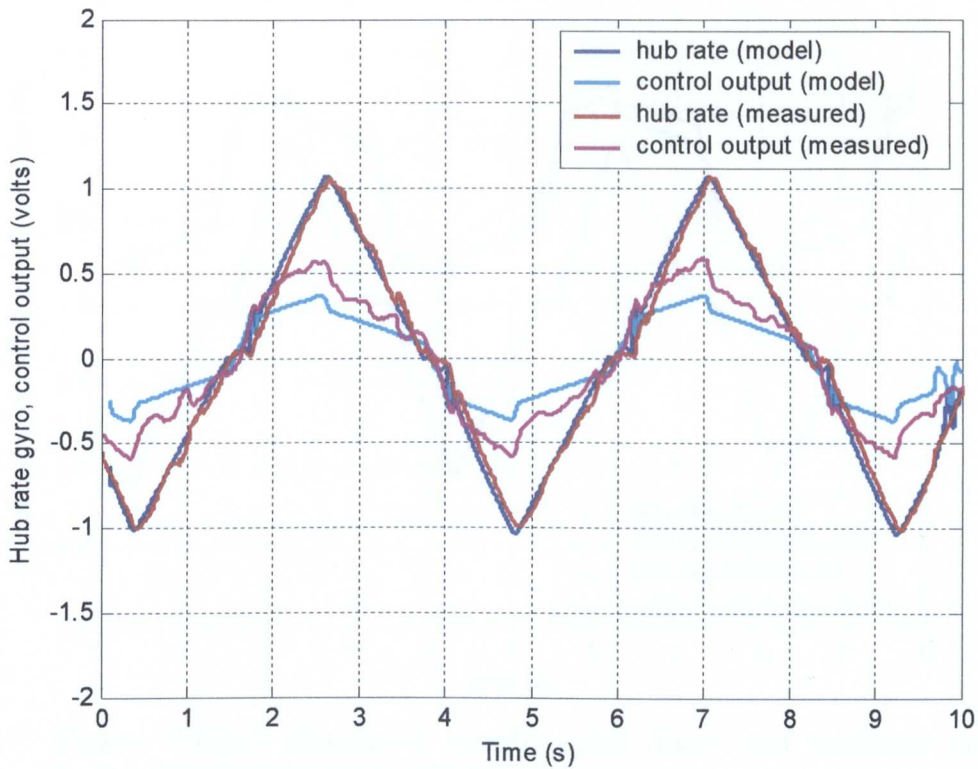


Figure 7-12(a): Comparing measured response with simulation results using a linear gain amplifier model for balanced system.

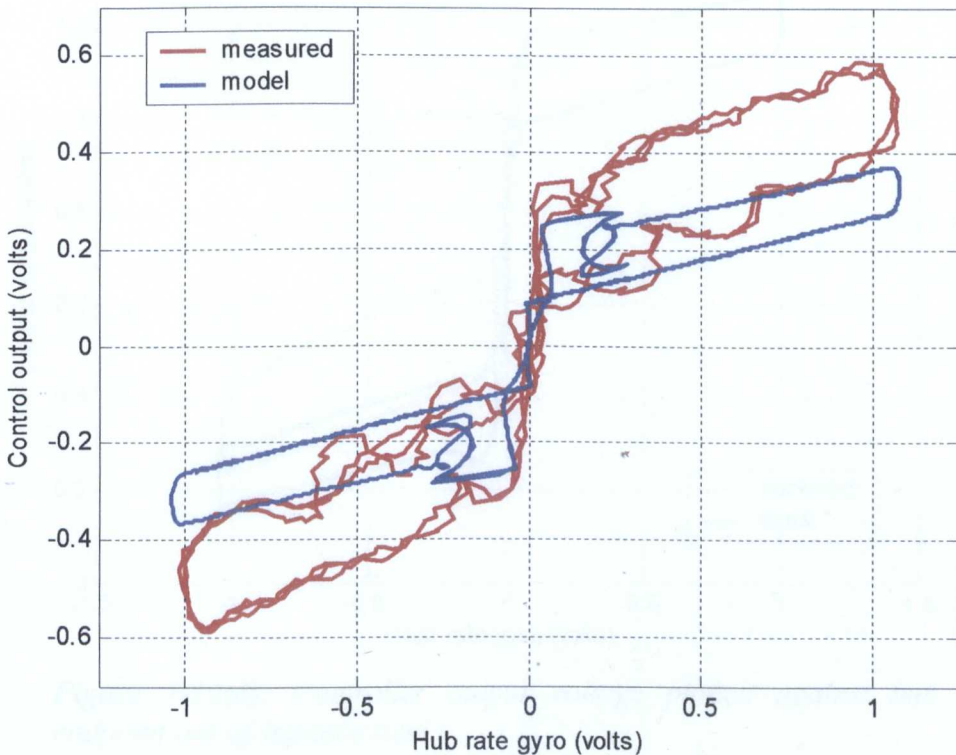


Figure 7-12(b): Comparing controller output against hub rate using linear gain amplifier model with measured results for balanced system.

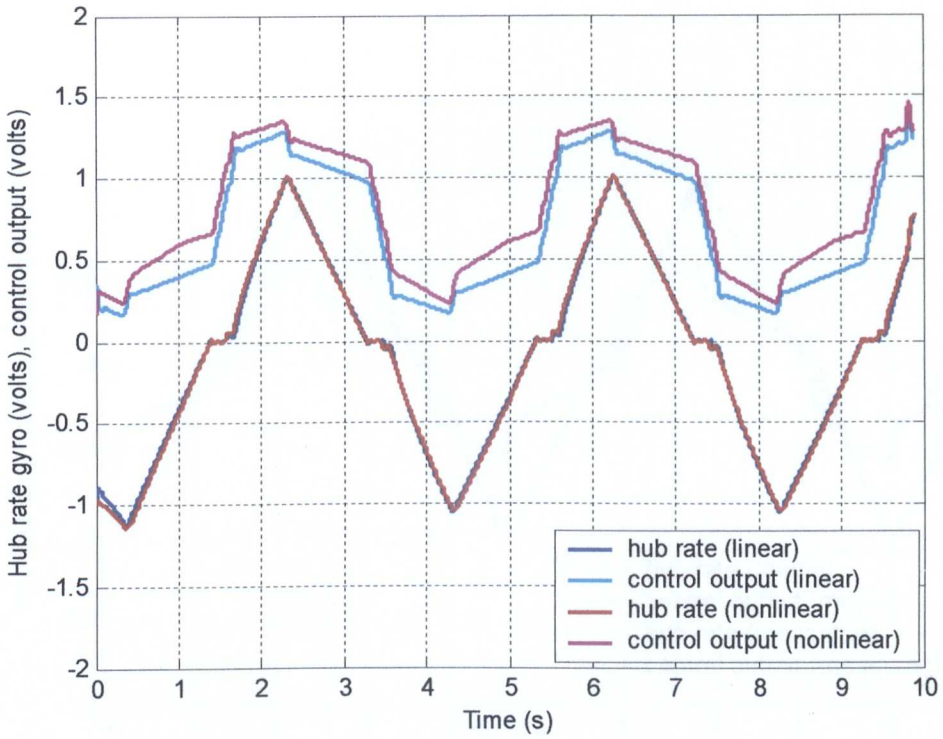


Figure 7-12(c): Simulation results, using linear and nonlinear amplifier model, for midpoint out-of-balance case.

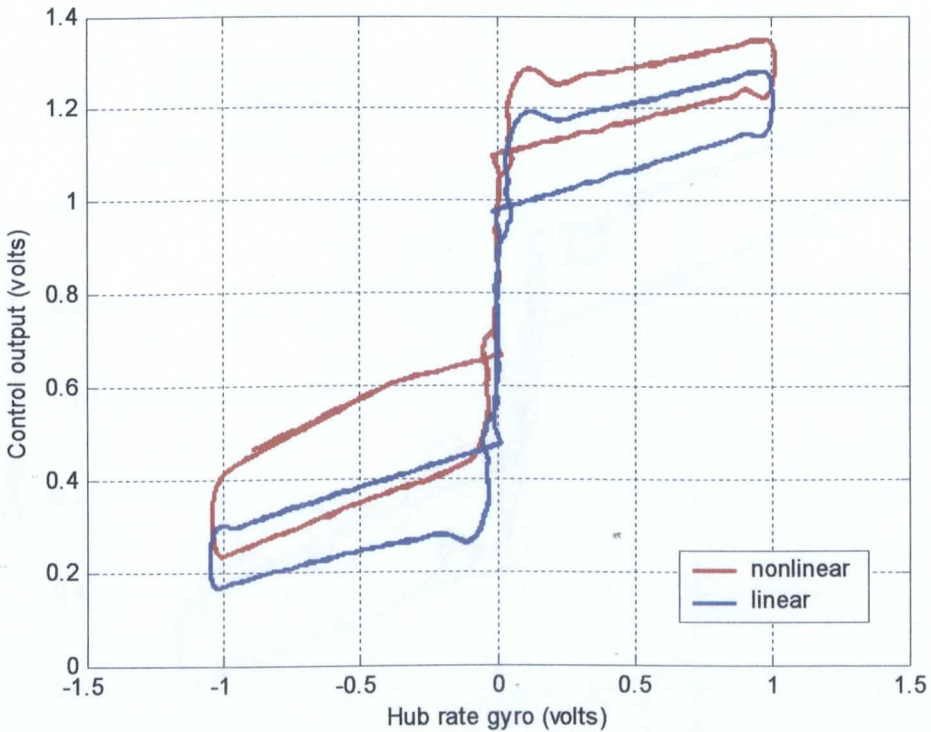


Figure 7-12(d): Controller output voltage plotted against hub rate for midpoint out-of-balance case.

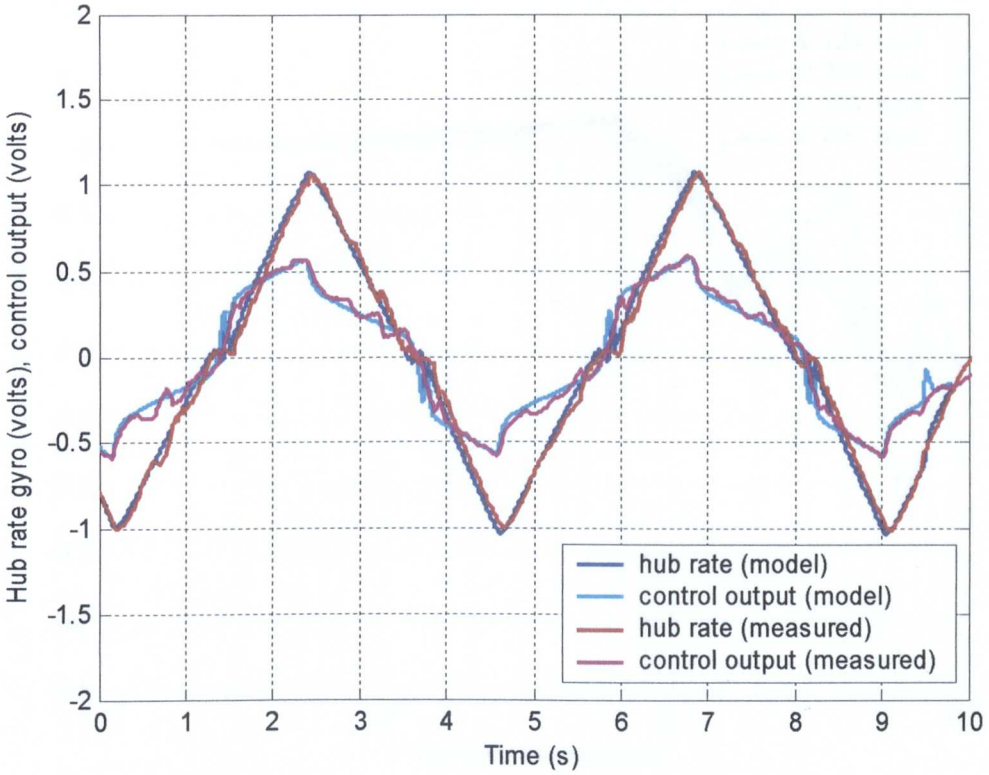


Figure 7-12(e): Comparing measured response of system with simulation results using a nonlinear amplifier gain for the balance system.

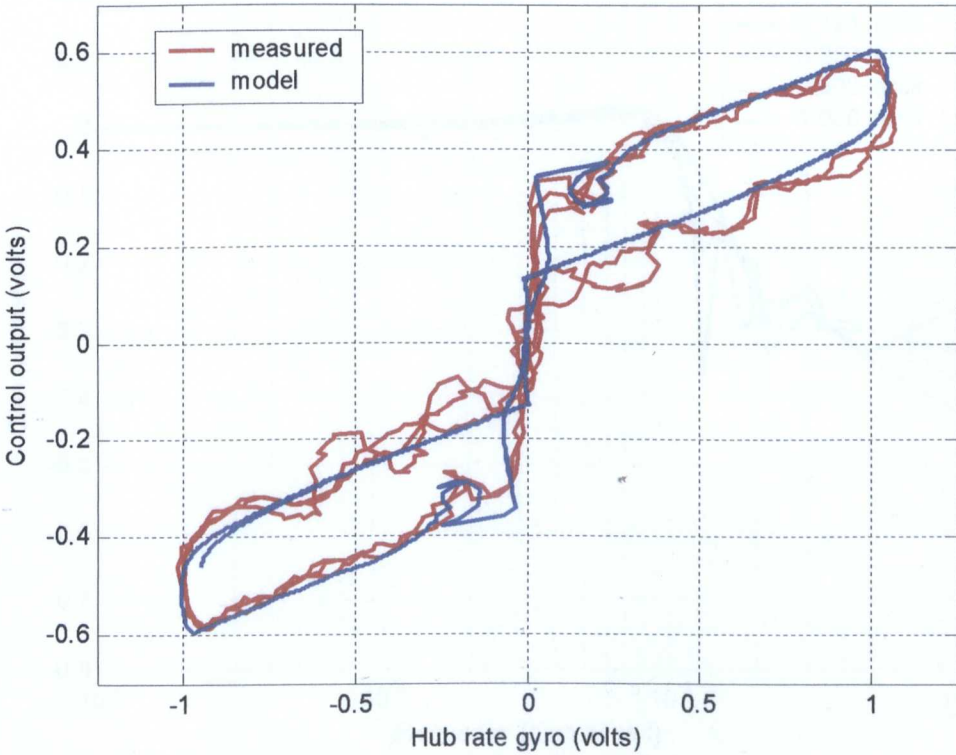


Figure 7-12(f): Comparing controller output voltage against hub rate using nonlinear amplifier model with measured results for the balance system.

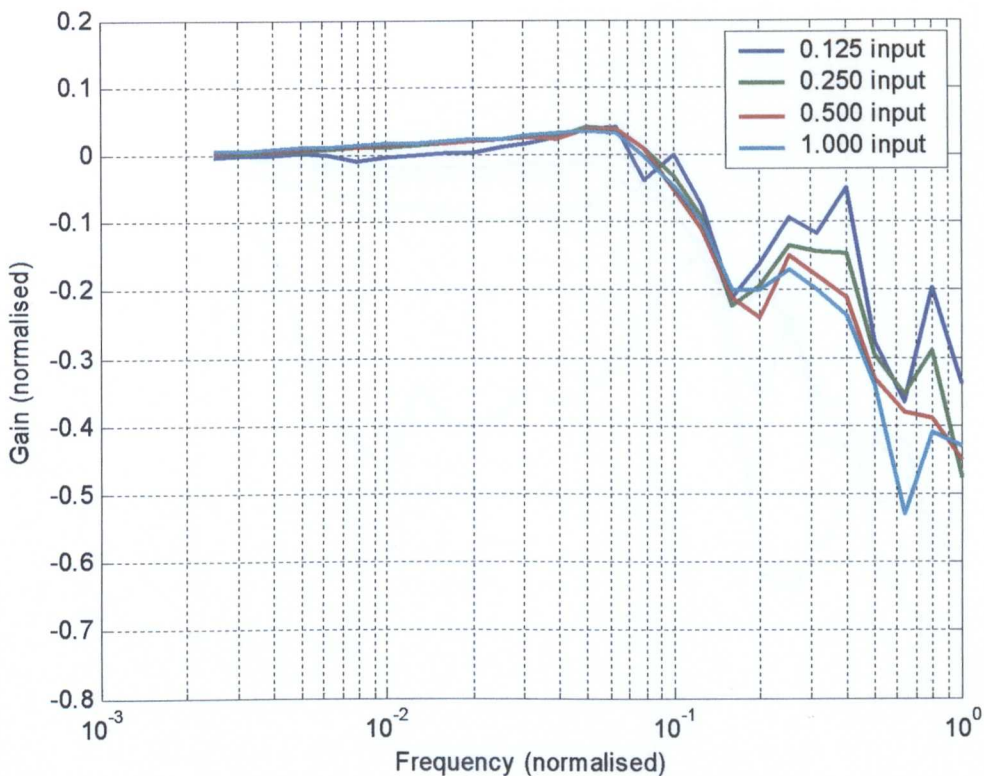


Figure 7-13(a): Measured closed-loop response of out-of-balance system with compensation.

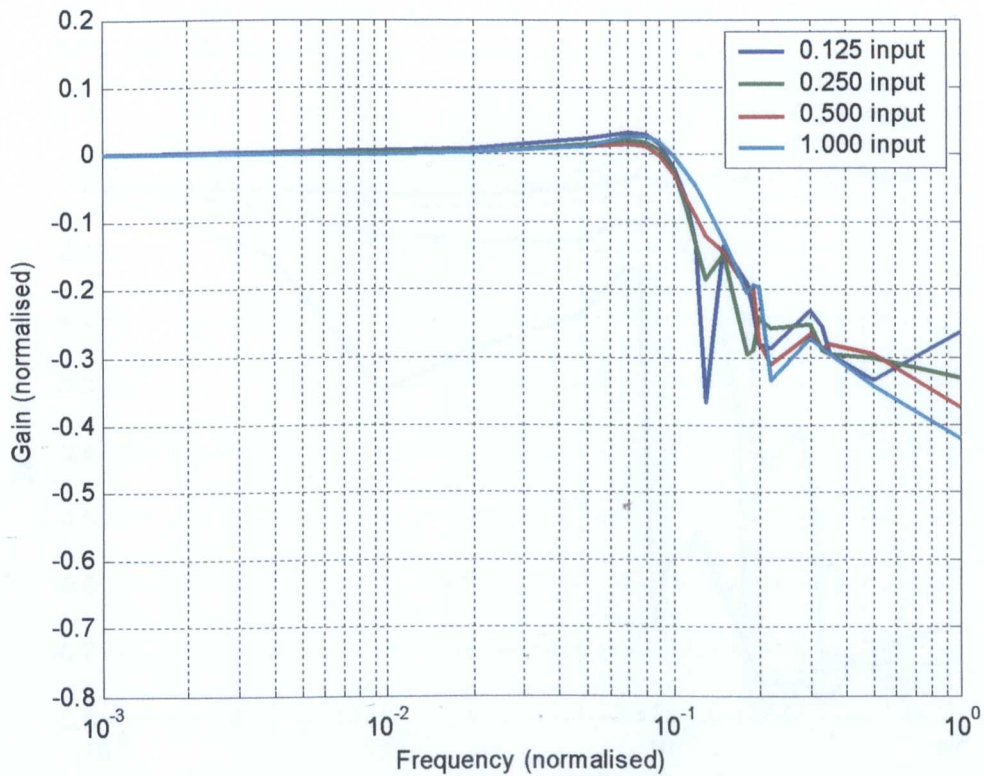


Figure 7-13(b): Simulated closed-loop response of out-of-balance system with compensation.

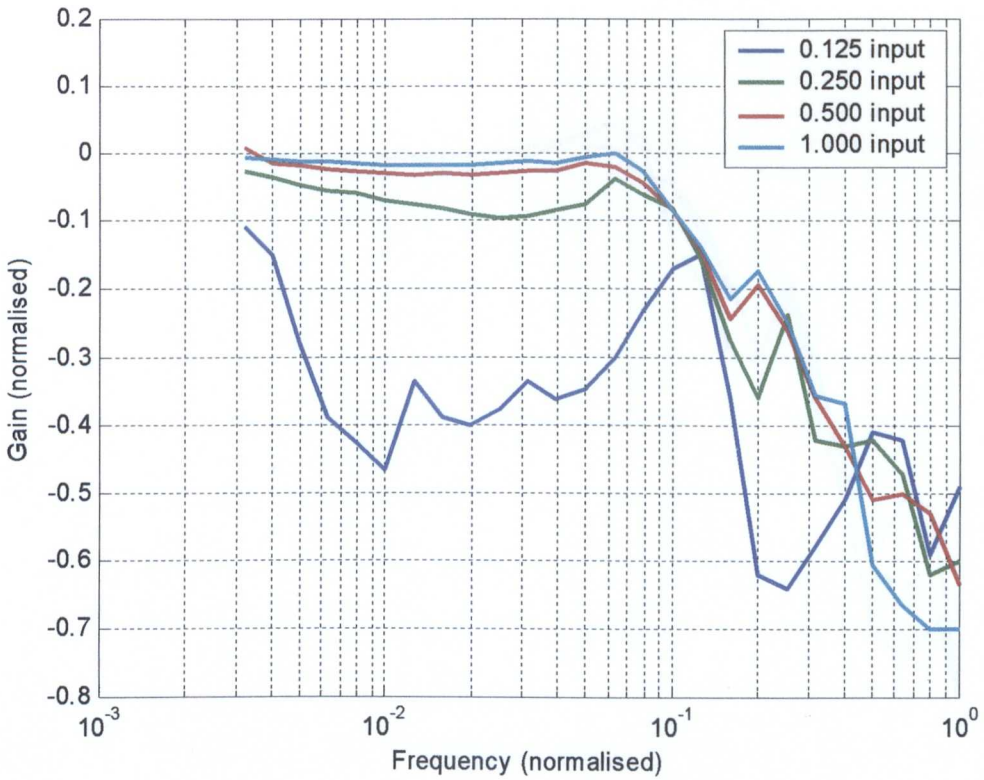


Figure 7-13(c): Measured closed-loop response of out-of-balanced system without friction compensation.

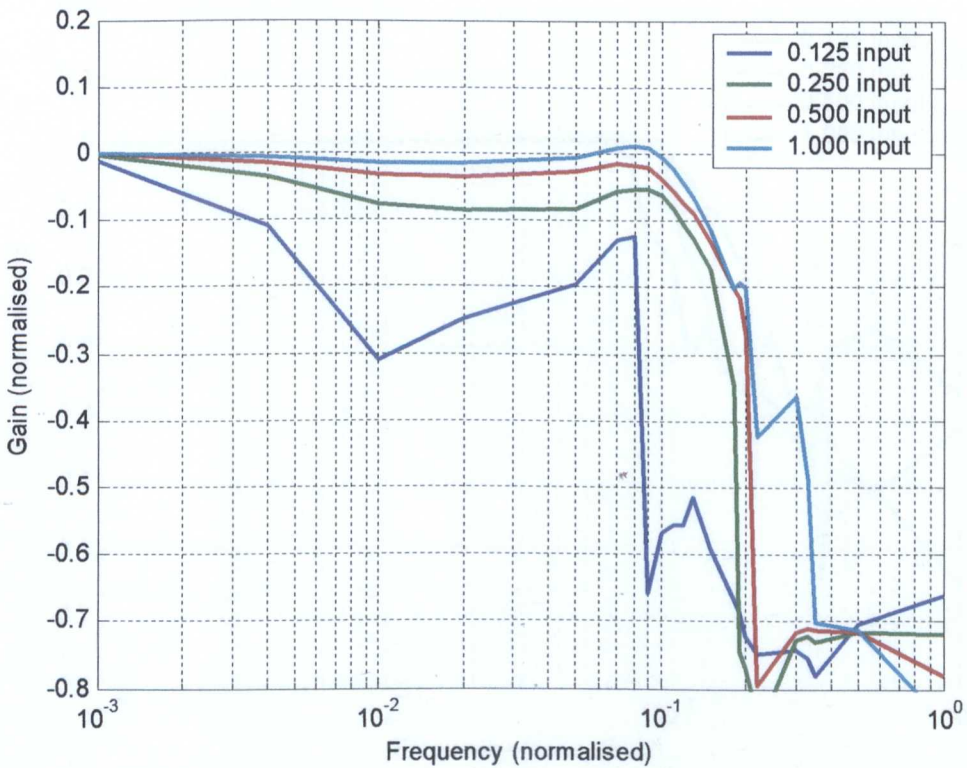


Figure 7-13(d): Simulated closed-loop response of out-of-balanced system without friction compensation.

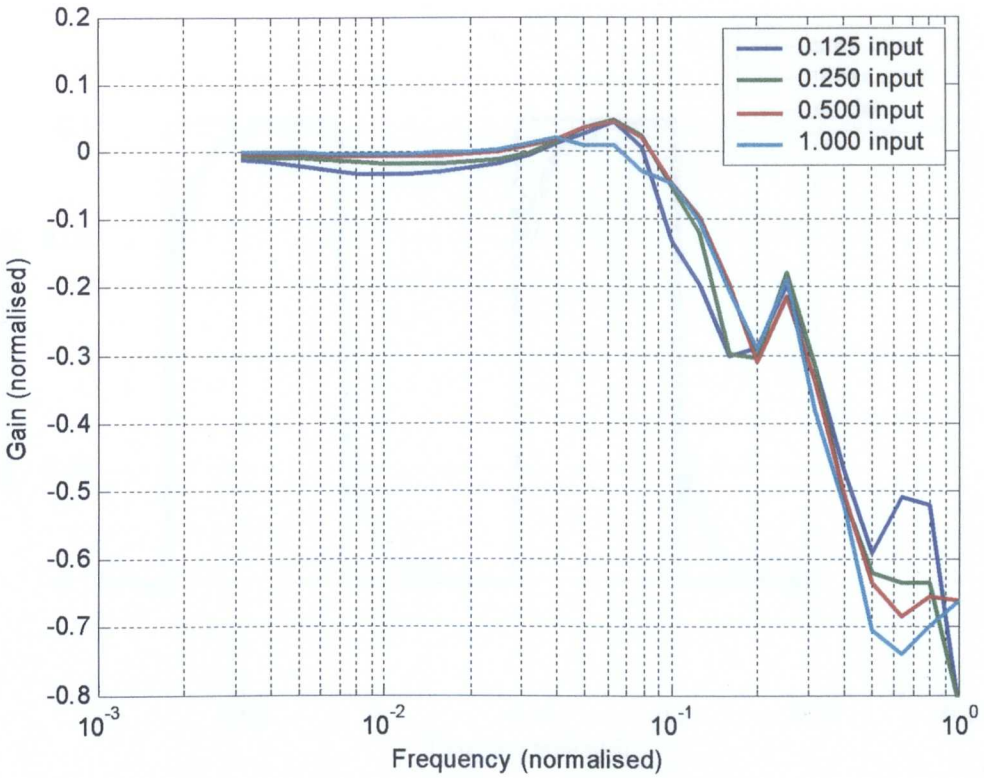


Figure 7-13(e): Measured closed-loop response of balanced system with friction compensation.

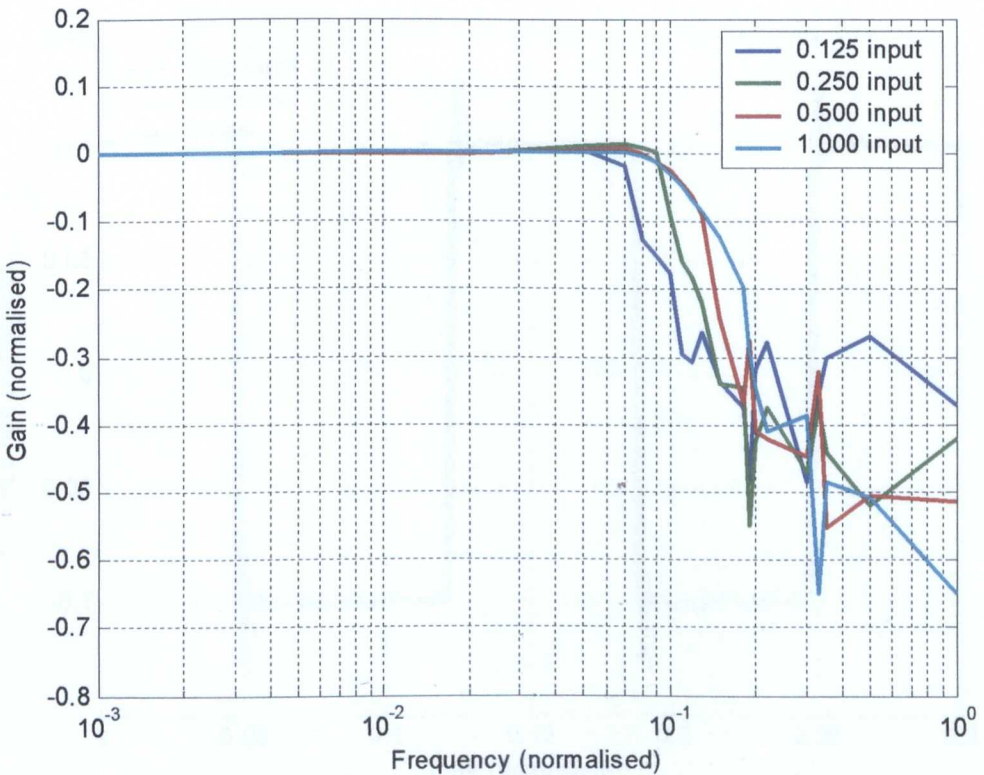


Figure 7-13(f): Simulated closed-loop response of balanced system with friction compensation.

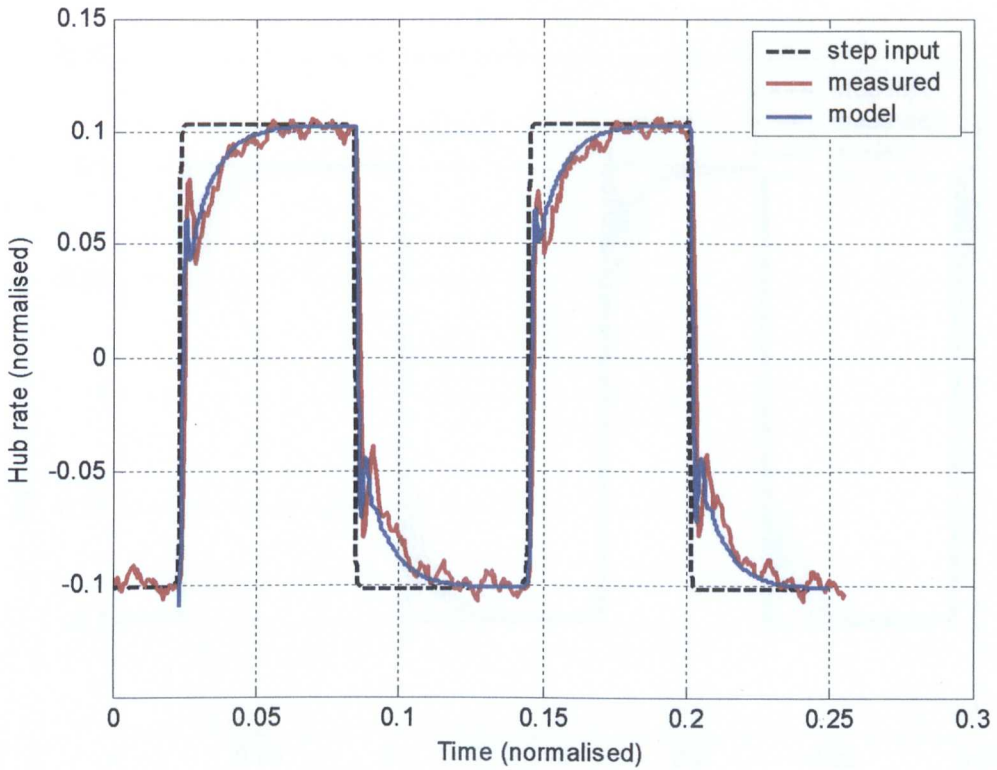


Figure 7-14(a): Comparing the simulation predictions with the measured results for the out-of-balance system without nonlinear compensation.

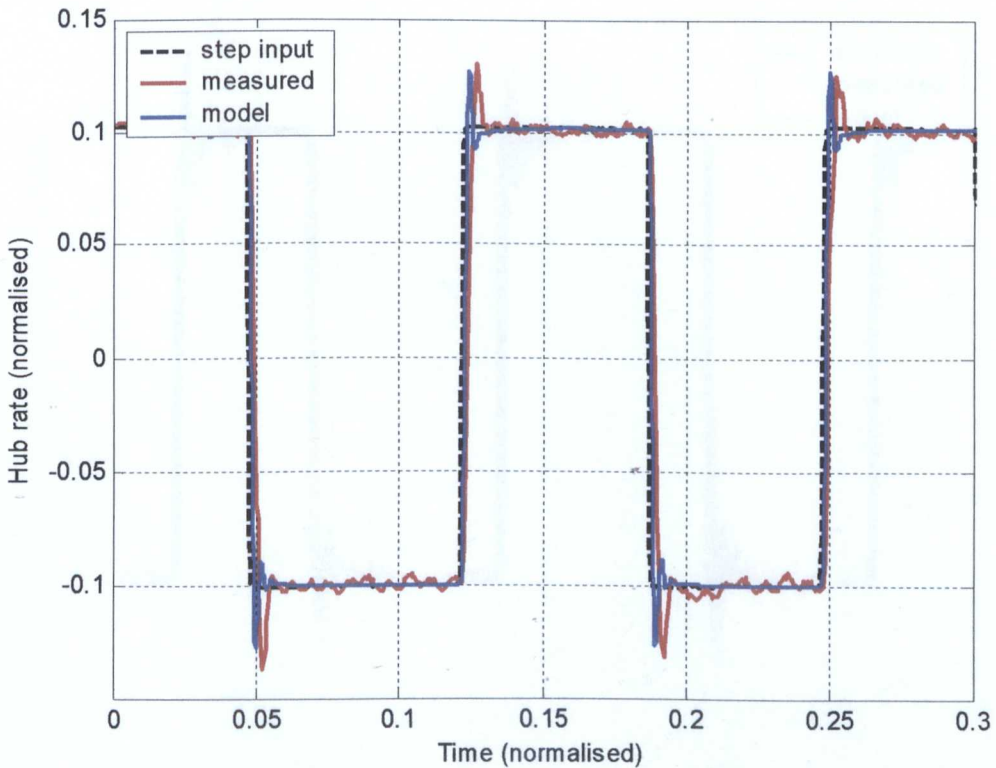


Figure 7-14(b): Comparing the simulation predictions with the measured results for the out-of-balance system with nonlinear compensation.

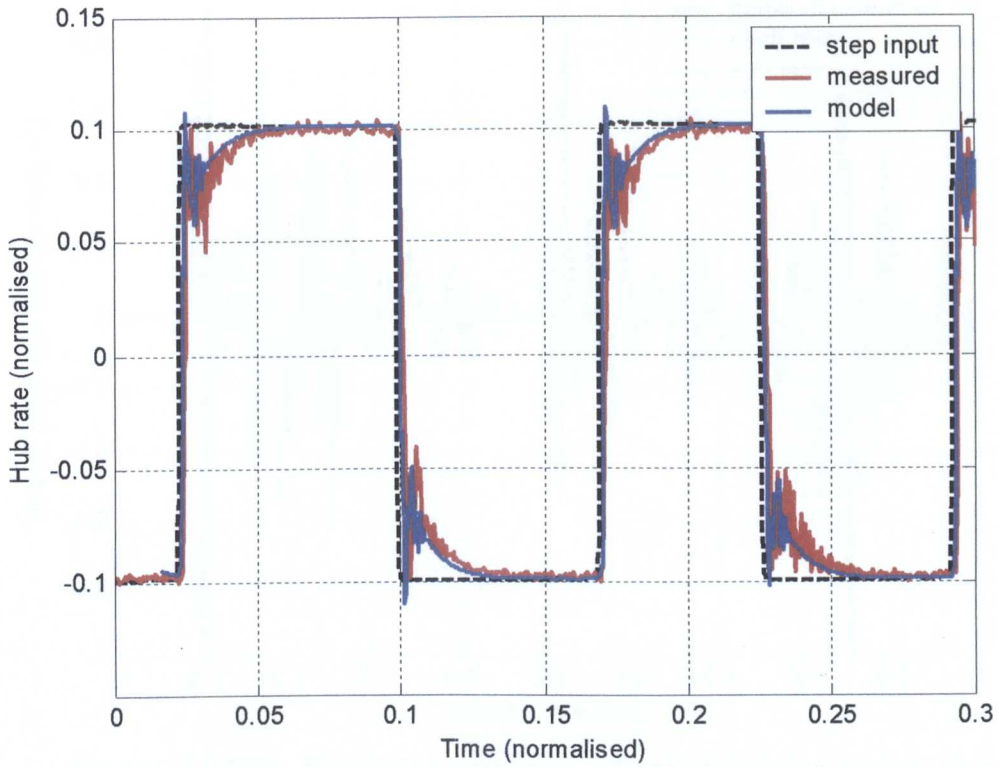


Figure 7-14(c): Comparing the simulation predictions with the measured results for the balanced system without nonlinear compensation.

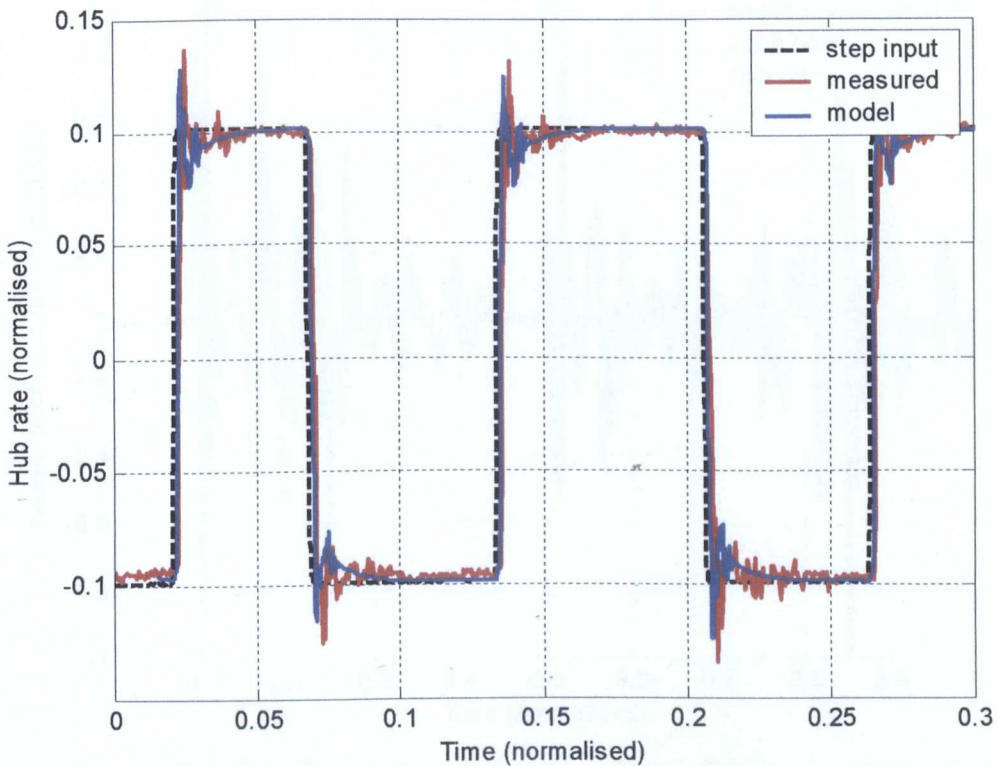


Figure 7-14(d): Comparing the simulation predictions with the measured results for the balanced system with nonlinear compensation.

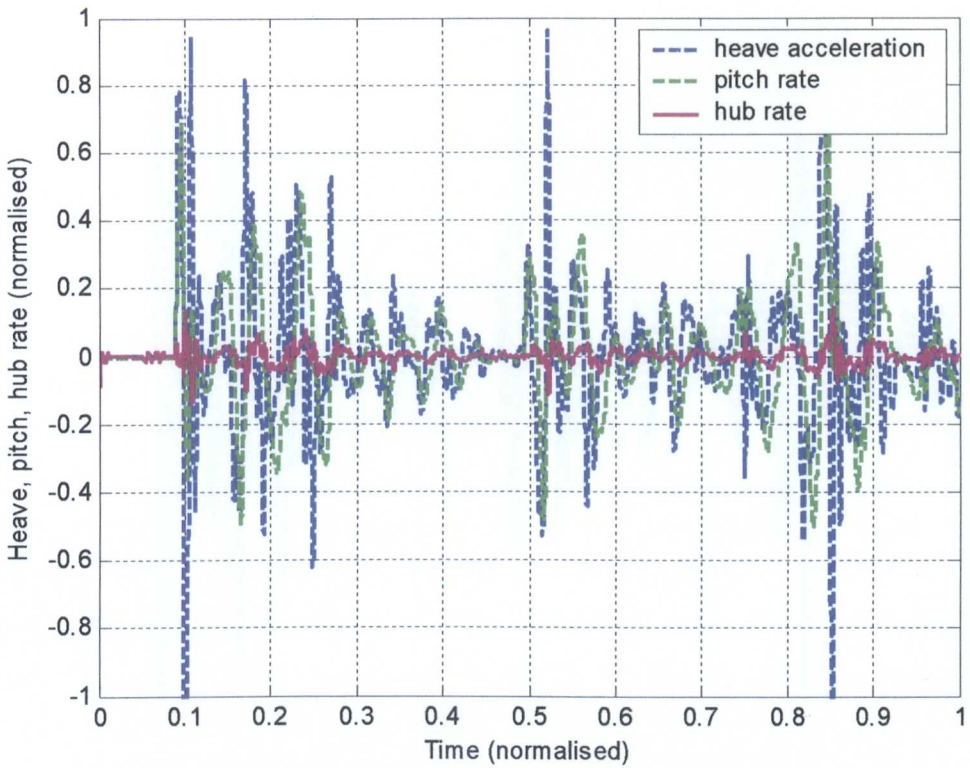


Figure 7-15(a): Simulation responses of out-of-balance system to external disturbances without feedforward.

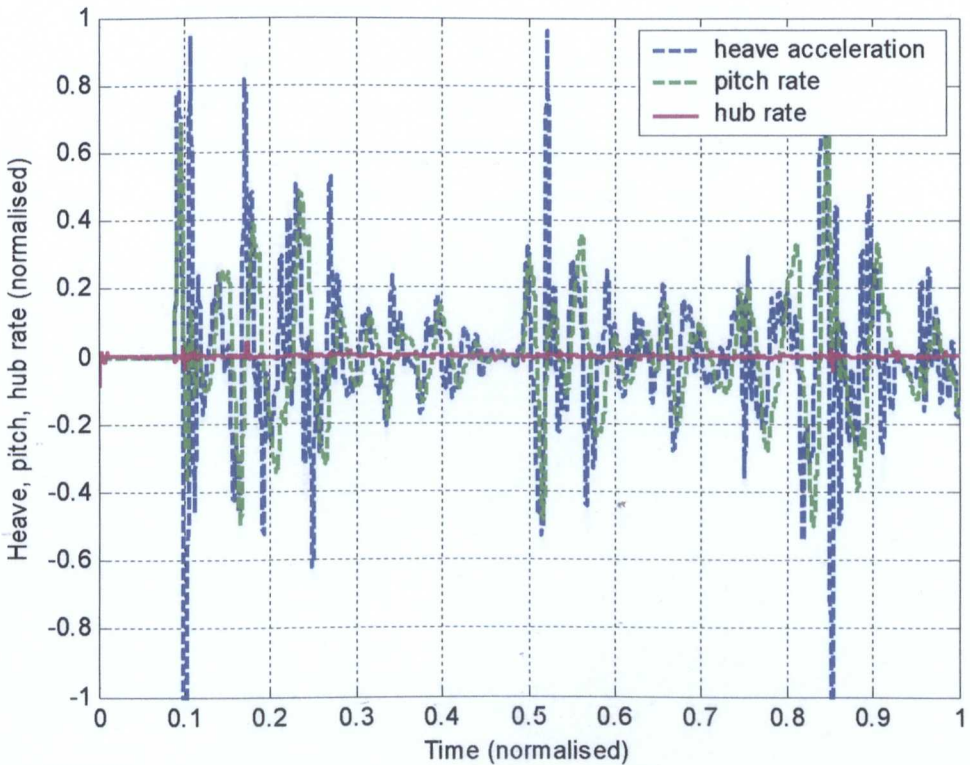


Figure 7-15(b): Simulation responses of out-of-balance system to external disturbances with both feedforward controllers.

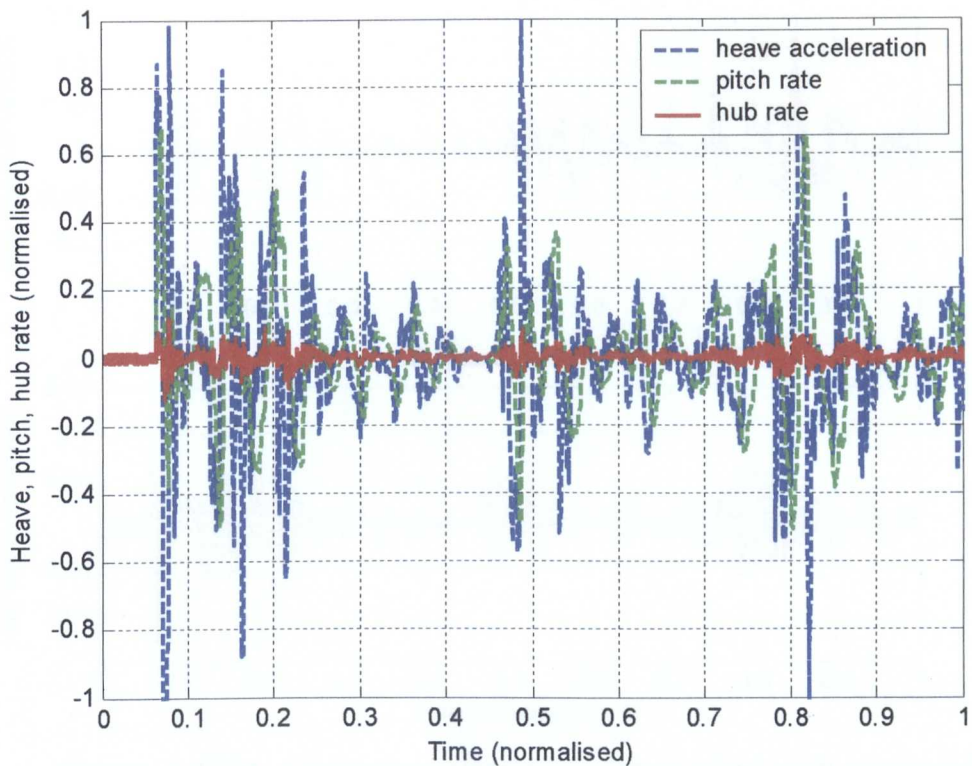


Figure 7-15(c): Measured response of out-of-balance system to external disturbances without feedforward.

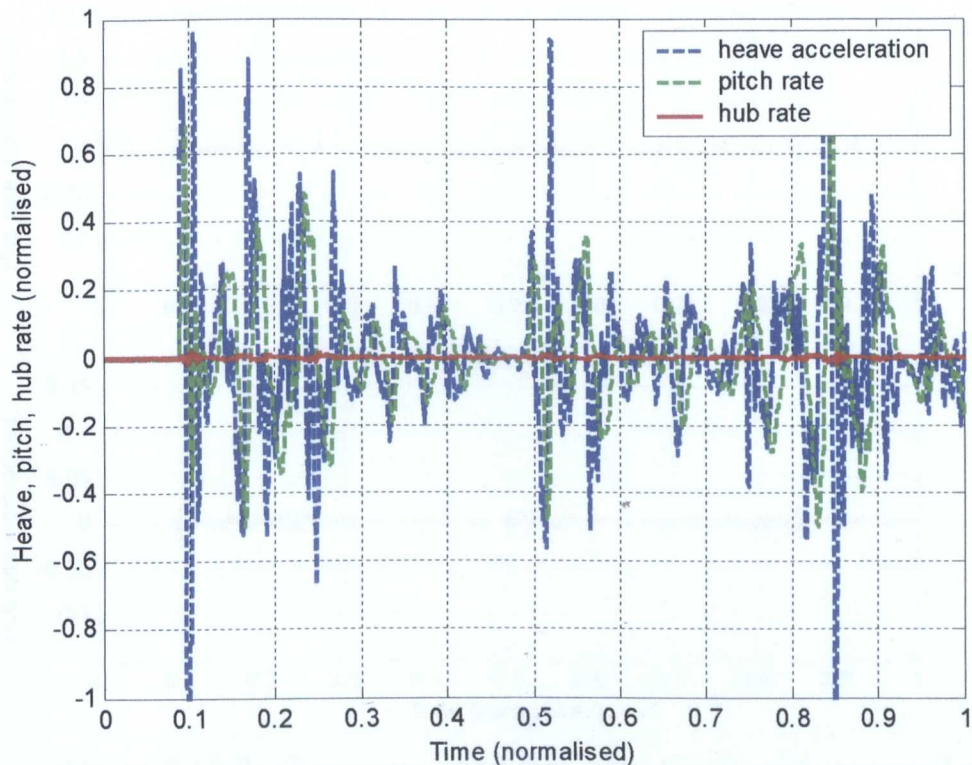


Figure 7-15(d): Measured response of out-of-balance system to external disturbances with both feedforward controllers.

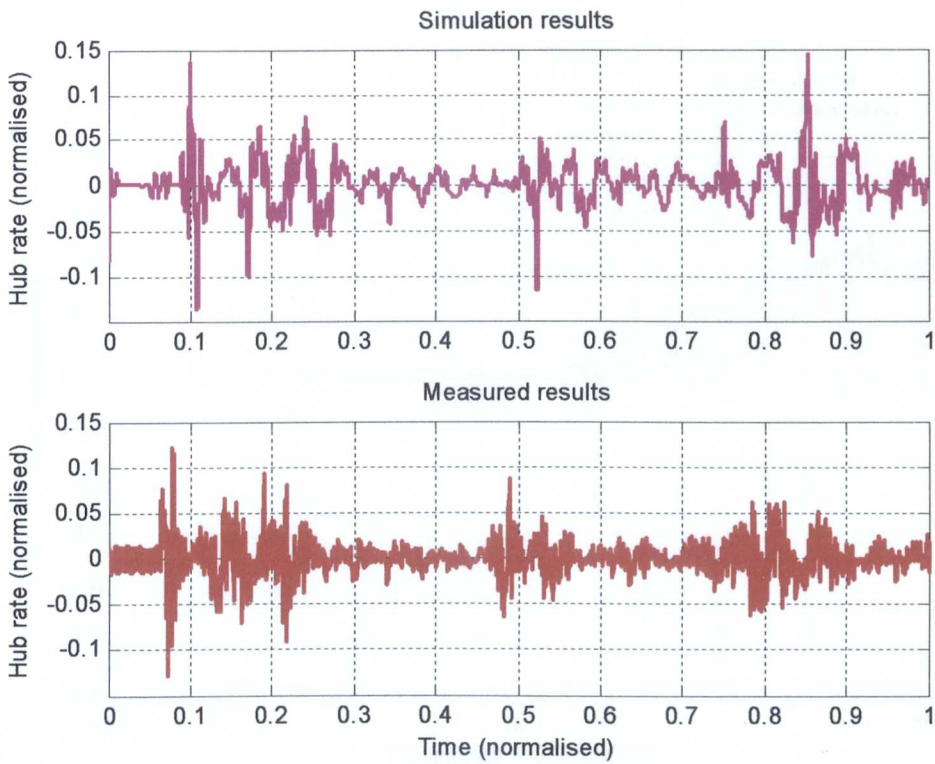


Figure 7-15(e): Comparing simulation output (top) with measured results (bottom) for out-of-balance system to external disturbances without feedforward controllers.

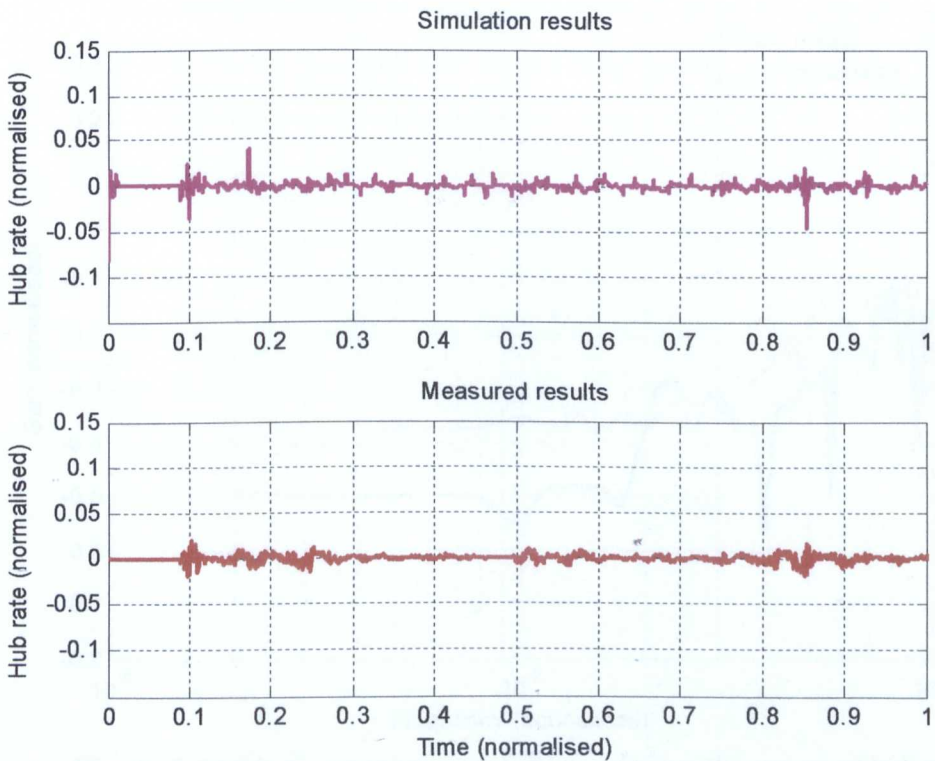


Figure 7-15(f): Comparing simulation output (top) with measured response (bottom) for out-of-balance system to external disturbances with both feedforward controllers.

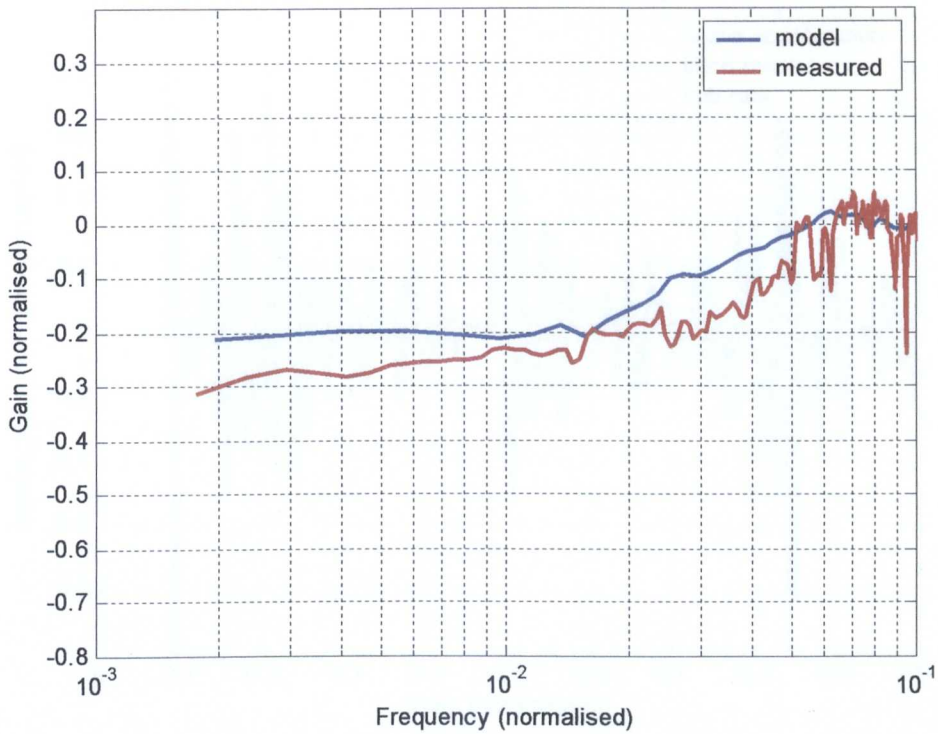


Figure 7-15(g): Comparing simulation output with measured hub response for the out-of-balance system without feedforward control.

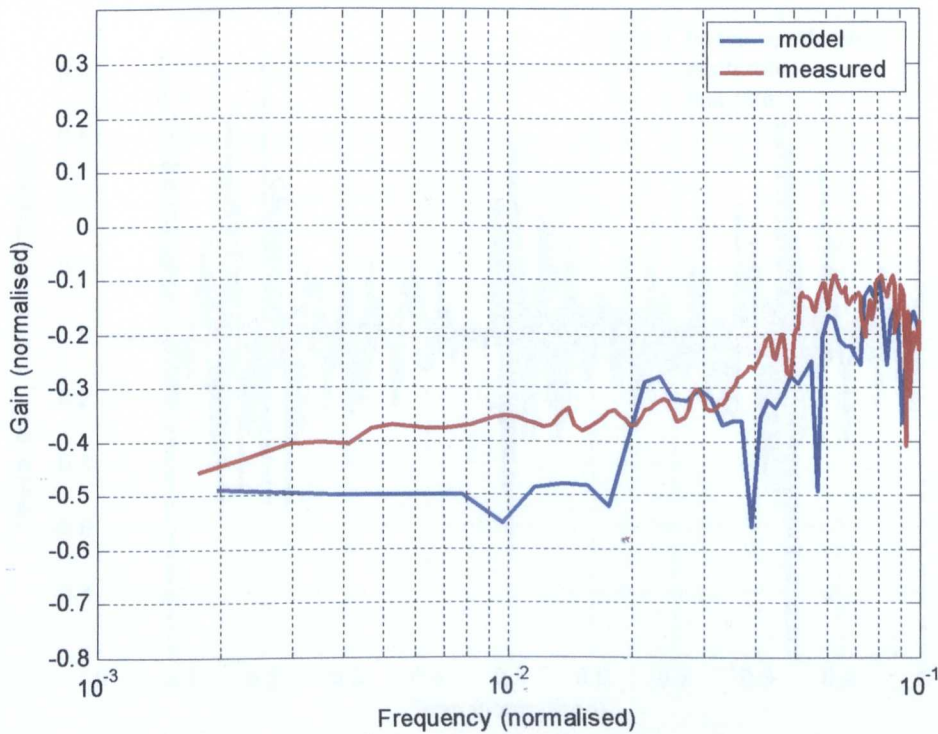


Figure 7-15(h): Comparing simulation output with measured hub response for the out-of-balance system with both feedforward controllers.

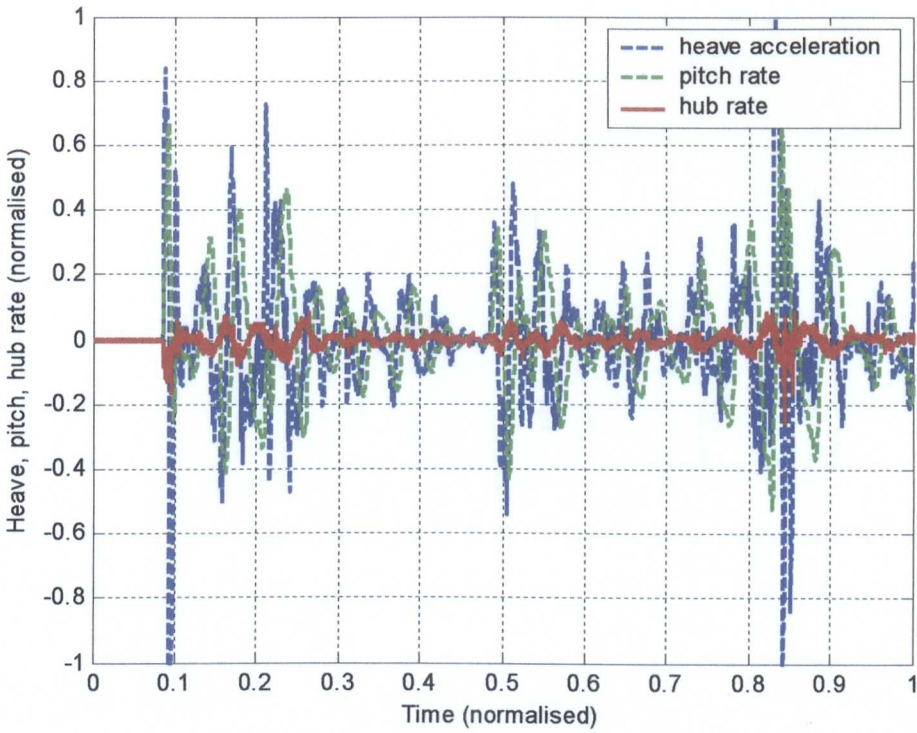


Figure 7-16(a): Measured response of balanced system to external disturbances without feedforward using the out-of-balance controller.

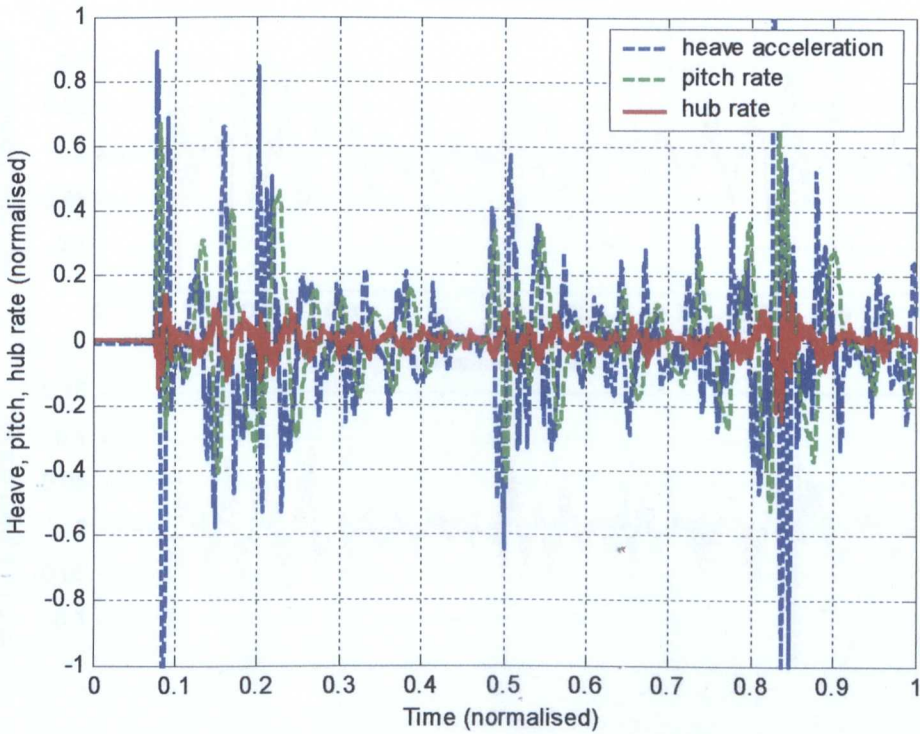


Figure 7-16(b): Measured response of balanced system to external disturbances with both feedforward controllers using the out-of-balance controller.

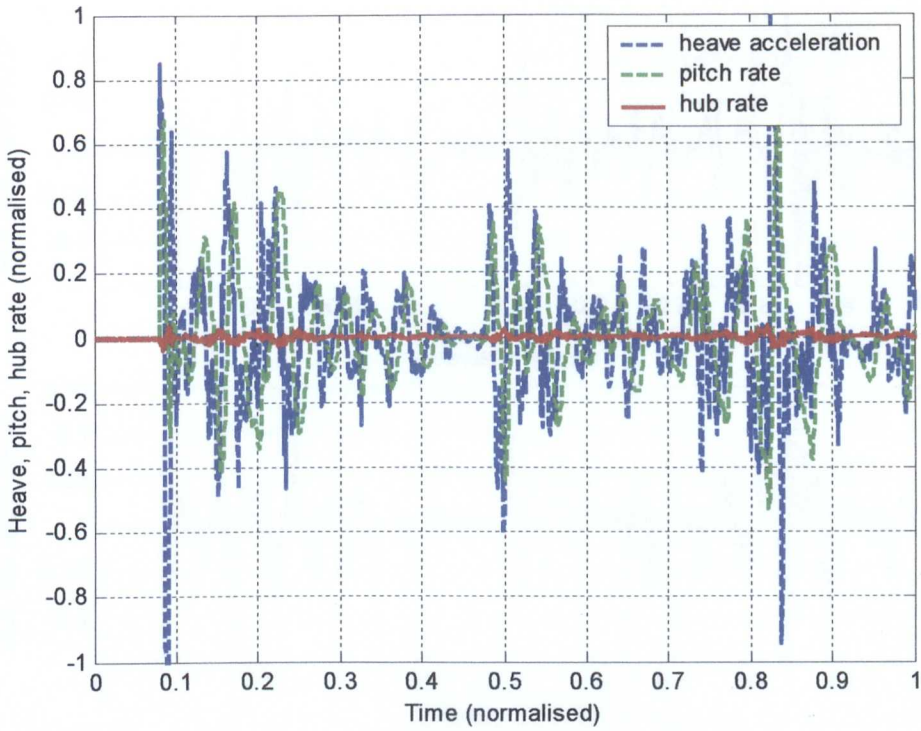


Figure 7-16(c): Measured response of balanced system to external disturbances with pitch feedforward using the out-of-balance controller.

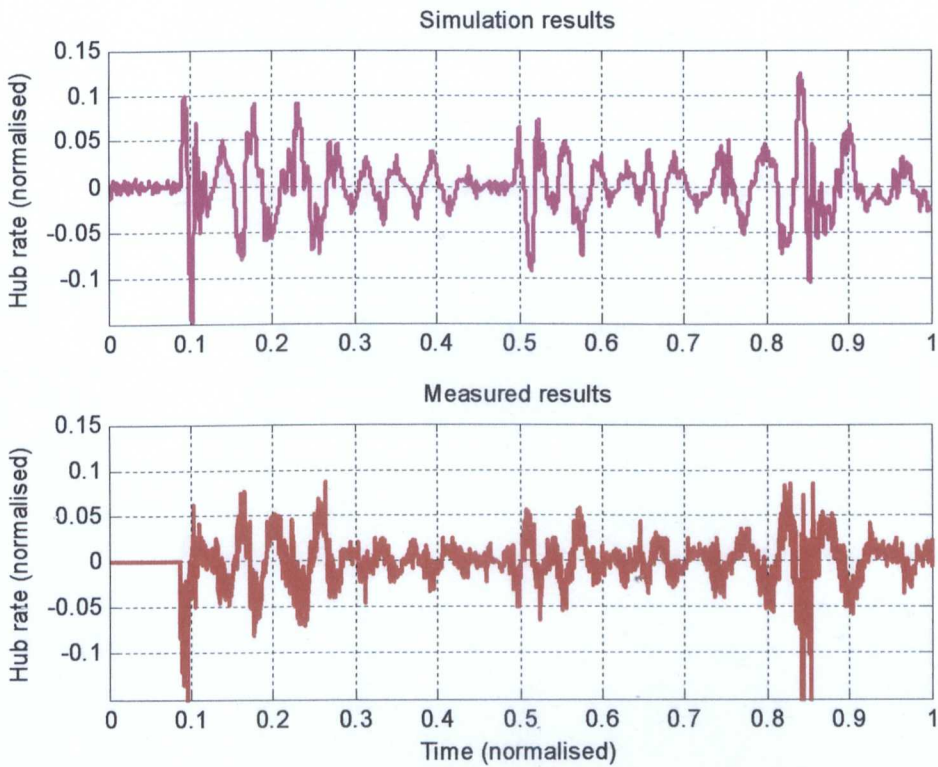


Figure 17-16(d): Comparing simulation (top) with measured response of the balanced system without feedforward controllers using out-of-balance controller.

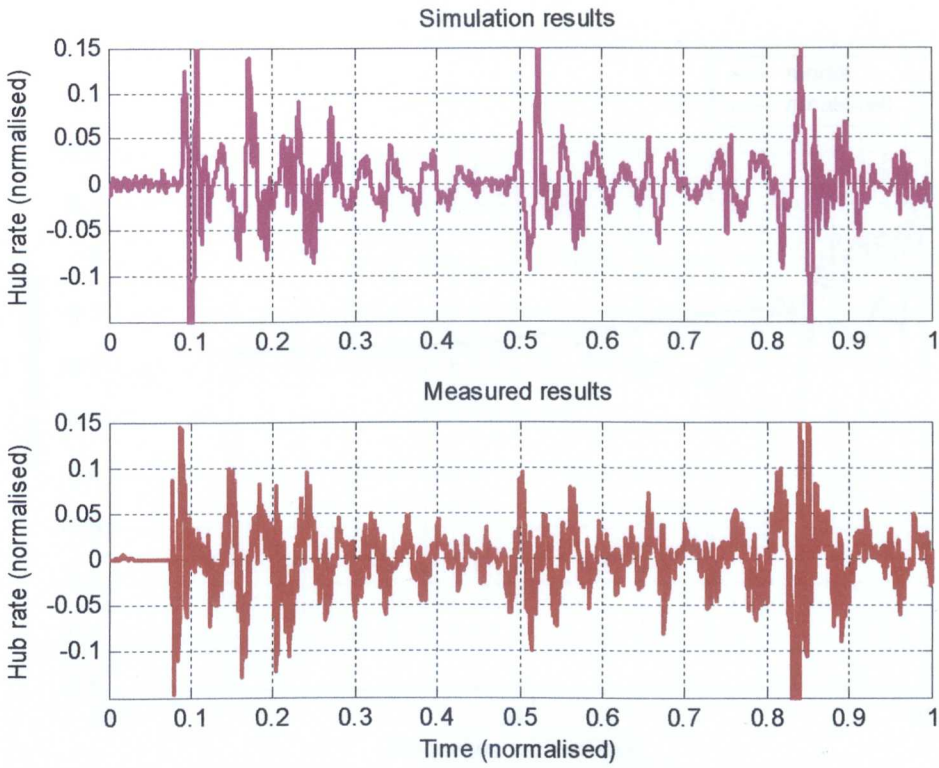


Figure 7-16(e): Comparing simulation output (top) with measured response for balanced system with both feedforward using out-of-balance controller.

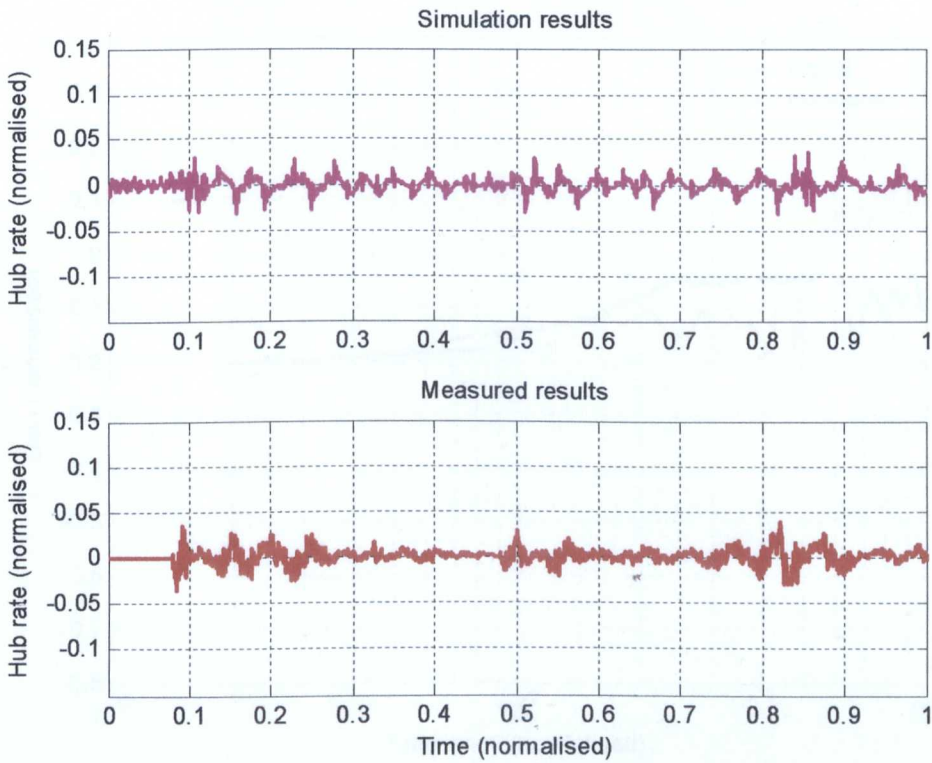


Figure 7-16(f): Comparing simulation (top) with measured response for balanced system with pitch feedforward using out-of-balance controller.

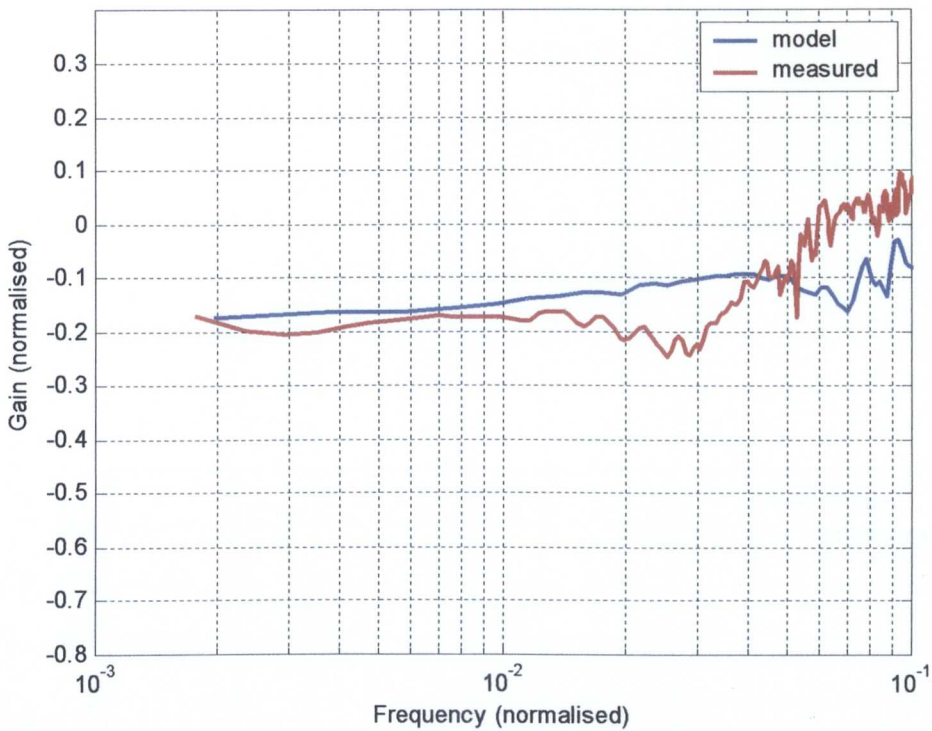


Figure 17-16(g): Comparing simulation output with measured hub response of the balanced system without feedforward using out-of-balance controller.

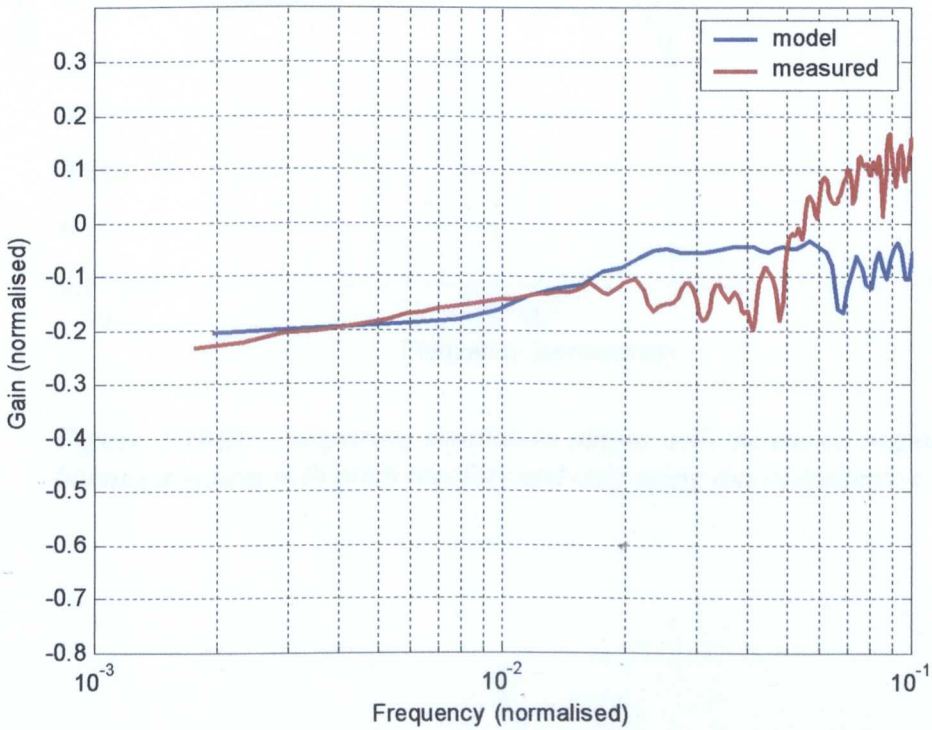


Figure 7-16(h): Comparing simulation output with measured response for the balanced system with both feedforward controllers using out-of-balance controller.

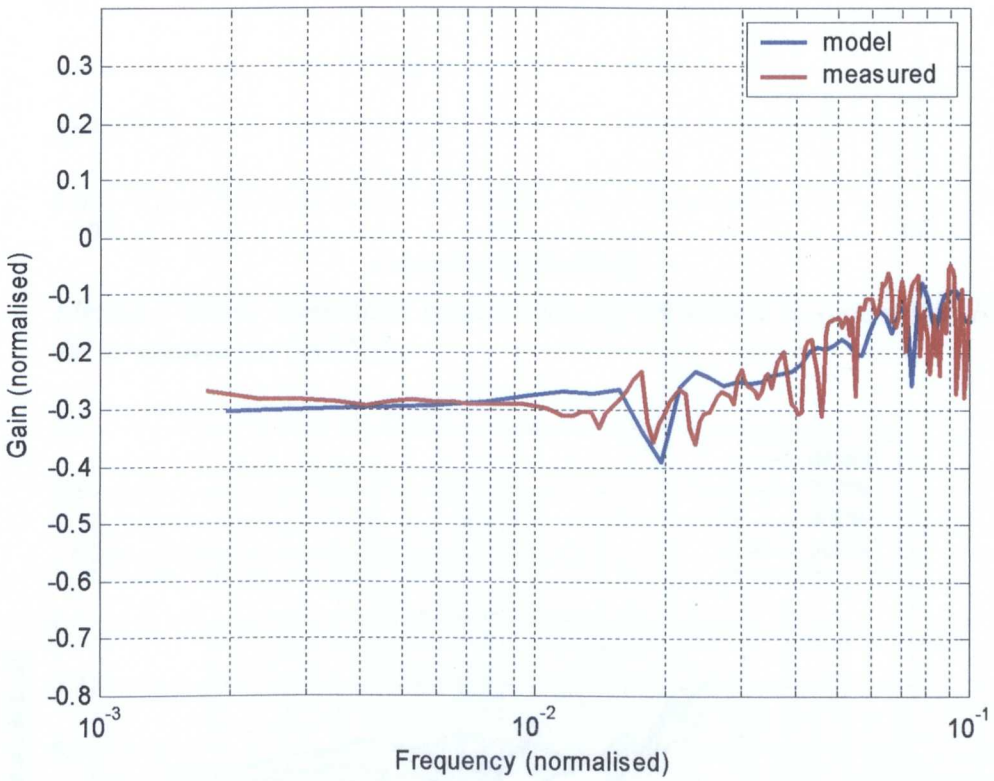


Figure 7-16(i): Comparing simulation output with measured response for the balanced system with pitch feedforward only using out-of-balance controller.

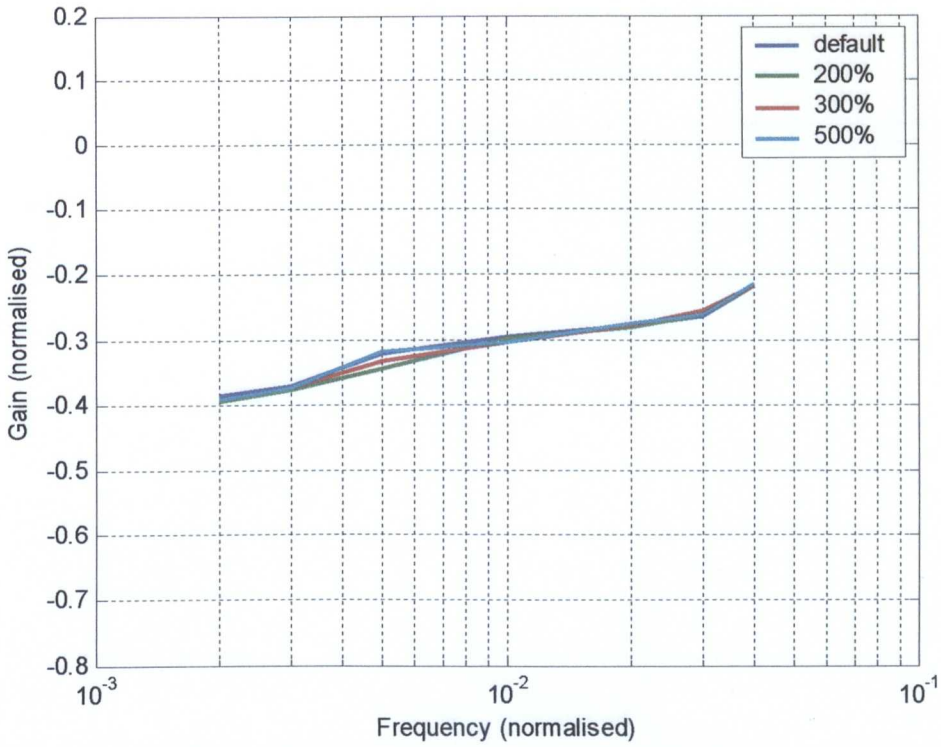


Figure 7-17(a): Simulation results showing variations in system stabilisation due to changes in backlash.

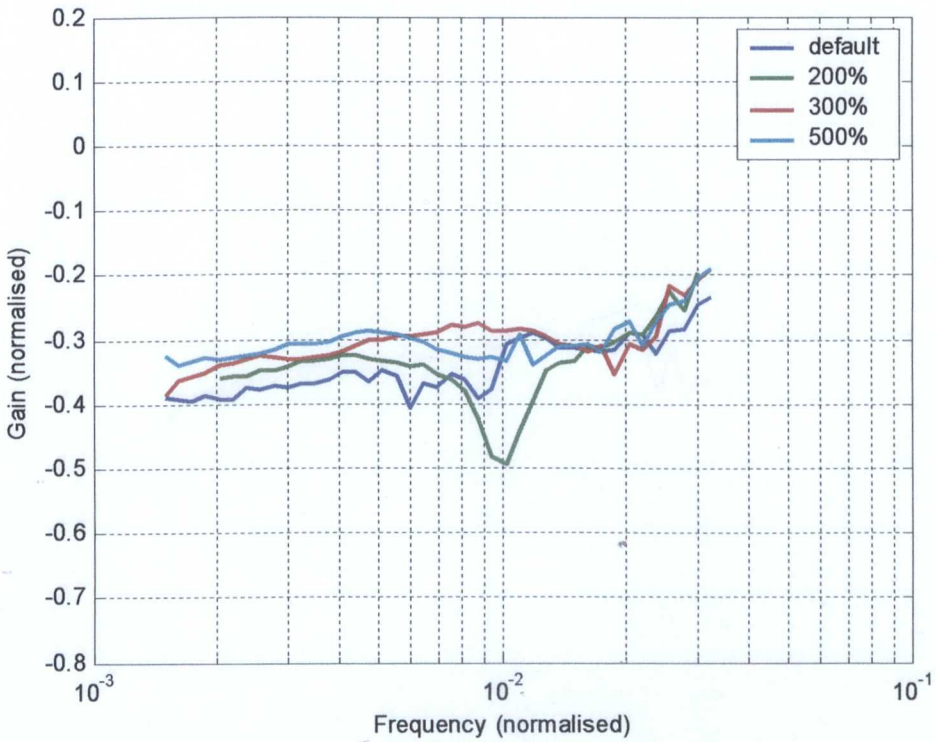


Figure 7-17(b): Measured results showing variations in system stabilisation due to changes in backlash.

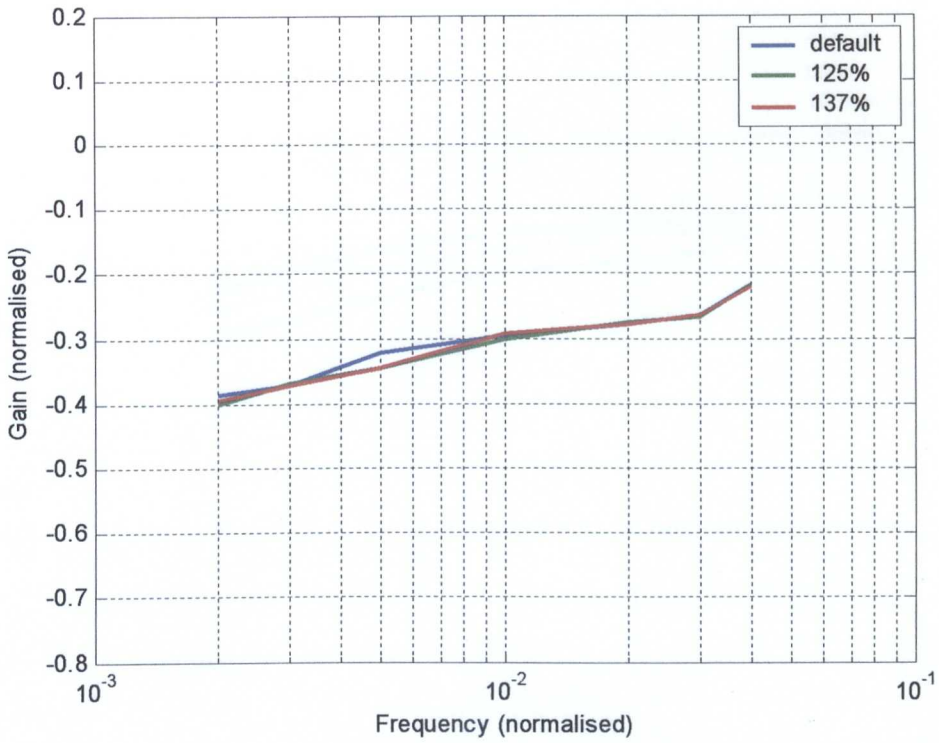


Figure 7-17(c): Simulation results showing variations in system stabilisation due to changes in inertia.

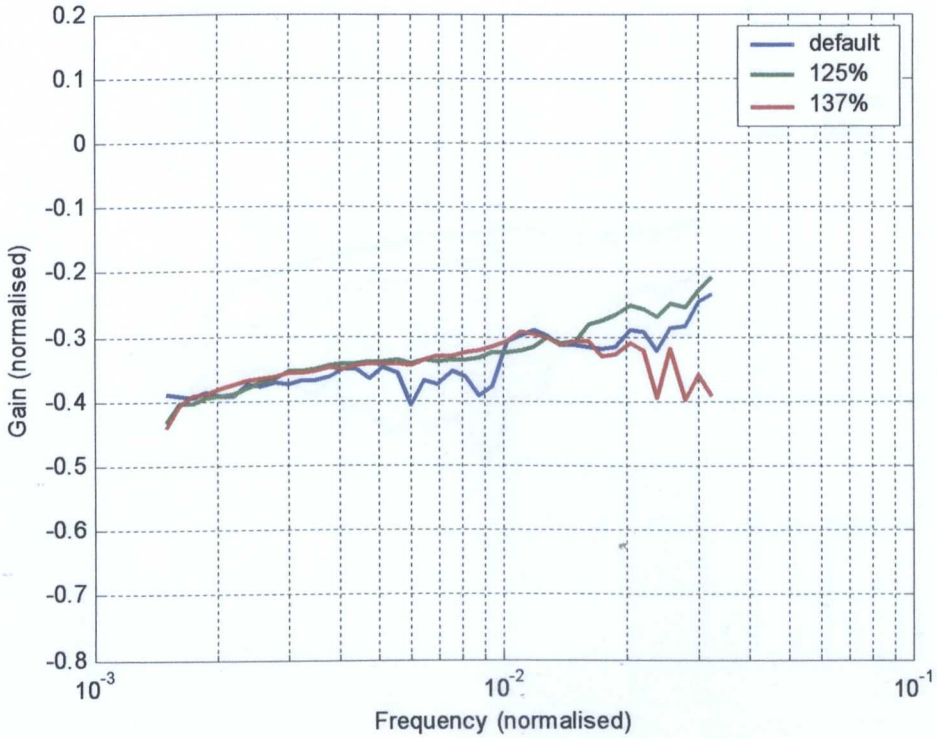


Figure 7-17(d): Measured results showing variations in system stabilisation due to changes in inertia.

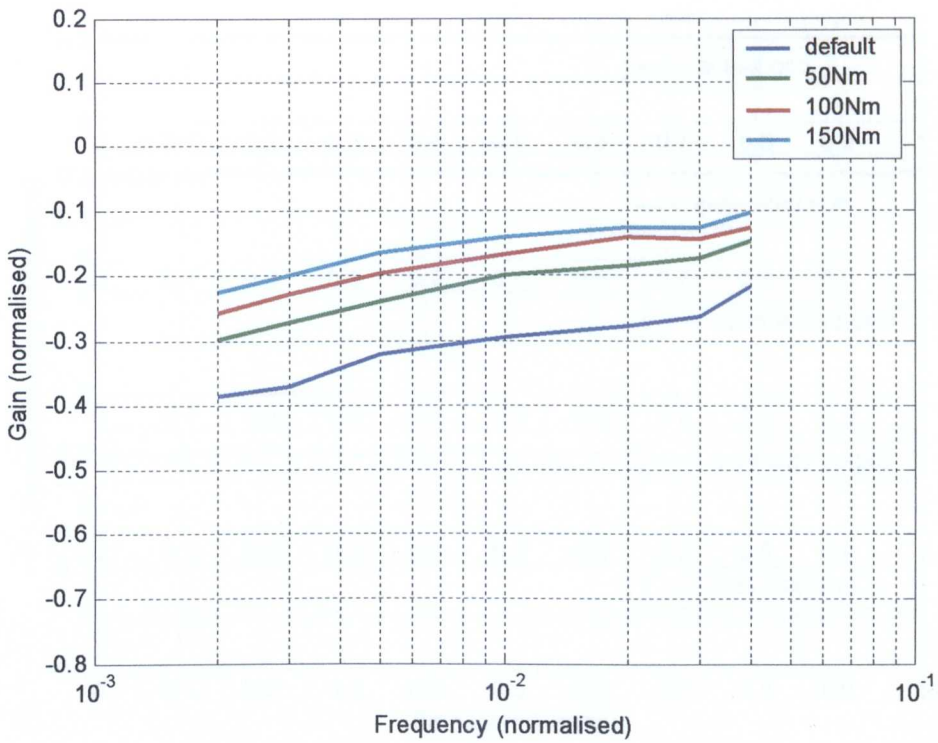


Figure 7-17(e): Simulation results showing variations in system stabilisation due to changes in friction.

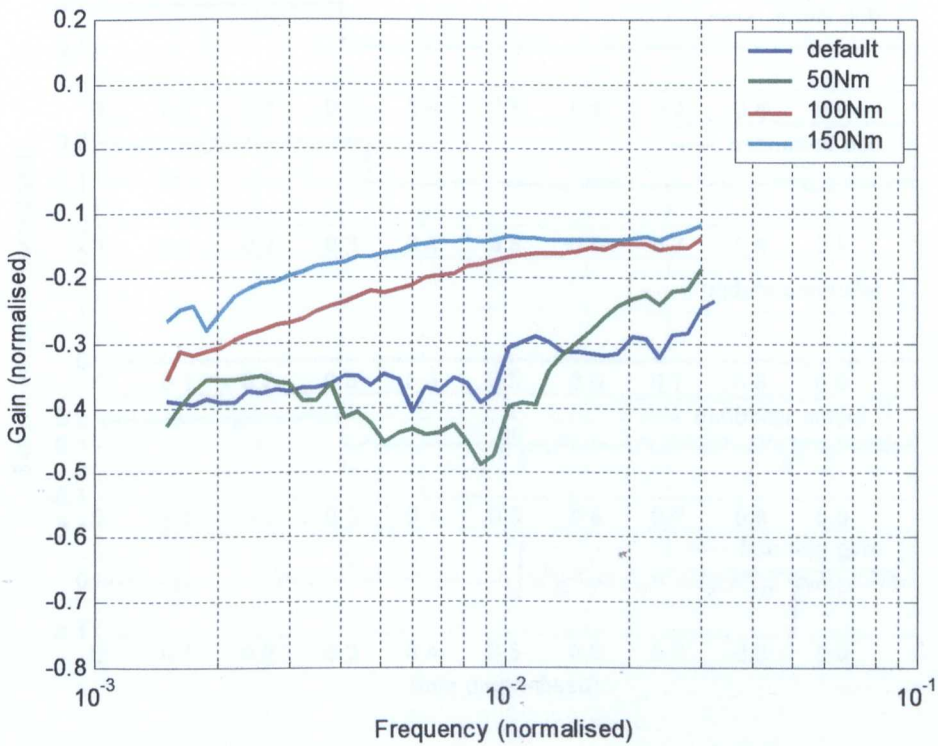


Figure 7-17(f): Measured results showing variations in system stabilisation due to changes in friction.

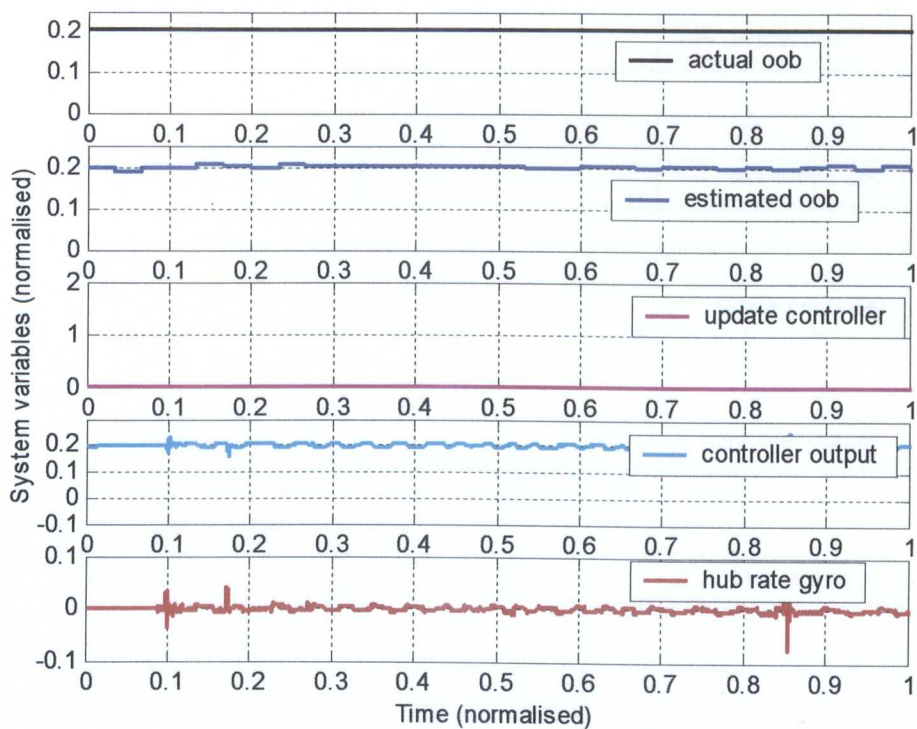


Figure 7-18(a): Various outputs from the system with default out-of-balance.

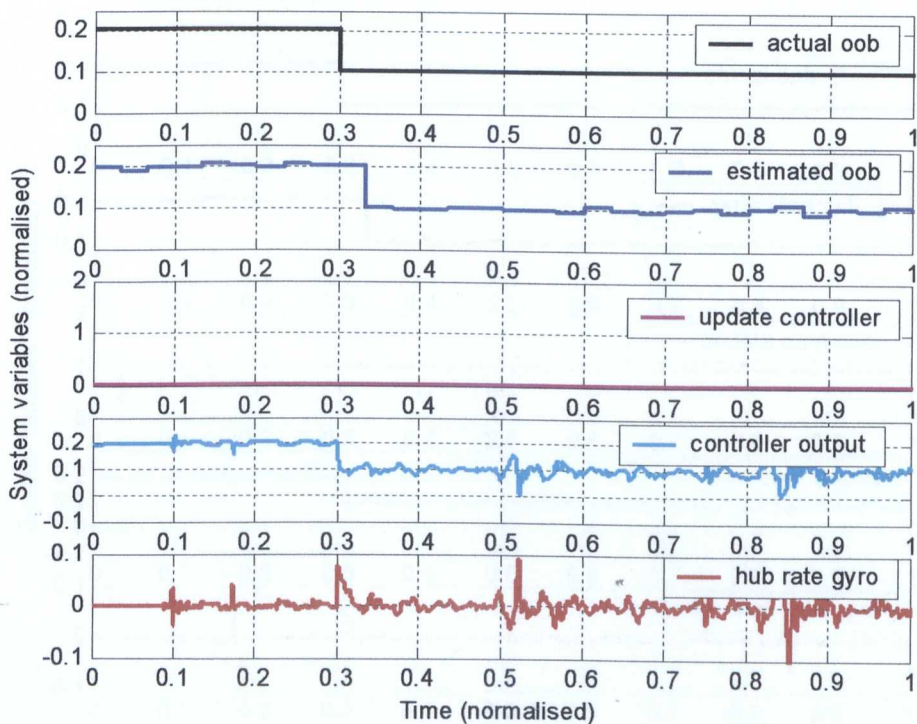


Figure 7-18(b): Various outputs when out-of-balance changes at 0.3 time.

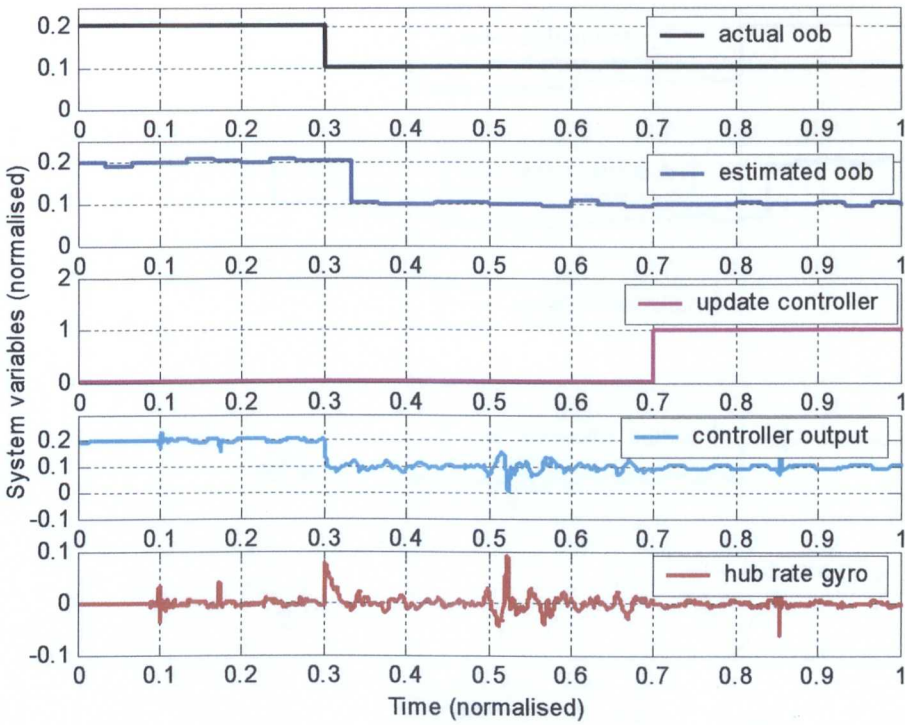


Figure 7-18(c): Various outputs when the system adapts at 0.7 time to out-of-balance change at 0.3 time.

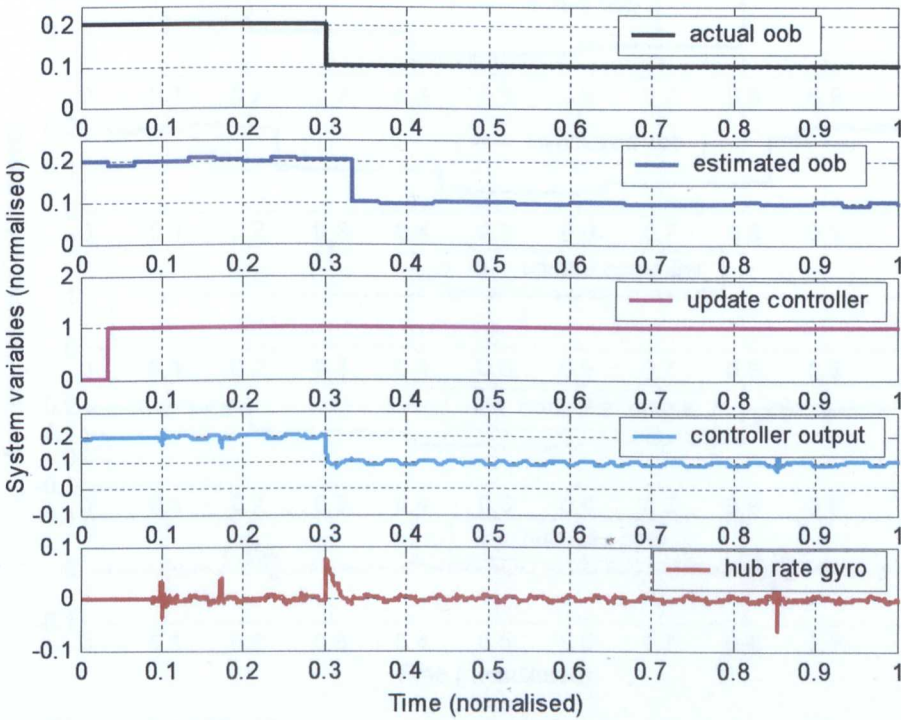


Figure 7-18(d): Various outputs when the system starts to adapts at 0.03 time and out-of-balance changes at 0.3 time.

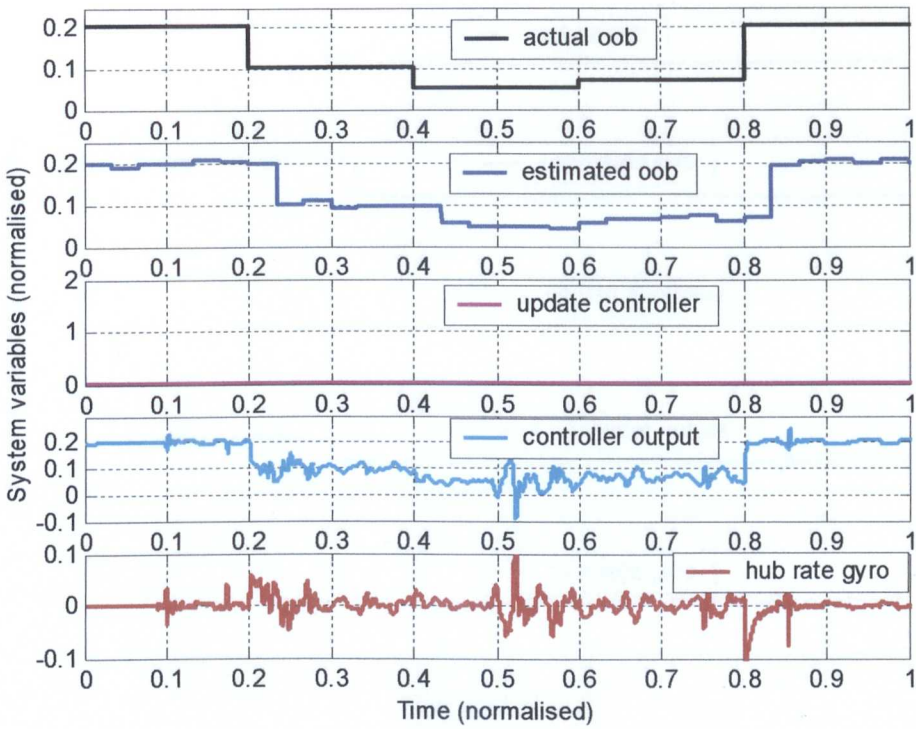


Figure 7-18(e): Various outputs when out-of-balance changes several times.

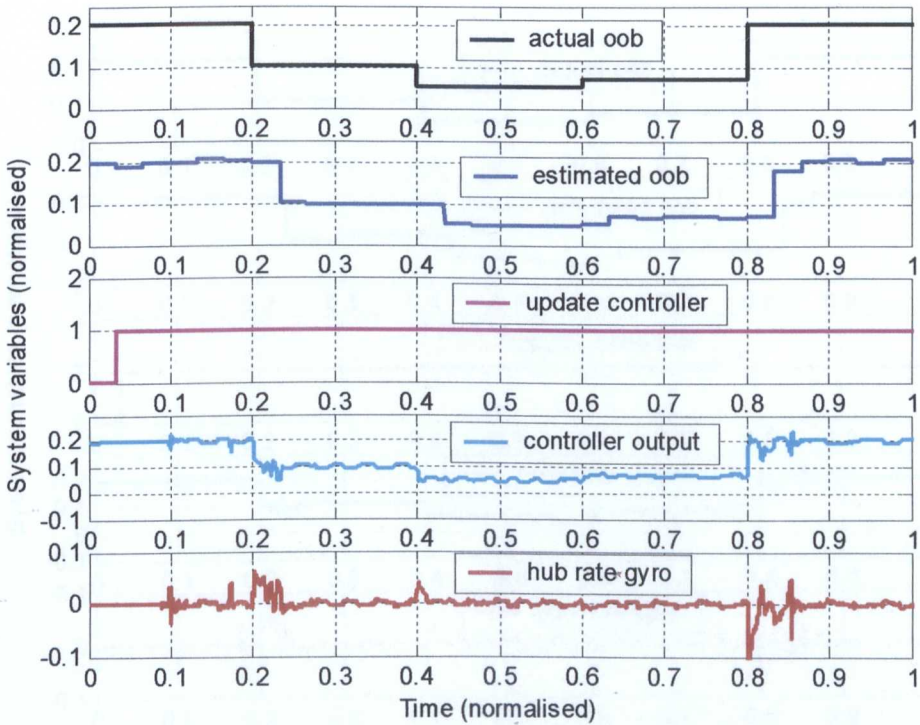


Figure 7-18(f): Various outputs when the system starts to adapt at 0.03time to several out-of-balance changes.

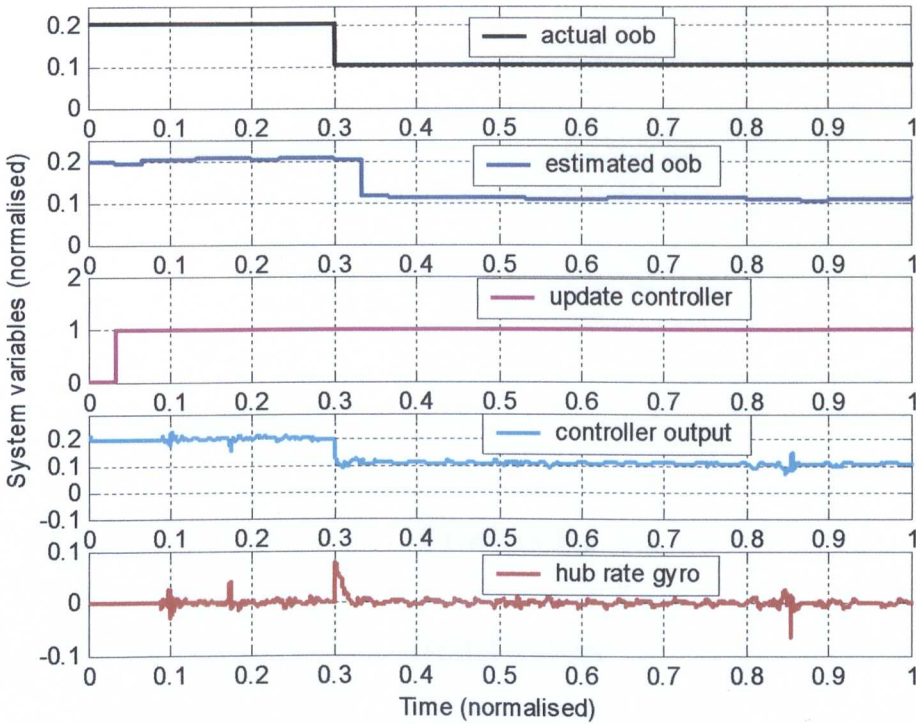


Figure 7-18(g): Various outputs when the system adapts at 0.03 time to out-of-balance changes at 0.3 time for system with the nonlinear amplifier gain.

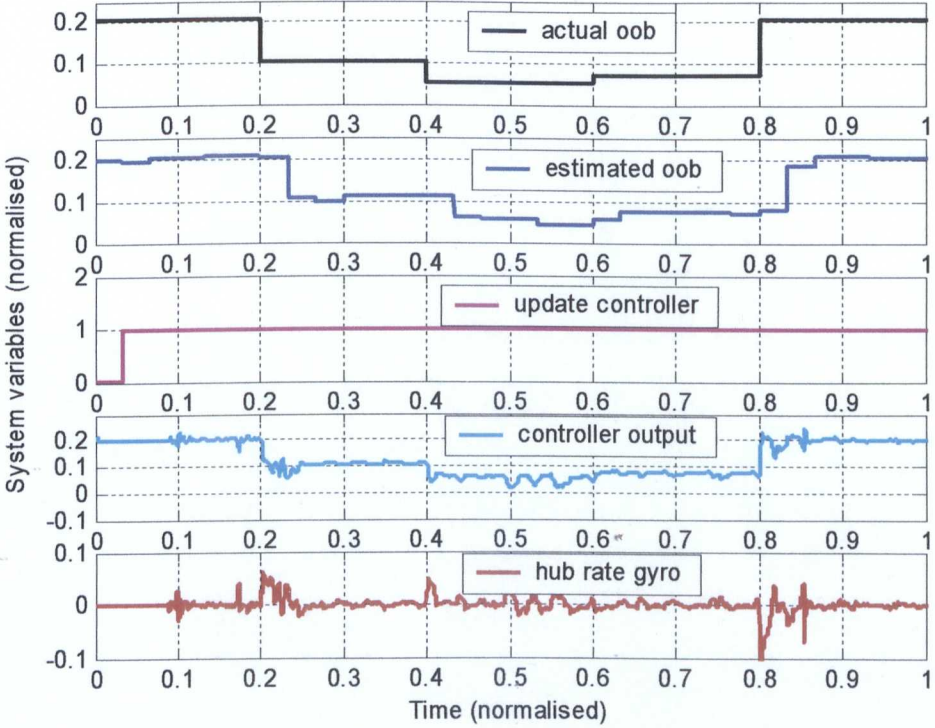


Figure 7-18(h): Various outputs when the system adapts to several out-of-balance changes for system with nonlinear amplifier gain.

CHAPTER 8

DISCUSSION

8.0 Discussion

8.1 Introduction

Difficulties in accurate positioning of stabilised systems are primarily caused by the presence of system nonlinearities, external disturbances, joint compliance and the inherently high-order coupled behaviour of mechanical structures. When presented together meeting the performance specifications can be a formidable challenge. System simulation greatly enhances the understanding of the system behaviour and plays an important part in the control system design process. The work presented in this thesis makes extensive use of simulations and a significant part of the work is devoted to modelling techniques and validation of the models. The discussion which follows brings together important aspects from each chapter is structured to address the aims and objectives presented in chapter 1.

8.2 Modelling of system nonlinearities

Although friction models can be traced back to renaissance period, circa 1500, it is only recently, 1986, that reliable frictions models for control systems work have been developed. Interestingly of the three dynamic friction models used in this research Dahl's[20],[21], model which was the first dynamic model to be developed, provides the most accurate prediction of friction characteristics when compared with experimental data in both the frequency domain and the time domain, presented in section 7.2. It also has the advantage that simulations which use the Dahl model run faster than simulations which use other dynamic or static friction models. The main limitation of the Dahl model is that it does not represent the forces due to stiction or capture the Stribeck effect. These deficiencies are addressed in the reset-integrator model [22]. Further developments of these models have resulted in the LuGre model [23] which includes both the Stribeck and stiction properties and in addition includes rate dependent friction phenomena such as varying break-away force and friction lag. The very close agreement of the Dahl model results with measured data indicates that in the cantilever mechanism used for the experimental studies these additional effects are of secondary nature. Further parametric study is required on reset-integrator and LuGre friction models to achieve a closer agreement with the measured results. The close agreement between the measured and

simulation results suggests that the time constant in the Dahl model is related to speed (RMS) and not acceleration as observed by Walrath[17]. At high input amplitudes all models, dynamic and static, show similar performance which is not unexpected as at high amplitudes the effects of pre-sliding displacement become less prominent.

In balanced systems which use large ratio gearboxes a single Dahl friction model located at the input or the output of the gearbox produces poor results when compared with measured results. Significant improvements are achieved by using two friction models – one located at the input and the other at the output of the gearbox. In the results presented for the balanced system the friction forces are allocated equally between the two models however results suggest that a ratio of 30:70 (motor to load) produces fairly acceptable results. In out-of-balance systems the ratio of friction forces changes and the most accurate results are obtained when a ratio of 10:90 (motor to load) is used. In simulation of out-of-balance systems, such as robots, cranes, large gun systems, where a single Dahl friction model is used then it should be located at the load end of the gearbox.

8.3 Identifying system parameters

It is very useful to be able to determine system parameters without resorting to the use of expensive instrumentation or specialized test procedures. A method proposed by Johnson and Lorenz[27] which has been used on robot gripper application is used in this study to identify the various parameters for the friction observer. The technique also provides a simple method for determining the system out-of-balance and has been extended so that the nonlinear gain characteristics of the amplifier can be extracted. The nonlinear gain obtained by this method shows excellent agreement with measured data. The details of the technique are described in chapter 7. The technique is applied directly to the closed loop system and uses the control signal and the hub rate output signal, both signals used to control the system. The plot of the control signal against the gyro signal provides a graphical illustration which can be used by operators in the field not be familiar with control system design techniques.

8.4 Modelling of flexible structure

The mathematical models developed in this thesis are generic models which can be used to carry out research into the stabilisation of cantilever mechanisms. The models incorporate bending and distortion of the structure, and angular movements caused by the pitch and heave motions of a mobile platform. In many studies, where tip movement is not required, these systems are assumed to be stiff and modelled using lump-parameter techniques. However, control systems designed using low order or truncated models can result in performance degradation caused by spillover effects. To study spillover effects two sets of models are produced. The 'high fidelity' distributed parameter models use finite element techniques and simpler models are developed using lump-parameter methods.

The FE models of the structure are developed and validated with experimental measurements using modal analysis. Several models of the flexible structure are developed ranging in complexity from a single element to 129-element model. As the cantilever mechanism is approximately tapered in cross-section two sets of models are produced. The first set uses elements with constant cross-sections, and a second set uses non-uniform cross-sectioned elements which enable the system geometry to be approximated using fewer numbers of elements or more accurately using the same number of elements. From the results it is established that a three element model gives a good representation of the system. The models which use non-uniform cross-sectioned elements are only marginally better than the constant cross-section elements and either model can be used without significant loss of accuracy. The FE models are developed from first principles for a cantilever mechanism which is a fairly simple shaped structure; for more complex structures the mass, stiffness and damping matrices can be obtained directly from commercially available FE packages and interfaced to the simulations as described in chapter 5. The main difficulty with these models is that they have to be reduced for control system design. Considerable care is required when using the reduction techniques as errors can be induced at low frequencies or additional modes can be introduced at higher frequencies which are not present in the original high order model. Comparison of the frequency responses at the hub of the FE models and lump-parameter models show good agreement at low frequencies but higher frequency modes are not present in the lump-parameter model which may be problematical in some applications.

8.5 Design of the control systems

The design of the control system is based on the H_2 robust control technique described by Grimble[63] and uses the MATLAB toolbox developed by Strathclyde University[68]. The control system which is primarily concerned with system stabilisation consists of three elements- feedback controller, heave feedforward and pitch feedforward. The design process involves the selection of the weighting functions for the three elements of the control system to obtain the appropriate controller characteristics to produce the required system response. Robust control techniques produce high order controllers whose complexity (order) is determined by the complexity of the weighting functions and the linear model of the system. The control system design algorithms fail when large order FE models of the system are used. These models are reduced using the techniques described in section 8.4. The performance of the controllers designed using reduced order models and lump-parameter models showed that in this application the effect of spillover effects is negligible. The performance of the controllers is verified on large order FE models.

H_2 robust control technique is a linear design technique which provides ideal performance when used on linear systems. The results, using the linear model, show that while the feedback control is able provide some rejection of external disturbances the inclusion of the two feedforward controllers provide substantial improvements. However, in the system under consideration friction is a dominant nonlinearity which causes substantial reduction in system accuracy and the results do not compare well with the linear model results. A nonlinear observer is incorporated in the control system which 'linearises' the nonlinear system. The parameters for the observer can be determined using the iterative identification technique presented in section 8.3.

The robustness properties of the control system are assessed using the nonlinear model of the out-of-balance system and it is shown that the control system is tolerant to changes in hub inertia and servo drive backlash, but is sensitive to changes in friction and system out-of-balance. The performance is particularly poor when system out-of-balance is changed. This degradation is caused by the limitations of the heave feedforward controller. The performance of the system is restored to the original levels by redesigning the controller with new out-of-balance values. In the redesigned controller the prominent

changes occur in the gain of the heave feedforward controller which is related to the change in magnitude of the out-of-balance. The pitch feedforward controller and the feedback controller remain unaltered.

A simulation study is presented for an adaptive control system which tracks the changes in system out-of-balance and automatically adjusts the heave feedforward controller to maintain the system performance to the required levels. The feedback control signal is used to determine the magnitude of system out-of-balance. The adaptive technique is able to adjust the controller parameters regardless of the platform being mobile or stationary. The adaptive control system produces excellent results when step changes in system out-of-balance are introduced.

8.6 Experimental results

From the outset it was intended that the research would provide practical solutions which could be incorporated in future systems and the techniques developed applicable to servo systems in general. To this end the practical work was carried out on a real system which was modified, without compromising its integrity, to include additional instrumentation, facilities to change system parameters and the control system hardware and software environment which enabled rapid development of control system algorithms.

The performance of the system is assessed using frequency and time-domain tests commonly used to specify control system requirements. The primary interest being the response of the system to input demand signals, the ability of control system to reject the heave and pitch disturbances and the robustness properties of control system to changes in system parameters. The design of the rig enabled the following parameters to be changed:

- Balance of system
- System inertia
- System backlash
- Friction at pivot

The response of the system to external disturbances is measured in the laboratory using a Platform Motion Simulator. The effects of heave motions are simulated by mounting the rig so that it was offset from the rotational axis of the PMS. Measured data from field trials used to drive the PMS and analysis of the PMS response showed that the heave motions can be simulated fairly accurately although the heave and the pitch motions cannot be controlled independently. The use of the PMS proved to be particularly useful as it enabled extensive experimental work to be carried out in a cost effective manner and enabled specific tests which are used in control system design and theoretical studies to be carried out. Some of the tests, particularly the frequency response tests, used to determine the friction characteristics, would have been very difficult and expensive to carry out in field trials.

The robust control design techniques produce large order linear controllers which were converted to digital form (z-domain), using the facilities provided in the CACSD package. These are converted into C code using automatic code generating software and integrated, as a function, into the rig control system. The process proved to very effective as portable software was developed quickly and imbedded into the rig control system.

The measured stabilisation results, in both the frequency and time-domain, showed good agreement with the predicted results. The theoretical frequency-domain results were obtained using a simulation of the frequency response analyser which enabled direct comparison with experimental results.

8.7 Concluding remarks

The results are promising and generally applicable to a wide variety of applications. Some of the techniques have been extended to other domains most notably the parameter identification technique which has been used to design control of actuators for an autonomous vehicle, Heyes and Dholiwar *et al.*[93].

CHAPTER 9

CONCLUSIONS AND RECOMMENDATIONS

FUTURE WORK

9.0 Conclusions and recommendations for future work

9.1 Conclusions

- a) The primary conclusion of the research is that out-of-balance systems can be controlled as effectively as balanced systems and provide stabilisation performance similar to those achieved for conventional balanced systems. However, the controller for an out-of-balance system is slightly more complicated, which requires the design of a feedforward controller and an additional transducer to measure the heave accelerations. In the vertical plane the servo system has to provide static torque to overcome the effects of gravitational acceleration. These torques can be many times greater than the torques required for the motion control resulting in higher powered servo components. This disadvantage can be overcome by using springs or equilibrators, to statically balance the system. The additional transducer and the higher capacity servo components result in increased system costs and increased power requirements which may be at a premium in some mobile applications.

- b) Stabilisation performance is sensitive to both changes in friction and changes in system out-of-balance. In the literature review, chapter 2, many papers are reported which describe techniques which compensate for changes in friction values. In this research the effects on system stabilisation performance due to the changes in system-out-of balance are addressed. Results of simulation study of an adaptive control system developed in this research show that changes in out-of-balance can be accommodated so that the system maintains the desired levels of stabilisation performance.

- c) The iterative technique used for nonlinear system identification provides an elegant method for parameter identification eliminating the need to install additional transducer or sensor systems. The friction characteristics, amplifier nonlinearities and out-of-balance torques were identified in this research. The out-of-balance torque identified using this technique provides a simple method for manually scaling the heave disturbance feedforward controller which enables the controller to cope with changes in system out-of-balance. Similarly the changes in friction can be

accommodated by tuning the parameters of the nonlinear observer. The graphical technique is particularly suitable for use in the field as operators who may not be familiar with control system design can make the necessary adjustments to the system.

- d) The three dynamic friction models, reset-integrator, LuGre and Dahl's model, used in this study display high order nonlinear behaviour at low inputs observed in the experimental results. Dahl's model provides the closest agreement with measured results. The two static models show the poorest agreement with measured results at low input speeds but show good agreement at higher amplitude inputs.
- e) A model of the flexible structure is developed and validated using modal analysis. The structure, which has a non-uniform cross-section, is modelled using finite element technique and the results show that it can be modelled fairly accurately using three elements.
- f) The results show that the H_2 robust control technique is able to cope fairly well with large changes in system parameters such as amplifier gain, hub inertia, and backlash but is sensitive to changes in system out-of-balance and friction. A friction observer is used in the control system design and both the simulation and experimental results show that it provides substantial improvements in performance for system stabilisation and response to input demand signals.
- g) The experimental work was carried out in the laboratory using a PMS, which has many advantages, in terms of cost, safe environment, etc. The PMS was used to determine the friction characteristics of the system. The main limitation of the PMS is that it only provides pitch disturbances. This limitation was overcome, by mounting the rig so that it was offset from PMS rotational axis, which enabled the research to be conducted on out-of-balance systems.

9.2 Recommendations for future work

The work has successfully fulfilled both the theoretical and experimental objectives of the research. However, completion of any work of this nature often highlights difficulties and uncovers areas in which further research is required. The discussion which follows first considers improvements in the work presented and then discusses new directions for future research.

- a) In the robustness tests the changes in friction were achieved using a fairly simple commercially available mechanism which did not provide accurate control of friction forces. The brake pads used in the system were made from synthetic material which did not represent changes in friction which would occur in metal to metal contact such as meshing gear teeth or bearing surfaces. A better designed system is required which enables more accurate control of various parameters of friction enabling more accurate assessment of the characteristics of friction which have an effect on system performance.
- b) The changes in system out-of-balance were achieved by installing additional masses at the hub which not only changed the balance but also changed the moment of inertia, and the mass of the system. An improvement in the mechanical design is required so that both the inertia and the out-of-balance can be changed independently while keeping the system mass constant.
- c) The parameter identification technique described enables the system out-of-balance to be estimated from the control signal which is then used to change the gain of the feedforward controller. This technique can only be used in the vertical plane where the static torque due to gravity produces an offset in the control system signal. For out-of-balance systems which operate in the horizontal plane such as the azimuth axis of a typical stabilised system or in zero gravity environment, other techniques are required to determine changes in system out-of-balance. The signal can then be used to scale the feedforward controller as described in section 7.
- d) Surprisingly the newer dynamic friction models, the reset-integrator and LuGre models, were not as accurate in predicting the friction characteristics as the Dahl

model when compared with the experimental frequency response data obtained from the motions of the platform and the cantilever mechanism. More detailed investigation is required to establish the reasons for this discrepancy and on the selection of parameters for these models.

- e) The controller in this research is based on H_2 control system design which is a linear technique and provides excellent results when used on linear models. It is recommended that the performance of other control techniques such as fuzzy logic control and variable structure control, which are both nonlinear techniques, should be applied to the stabilisation of out-of-balance mechanisms.

- f) In large stabilised cantilever mechanisms which are controlled using sensors mounted at the hub it has been shown that the motions at the tip can cause substantial errors in pointing accuracy. These errors can occur due to the thermal distortion caused by uneven heating of the system by the sun, due to deposit of snow and other debris or due to distortions caused by forces induced by the motions of the vehicle. Future research should address the stabilisation at tip for both balanced and out-of-balance systems. The techniques for modelling of these systems are presented in chapter 5 which covers system simulation.

REFERENCES

-
- 1 **Haessig D.**, Line of sight pointing and stabilisation control systems. The control handbook, (Levine W.S.), *IEEE Press*, ISBN 0-8493-8570-9, 1996, 1326-1338.
 - 2 **Moorty K., Marathe R., and Babu H.**, Fire control systems for mobile vehicles using fuzzy controllers. *Proc. of SPIE* . Vol. 6052, 60520A-1, 2005, 1-8.
 - 3 **Kennedy P. J., and Kennedy R. L.**, Direct versus indirect line of sight (LOS) stabilisation. *IEEE Trans. on control systems technology*, Vol. 11, N0.1, 2003, 3-15.
 - 4 **Profeta J. A., Vogt W. G., and Marlin M. H.**, Torque disturbance rejection in high accuracy tracking systems. *IEEE Trans. aerospace and electronic systems*, Vol. 26, No.2, March 1990, 232-238.
 - 5 **Bouazza-Marouf K., and Hewitt J. R.**, Control of a dynamic platform for offshore applications. *Mechatronics*, Vol. 3, No. 5, 1993, 589-609.
 - 6 **Henry A.**, Precision weapon stabilisation enables fire-on-the-move. *Defense systems review*, October 1984, 56-59.
 - 7 **Masten M. K., and Sebesta H. R.**, Line-of-sight stabilisation/tracking system: An overview. *Proc. American control conference ACC*, 2, 1987, 1477-1482.
 - 8 **Girvin D. L., and Book W. J.**, Numerical analysis of nonminimum phase zero for non-uniform link design. *Dynamics of flexible multibody systems*. AMD-Vol 141/dsc-Vol 37. ASME 1992, 5-16.
 - 9 **Armstrong-Helouvry B., Dupont P., and Canudas de Wit.**, A survey of models, analysis tools and compensation methods for the control of machines with friction. *Automatica*, Vol. 30, No.7, 1994, 1083-1138.
 - 10 **Armstrong Helouvry B.**, Control of machines with friction. *Kluwer academic publishers*, ISBN 0-7923-9133, 1991.
 - 11 **Radcliffe C., and Southward S. A.**, Property of stick-slip friction model which promotes limit cycle generation. *Proc. 1990 American control conference ACC*, San Diego, CA., 1198-1203.
 - 12 **Maqueira B., and Matsen M. K.**, Adaptive friction compensation for line-of-sight pointing and stabilisation. *Proc. American control conference ACC*, June 1993, 1942-1946.
 - 13 **Bird J. S.**, Measurement of tank gun dynamics in support of dynamic muzzle referencing systems. *Defence research establishment*, Ottawa. Report No. 1053. Dec 1990.
 - 14 **Joshi S.M., and Kelkar A.G.**, Control of flexible space structures. The Control handbook, (Levine W. S), *IEEE press*, ISBN 0-8494-8570-9, 1996,1318-1319.

-
- 15 **Balas M. J.**, Feedback Control of Flexible System. *IEEE Trans. automatic control*, Vol. AC-23, No.4, August, 1978, 673-679.
- 16 **Bigley W. J.**, and **Schupan F.**, Wideband base motion isolation control for a mobile platform. *Proc. of American control conference ACC*, 2, 1987, 1483-1490.
- 17 **Walrath C. D.**, Adaptive bearing friction compensation based on recent knowledge of dynamic friction. *Automatica*, Vol. 20, 1984, 717-727.
- 18 **Leonardo da Vinci.**, Codex Arundel. *British Library*, MS. 263, circa 1500, ff 40v-41.
- 19 **Morrison J. L. M.**, and **Crossland B.**, Introduction to the mechanics of machines, (The notebooks of Leonardo da Vinci translated by J Cope 1938). *Longman*, ISBN 0-582-44-7291, 422-423.
- 20 **Dahl P.R.**, A solid friction model. *Aerospace corporation*, El Segundo, California, USA. Tech report TOR-0158(3107-18)-1, 1968.
- 21 **Dahl P.R.**, Measurement of solid friction parameters of ball bearings. *Proc. Of 6th annual symposium on incremental motion, control system devices*, university of Illinious, 1977, 49-60.
- 22 **Haessig D.**, and **Friedland, B.**, On the modelling and simulation of friction. *Journal of Dynamic systems, measurement and control*, 113(3) 1991, 354-362.
- 23 **Canudas de Wit C.**, **Olsson H.**, **Astrom, K. J.**, and **Lischinsky P.**, A new model for control of systems with friction. *IEEE Trans. on automatic control*, Vol. 40, No 3, March 1995, 419-425.
- 24 **Tustin A.**, The effects of backlash and of speed-dependent friction on stability of closed-cycle control systems. *IEE Journal*, 1947, 94(2A), 143-151.
- 25 **Karnopp D.**, Computer simulation of stick-slip friction in mechanical dynamic systems. *Journal of dynamics, systems measurement and control*, Vol. 107, March 1985, 100-103.
- 26 **Gilbart J. W.**, and **Winston, G. C.**, Adaptive compensation for an optical tracking telescope. *Automatica*, Vol. 10, 1974, 125-131.
- 27 **Johnson C.T.**, and **Lorenz R.D.**, Experimental identification of friction and its compensation in precise, position controlled mechanisms. *IEEE Trans. on industrial applications*, Vol. 28, No 6, November 1992, 1392-1398.
- 28 **Dupont P. E.**, and **Armstrong Helouvry B.**, Compensation techniques for servos with friction. *Proc. of American Control Conference ACC*, San Francisco, June 1993, 1915-1920.

-
- 29 **Radcliffe C., and Southward, S. A.,** Property of stick-slip friction model which promotes limit cycle generation. *Proc. American Control Conference ACC*, San Diego, CA., 1990, 1198-1203.
- 30 **Kubo T., Anwar G., and Tomizuka M.,** Application of nonlinear friction compensation to robot arm control. *IEEE International conference of robotics and Automation*, San Francisco, 1986, 722-727.
- 31 **Shen C.N., and Wang H.,** Nonlinear compensation of a second and third order system with dry friction. *IEEE Trans. on applications and industry*, March 1964, 128-136.
- 32 **Hansson A., Gruber P., and Todtli J.,** Fuzzy anti-reset windup for PID controllers. *Proc. World congress on automatic control IFAC* Sidney, Australia, 1993.
- 33 **Himmel L. C., Geiger, G. J., and Fletcher, K. R.,** Examination of adaptive control based approaches to friction compensation in space craft gimbal control systems. *Proc. 14th conf. decision and control*, December 1985, 642-646.
- 34 **Hojjat Y.,and Higugi, T.,** Application of electromagnetic impulse force to precise positioning. *International Journal Japan Society Precision Engineering*, Vol. 25, No 1, March 1991.
- 35 **DeWeerth, S., Neilsen, C., Mead, C., and Astrom, K.,** A simple neuron servo. *IEEE Trans. on Neural Networks* 1991, PP 248-251.
- 36 **Lee S., and Meerkov S. M.,** Generalised dither. *IEEE Trans on Information Theory*, 37(1),1991, 50-56.
- 37 **Godfrey D.,** Vibration reduces metal to metal contact and causes an apparent reduction in friction. *ASLE Transactions*, 10(2), 1967, 183-192.
- 38 **Luh J., Fisher, W., and Paul, R.,** Joint torque control by direct feedback for industrial robots. *IEEE Trans. on automatic control*. Vol. AC-28, No., February 1983.
- 39 **Hashimoto M., Koreyeda K., Shimono T., Tanaka H., Kiyosawa Y., and Hirabayashi, H.,** Experimental study on torque control using harmonic drive built-in torque sensors. *IEEE International proceeding conference on robotics and automation*, Nice, 2026-2031.
- 40 **Bluen J., and Stuart K.,** Use of magnetic suspension for accurate pointing and tracking under static and dynamic loading. *SPIE*, Vol 1304, 1990, 33-45.
- 41 **Armstrong-Helouvry, B.,** Friction experimental determination, modeling and compensation. *IEEE Int. Conf. Robotics and Automation*, 1988, 1422-1427.

-
- 42 **Bo, L. C., and Pavelescu, D.,** The friction speed relation and its influence on the critical velocity of the stick-slip friction. *Wear*, 3, 1982, 277-289.
- 43 **Canudas de Wit C., Olsson H., Astrom, K. J., and Lischinsky P.,** A new model for control of systems with friction. *IEEE Trans. on automatic control*, Vol. 40, No 3, March 1995, 419-425.
- 44 **Bilman P.A., and Sorine M.,** Easy to use realistic dry friction models for automatic control. *Proc. of 3rd European control conference*, Rome, Italy, 1995, 3788-3794.
- 45 **Harnoy A., Friedland, B., Semenoek R., Rachoor, H., Aly A.,** Apparatus for empirical determination of dynamic friction. *Proc. American control conference ACC*, 1994, 546-550.
- 46 **Luh J., Fisher W., and Paul R.,** Joint torque control by direct feedback for industrial robots. *IEEE Trans. on automatic control*, Vol. AC-28, No.2, February 1983, 153-161.
- 47 **Leonard E. L., and Krishnaprasad P. S.,** Adaptive friction compensation for bi-directional low-velocity position tracking. *IEEE Proc. 31st conference on decision and control*. Tucson Arizona. 1992, 267-273.
- 48 **Kennedy P., Kennedy R., and Agard I.,** Adaptive compensation for pointing and tracking system applications. *IEEE Proc. of international conference on control applications*, 1999, 279-284.
- 49 **Craig J.,** Adaptive control of mechanical manipulators. *Addison-Wesley*, 1988.
- 50 **Paraskevopoulos P.N.,** Modern control engineering. *Marcel Dekker, Inc.*, 2002, ISBN 0-8247-8981-4, 2002, 637- 672.
- 51 **Pee H. M., Syed, V., and Lappen, J.,** Weapon control and stabilisation using modern control techniques. *FMC Corporation, Advanced systems centre*, Minneapolis, MN 55421. No date available
- 52 **Mathworks.,** Robust control toolbox user's guide. *The Mathworks Inc.* Natick, MA 01760-2098, June 2001.
- 53 **Mattice M., Coleman, N., Mattice M., Banks S., and Lin C. F.,** Robust weapon control system design. *IEEE 1992 American control conference*. June 1992, 429-433.
- 54 **Rao S., Mattice M., and Coleman N.,** Design of reduced order LQG/LTR controllers for turret -gun system. *IEEE Proc. of American control conference*, June 1989, 312-315.

-
- 55 **Rao S., and Mattice, M.,** Design of Robust controllers for turret-gun system using reduced order models. *ARDEC, Picatinny Arsenal, New Jersey, US report AD-E402 034*, April 1990.
- 56 **Rao S., Mattice N., and Coleman N.,** Design of Robust structural controllers for gun-turret systems. *Proc. of 7th US Army symposium on gun dynamics*. Newport, Rhode Island, May 1993, 334-348.
- 57 **Moorty K., and Marthe R.,** H_{∞} control law for line-of-sight stabilisation for mobile land vehicles. *Society of photo-optical instrumentation engineers*, 41 (11), 2002, 2935-2944.
- 58 **Moorty K., and Marathe R.,** LQG/LTR control law for a wideband controller for line of sight stabilisation for mobile land vehicles. *Proc., Int. conf. on electro-Optics*, Narosa, New Delhi, India 1999, 729-735.
- 59 **Li T., Lin C. F., Juang J., Coleman N., Mattice M., and Banks S.,** Fuzzy logic control of gun turret systems. *Proc. IEEE 1992 American control conference*, June 12, 1992, 440-444.
- 60 **Moorty K., Marathe R., and Babu H.,** Fuzzy controller for line-of-sight stabilisation systems, *Optical Engineering*, Vol. 43 (6), 2004, 1394-1400.
- 61 **Haug J., Lin, C., and Coleman, N.,** A nonlinear controller for the gun turret system. *1992 American control conference*, Chicago, Illinois. 424-429.
- 62 **Dana R., and Kreindler E.,** Variable structure control of a tank gun. *First IEEE conference on control applications*, Dayton Ohio, September. 1992, 928-933.
- 63 **Grimble M., and Diyar A.,** Introduction to the benefits of controllers with several degrees of freedom and the use of feedforward control, *Industrial systems and control*, ACT/TR12/95,1995.
- 64 **Purdy J., D.,** Comparison of balance and out-of-balance main battletank armaments. *Shock and Vibration*, 8, 2001, 167-174.
- 65 **D'Souza F.,** Design of control systems. *Prentice Hall*, ISBN 0-13-199951-6-025, 1988, 256-261.
- 66 **McNab R. J., and Tsao T.,** Frequency response based feedforward control design with uncertain considerations, *Proc. American Control. Conference*. 1997, Vol 5, 2726-2730
- 67 **Kavranoglu D., and Ahmed M. E.,** Hinf optimal feedforward process control, *Proc American control conference*, v1, 1992, 122-126.
- 68 **Grimble M. J. et al.,** Robust H_2 feedback/feedforward control design MATLAB toolbox polynomial approach. *Industrial control systems limited*, 1995.

-
- 69 **Solartron Instruments**, 1252 Frequency Response Analyser manual. *Solartron Instruments*, Farnborough, UK, 1982.
- 70 **Bendat J. S., and Piersol A. G.**, Engineering applications of correlation and spectral analysis, *John Wiley and Sons*, ISBN 0-471-05887-4, 1980, 43-76.
- 71 **Clephan J. S.**, The application of dynamic programming to the synthesis of an optimal controller for a tank gun control system. *Msc, report Royal military collage of science*, October 1982.
- 72 **Oats C., and Blower P.**, A study of an adaptive control for gun control equipment, *UMIST*, October, 1980.
- 73 **Meriovitch L.** Elements of vibration analysis. *McGraw-Hill*, ISBN 0-07-041340-1, 1975, 286-324.
- 74 **Craig R. R. Jr.**, Structural Dynamics, An introduction to computer methods, *John Wiley*, 1981.
- 75 **Clough R.W., and Panzani J.**, Dynamics of structures, *McGraw-Hill*, ISBN 0-071-011392-0, 1975, 336-339.
- 76 **Weaver W., and Johnston P. R.**, Structural dynamics by Finite Elements. *Prentice-Hall*, ISBN 0-14-853508-6 025, 1987, 164-167.
- 77 **Craig R. R., and SU T-J.**, Review of Model Reduction Methods for structural Control Design. *Proc. of 1st international conference*, Cranfield, UK, 15-18 May 1990, 121-134.
- 78 **Guyan R.J.**, Reduction of Stiffness and Mass Matrices. *AIAA Journal*, Vol.3, 1965, 380.
- 79 **Moore B.C.**, Principal component analysis in linear systems: Controllability, observability and model reduction. *IEEE Trans. on automatic Control*, AC-26, No.1, February. 1981, 17-32.
- 80 **ISI. Inc.**, Xmath model reduction module. No. 000-0025-002, *Integrated Systems Inc.*, Santa Clara, CA 95054-3309, January 1996.
- 81 **Gallagher R. H.**, Matrix dynamic and instability analysis with non-uniform elements. *International Journal for numerical methods in engineering*, Vol. 2, No. 2, 1970, 265-276.
- 82 **Anon**, Handbook of high performance motion control with brushless servo drives, *Reliance Motion Control Electro-Craft Corporation*, date unknown, 105-116.

-
- 83 **Kuo B.**, Incremental motion control. *SRL publishing company*, ISBN 0-9181852-02-x, 1978.
- 84 **Olson H., Astrom K. J., Canudas de Wit C., Gafvert M., and Lischinsky P.** Friction Models and Friction Compensation. *European journal of control*, 1998 (4), 176-19
- 85 **Laub A. J.**, Efficient Multivariable Frequency Response Computations, *IEEE Transactions on Automatic Control*, Vol. Ac-26 No2, April 1981. 407-408.
- 86 **Dholiwar D. K.**, The development of a pulse width modulated servovalve. *Msc. report, University of Bath*, 1980.
- 87 **Wellstead P. E.**, Frequency response analysis. *Solartron* 1982, technical report number 010/84.
- 88 **Luksic M.**, Exact frequency response simulation for any type of control systems. *IEEE 1st conf. on control applications*, 1992, 665-670.
- 89 **Dutton K., Thompson S., and Barraclough B.**, The Art of control engineering. *Addison Wesley*, 1997, ISBN 0-201-17545-2.
- 90 **Hughes P. C.**, Space structure vibration modes: How many exist ? Which ones are important ?, *IEEE control systems Magazine*, 27-28, February 1987.
- 91 **PAFEC**, PAFEC user's guide, PAFEC Ltd, *Strelley Hall, Nottingham, NG8 6PE*.
- 92 **MATLAB**, Control system toolbox, *MathWorks Inc, Natick, MA, USA*, 2000, 2.26-2.32.
- 93 **Heyes N., Peggs K., Baxter J., Franklin M., and Dholiwar D. K.**, Development of an autonomous UGV technology test bed for military operations. *Autonomous unmanned vehicle system international conference, L.A. California*, 2004.

APPENDICES

Appendix 1

A 1.0 Other techniques for control of systems with friction

Non-model based compensation schemes comprise impulse control, dither controllers, joint torque controllers and magnetic bearings to reduce friction.

A1.1 Impulse control

In impulse control small pulses are used to control the motion of the system. Several different schemes have been proposed for impulse control but the general idea is to apply impulses to the system when it is stationary or in 'stuck' condition and then use another control scheme when the system is in motion. Typical examples of work using impulse control are Hojjat *et al.*[1] and Deweerth *et al.*[2]; who use an ANN for their impulse control scheme.

A1.2 Dither control

In dither control a small high frequency oscillation is introduced to minimise the effects of the discontinuity, Lee and Meerkov[3], Godfrey[4]. This vibration can be introduced using external vibrators or the actuating signal can be modified. When external vibrators are used dither can be applied in a tangential or normal direction to the sliding contact. Vibrators called Dippers have been used on large guns to reduce the effects of nonlinear frictional. Experimental work by Leonard and Krishnaprasad[5], showed that the dither control used in conjunction with PID did not provide significant improvements in their application. They speculate that this may have been due to the low dither frequency used due to the sampling frequency limitation.

A1.3 Joint torque control

In joint torque control an inner loop is introduced which compensates for transmission and actuator friction. A torque transducer is required which measures the system output torque and has to be located as close as possible to the load. Amongst others Luh *et al.*[6], and Hashimoto *et al.*[7], have investigated the use of joint torque control. In the first paper, which deals with a robot drive system, describing function techniques are used to reduce oscillations caused by system backlash.

Hashimoto *et al.* show that joint torque control techniques provide substantial improvements in a position controlled system which uses PD for the primary loop. The work investigates the use of feedforward control, feedforward with friction model and a torque disturbance observer. The disturbance observer provides the best results and the feedforward the worst of the three. However, all three provide substantial improvements when compared to a system with no joint torque control. It should be noted that a fairly simple primary loop controller is used in this paper.

A1.3 Magnetic suspension

The work of Bleun and Stuart[8] on magnetic suspension is of particular interest as the experimental study shows that considerable improvement in stabilisation performance is achieved by using magnetic suspension system when compared to conventional bearing mounted systems. Their work on the azimuth axis of an electro-optic system showed the stabilised system performance is improved from -35dB to -60dB. The main disadvantage of the system is the complexity and the additional power requirements by the electro-magnetic system.

Appendix 1

References

- 1 **Hojjat Y., and Higugi, T.,** Application of electromagnetic impulse force to precise positioning. *International Journal Japan Society Precision Engineering*, Vol. 25, No 1, March 1991.
- 2 **DeWeerth, S., Neilsen, C., Mead, C., and Astrom, K.,** A simple neuron servo. *IEEE Trans. on Neural Networks* 1991, PP 248-251.
- 3 **Lee S., and Meerkov S. M.,** Generalised dither. *IEEE Trans on Information Theory*, 37(1),1991, 50-56.
- 4 **Godfrey D.,** Vibration reduces metal to metal contact and causes an apparent reduction in friction. *ASLE Transactions*, 10(2), 1967, 183-192.
- 5 **Leonard E. L., and Krishnaprasad, P.S.,** Adaptive friction compensation for bi-directional low-velocity position tracking. *IEEE Proc. 31st conference on decision and control*. Tucson Arizona. 1992, 267-273.
- 6 **Luh J., Fisher, W., and Paul, R.,** Joint torque control by direct feedback for industrial robots. *IEEE Trans. on automatic control*. Vol. AC-28, No., Feb. 1983.
- 7 **Hashimoto M., Koreyeda K., Shimono T., Tanaka H., Kiyosawa Y., and Hirabayashi H.,** Experimental study on torque control using harmonic drive built-in torque sensors. *IEEE International proceeding conference on robotics and automation*, Nice, 2026-2031.
- 8 **Bluen J., and Stuart K.,** Use of magnetic suspension for accurate pointing and tracking under static and dynamic loading. *SPIE*, Vol 1304, 1990, 33-45.

Appendix 2

A2.0 Robust control techniques

A2.1 Introduction

Classical control techniques are widely used and their continued success can be attributed to several factors. Firstly, these methods are relatively easy to learn. Secondly, the theoretical time and frequency domain results can be easily verified by experimental measurements. Thirdly, the graphical nature of these techniques, such as Nyquist and Bode diagrams, provide the designer with simple aids to manipulate and diagnose system performance. Fourthly, simple rules of thumb such as those provided by Ziegler-Nichols [1] can be used to obtain the desired performance. Finally, these low order controllers can be readily tuned on-line in the field. However, classical techniques struggle when used on MIMO systems which contain high degree of cross-coupling between several inputs and outputs of the controlled system. In contrast to the classical techniques the quadratic optimal control theories of the 1960's and 1970's are applicable to multivariable systems. However, it is difficult to incorporate robustness in the quadratic integral performance index used in the Linear Quadratic Gaussian (LQG) problem. In the 1980's robust multivariable approach to controller design was studied which resulted in, amongst other results, optimization theory known as H_{∞} .

Brief details of the three most commonly used techniques are outlined in this appendix and references are provided which give fuller details of the techniques. Excellent treatment of these techniques are presented in Skogestad and Postlethwaite[2], Dutton *et al.* [3] and tutorial examples can be found in MATLAB Robust control toolbox user's guide [4] which also gives details of the tools for solving the equations presented in this chapter.

A2.2 The LQG/LTR method

Although, The LQG/LTR method is applicable to SISO systems it is inherently a multivariable design method. It does not reduce a MIMO to a collection of SISO design problems. The LQG/LTR method involves two basic steps. In the first step a MIMO

target feedback loop (TFL) is generated. The TFL is selected to meet the performance specifications whilst maintaining the stability and robustness requirements. In the second step the LQG/LTR compensator is selected to approximate the performance of the feedback system to that of the TFL selected in the first step. The compensator has adjustable parameters which enable its characteristics to be manipulated to approximate the TFL. If the design plant model is minimum phase then the degree of approximation, or the recovery, of the target feedback can be quite good. If the design plant model is nonminimum phase then the recovery will depend on the location of the nonminimum phase zeros. Details of the design process are provided in reference by Athans[5], and some of the salient results from the paper are summarised below. Fuller details on LTR procedures are provided in the work by Kwakernaak [6], Doyle and Stein [7].

The design plant model (DPM) used in conjunction with the LQG/LTR method not only includes the nominal plant model, but also includes the scaling factors, augmented dynamics (such integrators) that the designer has included and reflects all the modeling errors to the output of the DPM, using multiplicative model error representation described by Doyle and Stein [8].

The DPM is represented by

$$\dot{\mathbf{x}} = \mathbf{Ax} + \mathbf{Bu} \quad (\text{A2-1})$$

$$\mathbf{y} = \mathbf{Cx} + \mathbf{Du} \quad (\text{A2-2})$$

Then the transfer function matrix (TFM) is given by

$$\mathbf{G}(s) = \mathbf{C}\Phi(s)\mathbf{B} \quad (\text{A2-3})$$

Where

$$\Phi(s) \equiv (s\mathbf{I} - \mathbf{A})^{-1} \quad (\text{A2-4})$$

The MIMO feedback loop is shown in Figure A2-1. The diagram shows the tracking error vector $E(s)$. For clarity the diagram does not show sensor noise and the disturbances acting on the system which is accounted for as an additive disturbance acting on the DPM output.

Target Feedback Loop (TFL)

The structure of TFL is shown in Figure A2-2. It is simply defined by the parameters \mathbf{C} and $\Phi(s)$ of the DPM and matrix \mathbf{H} which is called the filter gain matrix.

The loop Transfer Function Matrix (TFM) associated with the TFL is given by

$$\mathbf{G}_{KF}(s) = \mathbf{C}\Phi(s)\mathbf{H} \quad (\text{A2-5})$$

The sensitivity of TFM

$$\mathbf{S}_{KF}(s) = [\mathbf{I} + \mathbf{G}_{KF}(s)]^{-1} \quad (\text{A2-6})$$

And the complementary sensitivity function

$$\mathbf{C}_{KF}(s) = [\mathbf{I} + \mathbf{G}_{KF}(s)]^{-1} \mathbf{G}_{KF}(s) \quad (\text{A2-7})$$

For any filter gain matrix \mathbf{H} we can evaluate the TFL so that it meets the stability-robustness constraints and performance specifications.

The LQG/LTR compensator, $\mathbf{K}(s)$.

The LQG/LTR compensator illustrated in Figure A2-3 belongs to a class called the model-based compensators. The compensator contains the design plant model (DPM) and two feedback loops containing the gain matrix \mathbf{G} and gain matrix \mathbf{H} . These two matrices are the design parameters in the compensator.

The transfer function matrix of the model based compensator is defined by:

$$\mathbf{U}(s) = \mathbf{K}(s)\mathbf{E}(s) \quad (\text{A2-8})$$

and

$$\mathbf{K}(s) = \mathbf{G}[s\mathbf{I} - \mathbf{A} + \mathbf{BG} + \mathbf{HC}]^{-1}\mathbf{H} \quad (\text{A2-9})$$

The closedloop poles of the feedback system in Figure A2-1, when represented by equation A2, are the eigen values of $((A - \mathbf{B}\mathbf{G})$ and $(A - \mathbf{H}\mathbf{C})$.

In the LQG/LTR method when applied to model based compensator, the \mathbf{H} and \mathbf{G} matrices in equation A2-9 are selected as follows. \mathbf{H} is fixed to be the same as that in the TFL and the control gain matrix \mathbf{G} in $\mathbf{K}(s)$ is computed via the solution of the Linear Quadratic Regulator problem. Details of this solution are provided in reference by Doyle and Stein [8].

A2.3 Standard \mathbf{H}_2 and \mathbf{H}_∞ control

The limitations of LQG control were addressed in the 1980's which lead to the development of \mathbf{H}_∞ , with influential the work of Zames [9]. With further development the two approaches \mathbf{H}_2 and \mathbf{H}_∞ are now considered to be more closely related than originally anticipated. Skogestad and Postlethwaite [2] use a standard formulation to compare the two techniques. The general control configuration used is shown in Figure A2-4. The details of the system which is used to derive the equations presented in this section is shown in Figure A2-5.

The system is described by the following:

$$\begin{bmatrix} \mathbf{z} \\ \mathbf{v} \end{bmatrix} = \mathbf{P}_G(s) \begin{bmatrix} \mathbf{w} \\ \mathbf{u} \end{bmatrix} = \begin{bmatrix} \mathbf{P}_{G11}(s) & \mathbf{P}_{G12}(s) \\ \mathbf{P}_{G21}(s) & \mathbf{P}_{G22}(s) \end{bmatrix} \begin{bmatrix} \mathbf{w} \\ \mathbf{u} \end{bmatrix} \quad (\text{A2-10})$$

$$\mathbf{u} = \mathbf{K}(s)\mathbf{v}$$

Where

\mathbf{u} are control variables

\mathbf{v} are measured variables

\mathbf{w} are external signals such disturbances and demand

\mathbf{z} are error signals

The closed loop transfer function is as follows

$$\mathbf{z} = (\mathbf{P}_{G11} + \mathbf{P}_{G12}\mathbf{K}(I - \mathbf{P}_{G22}\mathbf{K})^{-1}\mathbf{P}_{G21})\mathbf{w} \quad (\text{A2-11})$$

Which can be written as:

$$\mathbf{z} = \mathbf{F}_l(\mathbf{P}_G, \mathbf{K})\mathbf{w} \quad (\text{A2-12})$$

Where

$$\mathbf{F}_l(\mathbf{P}_G, \mathbf{K}) = \mathbf{P}_{G11} + \mathbf{P}_{G12}\mathbf{K}(I - \mathbf{P}_{G22}\mathbf{K})^{-1}\mathbf{P}_{G21} \quad (\text{A2-13})$$

The \mathbf{H}_2 and \mathbf{H}_∞ control involve minimizing the function $\mathbf{F}_l(\mathbf{P}_G, \mathbf{K})$.

The \mathbf{H}_2 optimal control

The \mathbf{H}_2 control problem is to find a controller \mathbf{K} which minimizes the following

$$\|F_l(P_G, K)\|_2 = \sqrt{\frac{1}{2\pi} \int_{-\infty}^{\infty} F_l(P_g, K)(j\omega) \cdot F_l(P_g, K)(j\omega)^T d\omega} ;$$

The generalized plant model \mathbf{P}_G will include the interconnections and the weighting functions defined by the designer. The left hand side is called the 2 norm of error. This is minimizing the root-mean-square (RMS) of the error.

The \mathbf{H}_∞ optimal control

The alternative to the minimizing the average error is to minimize the peak value.

The \mathbf{H}_∞ optimal control is to find \mathbf{K} which minimize

$$\|F_l(P_G, K)\|_\infty = \max_{\omega} \sigma(F_l(P_G, K)(j\omega))$$

In practice it is much easier to design a suboptimal controller, which is close to optimal using the algorithm described by Doyle [10]

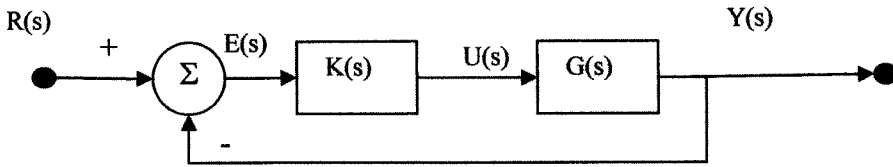


Figure A2-1: Closed-loop system with external disturbance

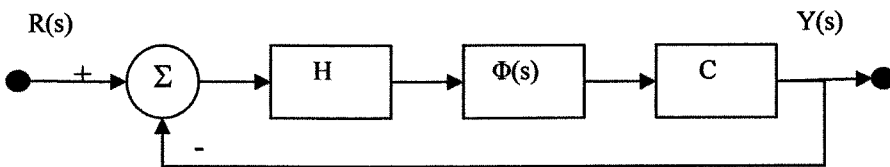


Figure A2-2: The target feedback loop structure

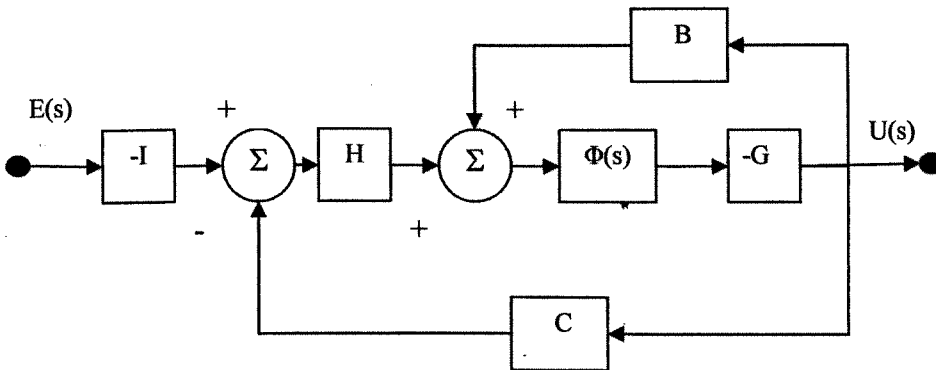


Figure A2-3: Structure of a Model based controller and an LQG/LTR compensator

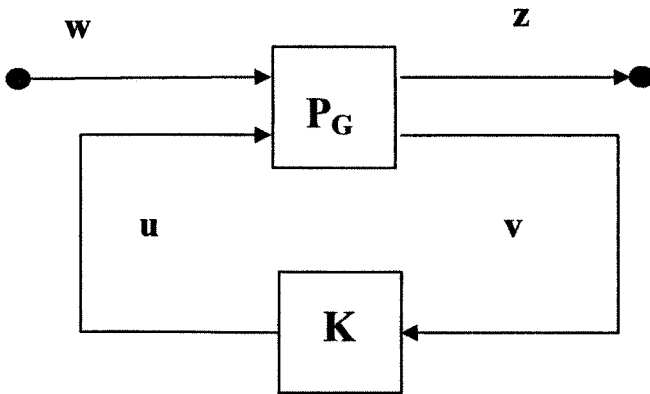


Figure A2-4: General control block diagram used for problem formulation

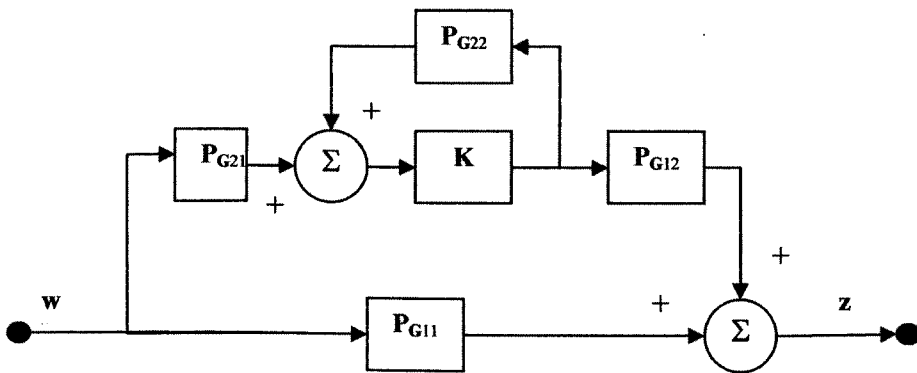


Figure A2-5: Block diagram of system.

Appendix 2

References

- 1 **Ziegler J.G., and Nichols N.,B.**, Optimum settings for automatic controllers. *Trans. Of ASME*, Vol. 64, 1942, 759-768.
- 2 **Skogestad S., and Postlethwaite I.**, Multivariable Feedback control analysis and design Structural Dynamics, An introduction to computer methods, *John Wiley and sons*, ISBN 0471 94277 4,1997.
- 3 **Dutton K., Thompson S., and Barraclough B.**, The Art of control engineering. *Addison Wesley*, 1997, ISBN 0-201-17545-2.
- 4 **Mathworks.**, Robust control toolbox users guide. *The Mathworks Inc.* Natick, MA 01760-2098, June 2001.
- 5 **Athans M.**, A tutorial on the LQG/LTR method. *IEEE Proc of American control conference*. Seattle, WA, June1986,1289-1296.
- 6 **Kwakernaak H.**, Optimal low-sensitivity linear feedback systems, *Automatica* ,5(3): 1969, 279-286.
- 7 **Doyle J., C., and Stein G.**, Robustness with observers, *IEEE Trans. on automatic control*, Vol. AC 24, August 1979, 607-611.
- 8 **Doyle J., C., and Stein G.**, Multivariable feedback design: Concepts for Classical/Modern synthesis, *IEEE Trans. on automatic control*, Vol. AC-26, February 1981, 4-16.
- 9 **Zames G.**, Feedback and optimal sensitivity: model reference transformations, multiplicative seminorms, and approximate inverse, *IEEE Trans. on automatic control*, Vol. AC-26, February 1981, 301-320.
- 10 **Doyle J., C., Glover K., Khargonekar P., P.,and Francis B., A.**, State-space solutions to standard H_2 and H_∞ : control problems, *IEEE Trans. on automatic control*, Vol. AC-34, August 1989, 831-847.

Appendix 3

A3.0 Feedforward control

The Transfer functions for the closed-loop system with external disturbance illustrated in Figure A3-1 are as follows:

$$Y(s) = \frac{G_1(s) G_a(s) G_2(s)}{1 + G_1(s) G_a(s) G_2(s)} R(s) + \frac{G_2(s)}{1 + G_1(s) G_a(s) G_2(s)} U(s)$$

The equations for the system with feedforward control illustrated in Figure A3-2 are as follows:

$$Y(s) = \frac{G_1(s) G_a(s) G_2(s)}{1 + G_1(s) G_a(s) G_2(s)} R(s) + \frac{G_2(s)[1 - G_f(s) G_a(s)]}{1 + G_1(s) G_a(s) G_2(s)} U(s)$$

If $G_f(s)$ is the inverse of $G_a(s)$ then from the above equation the term $[1 - G_f(s) G_a(s)]$ becomes zero and the effects of the disturbance are eliminated. However, it is not always possible to invert $G_1(s)$ in which case the term $G_f(s) G_a(s)$ is made to be close to unity. Typical example is a system which is non-causal. A system is causal if its output depends only on the past inputs, and non-causal if its outputs also depend on future inputs.

The main difficulty with feedforward control compensation is that it is an open-loop technique and if the transfer function $G_a(s)$ changes or is not known then the term $G_f(s) G_a(s)$ will not be close to unity. Secondly, with feedforward control the disturbance has to be known so that it can be used as an input to the feedforward controller.

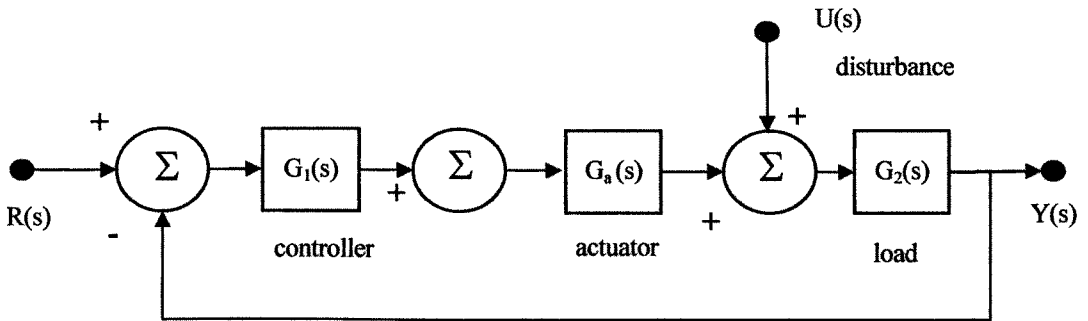


Figure A3-1: Closed-loop system with external disturbance

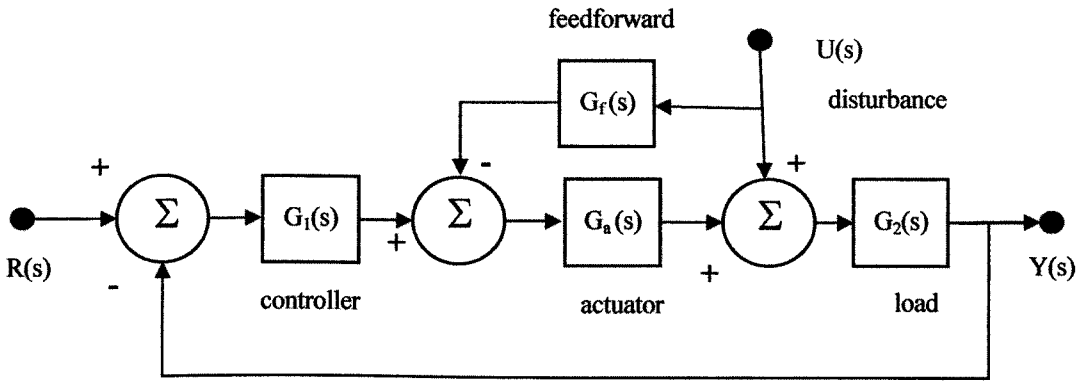


Figure A3-2: Closed-loop system with feedforward compensation

Appendix 4

A4.0 Control system hardware and development environment*

The rig is controlled using a digital system based on VME bus architecture. The system uses a MOTOROLA M68000/30 Central Processing Unit (CPU). Interface cards installed in the system enable it to be connected to the rig and provide communication links to other computer systems. The system has 32 differential analogue input channels (64 single ended) and 8 analogue output channels. The analogue input channels have a resolution of 16 bits which can be programmed to accept voltages which range from 0-5V to +/- 10V. The analogue output channels have a resolution of 12 bits which can be programmed to provide voltages similar to the input channels.

A digital I/O board supports 64 input and 32 output channels. The input channels are optically isolated and on-board relays isolate the output channels. The digital input channels are connected to limit switches, safety switches and other switches used to control the rig etc. The outputs are used to activate the system components such as safety brake, various alarms, and LEDs which monitor power amplifier operation such as temperature and current limits etc. A resolver input board, which has two channels, is used to measure the speed of the motor.

A timer counter board provides the real-time clock signal which is used to interrupt the Central Processing Unit. Communication to the VME system is via an Ethernet link connected to a PC.

A hard disk drive, installed in a rack system stores both the UNIX operating system and the LYNXOS Cross Development System [1] used to create the real-time software. The disk drive is also used to record experimental data from the various sensors. The experimental data stored on the hard disk, can be downloaded into the PC and analysed off-line using signal processing software such as MATLAB.

The sensor and the switches are connected to the computer system through a Sensor Interface Unit (SIU) which provides a buffer between the computer and rig. The buffer

* The design of the computer hardware is not part of the research, but details provided as background information.

enables sensors, which have low power outputs, to be connected to other devices such as plotters, tape recorders and oscilloscope. Analogue input signals connected to the computer were filtered using anti-aliasing filters.

The rig is protected by hard wired safety interlocks, safety switches and mechanical limit switches. These interlocks protect the system components such as power amplifier against excessive temperatures, high current demands, limit the travel of the structure to an arc of 30 degrees and enable the rig to be stopped quickly by activating the disc brake located on the gearbox. The disc brake can also be activated manually using the safety buttons.

An input unit is provided which enables the rig to be controlled manually or using external signal sources. This is used to test the response of the system to various input signals and also carry out open-loop and closed-loop frequency response analysis using the Frequency Response Analyser.

A4.2 Real-time software development

The software which controls the system consists of several subroutines (procedures) which are sequenced by the main program called the control executive. The program, developed using C programming language, provides all functions which manage the system such as system initialisation, input and output interfaces, Ethernet communication, data logging, BITE facilities etc. The work described in this thesis is concerned with the design of control system procedure which is summarised in a flow diagram illustrated in Figure A4-2. All the other software which control the peripheral functions are provided by the suppliers of the computer system.

	The VME bus computer system for control of the cantilever mechanism.
i)	CPU Board: MVME167 single board computer system, MOTOROLA. M68000/30 CPU Ethernet LAN transceiver Centronics printer port SCSI bus interface 64MB DRAM/8KB static RAM
ii)	Analogue I/O: VXME452, XYCOM. inputs 64 single-ended (32 differential) inputs 16 bits resolution, 0-5V, 0-10V, +/-5V, +/-10V input range 10 micro seconds conversion time outputs 8 channels 12 bit resolution 0-5V, 0-10V, +/-5V, +/-10V output range 4 micro second settling time
iii)	Digital I/O: AVME 9445I and 9426L, ACROMAG. input 64 opto isolated input channels 4-25 V or 20-55V DC input range 6 microseconds response output 32 mechanical relay 125V AC or DC 5milliseconds response
iv)	MPX 500B resolver input card, Pentland. 2/4 channel 2V input card 10-16 bit resolution accuracy +/-2,3,4 and 8 arc minutes 25millisecond settling time
v)	MPV 991 timer counter board, Pentland 10 general purpose 16 bit timer counters 5 internal frequency sources AM9519A VME Interrupt Bus 8 digital input and outputs
vi)	AB/ASF 1553 bus SBS dual channel 1553 bus interface
vi)	Disk drive 1.0GB and 3.5" floppy drive

Figure A4-1: Summary of the computer hardware

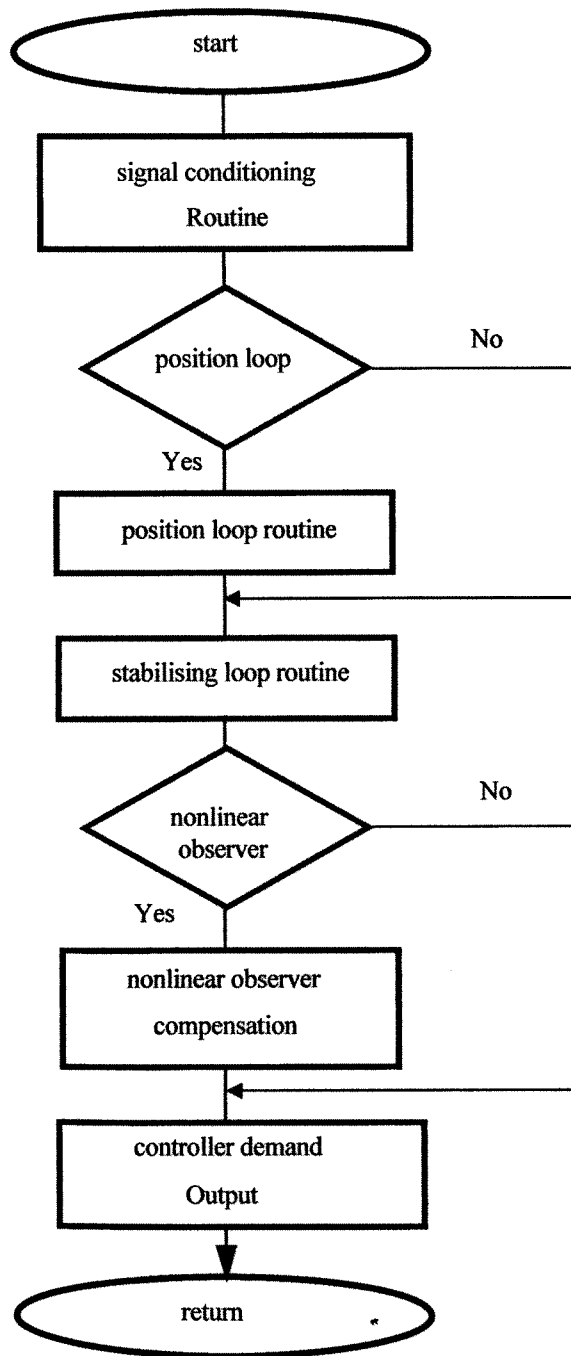


Figure A4-2: Flow diagram of the robust control procedure

Appendix 4

References

- 1 **Lynx Real-time Systems.**, LYNXOS reference manual V2.5. *Lynx Real-Time Systems Inc.*, San Jose California, 1997.

Appendix 5

A5.0 Details of the control system design

A5.1 Introduction

The design is based on the robust control technique described by Grimble *et al.* [1], and uses the MATLAB toolbox developed by Strathclyde University [2]. The H_2 control system design is a frequency domain technique which requires an estimate of the system transfer functions. Once a nonlinear model of the system has been obtained the next step is to select a suitable design point for the control system. The model is then linearised about this operating point and transfer functions are obtained. For the multi-input single-output (MISO) system under consideration transfer functions between each input and output are required.

Fundamental to the H_2 design is the selection of the weighting functions which determine the controller characteristics. Although general guidelines are known, many iterations in the selection of the weighting function characteristics are required to achieve the desired performance. The performance of the controller is verified using the linear models followed by the more detailed study using the nonlinear models. Several iterations of the above process may be required before a suitable controller is obtained.

In many applications the H_2 controller will result in a system which meets the designed objectives. However, in the system under consideration the H_2 controller does not provide the desired performance due to the influence of system nonlinearities. The method used to enhance the performance is based on the use of a nonlinear observer which is described in chapter 6 and 7.

A5.2 The design of hub controller

In chapter 6 the feedback controller is presented which produces 13% overshoot to step inputs. The control system can be refined to produce different responses. As an example a new control system, presented in this appendix, has been designed to produce smaller amplitude, 10%, overshoot. An additional controller, without integral control

(type 0), is also designed to show how the weighting functions can be selected to produce different controller characteristics.

A5.3 Defining the system transfer functions

The linear model, illustrated in Figure A5-1, is derived using Taylor's theorem. The transfer function model, required by the toolbox has a structure illustrated in Figure A5-2. The first transfer function is the open-loop response between the control signal and the hub output, the second transfer function is the response of the system to heave disturbance and the third transfer function is the response of the system to pitch disturbance. The three transfer functions are illustrated in Figure A5-3. The reduced order transfer functions are used for the control system design.

A5.3.1 Selecting the operating point

In nonlinear systems the transfer function changes with the operating point. However, in many systems a single transfer function is used as an approximation of the system dynamics to design a fixed term controller. The most suitable operating point is a matter of experience and engineering judgment. It may be selected to reflect the worst operating condition, which will result in a conservative design, or may be optimized at the mean operating condition, resulting in a controller which functions adequately at the extremes of operating conditions.

In the system under consideration the design point is selected by considering the operating range of the system. Responses at several points, within this range, were obtained to enable a suitable feedback transfer function to be selected. A similar process is used to obtain the transfer functions of the system-for the two external disturbances. The characteristics and magnitudes of the external disturbances were obtained from field trials carried out under typical operating conditions.

A5.4 The weighting functions

In robust techniques, such as H_∞ and H_2 , the controller is designed by selecting characteristics of two weighting functions, known as error weighting and controller weighting. Although, general guidelines for selecting the weighting functions are known the design process is problem specific and as a result it is not possible to provide definitive set of rules. One set of weighting functions may result in an entirely different controller if applied to another model with dissimilar characteristics.

However, as in any good design the controller should provide the following:

- a) Minimum steady state errors- high gain at low frequencies
- b) Rejection of high frequency noise- low gain at high frequencies
- c) Disturbance rejection at low frequencies -feedforward control
- d) Accurate tracking –tracking controller
- e) Operate within amplitude and rate limits of system components etc.

The weighting functions characteristics

The weighting functions for the controller with integral action are shown in Figure A5-4. The weighting functions for the controllers without integral control are shown in Figure A5-5. The resulting characteristics for the controllers are compared in Figure A5-6. The transfer functions for the weighting functions are provided below, where the coefficients (K_1 , a_1 and b_1 etc) are selected to provide the characteristics in Figure A5-4 and Figure A5-5.

Controller with integral

The final weighting functions for the controller with integral action are:

Feedback controller:

$$\text{Error weighting} = \frac{K_1}{a_1 s}$$

$$\text{Control weighting} = \frac{K_2(a_2 s + 1)}{1}$$

Linear disturbance feedforward controller:

$$\text{Error weighting} = K_3$$

$$\text{Control weighting} = \frac{K_4(b_4 s^2 + a_4 s + 1)}{1}$$

Angular disturbance feedforward controller:

$$\text{Error weighting} = K_5 \qquad \text{Control weighting} = \frac{K_6(b_6 s^2 + a_6 s + 0)}{1}$$

Controller without integral

The weighting functions for the controller without integral action are:

Feedback controller :

$$\text{Error weighting} = \frac{K_7}{(a_7 s + 1)} \qquad \text{Control weighting} = \frac{K_8(a_8 s + 1)}{1}$$

A5.5 The linear model results

The results from the linear simulations using the two controllers are presented in Figure A5-7 and Figure A5-8. The ability of the controllers to reject the effects of external disturbances are similar for the two control systems when the feedforward controllers are used as illustrated in Figures A5-7(c) and A5-8(c). However, from Figures A5-8(b) and A5-9(b), the response without feedforward control, it is noted that increased gain reduces errors caused by external disturbances.

The response of the system to step inputs shows that without integral control the system has a steady state error, and the system becomes more oscillatory.

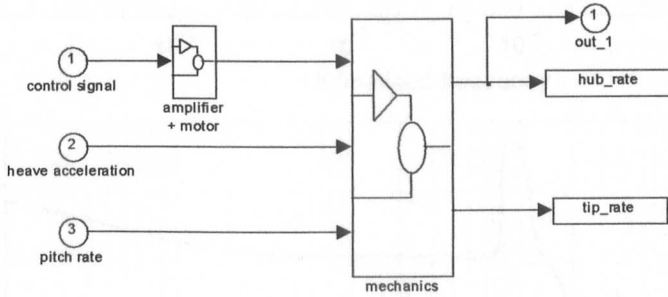


Figure A5-1: Linear model of the plant used to generate the three transfer functions

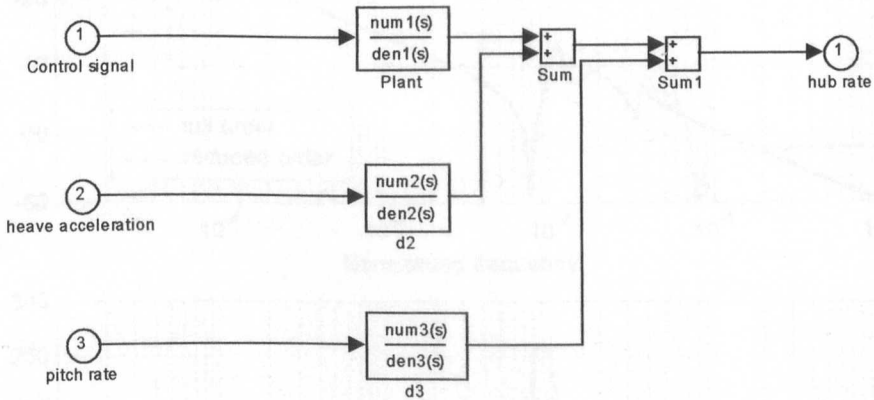


Figure A5-2: Transfer function model of the plant required by the toolbox.

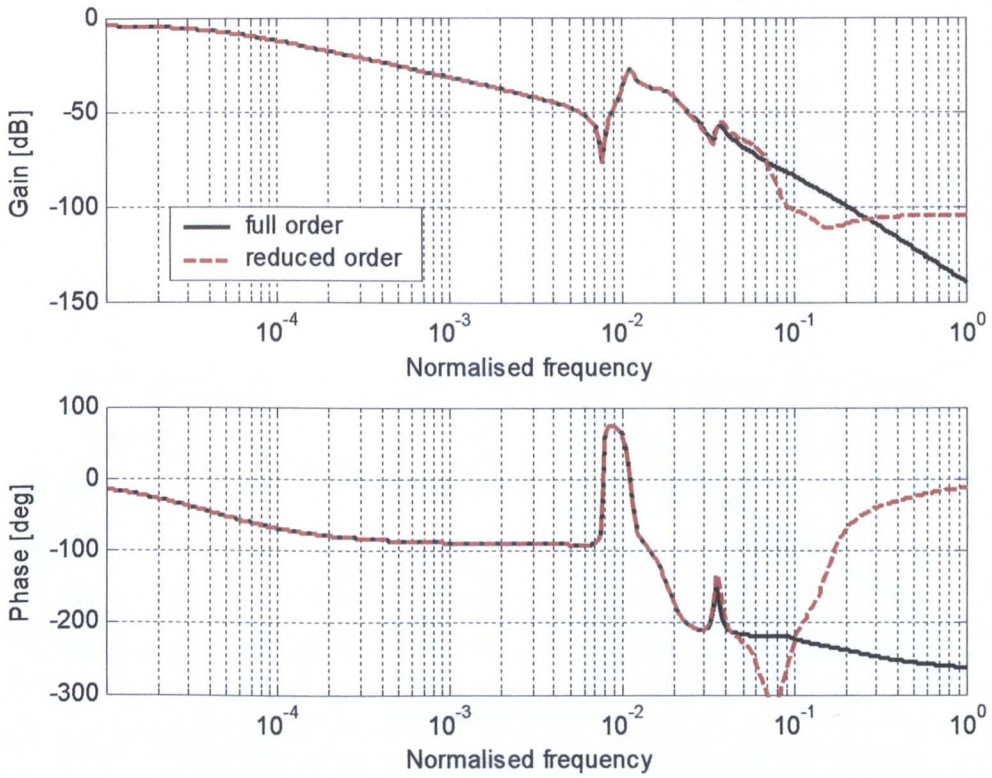


Figure A5-3(a): Frequency response of the plant to input signal and reduced order model used for control system design.

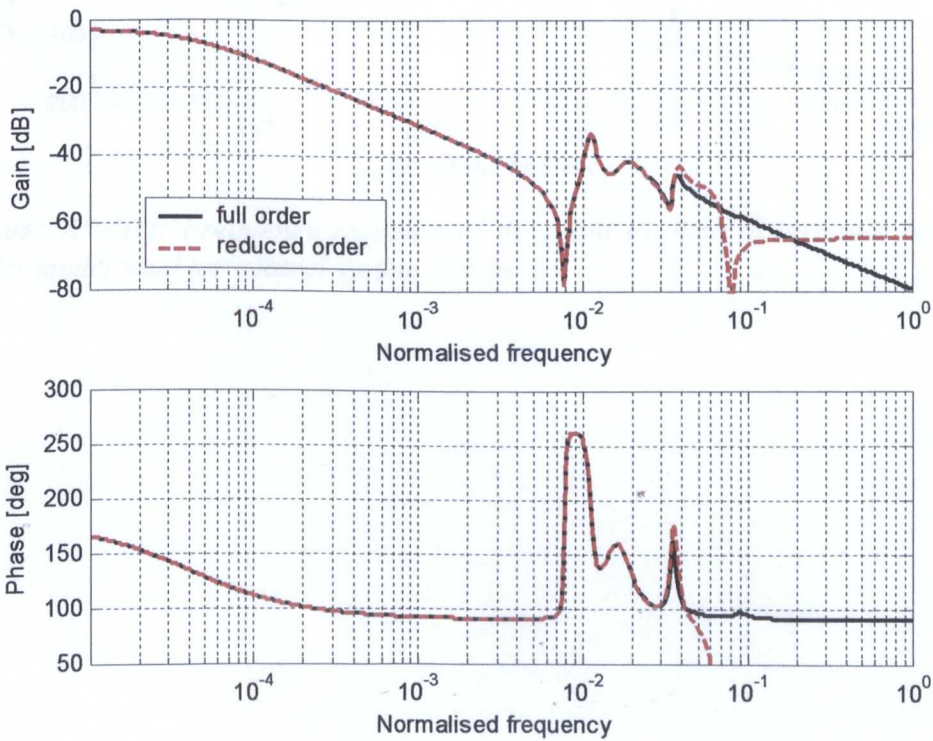


Figure A5-3(b): Frequency response of the plant to heave disturbance and reduced order model used for control system design.

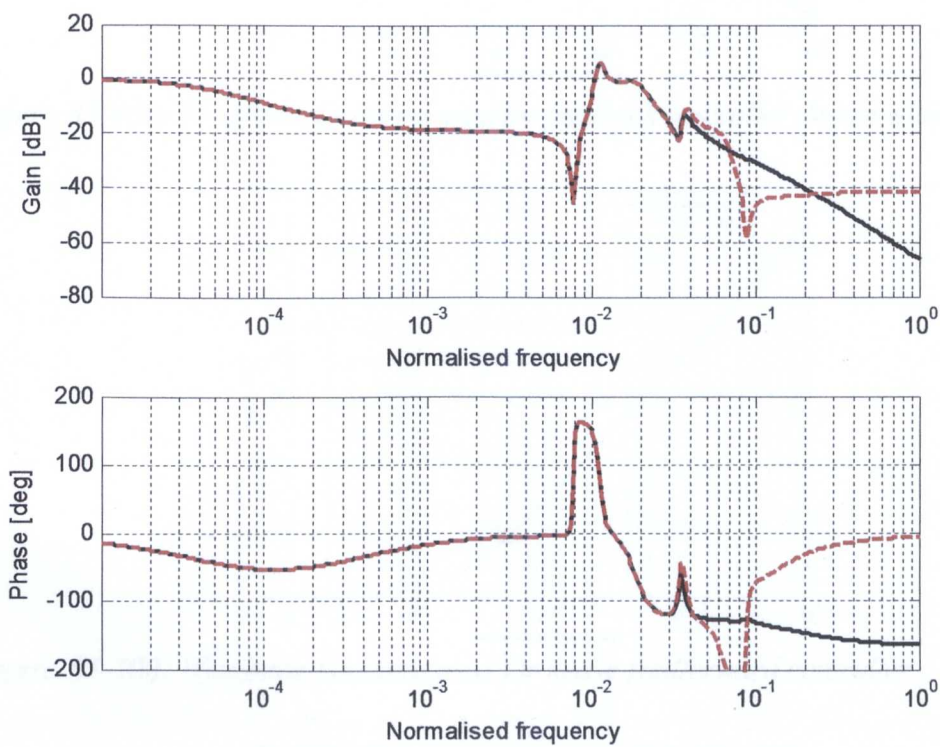


Figure A5-3(c): Frequency response of the plant to pitch disturbance and reduced order model used for control system design.

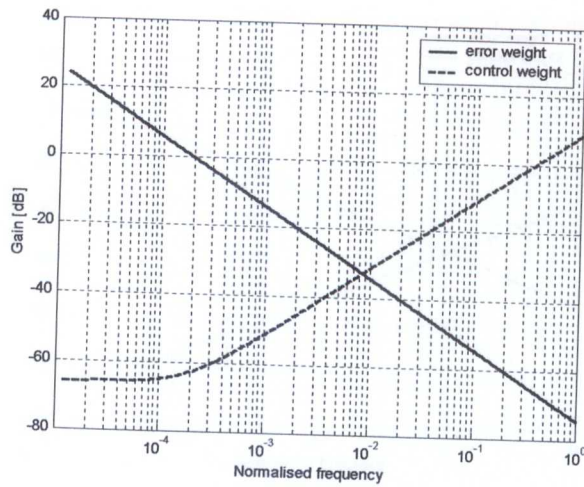


Figure A5-4(a): Weighting functions used for feedback controller design with integrator

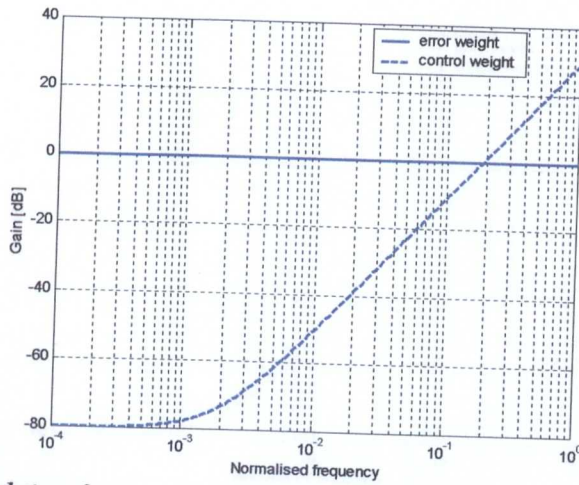


Figure A5-4(b): Weighting functions used for heavy feedforward controller

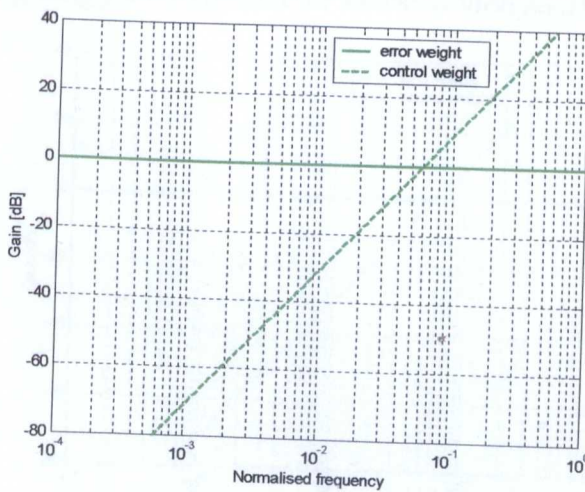


Figure A5-4(c): Weighting functions used for pitch motion feedforward controller

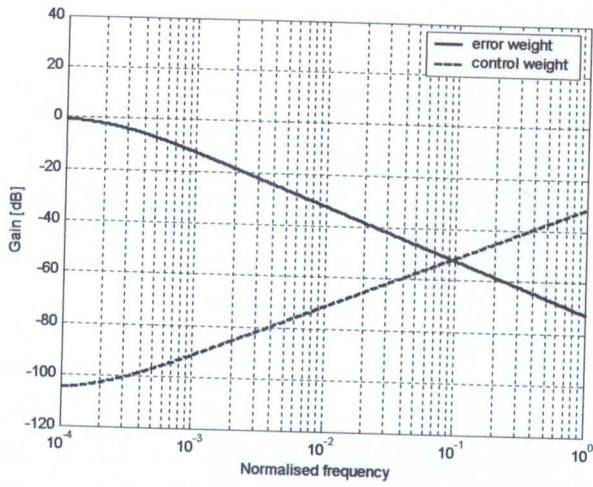


Figure A5-5(a): Weighting functions for controller without integrator

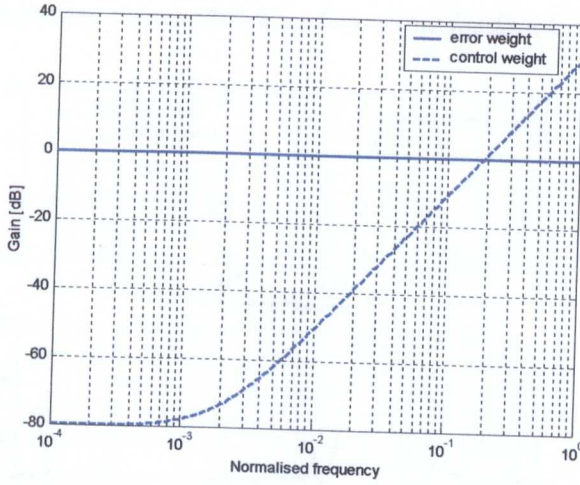


Figure A5-5(b): Weighting functions used for heave motion feedforward controller

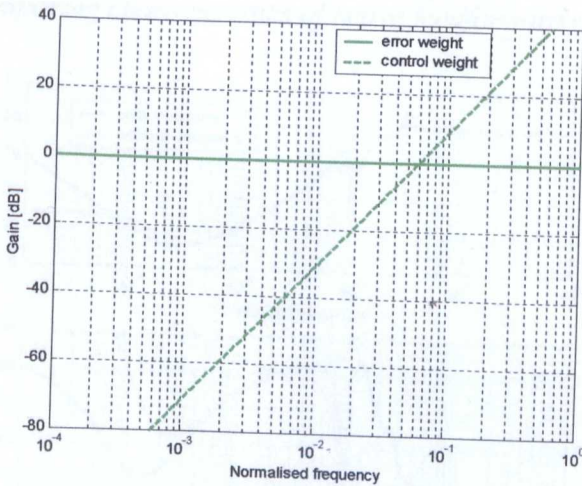


Figure A5-5(c): Weighting functions used for pitch motion feedforward controller

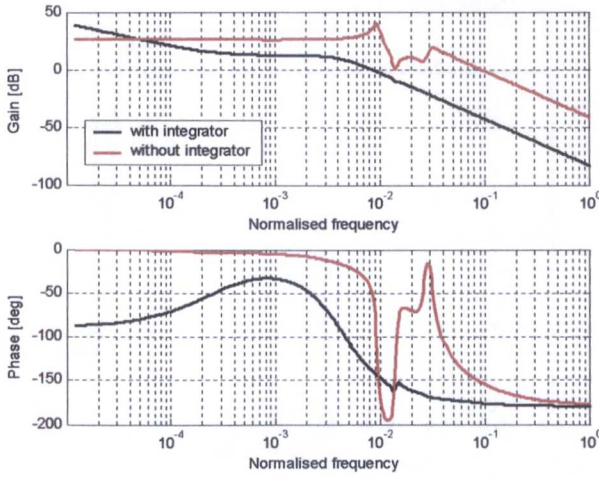


Figure A5-6(a): Comparing characteristics of the three feedback controllers

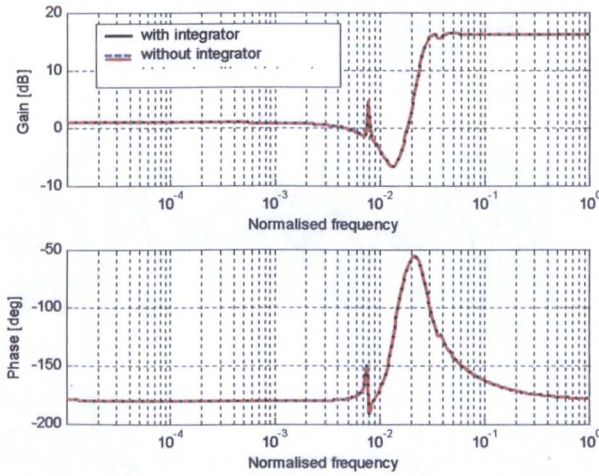


Figure A5-6(b): Comparing characteristics of heave feedforward controllers

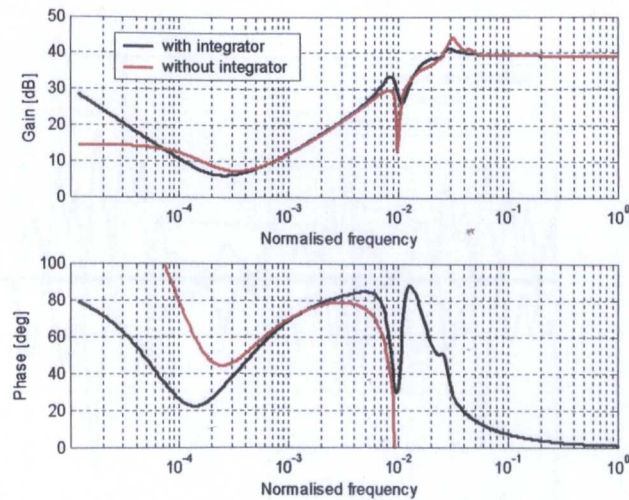


Figure A5-6(c): Comparing characteristics of pitch feedforward controllers

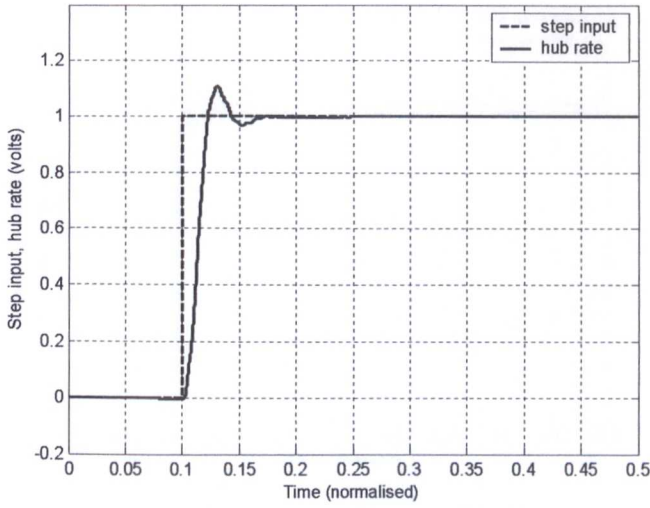


Figure A5-7(a): Linear simulation step responses using controller (with integrator)

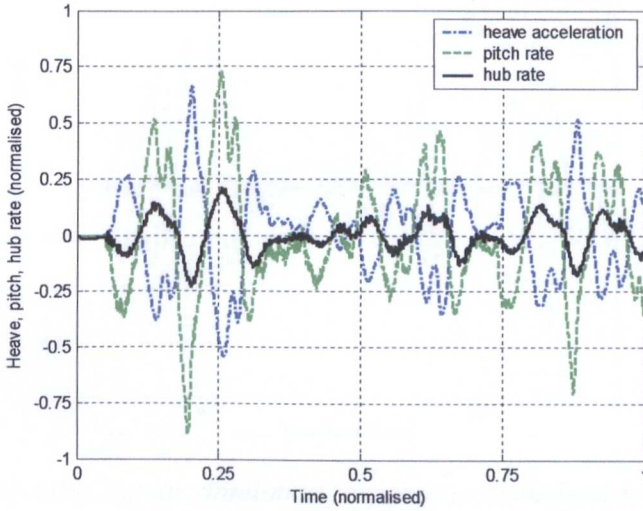


Figure A5-7(b): Linear simulation response to disturbances without feedforward control

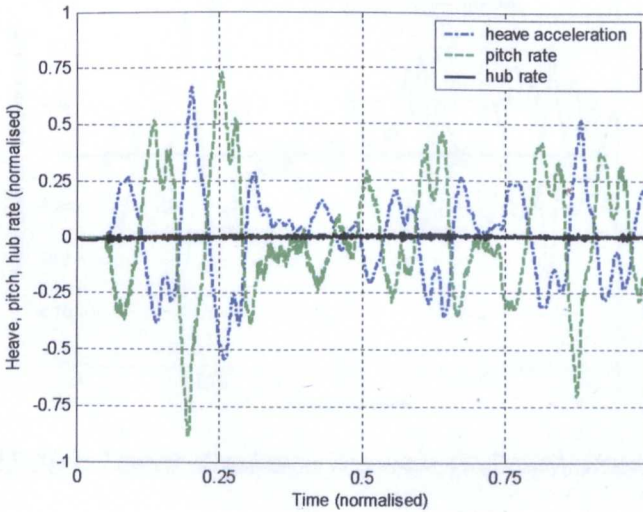


Figure A5-7(c): Linear simulation response to disturbances with feedforward control

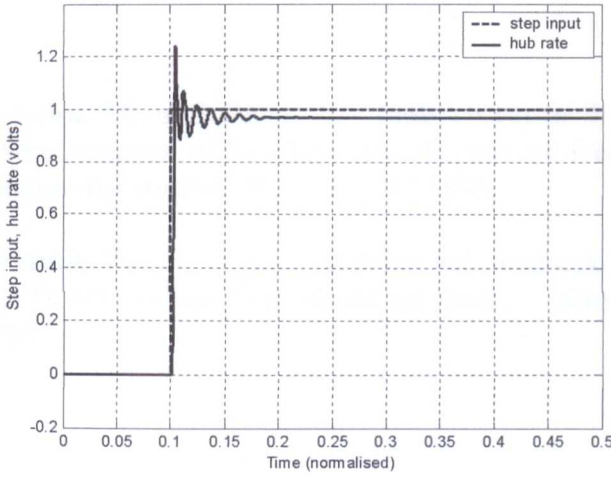


Figure A5-8(a): Linear simulation response of high gain controller without integrator

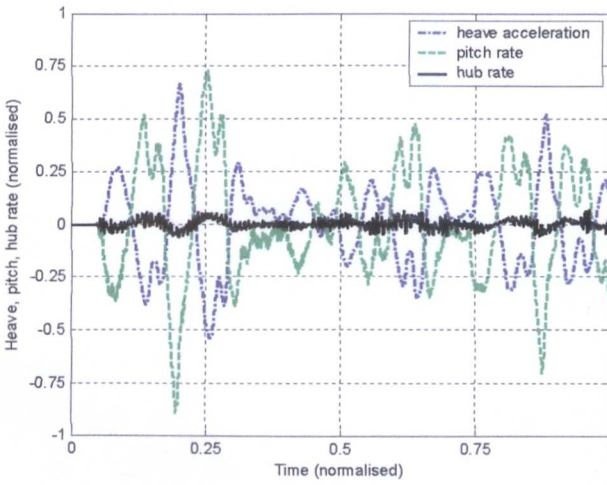


Figure A5-8(b): Linear simulation response to disturbances without feedforward control

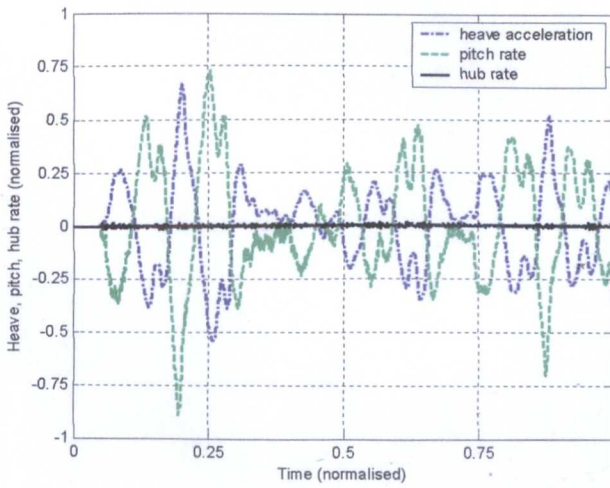


Figure A5-8(c): Linear simulation response to disturbances with feedforward control

Appendix 5

References

- 1 **Grimble M., and Diyar A.,** Introduction to the benefits of controllers with several degrees of freedom and the use of feedforward control, *Industrial systems and control*. ACT/TR12/95,1995.
- 2 **Grimble M. J. et al.,** Robust H2 feedback/ feedforward control design MATLAB toolbox polynomial approach. *Industrial control systems limited*. 1995.